Leather Inspection and Characterization using Non-Destructive Techniques

being a Thesis submitted for the Degree of

Doctor of Philosophy

in the University of Hull

by

José de Araújo Mendes

Engenheiro Electrotécnico, Universidade de Coimbra, Portugal, 1989

September 2000

Abstract

Leather is a widely used component of many products such as shoes, car seats, garments and other leather goods. Because it is a natural material, a tanned hide will contain visual and hidden flaws. In addition, its mechanical properties vary over the hide. At present, hides are inspected and assessed by skilled operatives. Further, current objective leather testing requires removal of samples and is either destructive and/or incompatible with real time operation, and little or no information about the rest of the skin is provided.

A novel mechanical scanning system was built for non-destructive leather testing. The investigation was focused on two of the most important physical leather properties, static compressibility across thickness and tensile properties for low strain regions. The results of static compression energy measurements for a compressive strain of 10 percent, showed a close agreement with the results of tests performed by a conventional compressibility tester. Further, the results of strain energy and stress measurements for a strain of 2 percent, revealed a very good correlation with the results of conventional tensile tests for a similar strain.

The application of infrared thermography, a non destructive and contact less technique, to leather characterisation and inspection was investigated in this work. It was shown that this technique could be used for detecting defects in leather, as well as for estimating their size and deepness. However, defect visibility by infrared thermography is conditioned by the fact that a defective area has to cause different material properties or produce an internal thermal resistance. Further, the prohibitive cost of infrared thermography cameras for automation is a serious limitation for its application in current leather testing.

It is recommended that the ideal testing system would be based on the combination of mechanical scanning, normal computer vision and infrared thermography. The normal computer vision part of this system would be responsible for measuring area and detecting defects that are visible in nature. The infrared thermography part of the system would be responsible for detecting the type of defects overlooked by the previous method, as well as some thermo-physical parameters. Finally, the Mechanical Scanning System would provide the physical properties of leather, like compressibility, tensile modulus, shear stress and softness that the vision based inspection systems are incapable of providing. In this way, every single skin could be completely characterised in terms of defects and physical properties.

To my grandfather

Acknowledgements

I am especially grateful to my supervisor, Paul Taylor, for his encouragement and confidence throughout this project. His helpful comments and suggestions have contributed considerably to the improvement of this work.

Thanks also go to my fellow colleagues with whom I had the pleasure to work with during these years: Didier Pollet, Andrew Kaiser and Sharon Brady. Thanks to Jo Aspland for her continuous support.

Special thanks go to my wife, my father and Jaime Fonseca for their continuous encouragement, support and help throughout the very difficult period of writing up, as well as Didier for his friendship during my stay in Hull.

Furthermore, I gratefully acknowledge the staff and technicians of the Department of Electronic Engineering in particular Dave Joyce for their mechanical support, Dave Glover, Ernie Thompson, Eric Wright and Sandra Batch for their helpfulness during these years.

I also would like to thank Professor Xavier Maldague from University of Laval, Canada, for his help with infrared thermography and Professor Daryl Almond from Bath University for the utilization of the infrared thermography facilities of the Department of Materials Science.

Finally, I wish to thank Fundação para a Ciência e Tecnologia for its financial support through the Portugueses research program "Praxis XXI".

Table of Contents

List of Illustrations

List of Tables

1

1 Introduction

Leather is an expensive component of many products such as shoes, furniture, car seats, garments and bags. Because it is a natural material, it will inevitably contain visual and hidden flaws. Actually, the manufacture of leather involves visual and tactile inspection and manual sorting at key stages of production by skilled operatives. Accurate sorting is fundamental for assuring the best return on the available material and customer satisfaction. Any lack of consistency by graders or between graders can prove very costly.

The development of an automatic inspection system is certainly the right answer to reduce the subjectivity associated with visual perception and varying skill of human sorters. The adoption of such system would undoubtedly have many advantages, such as: an infinite attention span and ability for continuous operation for long periods without mental or visual fatigue and without grade decision deterioration; equal attention to all areas of a skin, a manual sorter may overlook a certain area if lighting conditions are not appropriate. On the other hand, some disadvantages could be foreseen, for example: lack of human grader common sense in the decision-making process; faults disregarded by the human grader that can be tolerated; the system will only see the leather under one set of lighting conditions, whereas the human operator can change his viewpoint in order to check a suspected area.

Ideally, any effective inspection system should be able to cope with defects that vary greatly in size, from small spots, e.g. light spot and pinhole, through narrow linear faults such as, scratches, to larger area faults like ringworm, mange and putrefaction. Such system should have the ability to take into account the location, size, and nature of faults and produce numerical grades similar to those used at present. Furthermore, it should be capable to work at least as fast as currently achieved by human sorters.

Leather inspection is usually defined as the procedure of detection, mapping and assessment of the severity of defects, while leather characterisation is concerned with the performance properties of leather. In the case of this thesis, leather characterisation is restricted to the procedure of measuring physical and thermophysical properties and their mapping across the full skin or hide.

If leather inspection is very important for leather manufacture and leather goods industry, leather characterisation is of no less importance. Leather characterisation gives an indication of the fitness of a particular leather for a particular application. For this reason, many standards have been devised for leather characterisation, for example: tensile strength, tear strength and softness. Some of these tests are more objective than others, but almost all of them have in common the fact that they require removal of samples from the official sampling position (close to the butt region), and are either destructive and/or incompatible with real time operation.

Despite the fact that these tests are well accepted in today's industry, these testing standards have a major flaw. Leather is a natural material whose properties vary across the full skin or hide, i.e., each region of the skin has its specific characteristics that can be made even less uniform by the tanning process. This means that testing a particular region of a skin or hide gives little information about the properties of the rest of the material, which in turn makes the results of these tests of limited use. Again, the solution to this problem passes through the development of an automatic characterisation system.

An automatic characterisation and inspection system could also contribute decisively for the automation of the process of leather layout and cutting, as for each skin, a map of physical properties and defects would be produced, so CAD/CAM tools could use this information to maximise utilised area and lay out the right patterns on the best position. As an example, in the shoemaking industry, certain pieces must be cut from certain parts of the skin and in certain orientations in order to make the product easy to manufacture, and comfortable to wear or use.

Several attempts have been made to build such systems, mainly based on normal computer vision. Although good results are reported, it was concluded that some defects are not visual in nature and they are not detectable by a visual system. This fact greatly supports the view of the author that an effective automatic system for characterisation

and inspection of leather cannot be achieved by a single method but by a combination of several methods. Even though visual inspection is definitely relevant, it cannot provide information about, for instance, the thickness and compressibility of the material. Perhaps, the ideal solution would be a combination of mechanical, normal computer vision and other non-destructive evaluation techniques.

Normal computer vision has been object of intensive research and for this reason it is not further explored in this work.

1.1 Objectives of the Research

The aim of the research described in this thesis was the design of a mechanical system for leather characterisation without the need of cutting samples from the skin or hide. This system has to be able to scan leather properties that typical visual inspection systems would find impossible to measure. Also, it is aim of this research to assess the feasibility of utilisation of infrared thermography for leather characterisation and real-time flaw detection.

1.1.1 Mechanical Scanning System

A mechanical scanning system was built for leather testing in a non-destructive manner (see Figure 1.1). This system is capable of performing tensile testing for low strain regions, compressibility testing across thickness, softness, thickness and shear testing across thickness.

This testing device comprises two pairs of wheels between which the leather passes. By adjusting the speeds of the wheels and by measuring the applied torque and positions of the wheels, leather tensile characteristics can be measured. The compressibility across thickness can be determined by closing the nip formed by a pair of wheels and measuring the instant compression load and compressive strain. The shear stress across thickness can be determined using a pair of wheels, by slightly compressing the leather and rotating the two wheels in opposite directions, while measuring the applied torque.

1.1.2 Infrared Thermography

The application of infrared thermography, a non-destructive and contact less technique, to leather characterisation and inspection was investigated in this work. A transient thermography set-up was used; a thermal stimulation is impinged on the leather surface and from the observation of the emitted thermal radiation subsurface defects can be

detected and their size determined. Figure 1.2 displays an infrared image, of a leather specimen with two small and not very severe real defects ("flay-cuts").

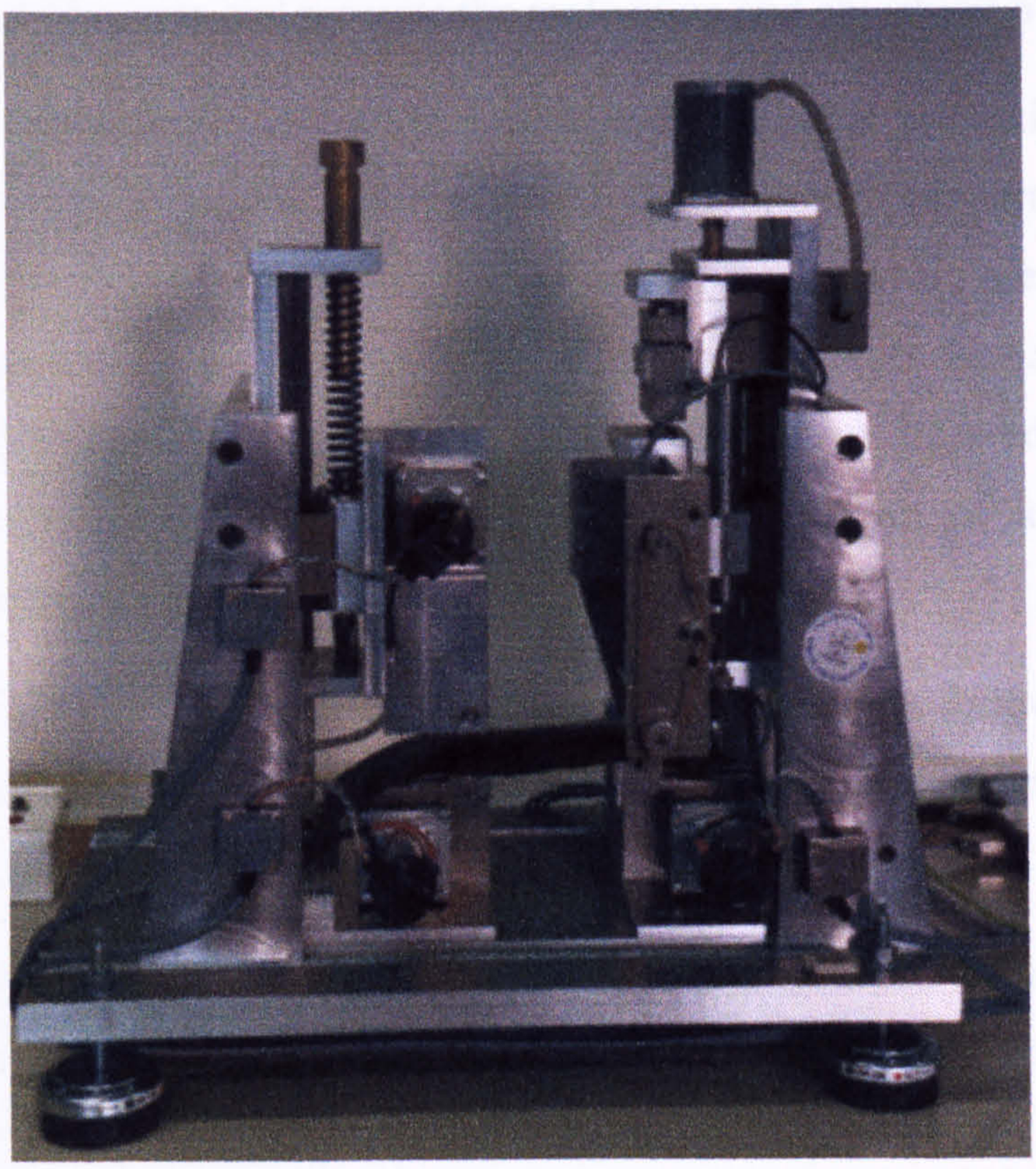

Figure 1.1-View of the Mechanical Scanning System.

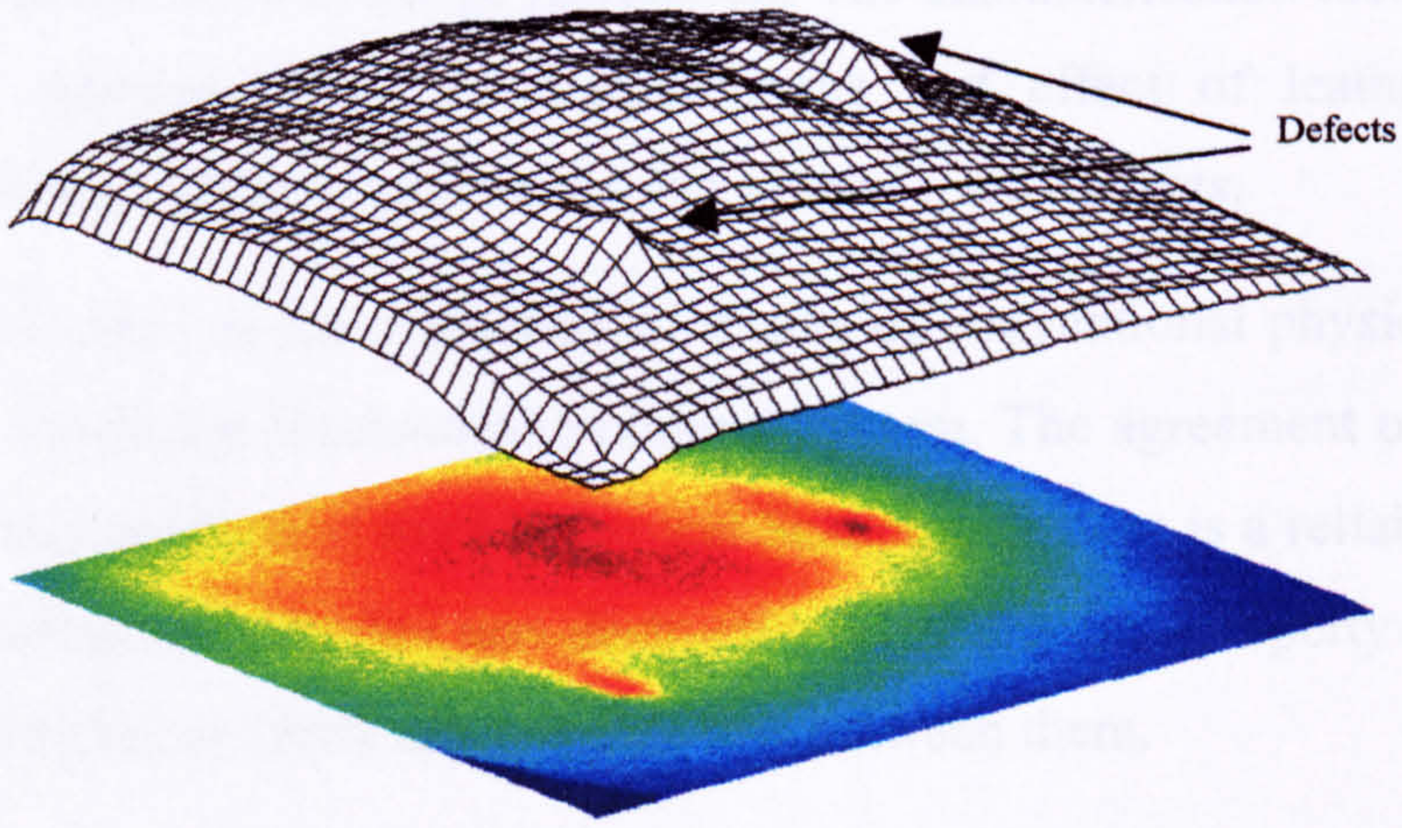

Figure 1.2-Infrared thermography image of a leather specimen with two small defects.

1.2 Organisation of the Thesis

This chapter introduces the subject of leather characterisation and inspection using non-destructive techniques and presents the motivation and objectives of this thesis.

Chapter 2 provides an overview of the most relevant physical properties of leather, as well as the structure of leather and the spatial distribution of properties over a hide. Most relevant conventional and current leather testing standards are presented, followed by an assessment of a range of non-destructive testing techniques that could be used for leather characterisation and inspection, with emphasis on infrared thermography. Finally, the author gives an overview of the state of the art of leather automatic inspections systems.

The following chapter, Chapter 3, introduces the procedure followed for sample selection and handling. The results of conventional physical tests of the specimens used in this work are also presented.

Chapter 4 concerns the philosophy, design and implementation of a non-destructive leather testing cell designated Mechanical Scanning System and the presentation of the results of experiments performed with this device.

Chapter 5 is concerned with leather inspection and characterization using infrared thermography. A description of the transient thermography system is given, followed by considerations about infrared image restoration. The characterisation results of infrared thermography, thermal diffusivity measurements and effect of leather anisotropy, precedes the divulgation of inspection results of man-made defects.

Chapter 6 is dedicated to the evaluation of results of conventional physical testing and results obtained with the Mechanical Scanning System. The agreement of the results is discussed in order to assess if the Mechanical Scanning System is a reliable and correct method of characterising leather non-destructively. A physical property and a thermal property are analysed to verify any possible link between them.

Finally, main conclusions are drawn and recommendations for future work are given.

2

2 Literature Survey

2.1 Introduction

This chapter provides reasonable background knowledge for the entire thesis and an overview of the state of the art of subjects here presented.

Firstly, an overview of the most relevant physical properties of leather for this work is given. The structure of leather is examined, as well as its density, tensile strength and elongation at break. The spatial distribution of properties over a hide, follows a brief study of compressibility of leather. The softness of leather and the viscoelastic behaviour of leather are focused on too.

Secondly, the most relevant conventional and current leather testing standards are referred to, pointing out some of its weaknesses.

Thirdly, an assessment of a range of non-destructive testing techniques that could be used for leather characterisation and inspection is carried out. A theoretical background of infrared thermography, a relatively new non-destructive technique, is presented as well as many aspects of its usage. A hypothesis of linking thermal properties, measured by infrared thermography in a non-destructive and contact less manner, with physical properties is put forward.

Finally, the author gives an overview of the state of the art on leather automatic inspection systems.

2.2 Physical Properties of Leather

A wide variety of animal hides and skins are used for leather making, for instance, cattle, sheep, goats, pigs, horses and kangaroos. Other species like reptiles, fish and birds are also used but of much less commercial importance. The term skin is usually

applied to smaller animals, while the term hide is applied to animals with a body surface area bigger than 1 m^2.

The hide or skin of each species has its own characteristic width, length, thickness, fibre structure and grain surface. The physical properties of leather depend upon these characteristics and many others. Variations from species to species, from one individual specimen to another, and even from one region to another within an animal's skin can also be observed. The structure of leather has a higher degree of complexity than that of any artificial material. Thus, the structure of leather will now be looked at in more detail.

2.2.1 Structure of Leather

Leather consists of an entangled three-dimensional network of collagen fibre bundles, which can be divided in two distinct layers: the grain (surface) layer and the corium layer (underneath). In the living animal, an epidermal layer covers the grain layer, but it is removed during the tanning process. All skin from mammalians is covered in hairs, which are also removed except for fur production.

The epidermal layer, usually called epidermis, protects the skin from abrasion. Keratin is the basic component of this layer. It consists of epidermal cells that are formed in the lower layer of the epidermis. As time goes by, the skin grows in thickness and the epidermal cells gradually change and dehydrate. Newer cells are continuously being formed below, while older cells are being pushed toward the surface and lost as horny flakes. In Figure 2.1, it is shown that the epidermal layer also covers the hair follicles that penetrate deep into the grain layer.

The layer just below the epidermis is the grain layer. It has a very important function in the living animal, which is known as the thermostatic layer. Its main composition is elastin fibres, fat cells, hair follicles, muscle tissue, sebaceous glands, and sweat glands. The grain layer consists of very fine, numerous and densely packed fibre bundles that are arranged more or less perpendicular to the plane of the skin. After tanning, this layer becomes the upper surface of the leather. Its full thickness is reached quite early with age, increasing only slightly in depth but very much in area.

In mammalian skins, the hair shafts within the grain layer produce a distinctive pattern. The size and configuration of these follicles is a characteristic of the animal and its age.

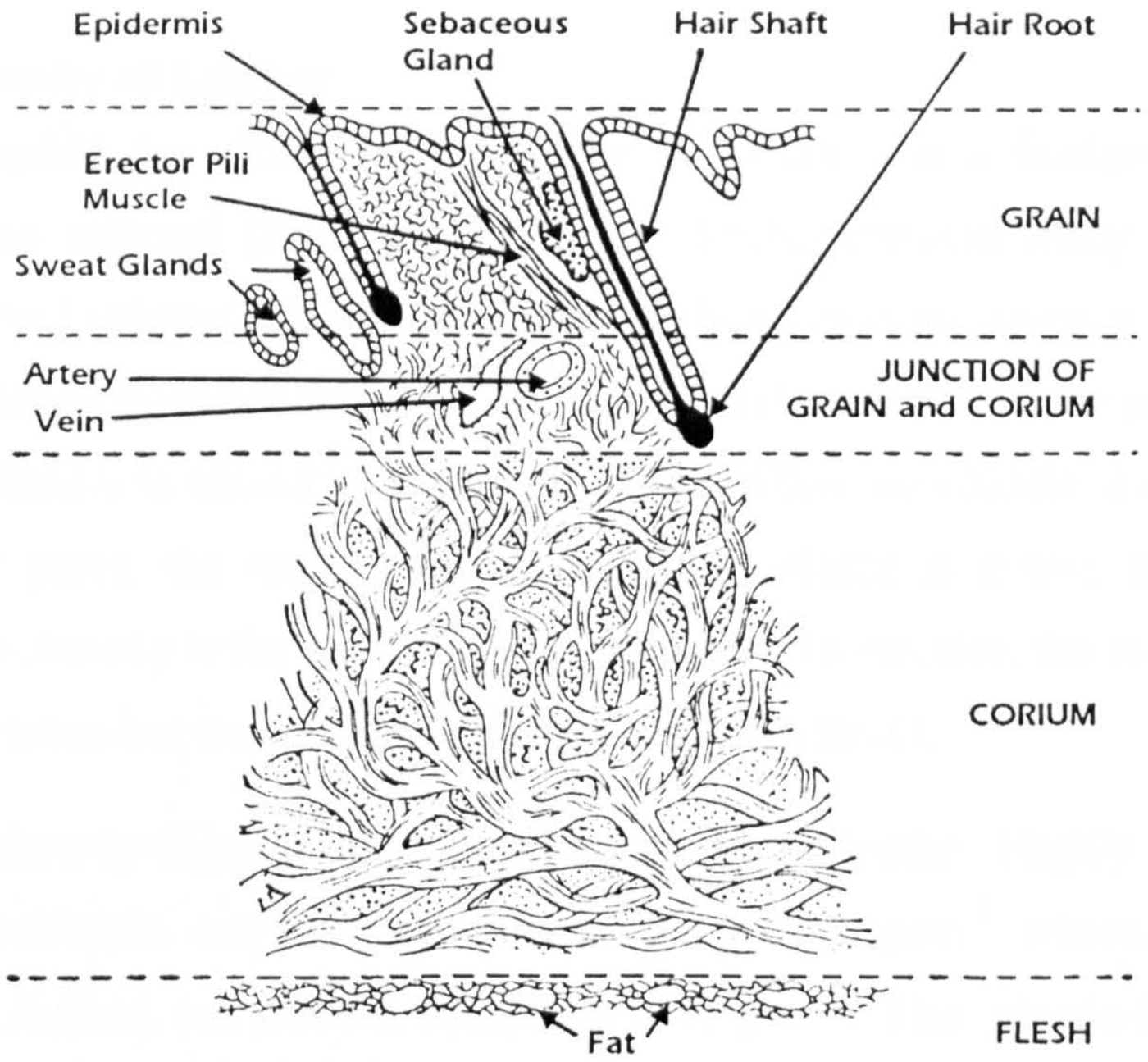

Figure 2.1-Typical structure of a mammalian skin [SATRA 92].

The corium layer, the part of the skin below the grain layer, comprises almost entirely large coarse fibre bundles of collagen fibres with a scattering of elastin fibres. The interweaving of the fibre bundles is done at varying angles but in a much less compact manner than in the grain layer. The thickness of this layer increases with age and is the source for the strength of the leather. Another relevant aspect for the material properties of leather is that, the corium layer thickness varies greatly from one region of a hide to another. On the other hand, the grain layer is fairly constant across the full hide. These facts partially explain the lack of homogeneity of leather.

The layer just below the corium layer, which should be removed before the tanning process, is known as the flesh layer. The presence of fatty and muscle tissue, blood vessels and nerves diminishes the penetration of tanning agents in the corium layer. The back surface of leather is also known as flesh. Here, the angle of weave of the fibre bundles decreases, lying in the plane of the skin.

The angle of weave and configuration of the fibre bundles in the distinct layers also changes smoothly from one location to another in an individual skin. The most compact fibre bundles, with the corium fibres interweaving at about 45° to the surface, can be

found on the animal's back and butt. Therefore, this region is likely to be firmest and tightest than the rest of the skin.

2.2.2 Density of Leather

Density of leather, the ratio of its mass by its volume, is a fundamental physical property of any material [Kanagy 65]. Because leather contains many different sized pores, the correct volume calculation of the fibre bundles is not an easy task. When the volume calculation does not take into consideration the volume of the pores, the value obtained for density is known as apparent density. When the volume is calculated with allowance for pores, the ratio of the mass to the volume is known as real density. Therefore, real density is the real density of the fibres. In practice, the real volume is of difficult calculation but the apparent volume is not as difficult.

The apparent density depends on the pore volume of the leather. Highly porous leather, for example buckskin, can have a density as low as 0.52 gcm^{-3}, whereas sole leather, highly dense leather, can have a density of 1.15 gcm^{-3}. This physical property also depends on the type of tanning, as the impregnation of tanning agents in the flesh side can increase the apparent density to about 1.17 gcm^{-3}, this being a value close to the maximum that can be obtained [Kanagy 65].

Another very important observation of Kanagy is that the apparent density is an indication of the substance of a hide; Kanagy showed that, within a hide, it could vary from 0.57 gcm^{-3} in the shoulder area to 0.66 gcm^{-3} in the butt area [Kanagy 55].

Different real density measurements produced density values in the range of 1.38 gcm^{-3} to 1.55 gcm^{-3}. Other researchers showed that real density of the grain layer is higher than the rest [Randall 52].

Wang, in her study "Characteristics of Brazilian Goat and Sheep Skin and Leather" of physical properties of leather, carried out several different physical measurements, such as: apparent density, tensile strength, tear strength, softness and compression. With the available data, Wang performed several plots of these properties against other parameters, like: apparent density vs. age of the animal, apparent density vs. collagen content, apparent density vs. compactness of skin, tensile strength vs. apparent density, tear strength vs. apparent density, compressive strain vs. apparent density. Wang reported that the density of leather was highly correlated with the tensile strength of

leather and a good correlation between tear strength and density was also obtained [Wang 92].

2.2.3 Tensile Strength and Elongation at Break

Strength certainly is one of the most important properties of leather. The tensile strength test is used in leather evaluation as strength gives a good indication of fibre quality. Low tensile strength may be a sign of poor fibre quality or may even indicate degradation. The tensile strength and elongation at break are closely dependent on the width of the specimens to test, and both are higher for wider samples [Roddy 56]. Damage to the fibre structure near the edge of narrow specimens, when they are cut, is the most likely explanation for those lower values of tensile strength and elongation at break.

When a tensile load is applied to a specimen, the woven fibre matrix of the hide gets aligned in the same direction. The application of a tensile load to a specimen causes its elongation and consequent narrowing; the fibres initially oriented in the direction of the load get closer to each other, making the cross section narrowing inversely proportional to the number of fibres oriented in that direction [Mitton 45, Mitton 48].

In the case of the shoe upper leather, its tensile strength can be increased by the presence of grease and moisture [Roddy 56]. The extension rate also influences the observed elongation and strength [Maeser 65]. The grease and moisture influence is believed to take place due to a lubricating action in which fibres are allowed to slide against each other without rupturing. A gradual application of the load permits the rearrangement of the fibres, whilst a rapid application of the load prevents this rearrangement and, consequently, rupture takes place earlier.

Kanagy performed tensile tests on upper leather in two directions [Kanagy 55], parallel and perpendicular to the backbone over the entire area of a skin. The results show that the product of the tensile strength and elongation in one of these directions is equal to the product of the tensile strength and elongation in the direction at right angles. This indicates proportionality between strength and elongation and that a high strength usually indicates low failure strains, whereas low strength indicates high failure strains. Most of the stretching observed in tensile tests is caused by the rearrangement of the fibres network rather than fibres elongation [Mitton 45]. The elongation of a fibre alone at failure is about 15%. Therefore, the amount of narrowing of the test specimens in the

transverse direction of the test is inversely proportional to the number of fibres that support the load.

The tensile strength of upper leather is in the range 15 MPa to 40 MPa. The elongation for shoe upper leather lies in the range 29.5% to 73.0% but that for sole leather lies in the 10.0% to 30.0% range [Bailey 89].

Measurements of the initial strain energy of leather conducted by Liu showed that a prediction of the tensile strength might become feasible without breaking the leather. A statistical model was established for the relationships among tensile strength, initial strain energy, strain rate and moisture content, allowing its application in Non-Destructive Evaluation of partially processed leather before fat-liquoring and staking. Liu concluded that by simply stretching the leather to 10% and measuring the initial strain energy at any sampling angle, tensile strength can be predicted without breaking the leather [Liu 97].

2.2.4 Compressibility

Compressibility (across thickness of the material) is a physical property that is mostly used for characterising sole leather, because it is closely related to hardness or firmness.

However, in the textile area, compressibility is regarded as a basic mechanical property closely related to fabric handle [Kawabata 80]. A fabric that compresses easily is likely to be deemed soft, and found to possess a low compression modulus and high compression.

Lokanadam and collaborators confirmed that compressibility reflects the softness of soft leather. This research group compressed leather between two flat surfaces across its thickness with an increasing load while the changing distance between surfaces was recorded. The logarithmic plot of the thickness against the load showed that higher negative slopes were associated with leather considered to be softer [Lokanadam 89].

Additionally, Wang reported a good correlation between compressive strain at 200 N load with the softness obtained by hand evaluation. Also, a negative correlation coefficient (-0.91) was found for the correlation of compressive strain with apparent density [Wang 92a].

Smith also performed some compressibility tests in order to predict the drift of a piece of leather when compressed between moving rollers [Smith 91]. Smith obtained compression curves that are divided in four regions as shown in Figure 2.2.

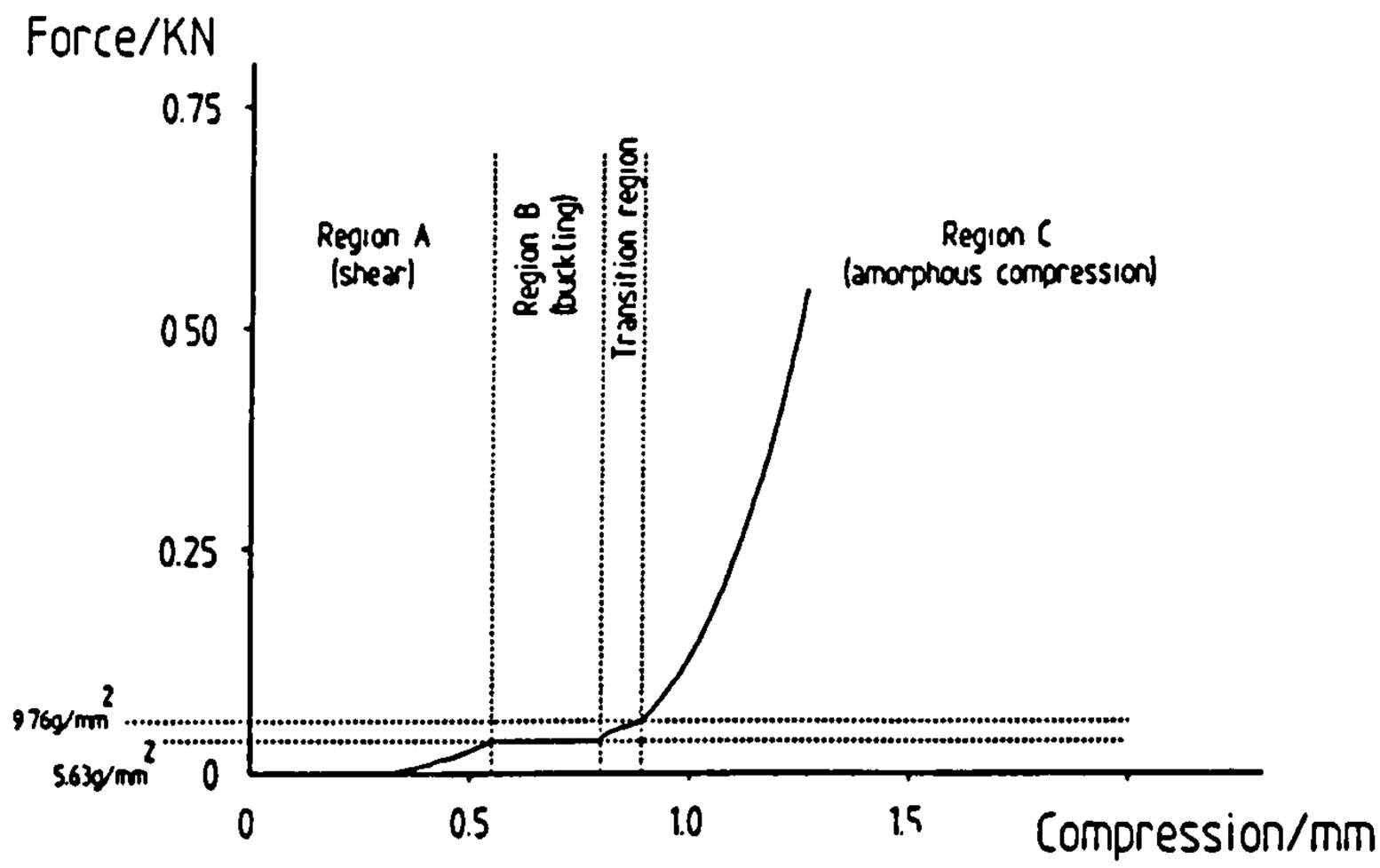

Figure 2.2-Compression curve by Smith [Smith 91].

However, the author was not able to reproduce such results and Lokanadam never reported similar findings.

2.2.5 Splitting and Failure of Leather

The strength of leather is not uniform right through its thickness. Most cattle hides are split in to two or even three layers.

The grain layer is weaker than the corium layer. In the grain layer, thinner fibre bundles and a more compact structure are responsible for less room for fibre reorientation when under stress. Consequently, failure under stress occurs earlier for the grain than for the corium layer that is characterised by a much looser fibre structure. The majority of the strength is in the corium layer and the overall strength is dependent upon the thickness of this layer. When a hide is split there is a loss in strength, the sum of the strength of the splits is always lower than the strength of the unsplit [Maeser 54].

O'Leary studied thoroughly the differences in strength between the grain and corium layers of bovine leather, concluding that the greater resistance of the corium layer is due to the process of fibre debonding and pull out. The viscoelastic nature of the grain and

corium material was also investigated by examining its tensile properties at different deformation rates [O'Leary 96].

2.2.6 Spatial Distribution of Properties

Vos performed a study on the topographic differences in physical properties of different kinds of leather, concluding that the curves of 'similar' individual skins may differ considerably from the average curves [Vos 73]. This same view is corroborated by other research teams [Muthiah 76] [Boccone 77].

The butt area of a leather side tends to be the firmest and tightest with a fine break. These properties drop across shoulder areas and the belly and neck areas are much looser with a coarser break. In Figure 2.3, typical lines of tightness in a cattle hide are presented.

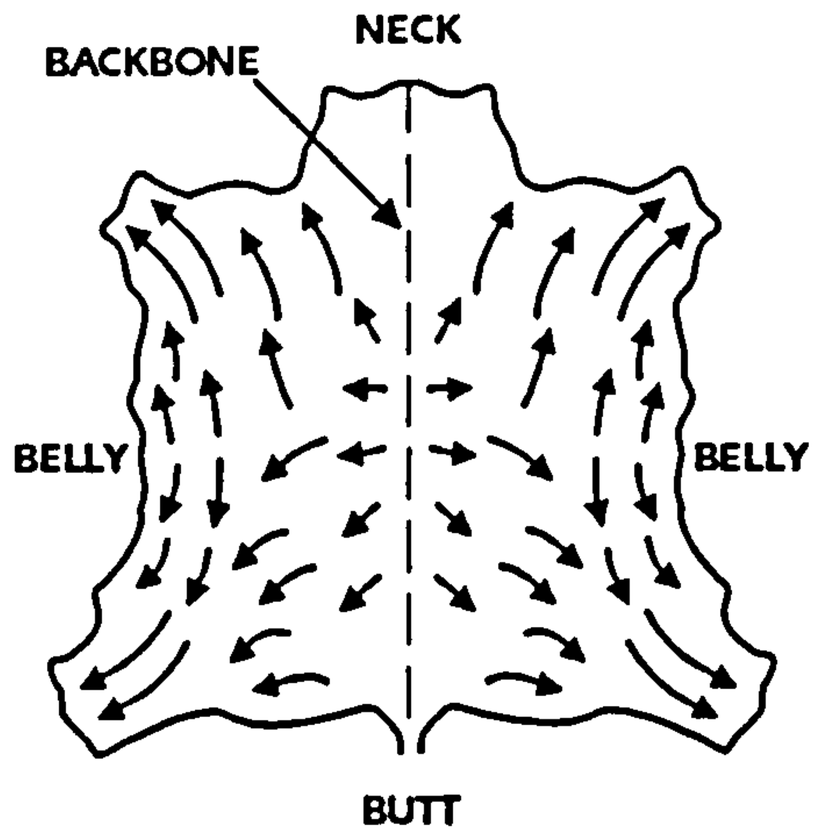

Figure 2.3-Typical lines of tightness of a cattle hide [Satra 92].

The spatial distribution of leather properties across a full hide has its obvious implications on leather utilisation, in shoe manufacturing in particular. Whole or part vamp patterns of shoes must be cut from higher quality butt areas. The less visible parts of shoes, for instance quarters and tongues, may be cut from the lower quality shoulder and belly regions. A vamp of a shoe should be cut in a way that the toe-heel direction should be the least stretchy, i.e., cut in the backbone direction. However, this characteristic follows complex patterns and the positioning of vamps should be adapted to the particularity of each skin [Satra 92].

2.2.7 Softness of Leather

Softness is a very important property of leather, in particular in the shoemaking industry. However, this is a subjective property of leather and commonly different operators cannot agree on a value of softness for a given sample. Leather is a tactile material and softness clearly depends on the way it feels.

Softness is not an absolute parameter, in contrast with for instance tensile strength. It also depends among other elements on fullness, tightness, compressibility, thickness, flexibility and elasticity. Thus, the overall perception of softness is influenced by other factors, being tightness/looseness one of the most important.

Presently, a device developed by BLC (BLC ST300 Softness Gauge) is being used for quality control. This device measures softness non-destructively and measurements correlate well with manual judgements [Alexander 93].

2.2.8 Behaviour of leather

The extension of leather short of rupture levels and later release causes deformation of the said material. The leather does not recover its original length but remains partially extended. This deformation is due to the plastic behaviour of leather, which is quantified as percentage set. This characteristic is of particular importance in the shoe making industry as it is responsible for the shape retaining properties of leather, making the shape and fitting of shoes not dependent only on the shape of the last.

Butlin investigated the plasticity and related properties of shoe upper leather [Butlin 63]. The samples were left in a stretched condition for a required time. Upon release, the shoe upper leather sample contracted and the amount of contraction was measured after a given time (usually 24 hours). The experimental results showed that the percentage set can be augmented either by increasing strain or increasing time under strain.

The plasticity of leather can also be improved by increasing the moisture content of leather. In the shoe construction process, the upper leather is heated before stretching as this operation further contributes for better plasticity. When moisturised or heated, leather becomes softer and more flexible.

The percentage set of leather decreases with the increasing time of relaxation. The reorientation of individual fibre bundles within the three-dimensional fibre structure in

order to relieve the strain developed amongst them, is the most plausible explanation for the referred behaviour. This behaviour confirms that leather is also a viscoelastic material.

2.3 Conventional Testing of Leather

Currently, there are several well-established official testing standards, for instance: ASTM-American Society for Testing and Materials; ISO-International Standard Organisation; BS-British Standard. Some institutions, like SATRA-Footwear Technology Centre, also have their own testing methods and, in this case, they are oriented towards the shoemaking industry.

The conventional testing of leather, in particular for the shoe making industry, comprises three categories of methods, adhesion methods, chemical methods and physical methods.

Despite the fact that these tests are well accepted in industry, these physical methods give little information on properties like handle or feel properties of light leather, which are of up most importance for the shoemaking, garment and automotive industry. Further, because most tests are in their nature destructive and performed only on a specific portion of a skin, the results of these tests are of limited use.

The standards here briefly described belong to the American Society for Testing and Materials (ASTM) because they were of easier access. In this thesis, only physical methods will be looked at and the first step for conventional leather testing, either physical or chemical, is the gathering of test specimens.

2.3.1 Specimen Selection

The leather test specimen for physical tests must be free from visual defects, such as scratches, cuts and other obvious flaws.

The ASTM standard D 2813-91, "Sampling Leather for Physical and Chemical Test", covers the sampling of finished leather and fabricated leather for physical and chemical tests. The leather is supposed to be in lots that are randomly sampled in such a way to yield a representative sample of the lot. The sample may be used to find out compliance of the lot with applicable specification requirements, leading to the acceptance or rejection of the lot in its entirety.

In this standard, a considerable variability of physical and chemical properties (depending on location on the side, side or skin from which the test sample is taken) is recognised. Because leather is a natural product, it is subject of extensive variability of its properties.

For lots of less than 15 units (sides or skins) each unit should be sampled. In case of cattle hides, the sampling in most instances should be done on the butt region, close to the backbone (one of the best quality areas), cutting a test piece of 203 mm by 203 mm.

From this short description of the ASTM leather sampling procedure, a strong contradiction is evident: on one hand, leather properties are subject to extensive variability even on the same skin; on the other hand, this sampling is trying to obtain a representative sample of a lot of skins. These two arguments are logically incompatible. A conclusion that can be drawn is that all this testing is much more important to fulfil the quality certificate hunger of buying companies than of any practical use in a production process. In addition to this, many tests to be performed on these cuttings are completely destructive.

2.3.2 Testing Methods

The ASTM standards for leather testing specify unambiguously the exact procedure for a vast list of tests. Here, a short description of the most relevant leather physical tests for is presented.

The ASTM standard D 1610-91, "Conditioning Leather and Leather Products for Testing", specifies the conditions of all units and specimens of leather prior to testing and during testing. Temperature and principally humidity have an immense influence on many physical properties of leather. Standardised environmental conditions contribute for equal moisture values of all tested samples, thus allowing reliable comparisons among different leathers and laboratories. This standard defines the standard temperature as 23 ± 2°C and the standard humidity as 50 ± 4%. Specimens should be stored under these conditions until they reach mass equilibrium, which usually requires up to 24 to 75 hours, depending on the leather and its thickness.

Other standards define different values for atmospheric conditions, for instance, standard temperature as 21 ± 2°C and the standard humidity as 65 ± 2%.

A standard for measuring apparent density of leather is also defined, ASTM standard D 2346-91. This test method determines the apparent density of specimens from their area and thickness, which in turn are obtained by applying test methods, respectively D 2347-91 and D 1813-89. For the computation of the apparent density, the weight of the specimen to the nearest 0.001 gram is divided by the product of the area and thickness.

The ASTM standard D 2209-90, "Tensile Strength of Leather", covers the determination of the load required to break apart a leather test specimen of certain dimensions, being the tensile strength obtained by dividing the rupture load by the original unstretched cross-sectional area. In the "Significance and Use" section of the standard, the tensile strength is referred as being a reliable indicator of the quality of the leather, as well as being an excellent method, among other things, for control, specification acceptance and service evaluation of leather.

The stretching of the leather should be performed at a uniform speed of 4.2 ± 0.8 mms^{-1}, in strict observation of a list of other conditions. The leather specimen for this test must be dumbbell in shape, cut by means of a die and in the direction of the long dimension in relation to the backbone noted.

The determination of the elongation of the stretched leather in the tensile strength tests is well defined in the ASTM standard D 2211-89.

2.4 Non-Destructive Techniques

Non-Destructive Evaluation (NDE) or Non-Destructive Testing (NDT) is a procedure that comprises the inspection and/or testing of any material, component or assembly in a manner, which does not affect its current or future use. At present, there are several well-established NDE methods covering many different fields, such as: material analysis, operation and maintenance of structures and buildings, maintenance of electric utilities, inspection of nuclear power plants.

The most important and widely used methods are radiographic, ultrasonic, magnetic, electrical and penetrant, but all can be subdivided. In addition to these, there are other emerging techniques like infrared thermography.

2.4.1 Industrial Radiography Technique

Industrial Radiography is a technique that includes a number of methods of using energy radiation for the examination of opaque objects. The beam energy can be generated electrically (e.g. X-rays between 70kV to 250kV) or radioactive isotopes may be used to produce gamma rays and nuclear reactors to produce neutron radiation. A shadowgraph on a photographic film or fluorescent screen is the typical output of such a system that records the variations of density and thickness. This property makes this technique useful for detecting porosity, cracks parallel to the radiation, thinning and inclusions. The main advantages of this technique are the ability to detect internal defects and that it can be used for a vast range of materials. However, this is an expensive technique and very demanding from a safety point of view because of the radiation hazard. It is also a technique that is not compatible with real time operation and of difficult application to complex geometries. A further disadvantage is that access to both sides of the component being inspected is mandatory [Halmshaw 91].

2.4.2 Ultrasound Technique

Another main technique is based on the emission of ultrasound waves, using a piezoelectric transducer (usually a short pulse frequency of 500 kHz to 10 MHz), in a narrow beam into a specimen and to detect any echoes returning from a defect with the same or another transducer. The echoes are usually displayed on a flaw detector, which displays a waveform using a time base that starts with the emitted pulse and is calibrated horizontally in terms of distance within the specimen. Most times, having a coupling agent, like gel, between transducer and specimen is mandatory. Water immersion is another example of a good coupling technique.

Many industries prefer to use an ultrasound controlled scanning technique called C-Scan. It displays the size and position of a defect in the plane of the surface of the component, as well as, an indication of the defect depth using different shades of grey or colours. Essentially, the C-Scan technique makes use of a grid system to manage the position of the transducer and to associate the correspondent output from the flaw detector. The position of the transducer is controlled by a two-dimensional positioning system allowing the full coverage of the surface of the component.

The ultrasound technique has several advantages worth mentioning: its great penetration power enables examination and measurement of materials of considerable thickness;

access to one surface of the component is sufficient; its high sensitivity and fast response; it is harmless in contrast with industrial radiography; it is sensitive to planar defects; as it is an electronics based operation suits automated inspection applications. On the other hand, there are also several disadvantages: it requires experienced operatives; it requires a couplant as a medium for wave propagation; it is insensitive to defects very near the surface; it is time consuming if large areas are to be scanned; it is very difficult to apply to coarse grain materials and rough surfaces due to ultrasound wave attenuation. Because leather structure contains many small air pockets, ultrasound waves are highly attenuated, therefore low frequencies must be used if any results are to be obtained.

Kronick performed acoustic emission studies on leather during deformation, concluding that by observing the increase in energy and frequency of acoustic pulses, it is possible to predict leather failure well before it tears [Kronick 92]. It was also observed that breakage of adhesions and fibres occurred earlier in corium than in grain.

2.4.3 Eddy Current Technique

The eddy current technique is based on the placement of an inductive coil with an alternating current close to the component to examine. A circulating eddy current is generated in the sample very near the surface. This current, flowing in the component, creates an electromagnetic field that is affected by the presence of a defect. The electromagnetic field is measured using a sensing coil.

The main advantages of this technique are the following: it is very fast; plenty of information can be obtained, such as, amplitude and phase information of probe impedance; as it is a non-contact method, can be carried out remotely. The most relevant drawbacks are: its difficulty to penetrate deep into thick material because of the electromagnetic field attenuation below the surface; no defect shape information is obtained; it is only applicable to materials with significant electrical conductivity. This last disadvantage clearly rules out the application of this method for defect detection in leather [Halmshaw 91].

2.4.4 Infrared Thermography

Infrared thermography is a relatively new approach to non-destructive testing that uses invisible thermal radiation to detect changes in material properties. From the invisible thermal radiation, an image of the heat distribution over the surface of an object is

obtained. Heat flow in a material with variations of its properties, causes variations on the emitted infrared radiation.

2.5 NDT by Infrared Thermography

The development of detectors of infrared radiation, associated theory and electronics allowed non-contact temperature measurement by quantifying the infrared radiation. Recent advances in infrared technology, specifically development of high-density imaging sensors have opened a new level of applications unreachable prior to the availability of this technology. Since then, many applications of infrared technology have been conceived, such as: buildings and structures operation and maintenance, printed circuit boards evaluation, nuclear power industry, real-time welding quality control, military applications, aerospace industry, medical applications and material analysis and non-destructive testing. This last field, material analysis and non-destructive testing, is the most interesting for leather characterisation and inspection.

Materials analysis supposes excitation of an object, recording the object's response and then extracting information about its physical properties, in particular its thermal properties when infrared technology is used. Material defects can be regarded as smooth or sharp variations in the physical properties of sound material. Thus, "material analysis" is widely accepted as complete characterization of an object, while "non-destructive testing" concerns mapping of the spatial distribution of physical properties inside a sample. In general, defects can be regarded as a deviation from an accepted standard.

All NDT techniques have their own strengths and weaknesses. Infrared thermography has the following advantages: high inspection rate; no contact is needed and access to only one side of the material is required; no harmful radiation is involved, there are no personnel safety concerns; the results are presented in form of an image and easily interpretable; wide span of applications. On the other hand, there are several difficulties affecting this technique: difficulty in achieving a quick, uniform and highly energetic thermal stimulation over a large area; effects of thermal losses (convective, radiative) that affect the reliability of interpretation; very costly equipment (infrared camera and thermal stimulation units); capability to detect only defects that cause measurable change of thermal properties; ability to inspect only a limited thickness of material under the surface; emissivity problems. These last two disadvantages are not relevant

for leather inspection as leather is a relatively thin material and possesses high infrared emissivity [Maldague 94].

For a better understanding of the basics of infrared thermography a brief introduction to its most relevant aspects is presented below.

2.5.1 Principles of Infrared Radiation

Sir William Herschel, in 1800, discovered by accident the presence of thermal radiation outside the spectrum of visible light. He verified that beyond the red part of the spectrum of visible light there was an invisible radiation. The energy of this radiation was able to produce a maximum elevation of temperature of a mercury thermometer when compared with all the bands of the spectrum of visible light. This radiation was named *infrared* and it is just a continuation of the well-known spectrum of visible light [Hudson 69].

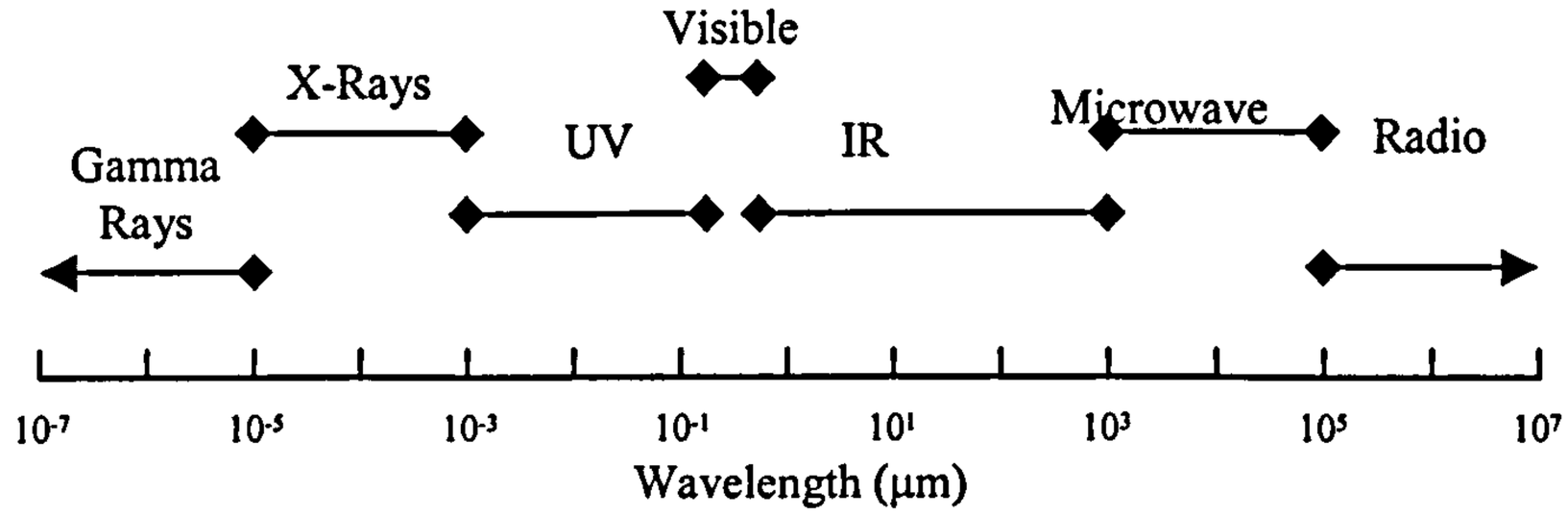

Figure 2.4-The electromagnetic spectrum.

The infrared radiation obeys exactly to the same laws as any electromagnetic wave. Infrared radiation is characterised by longer wavelengths than the visible spectrum, between 0.75 μm and 1000 μm (see Figure 2.4). The range 0.75 μm to 1.5 μm is known by *near infrared*, the range 1.5 μm to 20 μm is known by *middle infrared* and the range 20 μm to 1000 μm is known by *far infrared*.

The *middle infrared*, also known as thermal infrared, is the radiation range most important for infrared thermography. As an example, infrared cameras have typically two radiation working regions, 3 μm to 5 μm and 8 μm to 12 μm.

Electromagnetic radiation is continuously emitted and absorbed by matter. The emission process involves molecular excitations within the material, which generate radiative transitions in its constituent particles. An augment in temperature causes an increase in

molecular excitation in the material, which in turn is beneficial to the generation of radiation.

Thermal emission by solids is typically presented in terms of the concept of a blackbody. A *blackbody* is defined as an object which absorbs all radiation that impinges upon it at any wavelength. A blackbody capable of absorbing all radiation at any wavelength is equally capable in the emission of radiation.

Three fundamental laws were postulated to describe the behaviour of a blackbody: Planck's law, Wien's displacement law and Stefan-Boltzmann law.

Planck's Law

Max Planck was able to describe the spectral distribution of the radiation from a blackbody by means of the following formula:

$$W_{\lambda b} = \frac{2\pi \cdot h \cdot c^2}{\lambda^5 \cdot \left[e^{\frac{h \cdot c}{\lambda \cdot k \cdot T}} - 1 \right]} \qquad (2.1)$$

where $W_{\lambda b}$ is the blackbody spectral radiant emittance within a spectral interval 1 μm wide at wavelength λ, c is the velocity of light, h is Planck's constant, k is Boltzmann constant, T is the absolute temperature. The significance of the 1 μm wide spectral interval in the value of $W_{\lambda b}$ is that the instrument used for measuring spectral emittance characteristics must use a narrow band of radiation in order to register a reading. Thus, a value of spectral radiant emittance is meaningless unless the spectral interval is also specified.

For any temperature, the spectral emittance is zero at $\lambda = 0$, then increases rapidly to a maximum at a wavelength λ_{max} and after passing it decays to zero again at very long wavelengths. The higher the temperature, the shorter the wavelength at which the maximum occurs.

Wien's Displacement Law

Differentiating Planck's formula with respect to λ, and finding the maximum, Wien's displacement law is obtained and is given by the following formula:

$$\lambda_{max} = \frac{2898}{T} \qquad (2.2)$$

This formula expresses mathematically the common observation that colours vary from red to orange or yellow as the temperature of a thermal radiator increases. The wavelength of the colour is the same as the wavelength calculated for λ_{max}. For instance, a very hot star such as Sirius (11000°K), emitting bluish-white light, radiates with the peak of spectral radiant emittance occurring within the invisible ultraviolet spectrum, at wavelength 0.27 μm. The sun (approximately 6000°K) emits yellow light, peaking at about 0.5 μm in the middle of the visible light spectrum. At room temperature (300°K) the peak of radiant emittance lies at 9.7 μm, in the middle infrared; while at the temperature of liquid nitrogen (77°K) the maximum of the almost insignificant amount of radiant emittance occurs at 38 μm, in the far infrared [Casado 95].

Stefan-Boltzmann Law

Integrating Planck's formula from $\lambda = 0$ to $\lambda = \infty$, the total radiant emittance W_b of a blackbody is obtained and given by the following formula:

$$W_b = \sigma \cdot T^4 \tag{2.3}$$

where σ is the Stefan-Boltzman constant. The Stefan-Boltzman law states that the total emissive power of a blackbody is proportional to the fourth power of its absolute temperature. Graphically, W_b represents the area under the Planck curve for a particular temperature. It can be shown that the radiant emittance in the interval $\lambda = 0$ to $\lambda = \lambda_{max}$, is only 25 percent of the total, which represents about the amount of the sun's radiation which lies inside the visible light spectrum.

The previous concepts can only be applied to blackbodies. Real objects almost never comply with these laws over an extended wavelength region, although they may approach the blackbody behaviour in certain spectral intervals.

There are three processes that prevent a real object of acting like a blackbody: a fraction of the incident radiation α (spectral absorbance) may be absorbed, a fraction ς (spectral reflectance) may be reflected and a fraction τ (spectral transmittance) may be transmitted. Moreover, these factors are more or less wavelength dependent. However, for any wavelength the three fractions must always add up to the whole, so the following relation is achieved.

$$\sigma + \varsigma + \tau = 1 \tag{2.4}$$

Another important factor, ε emissivity, is required to describe the fraction of the radiant emittance of a blackbody produced by an object at a specific temperature. Spectral emissivity is also wavelength dependent and is the ratio of the spectral radiant power from an object to that from a blackbody at the same temperature and wavelength.

Usually, there are three types of radiation source, distinguished by the ways in which the spectral emittance of each varies with wavelength: a blackbody $\varepsilon = 1$ for all wavelengths; a graybody ε = constant (less than 1) for all wavelengths; and a selective radiator where ε varies with wavelength.

Emissivity has its implications in Stefan-Boltzmann law, which is shown in the following formula.

$$W_b = \varepsilon \cdot \sigma \cdot T^4 \tag{2.5}$$

From this formula, it can be stated that the total emissive power of a graybody is the same as a blackbody at the same temperature reduced in proportion to the value of emissivity for the graybody.

2.5.2 Thermal Stimulation

In terms of experimental set-up configurations of infrared thermography, two methods can be used: the active and passive approach. In the passive approach, an image of the object to test is obtained while no external thermal perturbation is applied. In the active approach, externally applied thermal stimulation is required to generate meaningful contrasts which will lead to abnormality detection. Without such extraneous applied thermal perturbation, no information can be obtained from the inspection since the surface temperature distribution is not related to the subsurface structure [Maldague 93].

For leather characterisation and inspection the active approach is certainly the most interesting. Regarding the thermal stimulation of materials a vast number of modes have been proposed and an overview of the most interesting for practical infrared thermography, such as, Pulse Thermography, Step Heating and Lock-in Thermography is given in this thesis.

Pulse Thermography

In Pulse Thermography, also known as Transient Thermography, a thermal pulse is applied to the material to be inspected. Following this input of thermal energy, a

measurement of the temporal evolution of the surface temperature of the specimen is carried out with an infrared camera allowing subsurface flaws to be exposed, in the following manner. The temperature of the specimen changes rapidly after the initial thermal perturbation as the thermal front propagates, by diffusion, under the surface. The presence of defects affects the diffusion rate, thus when observing the surface temperature, defects show up as zones of different temperatures with respect to neighbouring sound zones once the thermal front has reached them. As a consequence, deeper defects will be observed later and with reduced contrast. In reality, the observation time t is a function (in a first approximation) of the square of the depth z [Cielo 87] and the loss of contrast c is proportional to the cube of the depth [Allport 88].

$$t \approx \frac{z^2}{\delta} \qquad and \qquad c \approx \frac{1}{z^3} \tag{2.6}$$

where δ is the thermal diffusivity of the material. An empirical rule of thumb by Vavilov [Vavilov 82] says that:

> *"the radius of the smallest detectable defect should be at least one to two times larger than its depth under the surface"*

This empirical rule is applicable to isotropic materials, however in case of anisotropic materials it is more constrained.

The thermal energy impingement on the sample can be performed in several ways, particularly for point, line and surface inspection. In the case of point inspection, a laser or a focused light beam is used for that purpose with good repeatable heating and uniformity; on the other hand there is a need to move the inspection head or the material to cover a surface slowing down the process. Line inspection using line infrared lamps allows faster inspection rate and good uniformity due to the lateral motion of the scanning head or material. Surface inspection uses lamps and complete analysis of covered area is possible, however the non-uniformity of the heating creates additional problems.

Sometimes, the temperature of the part to inspect is already higher than the ambient temperature due to, for instance, the manufacturing process; it may be more advantageous to use a cold thermal source. The propagation of the thermal front is not dependent on the type of source (cold or hot), what is important is the temperature

differential between thermal source and the material being inspected. Another aspect that must be realized is that the stimulation source must stay non-destructive, neither causing any chemical or physical damage to the specimen being inspected.

The observation of the response to the application of a thermal perturbation can be achieved by two modes: reflection mode, both the thermal source and the detector unit are located on the same side of the specimen being tested; transmission mode, where the thermal source and the detector unit are located on opposite sides of the specimen being tested.

The reflection mode offers better resolution but for a smaller maximum thickness. In the transmission mode a greater thickness can be inspected but the depth information is lost [Sayers 84]. Further, observation in transmission mode is not always feasible especially for more complex structures. In general, the reflection approach is best used for detection of flaws close to the heated surface, while the transmission mode is best suited for detecting defects closer to the rear surface.

Step Heating

For another thermal stimulating scheme, step heating (long pulse), the interesting feature is the increase of the surface temperature during the application of a step heating pulse. Similarly to the previous thermal stimulating mode, changes of surface temperature are closely related to specimen features. This technique has many applications for example for coating thickness evaluation and integrity of the bond of coating-substrate [Spicer 91].

Lock-in Thermography

Lock-in Thermography is a thermal stimulating mode based on thermal waves generated inside the specimen under scrutiny [Busse 92]. This concept is well know in electrical circuits analysis field, for which the stationary regime response to a sinusoidal input signal is also a sinusoidal signal with specific amplitude and phase, if the system is linear. If a sinusoidal thermal stimulation is applied to a specimen, a highly attenuated and dispersive wave is found inside the material (in a near surface region). This wave is designated as a "thermal wave". The most interesting part is that these waves can be created and detected remotely. The stimulation with a sinusoidal deposition of heat on the surface specimen and the recording of the thermal infrared emission is known as lock-in thermography. The outcome of lock-in thermography is rather different than

from pulse thermography, here the interesting data is the amplitude and phase images; specially the phase image which is related to the propagation time and is independent of the optical surface properties of the specimen.

2.5.3 Thermal Image Degradation

Infrared image degradation can occur in three forms, radiometric distortion, geometric distortion and noise.

Radiometric distortion is caused by the non-linear response of the system to the full input range of radiation. For instance, a thick high thermal conductivity material (copper) is heated to a temperature higher than the ambient temperature. The infrared image from this heated plate is recorded. In most cases this image will not be uniform; and more surprisingly the non-uniformity will depend on the plate temperature. This example shows that some radiometric corrections might be necessary especially for performing quantitative measurements.

Spatial geometric distortion is caused by the intrinsic fuzziness of thermal images caused by lateral propagation of heat. Other geometric distortions like vertical to horizontal ratio distortion may also affect systems.

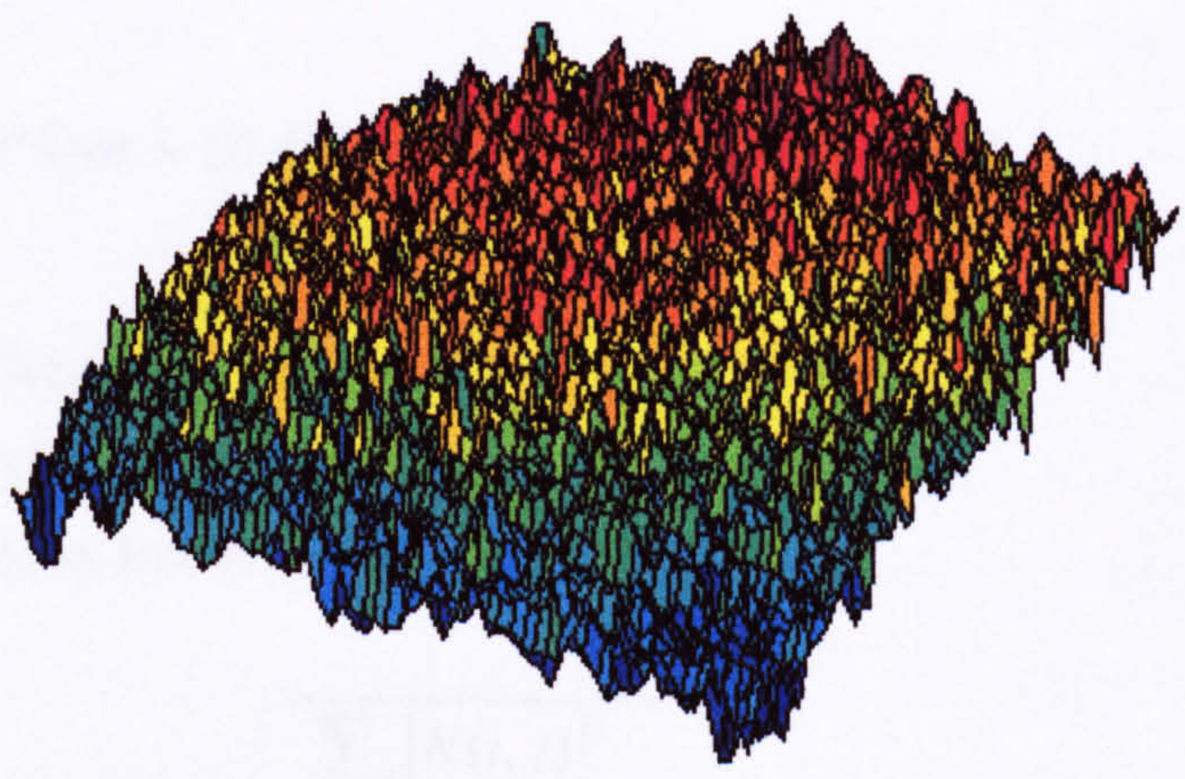

Figure 2.5-Raw thermal image of leather where high frequency noise is clearly visible.

This image was obtained with the infrared thermography system available at Bath University.

Finally, noise greatly affects thermal images (see Figure 2.5), in particular high frequency noise that certainly has to be taken into account when processing thermal

images. There are many noise sources, such as, noise from infrared detector, background radiation, and noise caused by object inhomogeneity (emissivity variations, volumic noise i.e., variations in thermal properties that are not regarded as defects).

Averaging N images of a stationary scene contaminated by random noise increases the signal-to-noise amplitude ratio by a factor of $\sqrt{N}$ [Castleman 96]; this is a simple method of reducing noise. Smoothing of noisy thermograms can also be achieved by filtering infrared images using a median filter or more complex methods by sliding gaussians [Hayden 87]. Averaging frames of the same scene is simple and it does not affect edges, which due to their nature are already quite blur.

Despite some image degradation may be corrected, great care has to be taken with these corrections because there are always unavoidable uncertainties in these transformations.

2.5.4 Noise Evaluation

Using a technique proposed by Fisher *et al.* [Fisher 95], image noise quantification of any images can be easily obtained by recording two images of the same scene. It is assumed that if they are acquired in the same conditions the only difference between them is noise. The peak signal-to-noise ratio (PSNR) of two indexed images can be calculated using the following equation:

$$\mathrm{PSNR} = 20 * \log_{10}\left[\frac{\text{Max Intensity}}{\mathrm{rms(N)}}\right] \quad \text{(dB)}$$

$$\text{Where N} = \text{noise} \cong |\text{A - B}|$$
$$\forall ij, 0 \le \text{A}(i,j), \text{B}(i,j) \le 1$$
$$\text{Max Intensity} = 1 \qquad (2.7)$$

$$\text{rms (N)} = \sqrt{\frac{\sum_{ij}[N(i,j)]^2}{\text{Maxcol Maxrow}}}$$

$$i = 0,1,\ldots,\text{Maxrow - 1 (Maxrow rows in images)}$$
$$i = 0,1,\ldots,\text{Maxcol - 1 (Maxcol columns in images)}$$

It is assumed that indexed images have pixel values between [0..1]. The PSNR is given in decibel units (dB), which measure the ratio of the peak signal and the difference

between two images. An increase of 20 dB corresponds to a ten-fold decrease in the root mean squared difference between two images.

2.5.5 Thermal Image Processing

In infrared thermography, the two most important quantities are temperature spatial distribution and its time relationship. From these quantities other parameters can be derived such as the *temperature contrast* which is of interest since is less affected by noise (a time domain analysis provides a more reliable procedure since volumic noise has a smaller effect).

Many temperature contrast definitions are used in infrared thermography, the most common are: the increased or excess temperature, the running contrast, the normalized contrast and standard contrast.

The increased or excess temperature signal is $\Delta T(t)$ is given by thefollowing expression:

$$\Delta T(t) = T_i(t) - T_s(t) \tag{2.8}$$

where T is the temperature signal, t is the time variable, indexes i and s refer to a suspected defective area and over sound areas respectively. Usually, a sound region is identified automatically or by an operator. With this kind of data processing a better visualisation of the defect is obtained, however ΔT is linearly related to the absorbed energy and this limits comparisons among experiments. This contrast computation makes use of the "spatial reference technique" in which sound values are subtracted from suspected values to improve visibility [Maldague 93a].

The running contrast $C^r(t)$, computed by Equation 2.9 is less affected by surface optical properties, if suspected and sound areas are located over regions of same emissivity/absorptivity. Also, the running contrast is less dependent on the absorbed energy [Grinzato 95] .

$$C^r(t) = \frac{\Delta T(t)}{T_s(t)} \tag{2.9}$$

The normalised contrast $C^n(t)$ is a contrast calculated with respect to the values of temperature at the instant t_m when the excess temperature is maximum (see Equation 2.10).

$$C^n(t) = \frac{T_i(t)}{T_i(t_m)} - \frac{T_s(t)}{T_s(t_m)} \tag{2.10}$$

Obviously, this parameter is dependent on the heating stimulation parameters. Normalisation may also be computed with values at the end of the thermal process.

The standard contrast definition $C^s(t)$ is another definition that is computed with respect to before heating temperature distribution at time t_0 (to minimise the adverse contributions from the surrounding environment) and normalised by the behaviour of a sound area (see Equation 2.11).

$$C^s(t) = \frac{T_i(t) - T_i(t_0)}{T_s(t) - T_s(t_0)} \tag{2.11}$$

In standard contrast computations, a unit value is obtained over a non-defective area. Standard contrast is widely spread as the definition of thermal contrast. Interestingly, standard contrast reduces the spurious effects of emissivity since its negative contribution cancels out in the division, if assumed uniform over the specimen surface.

On the whole, thermal contrast images are generally cleaner than raw thermograms, or thermal images. Contrast is often computed as a first step in the analysis of thermal image sequences.

2.5.6 Defect Sizing

Defect sizing is not a straightforward task in infrared thermography. Nevertheless, defect sizing is an important aspect of nondestructive testing because size is an important factor in the assessment of the severity of a defect.

The traditional approach for defect sizing is based on a "gradient image" (high-pass filtered contrast image) of the contrast image recorded when standard contrast is greatest. The gradient image is then used for defect size computation. This approach is based on the fact that defect visibility is greatest at peak contrast when the defect detection is more likely to occur. This is particularly true for weaker defects.

More recently, however, another argument was brought into consideration: if one has to wait for maximum contrast to develop, the visibility of a defect will be enhanced but, on the other hand, waiting for this to happen also blurred the edges of the defects due to the three-dimensional spreading of the thermal front. In this respect, Krapez suggested to

rely on the contrast image as soon as it emerges from the noise [Krapez 94] or when the slope of the contrast curve is at its peak [Favro 95].

Another refinement to the early detection procedure was proposed by means of an iterative technique to correct the shrinkage resulting from the thermal front spreading up to the time of defect detection. A series of images are recorded following the pulse heating and, for each image, defect size is taken as half the maximum amplitude. A plot of defect size as function of the square-root of the time, is then created and the fit line at time zero gives the defect size with a small overestimation (4% was noticed in the case of mild steel) [Almond 94]. This approach is not exempt of problems because, for very small defects or at very long times it fails.

2.6 Thermal properties vs. Physical properties

In some cases, measurement of a certain thermophysical property is directly related to the value of another material property. Some research has been done on linking thermal properties with physical properties, using infrared thermography.

Peralta *et al.* reported consistent differences in thermal diffusivity of high purity aluminum specimens depending on the degree of specimen recrystallization [Peralta 91].

Connolly studied the effect of porosity on the apparent diffusivity of composite materials [Connolly 92]. In this study, a face of a sample is heated with a high power laser, while the thermal response on the other face is observed and recorded. Experiments were conducted on carbon-epoxy samples with a range of known porosities and varying thickness. A good correlation between the diffusivity and the porosities for the tested samples was obtained. These results were explained in terms of the influence of the porosity on the thermal diffusivity. Small pores create a higher thermal resistance and retard the heat flow through the material.

Thus, thermal diffusivity seems to be a good indicator for porosity assessment because it is linked to apparent density and can be measured through infrared thermography.

2.6.1 Thermal Diffusivity Measurement of Materials

Thermal diffusivity of a material, δ, is given by Equation 2.12, where ρ is the density, c is the specific heat and k is the thermal conductivity.

$$\delta = \frac{k}{\rho \cdot c} \tag{2.12}$$

Thermal diffusivity of a material can be measured in a relatively simple non-contact manner using infrared thermography.

One of the best known methods of measuring thermal diffusivity [Parker 61], also known as classical method, consists of heating a specimen and observing the temperature evolution of either the front or the back surface. In case the back face is monitored, Parker *et al.* showed that for a sheet of material with a thickness L, the time $t½$ (i.e., the time for the monitored surface to reach half its maximum temperature) can be defined by:

$$t_{1/2} = \frac{1.38L^2}{\pi^2 \delta} \tag{2.13}$$

However, this expression assumes a one-dimensional heat flow within a semi-infinite medium. Hobbs *et al.* carried out computations of t½ for a range of materials and they concluded that $t½$ for copper is only 0.13 seconds while for a 10 mm thick composite plate is 33 seconds [Hobbs 91].

Two other methods can be used for thermal diffusivity measurements, namely, Diffusivity Measurement Method based on the Laplace Transform and Diffusivity Measurement Method based on Phase Measurement. Despite these methods being more accurate than the classical method, they have the inconvenient of requiring more resources.

From this short study, one can hypothesize that if the thermal diffusivity of a material depends on its porosity, it is very likely that it also depends on the apparent density of the same material. A more porous material has a smaller apparent density. Wang reported a high correlation between tensile strength and density of leather [Wang 92]. Thus, it is proposed that a relationship between diffusivity and the tensile strength of leather may exist. The confirmation of this hypothesis would be a major breakthrough in leather characterisation, as it would be possible to partially characterise leather in a non-destructive and contact less manner.

2.7 Leather Characterisation and Inspection

The manufacture of leather involves visual inspection and manual sorting at key stages of production by skilled operatives. Accurate sorting is fundamental for assuring the best return on the available material and customer satisfaction. Any lack of consistency by graders or between graders can prove very costly. The development of an automatic characterisation and inspection system is certainly the right answer to reduce the subjectivity associated with visual perception and varying skill of human sorters.

The adoption of such system would undoubtedly have many advantages, such as: an infinite attention span and ability for continuous operation for long periods without mental or visual fatigue without grade decision deterioration; equal attention to all areas of a skin, a manual sorter may overlook a certain area if lighting conditions are not appropriate.

However, some disadvantages could also be foreseen, for example: lack of human grader common sense in the decision-making process; faults disregard by the human grader that can be tolerated; system will only see the leather under one set of lighting conditions, whereas the human operator can change his viewpoint in order to check a suspected area.

Ideally, any effective inspection system should be able to cope with defects that vary greatly in size, from small spots, e.g. light spot and pinhole, through narrow linear faults such as, scratches, to larger area faults like ringworm, mange and putrefaction. Such system should have the ability to take into account the location, size, and nature of faults and produce numerical grades similar to those used at present. Furthermore, it should be capable of working at least as fast as currently achieved by human sorters.

Such system could also contribute decisively for the automation of the process of leather layout and cutting. For each skin, a map of physical properties and defects would be produced, so CAD/CAM tools could use this information to maximise the utilised area and lay out the right patterns on the best position.

Several attempts have been made to build such system without much success. These systems are mainly based on normal computer vision.

Gaffron *et al.* developed an automatic inspection system based on a CCD line scan camera. Its main objectives are to be able to recognise and classify grain defects. These

are expressed in form of a fault map or single numerical grade prior to samming or after toggling. In order to explore the system potential, faults were divided in three geometric categories (dot, linear, area) and graded by three levels of severity of detection (E for easy, D for difficult, R for in between faults). The reported results show a detection rate of 83% for E and R faults and several of the class D faults [Gaffron 94].

Hilton presents another inspection system based on image analysis. Simultaneous acquisition of multiple images using laser-scanning techniques is reported. Three different types of images are produced: reflection, transmission and fluorescence. The transmission image is best used for restricting the working area and detect penetrating defects or thickness variations. The reflection image is suited to faults that cause contrast changes on the surface. The fluorescence image is ideal for highlighting healing and structural defects. However, no quantified results are presented [Hilton 95].

Pölzleitner designed a flexible real-time system for 2D defect and texture classification of wooden materials that was successfully applied to leather inspection. A line scan camera is used for image acquisition and several algorithms for object segmentation and recognition are applied. Furthermore, texture classification is also performed in real-time [Pölzleitner 95].

The exhaustive work of Hoang *et al.* on achieving automation in leather surface inspection, concentrated on the development of algorithms for defect detection, defect classification and material handling [Hoang 97]. This research group experienced some difficulties during the image acquisition process, as the geometry and/or position of some defects against the light source and CCD line scan camera are not dominant enough to be detected. Although good results are reported, it was concluded that some defects are not visual in nature and they are not detectable by a visual system.

This last conclusion of Hoang *et al.*, is extremely important and greatly supports the view of the author that an effective automatic system for characterisation and inspection of leather cannot be achieved by a single method but by a combination of several methods. Although visual inspection is definitely relevant, it cannot provide any information about the thickness or material properties. Perhaps, the ideal solution would be a combination of mechanical, normal computer vision and infrared thermography.

3

3 Physical Testing and Results

3.1 Introduction

This chapter starts by the presentation of the sample materials used in the experiments performed throughout this work, and how specimens were obtained and handled.

Next, a brief description on how thickness measurements are carried out is given. Tensile tests, apparent density and surface roughness measurements, follow the section devoted to static compressibility tests. For each test, a description of the procedure, instrumentation, results computation methods and results is given.

The main of objective of conventional physical tests is to characterise the specimens used in this work in a conventional manner and then compare these results with the data obtained by the Mechanical Scanning system and by Infrared Thermography.

3.2 Sample Materials

3.2.1 Sample Selection

Three sides of leather were used in this work as well as some random specimens from a spread of leathers. Specimens are coded to facilitate the comparison and storage of results.

Two bovine sides of crust leather with an average thickness of about 1.1 and 2.2 mm were selected and kindly offered by Holmes Hall Tanners, Plc. Hull. These two sides were tanned under the same procedure, in this way, one can be assured of "similar" properties on different skins and different areas apart from natural variations of density, thickness, defects, structure of fibres and orientation of fibres. A single side of a bovine hide (2.5x1 m) can easily provide seven sampling positions with adequate variety of properties for this study [Muthiah 76]. The selected positions correspond to: Shoulder,

Butt 1, Butt 2, Tail end, Front Shank, Belly and Back Shank (see Figure 3.1). These sampling positions were numbered from 1 to 7 as shown in the same figure.

A corrected grain sheepskin side 1 mm thick was also selected in order to cover a wider range of leather. However, due to the sheepskin size, only two similar sampling positions can be obtained (Front and Back respectively numbered 1 and 2).

From each sampling position, an oblong piece of leather was removed. From this piece, a set of specimens for each location was cut in order to perform destructive and non-destructive tests. Figure 3.2 shows the layout of a set of specimens within a sampling position.

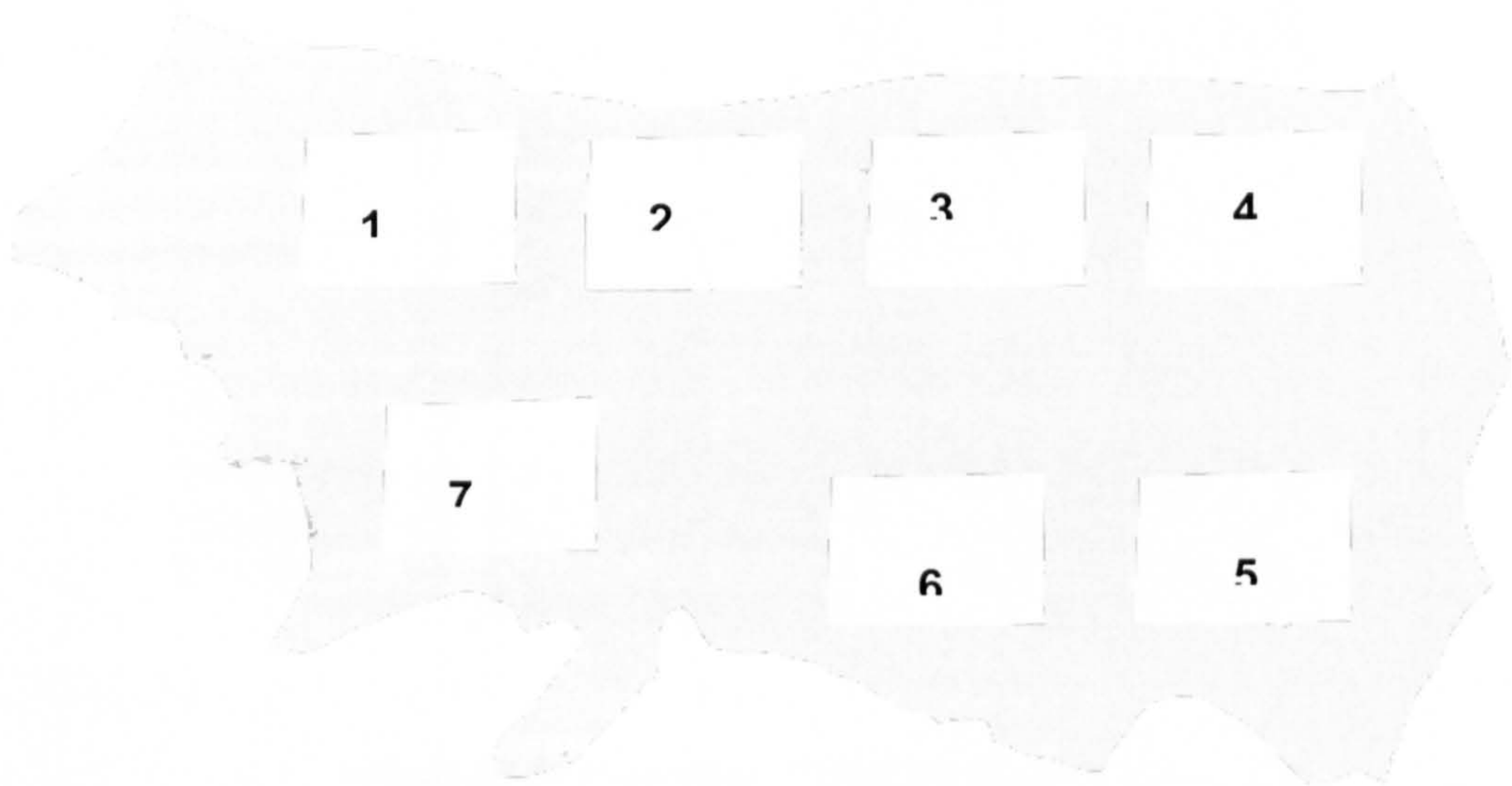

Figure 3.1-Selected sampling positions within a side.

Each specimen within a set is unambiguously identified by an alphanumeric code, which is composed by several letters, e.g.: S14A3. Here, "S1" stands for the side with thickness around 1 mm, "S2" for 2 mm thick side and "S3" for the sheepskin side. The second digit identifies the sampling position relatively to the side and, according to Figure 3.1 ranges from 1 to 7 for "S1" and "S2", and ranges from 1 to 2 for "S3". The following letter represents the shape of the specimen according to Figure 3.2. Finally, the last digit identifies the number of the specimen in case there is more than one.

The primary objective of each specimen was as follows: "A1" to "A3" and "B1" to "B3" are provided for tensile strength and elongation testing, parallel and perpendicular to the backbone; specimen "C" and "D" were used for friction and roughness tests and could also be used for tear strength tests; high voltage tests were carried out on "E1" to "E3"; softness and static compressibility tests were done on specimen "F"; specimens

"HW" were used for static compressibility tests but on specimen "HW" impact compressibility tests also take place; further, specimen "HN", "HW", "GN" and "GW" are utilized for all the testing that can be performed by the Mechanical Scanning System; for infrared thermography testing and diffusivity measurements specimen "I" was selected, while some "HW", "C" and "D" specimens are also used for infrared testing, in particular after inducing some artificial faults.

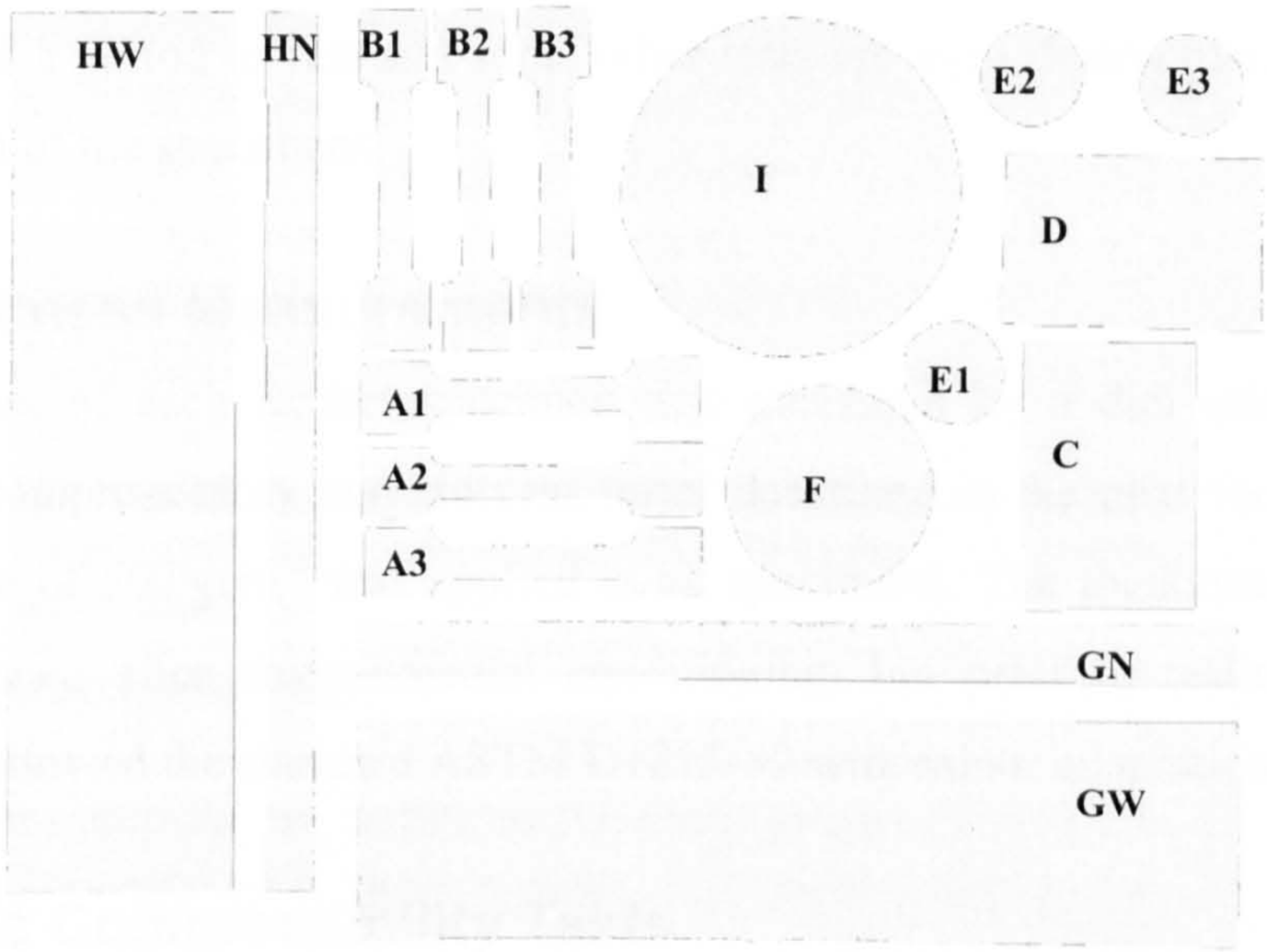

Figure 3.2-Set of specimens within a sampling position.

The precise dimensions of the specimens are presented in Appendix A.

The main objective of having wide leather strip specimens was to emulate the behaviour of a skin, so results from testing wide specimens would be considered as results from testing the full skin without cutting of specimens.

The layout of the specimens within a sampling position was thought to enable the correlation of results from different tests, assuming a smooth transition of properties between adjacent specimens.

3.2.2 Sample Conditioning

Leather specimens are conditioned at standard testing atmosphere (23°±1°C, 50±4% r.h.), according to ASTM D 1610-91 for at least 48 hours before testing . Most of the time, a maximum variation of 4 % on the relative humidity and 1°C on the temperature was not feasible because of the limitations of the air conditioning control

system available at The University of Hull. All tests were performed in the same room where the leather samples were conditioned, with the exception of the infrared thermography experiments that were performed at the Department of Materials Science of the University of Bath.

3.2.3 Testing sequence

Leather testing in this work followed a precise sequence in order to be able to combine tests of different nature. Some tests simply do not affect tested specimens, while other tests demand a period of rest and some other tests are even destructive, preventing the re-utilisation of the specimens.

3.3 Thickness Measurements

The thickness of each leather specimen was measured by a dial micrometer gauge and/or the compressibility and softness tester described in the next section. A similar contact force of 500 gcm^{-2} was applied to all specimens. The thickness measurements were performed after environmental conditioning, but prior to testing. The testing procedure followed the standard ASTM D1813-89 with minor adaptations.

3.4 Static Compressibility Tests

Compressibility is defined as the decrease in intrinsic thickness with an appropriate increase in pressure across thickness. The intrinsic thickness of leather is in fact the maximum leather thickness that can be measured and is determined as the thickness of the space occupied by the leather subjected to a defined pressure. Two effects are noteworthy in compression. At first, there is the irrecoverable strain during the initial compression cycle, and secondly, there is a mechanical hysteresis observed during a compression-release cycle (see Figure 3.3) resulting in a lower volume during the release cycle. In order to compare different compression curves of fabric, Kawabata [Kawabata 80] introduced four parameters as part of the compression test in his KES-F system (a system aiming objective fabric evaluation). The KES-FB3 compression test takes several thickness measurements between T_0 and T_m at a 0.5 $gf.cm^{-2}$ and 50.0 $gf.cm^{-2}$ (P_m) pressure interval, respectively. The following four parameters express the work of compression, *WC*, as the area under the pressure-thickness curve; (*WC'* area release curve), the linearity, *LC*, as the deviation from a straight line between the

thickness limits; the resilience or hysteresis of the fabric compression, *RC* and the relative compressibility, *EMC*.

$$\begin{aligned} WC &= \int_{T_0}^{T_m} P\,dT \\ LC &= WC/\left(0.5P_m\left(T_0 - T_m\right)\right) \\ RC &= WC'/WC \\ EMC &= 1-\left(T_m/T_0\right) \end{aligned} \tag{3.1}$$

Lokanadam concentrated his work mainly on the compressibility index, plotting the logarithm of leather thickness against the logarithm of measuring load. The negative slope of a fitted straight line represents the compressibility of the leather, *C*, and according to Onions *et al.* [Onions 67] is given by:

$$C = -\frac{d_p}{d_t}\cdot\frac{p}{t} = -\frac{\textit{the fractional change in thickness}}{\textit{the fractional change in pressure}} \tag{3.2}$$

being p the applied pressure, t the thickness, d_p changes in pressure and d_t changes in thickness.

In the process of leather compression, three stages can be distinguished depending on the pressure (see Figure 3.3), as it happens in fabric [Postle 71, de Jong 86 and Matsudaira 95]. First at low pressure, the pressure foot starts to compress the leather causing a certain amount of shear stress while the compression force varies linearly with the thickness. An increase in the pressure might cause the rearrangement of fibre bundles overcoming interfibre friction. The leather thickness decreases non-linearly with increasing pressure in this second region. Increasing the pressure even further compresses the rearranged and compacted fibre bundles, hence the pressure rises greatly for a small reduction in thickness. This third region can be considered as the initial elastic region of the fibres.

In this thesis, the author uses the concept of compression energy *CE* to characterise leather. This concept is defined as the energy needed to compress leather, for instance to 10% compressive strain. If the compression load *CL* compresses the leather by an amount *dl*, the compression energy is computed according to Equation 3.3.

$$CE = \int_0^{10\%} CL\,dl \tag{3.3}$$

Graphically, the compression energy *CE* represents the area under the curve, compression load function of compression length, from 0 to 10 percent compressive strain, as shown in Figure 3.3.

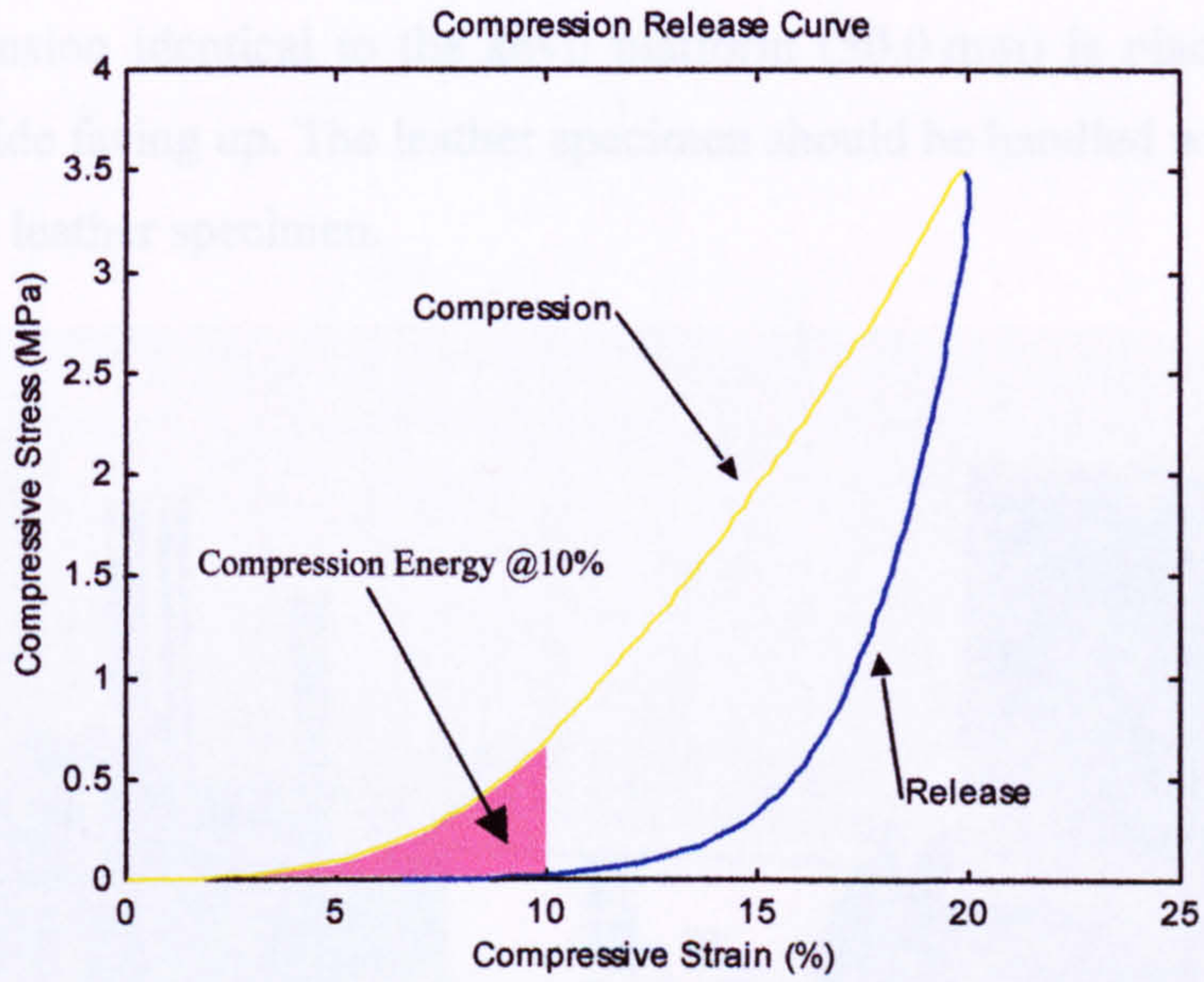

Figure 3.3-Real compression-release curve ("S24HW").

3.4.1 Instrumentation and Method

The author built an automated compression tester, shown in Figure 3.4, which can also be used for softness measurements. The testing device measures electronically the applied pressure with a load-cell (OMEGA® LCCA-50, range 100 lbs compression and tension). The reducing leather thickness is measured with a 4 mm range inductive displacement sensor (TQ 402/5M) attached to the moveable platform. Both sensors are connected via a PC30AT data acquisition card (12-bit analog-to-digital conversion) to a computer, which logs the data and controls the compression tester.

The compression tester has been built according to the ASTM D1813-89 specifications with slight modifications of the pressure foot and anvil diameters. The new anvil and pressure foot characteristics are: a flat anvil with 7.8 mm diameter projecting 2.5 mm from the surface of a flat circular platform about 50 mm diameter; a flat pressure foot with 7.8 mm diameter having an effective compression area of 48 mm^2. Further, both compressing surfaces were lapped to give a mirror finish and are parallel to within 10 μm. As a matter of comparison, Lokanadam selected a pressure foot with the radius

of 3.11 mm [Lokanadam 89]. Further details on the rig and the sensors can be found in Appendix B.

A typical compression test is performed as follows. The leather specimen with a minimum dimension identical to the anvil platform (50.0 mm) is placed on the anvil with the grain side facing up. The leather specimen should be handled with care to avoid alteration of the leather specimen.

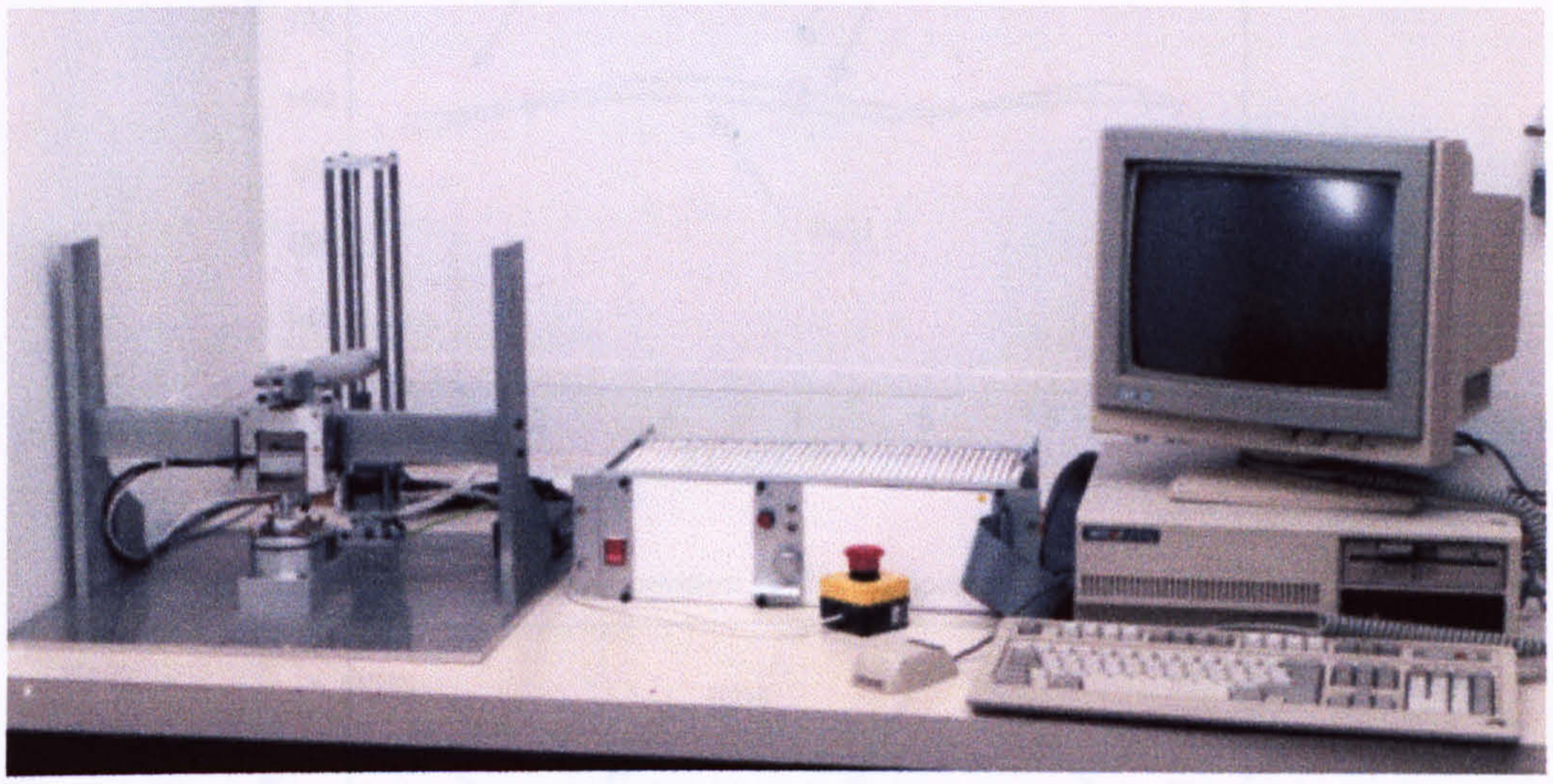

Figure 3.4-Full view of the static compressibility and softness tester.

3.4.2 Static Compressibility Testing Results

Static compressibility tests were performed on each "H" specimen of each sampling location of the three available sides. The main objective of this test is to compare its results with those from tests executed with the Mechanical Scanning System.

The compression rate of these conventional compressibility tests is about 50 μms^{-1}. Each final result is the average of six similar experiments, performed under the same conditions.

The compression test results are presented in Figure 3.5, the compression vs. sample position at 10 percent compressive strain is plotted, as well as the compression energy vs. sampling position at the same compressive strain.

The compression energy *CE* concept used in this test was described above and is computed according to Equation 3.3.

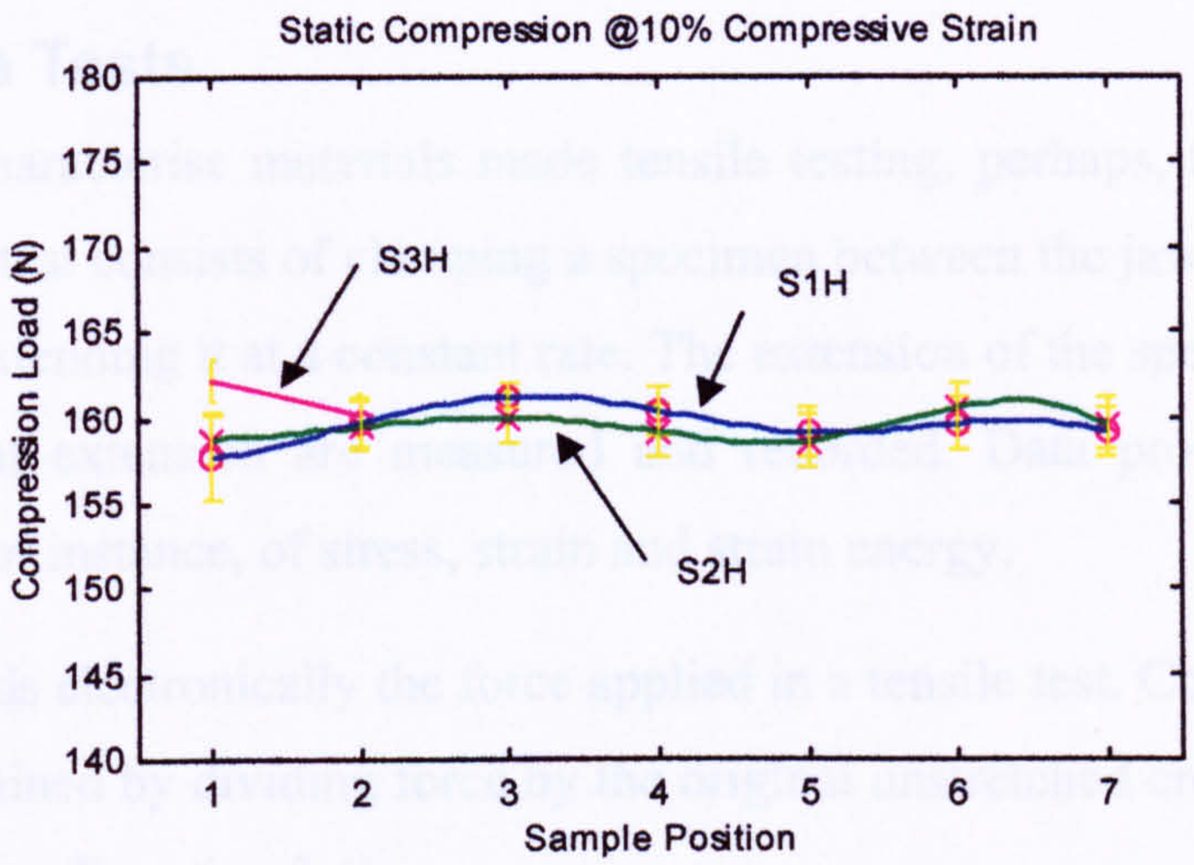

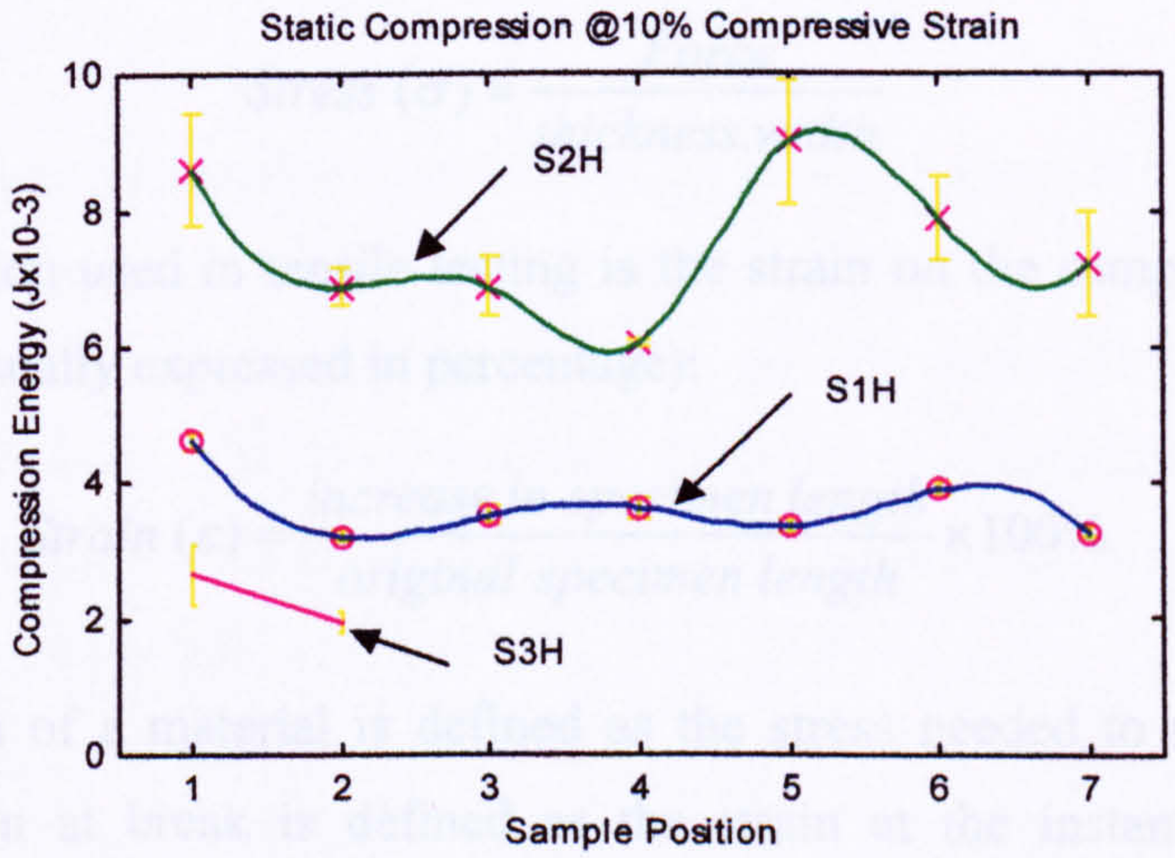

Figure 3.5-Conventional static compression test results.

All data was calculated in MATLAB with functions developed by the author. In Figure 3.5 the compressive load of, for instance, specimen S14H (side 1, position 4, specimen H) is read from the curve S1H "Sample position" 4.

3.5 Tensile Tests

The need to characterise materials made tensile testing, perhaps, the most commonly used test. This test consists of clamping a specimen between the jaws of a tensile testing machine and extending it at a constant rate. The extension of the specimen and the force needed for that extension are measured and recorded. Data processing enables the computation, for instance, of stress, strain and strain energy.

A load cell reads electronically the force applied in a tensile test. Conversion from force to stress is obtained by dividing force by the original unstretched cross-sectional area of the specimen (see Equation 3.4).

$$Stress\ (\sigma) = \frac{Force}{thickness.width} \tag{3.4}$$

Another definition used in tensile testing is the strain on the sample and is defined in Equation 3.5 (usually expressed in percentage):

$$Strain\ (\varepsilon) = \frac{increase\ in\ specimen\ length}{original\ specimen\ length} \times 100\% \tag{3.5}$$

Tensile strength of a material is defined as the stress needed to rupture a specimen, while elongation at break is defined as the strain at the instant of rupture of the specimen and is usually expressed in percentage.

Another definition used in this thesis is the strain energy *SE* concept, which is defined as the energy needed to extend leather to 1 or 2 percent strain. If the extension load *EL* extends the leather by an amount *dl*, the strain energy is computed according to Equation 3.6:

$$SE = \int_{0}^{1\%\ or\ 2\%} EL\, dl \tag{3.6}$$

Graphically, the strain energy *SE*, represents the area under the curve extension load vs. extension length from 0 to 1 or 0 to 2 percent strain. All data was calculated in MATLAB with functions developed by the author.

Figure 3.6 shows the result of a tensile strength test of specimen S21A1, where the maximum stress was 17.9 MPa at 47.1 % strain.

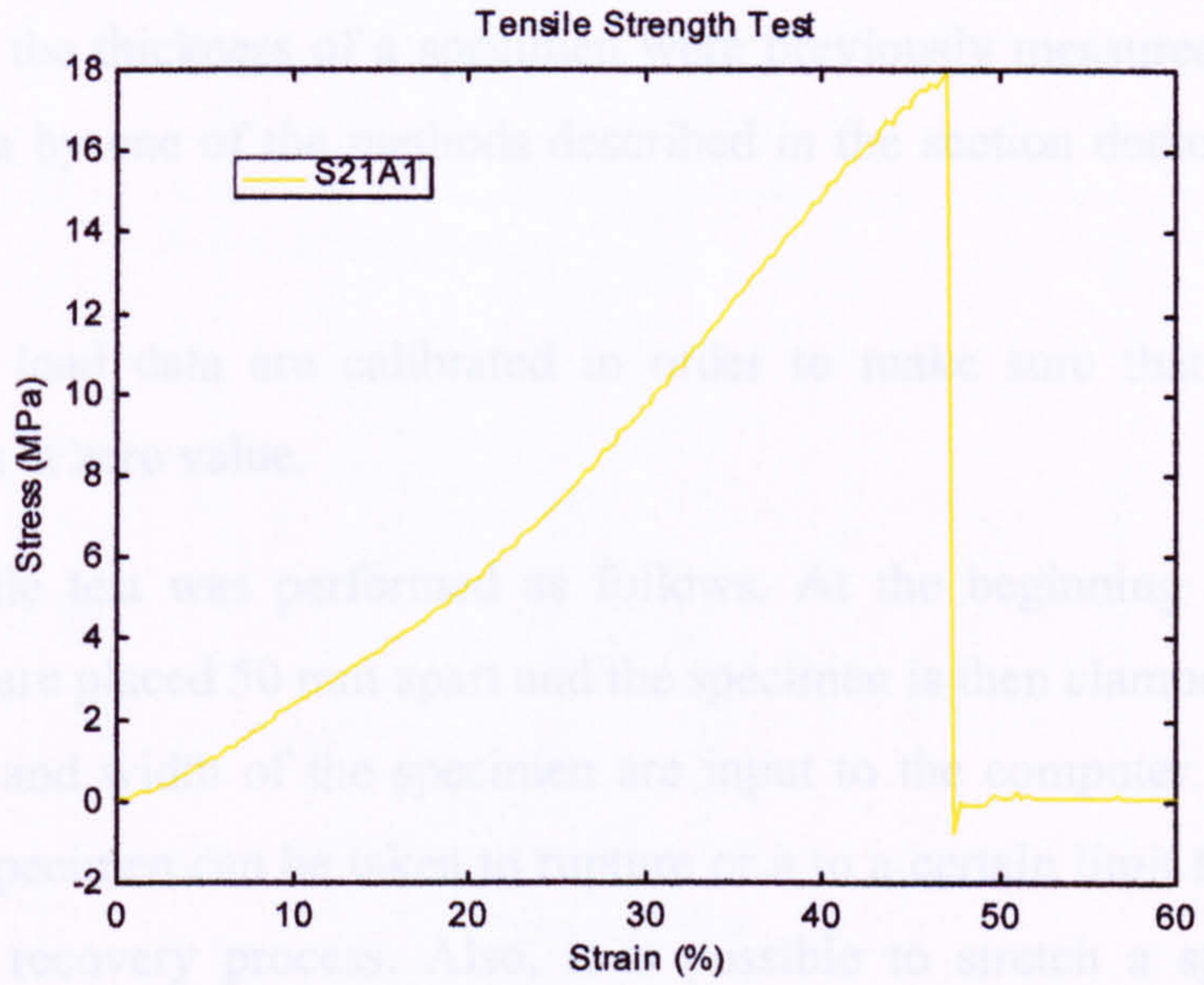

Figure 3.6-Tensile strength test result of specimen S21A1.

The shape and dimensions of the specimens for tensile testing of leather are shown in Figure 3.7. The standard ASTM D2209-90 recommends quite a large dumbbell shaped specimen, however for leather saving reasons a medium sized IUP/6 (Official Methods of Analysis) specimen has been adopted. O'Leary also adopted successfully this specimen shape and dimensions for his study of the differences in strength between the grain and corium layers [O'Leary 96].

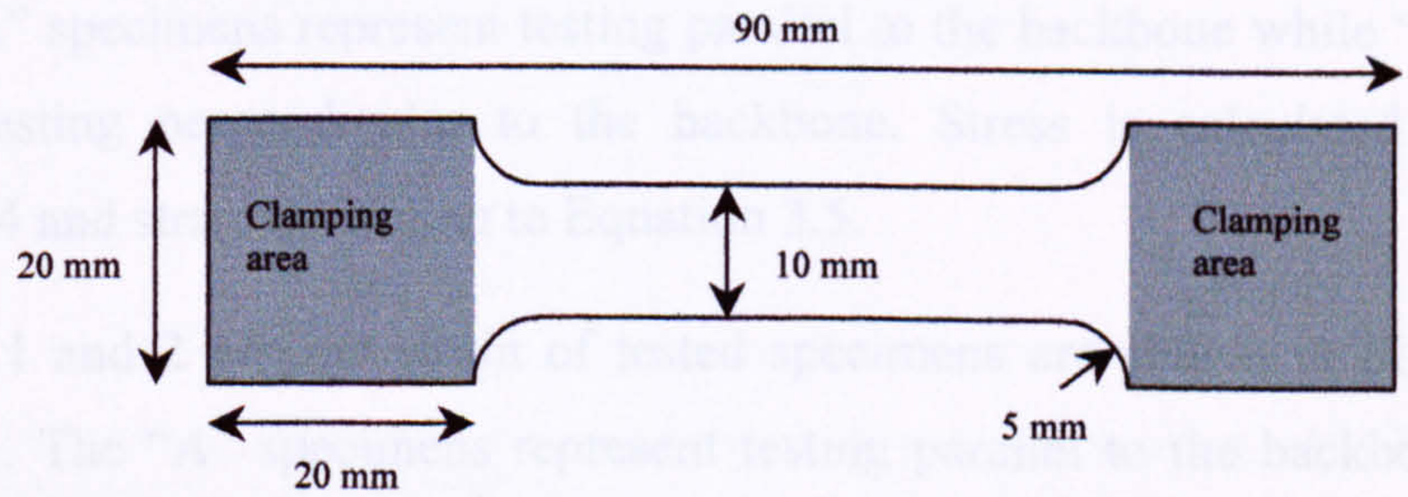

Figure 3.7-Shape and dimensions of specimen for tensile testing.

3.5.1 Instrumentation and Method

A tensile testing system built in house was used for performing tensile strength, elongation at break and stress-strain cycles.

The testing device measures electronically the extension force with a load-cell (OMEGA® LCCA-100, range 200 lbs compression and tension). The distance between

clamping jaws is given by the position encoders of the pulling jaw. A PC controls the rate of extension and saves all data in a MATLAB format file.

The width and the thickness of a specimen were previously measured in the centre of the narrow area by one of the methods described in the section dedicated to thickness measurements.

Extension and load data are calibrated in order to make sure that initial load and extension begin at zero value.

A typical tensile test was performed as follows. At the beginning of each test, the clamping jaws are placed 50 mm apart and the specimen is then clamped. The extension rate, thickness and width of the specimen are input to the computer. Then, stretching starts and the specimen can be taken to rupture or a to a certain limit force followed by measuring the recovery process. Also, it is possible to stretch a specimen up to a particular strain followed by the measurement of the recovery process.

3.5.2 Tensile Testing Results

Tensile testing of specimens "A" and "B" was carried out as conventional tests whose results were to be used to compare and validate measurements performed with the Mechanical Scanning System. A similar extension rate, $0.52\,mms^{-1}$, was used to perform extensions up to 2 percent strain.

Stresses at 1 and 2 percent strain of tested specimens are shown in Figure 3.8 and Figure 3.9. The "A" specimens represent testing parallel to the backbone while "B" specimens represent testing perpendicular to the backbone. Stress is calculated according to Equation 3.4 and strain according to Equation 3.5.

Stresses at 1 and 2 percent strain of tested specimens are shown in Figure 3.10 and Figure 3.11. The "A" specimens represent testing parallel to the backbone while "B" specimens represent testing perpendicular to backbone. Strain energy is calculated according to Equation 3.6.

Each result presented in Figure 3.8, Figure 3.9, Figure 3.10 and Figure 3.11 represents the average of six similar experiments.

In Figure 3.8, the stress at 1 percent of strain of, for instance, specimen S14A1 (side 1, position 4, specimen A1) is read from the curve S1A "Sample position" 4.

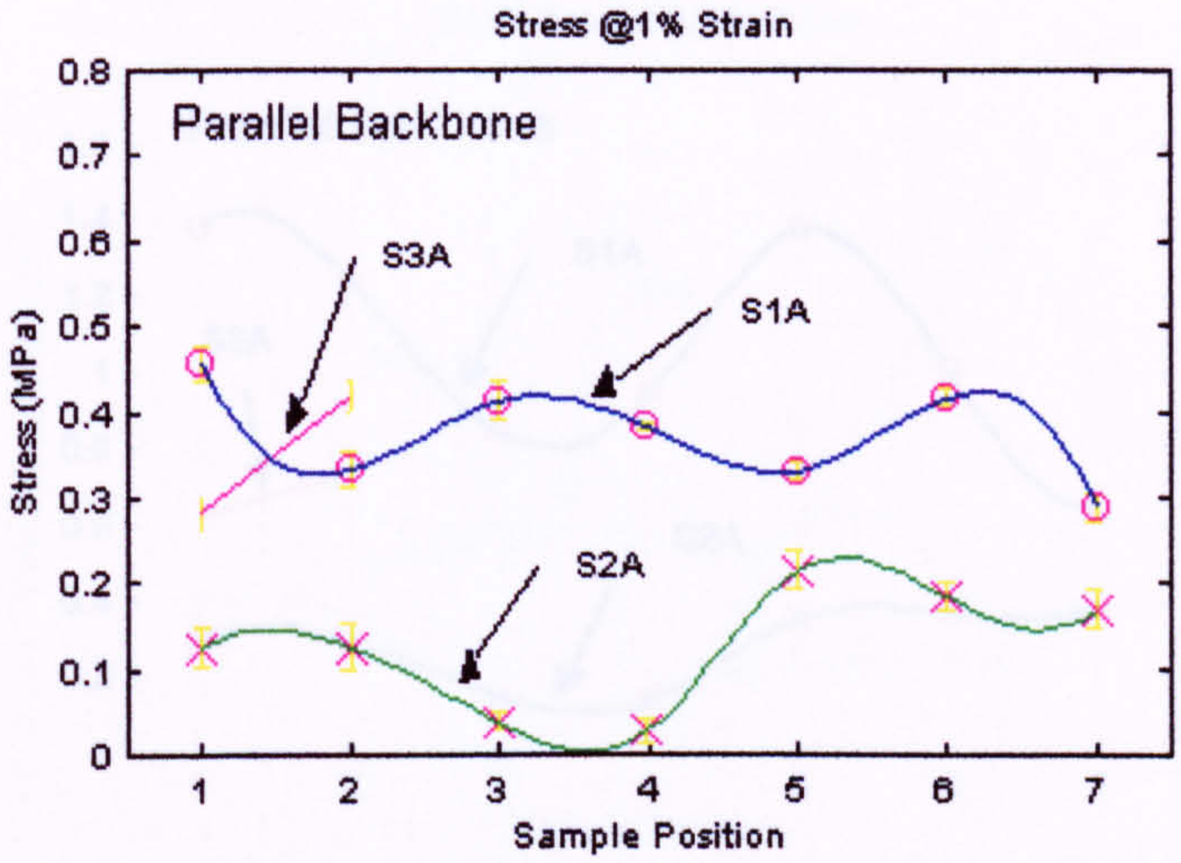

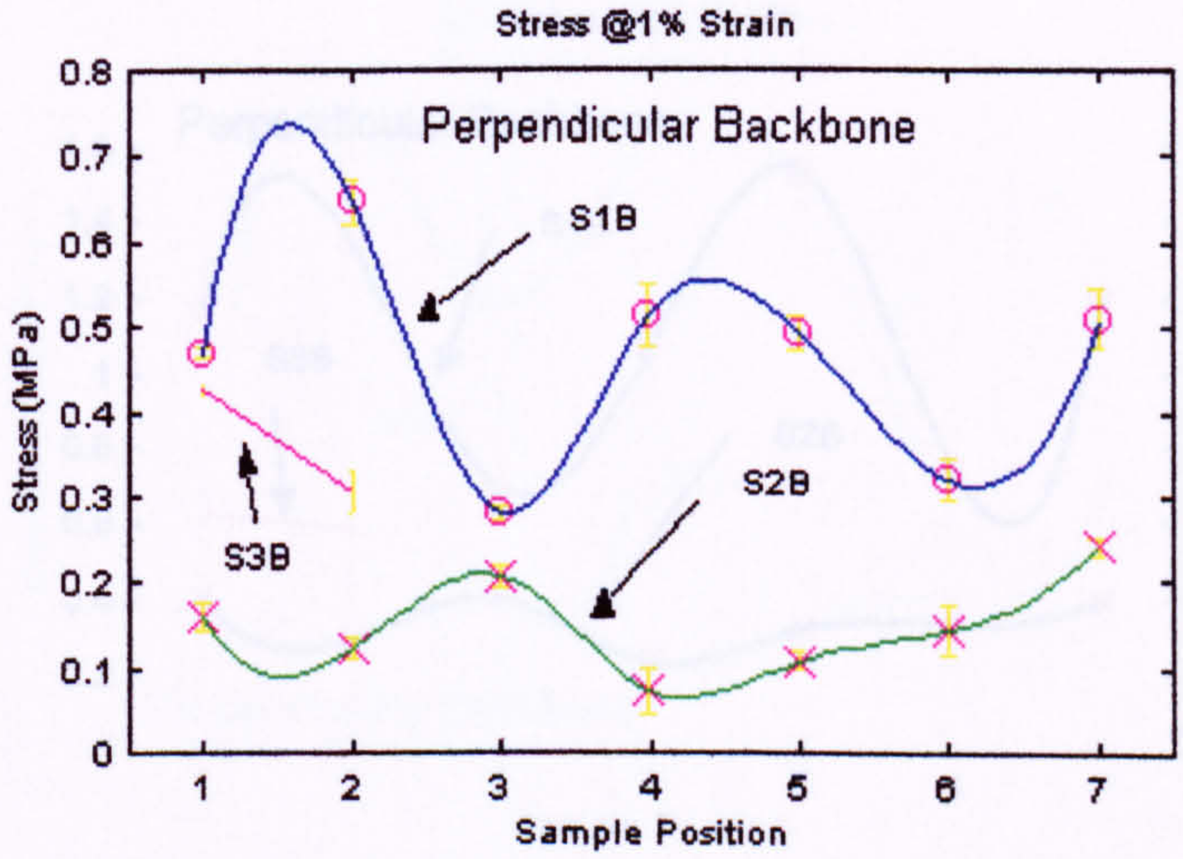

Figure 3.8-Plot of stress @1% strain for A1 and B1 specimens.

Tests were performed under standard conditions, and the extension rate was of 0.52 mms^{-1}.
Each result is the average of six runs.

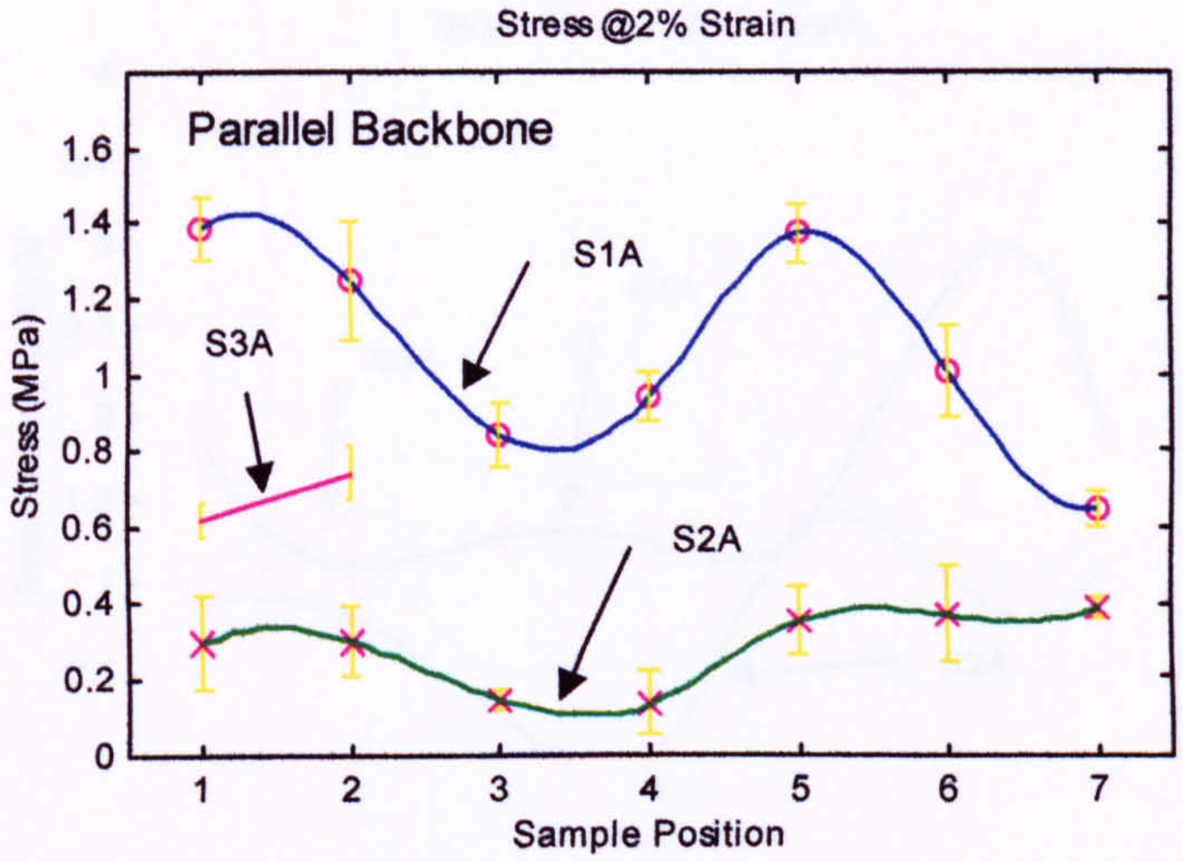

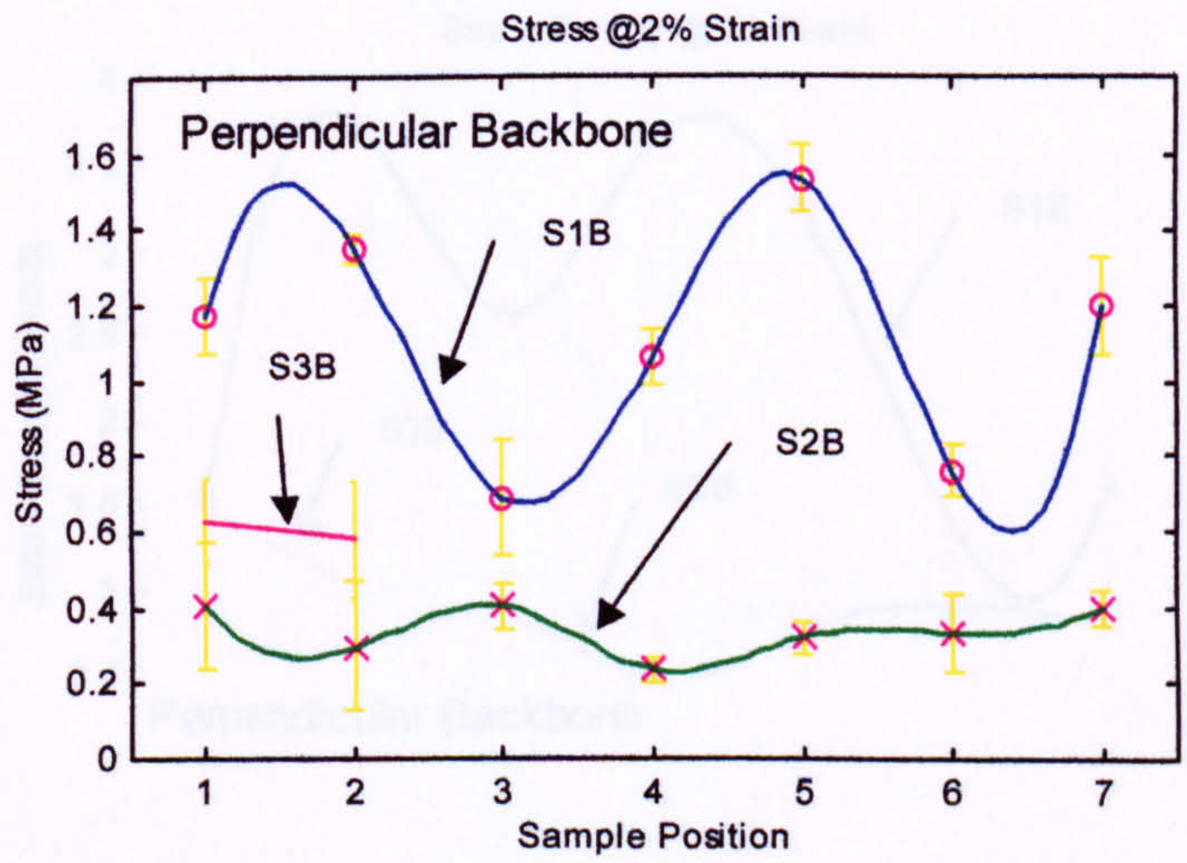

Figure 3.9-Plot of stress @2% strain for A1 and B1 specimens.

Tests were performed under standard conditions, and the extension rate was of 0.52 mms^{-1}. Each result is the average of six runs.

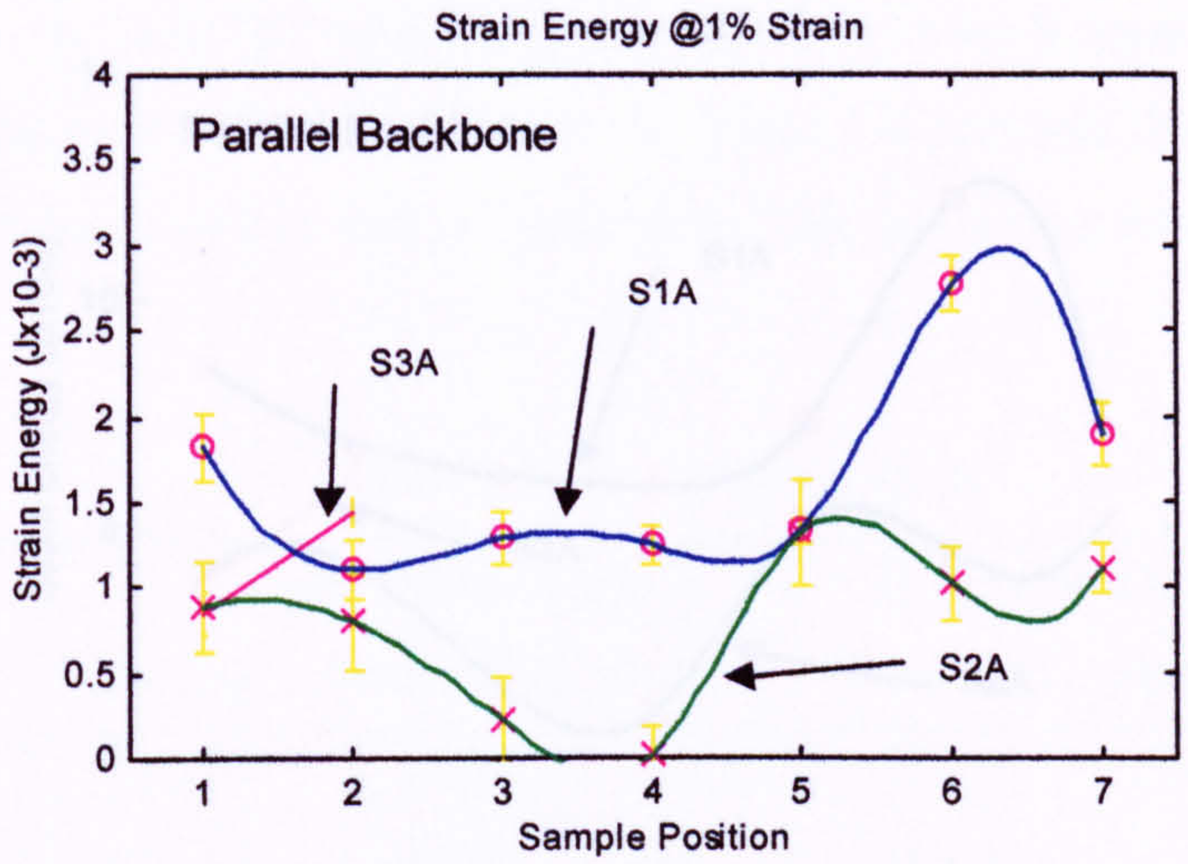

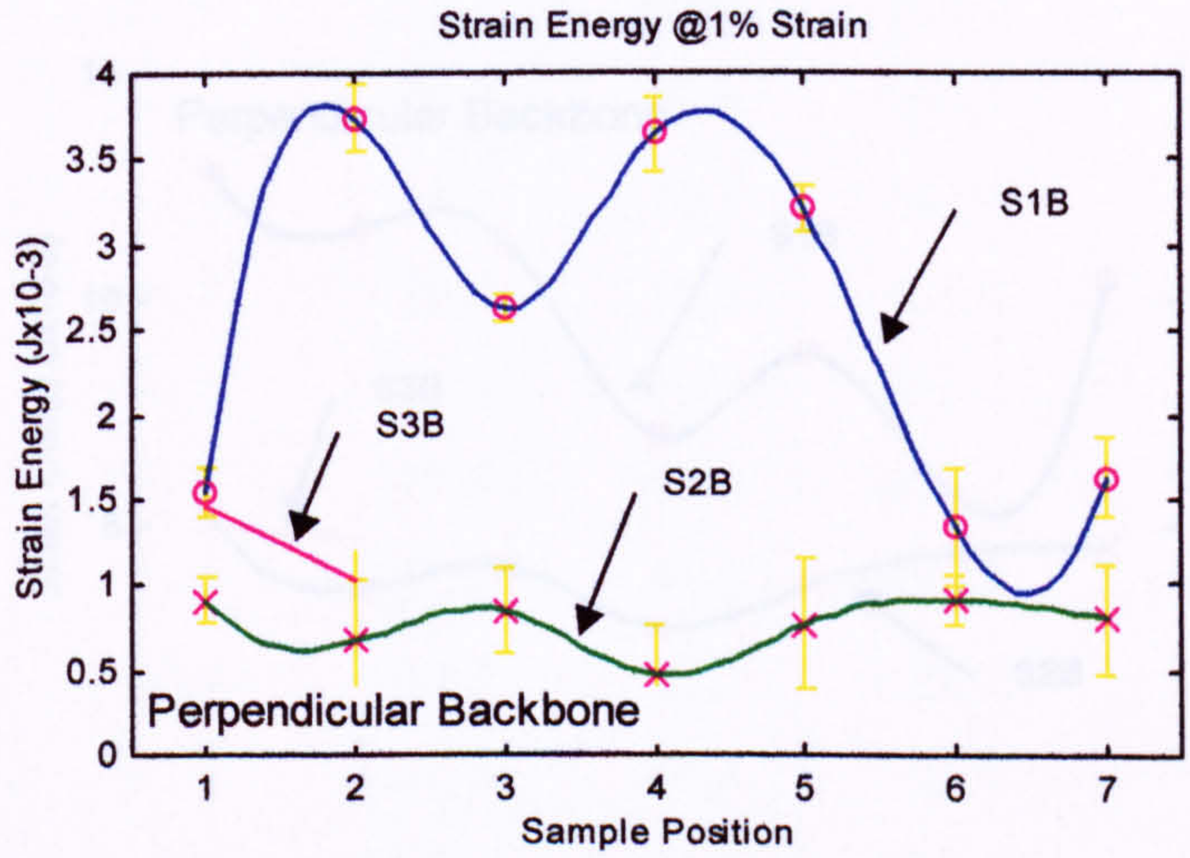

Figure 3.10-Plot of strain energy @1% strain for A1 and B1 specimens.

Tests were performed under standard conditions, and the extension rate was of 0.52 mms^{-1}.
Each result is the average of six runs.

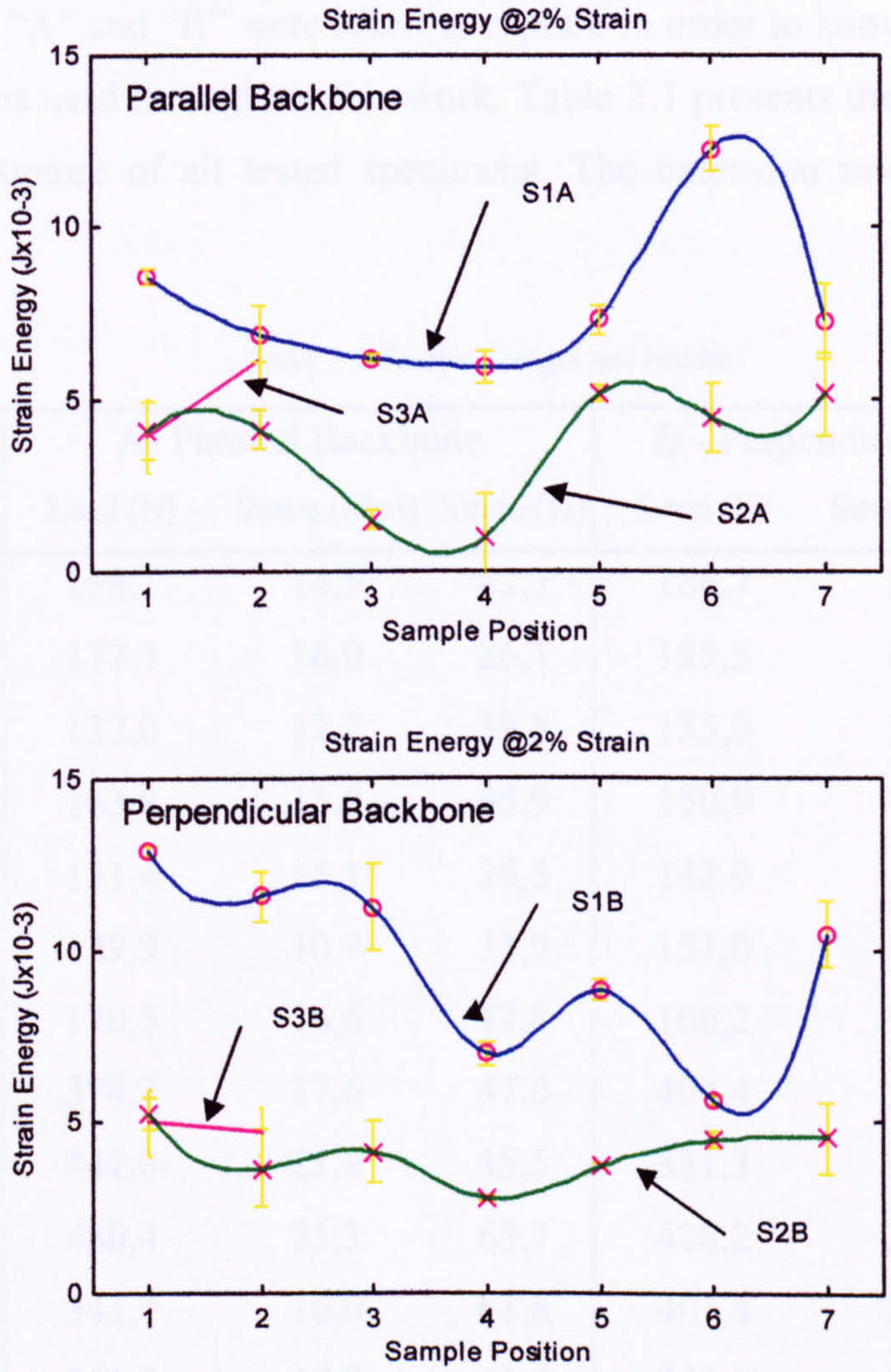

Figure 3.11-Plot of strain energy @2% strain for A1 and B1 specimens.

Tests were performed under standard conditions, and the extension rate was of 0.52 mms^{-1}. Each result is the average of six runs.

3.5.3 Tensile Strength Results

The load to rupture a specimen divided by its original unstretched cross-sectional area gives the tensile strength.

The specimens "A" and "B" were taken to rupture in order to know the tensile strength of the specimens used throughout this work. Table 3.1 presents the average load, stress and strain at rupture of all tested specimens. The extension rate of these tests was 0.52 mms^{-1}.

Table 3.1-Tensile strength test results.

Specimen	A- Parallel Backbone			B - Perpendicular Backbone		
	Load (N)	Stress (Mpa)	Strain (%)	Load (N)	Stress (Mpa)	Strain (%)
S11	158,1	14,9	42,7	186,7	17,5	36,6
S12	177,5	16,0	26,1	195,5	17,0	34,1
S13	132,0	12,2	39,8	155,0	13,6	40,4
S14	163,8	15,0	45,9	150,9	13,6	32,2
S15	151,4	15,1	29,3	142,9	14,3	35,3
S16	129,9	10,9	31,9	151,0	12,8	30,9
S17	170,5	16,6	47,8	160,2	14,3	26,4
S21	374,7	17,6	47,6	404,4	19,0	45,2
S22	441,0	21,9	45,5	331,3	16,8	55,4
S23	480,4	23,3	63,7	428,2	20,8	45,8
S24	341,7	16,0	61,8	401,4	19,0	45,9
S25	361,1	19,0	41,4	333,0	17,5	41,4
S26	364,3	19,3	44,6	396,6	20,2	52,2
S27	410,3	21,8	45,5	414,3	22,0	40,4
S31	421,9	41,0	39,2	290,0	29,0	45,5
S32	369,1	31,8	46,8	331,5	28,8	45,2

Tests performed under standard conditions, extension rate of 0.52 mms^{-1}, whenever rupture occurred close to the jaws, tested specimen was replaced by similar specimen cut from "HW" or "GW" specimens.

3.6 Apparent Density Measurements

The standard ASTM D2346-91 defines a method for measuring the apparent density of leather. This method is based on two other ASTM standards, ASTM D1813-89 Measuring Thickness of Leather Test Specimens and ASTM D2347-91 Measuring Area of Leather Test Specimens.

Measurements of apparent density comprehend four steps, measuring weight, measuring area, measuring thickness and perform calculation of apparent density.

The measurement procedure starts with accurate measuring of the mass of the specimen with an electronic balance (METTLER Toledo PB302, resolution ± 0.01 g).

Next, the area of these circular specimens is obtained by measuring the diameter of the specimen with a steel ruler. The ruler is placed across its widest girth and four measurements are taken at radii approximately 45° to each other.

Next, eight thickness values are taken at radii approximately 45° to each other, equidistant from the rim and the centre of the specimen.

Finally, all data is introduced in MATLAB and a script averages the four diameter measurements as well as the eight thickness values, computes the area and apparent density. Apparent density is computed by dividing the weight of the specimen in kilograms by the product of the area in square metres by the average thickness in metres. The MATLAB script also saves all data in a MATLAB format file.

Despite specimens "I" being larger than recommended by the ASTM standards for apparent density measurements, their apparent density was measured.

The plot of Figure 3.12 presents the apparent density values of the tested "I" specimens measured according to the procedure described above. In Figure 3.12, the apparent density of, for instance, specimen S14I (side 1, position 4, specimen I) is read from the curve S1I "Sample position" 4.

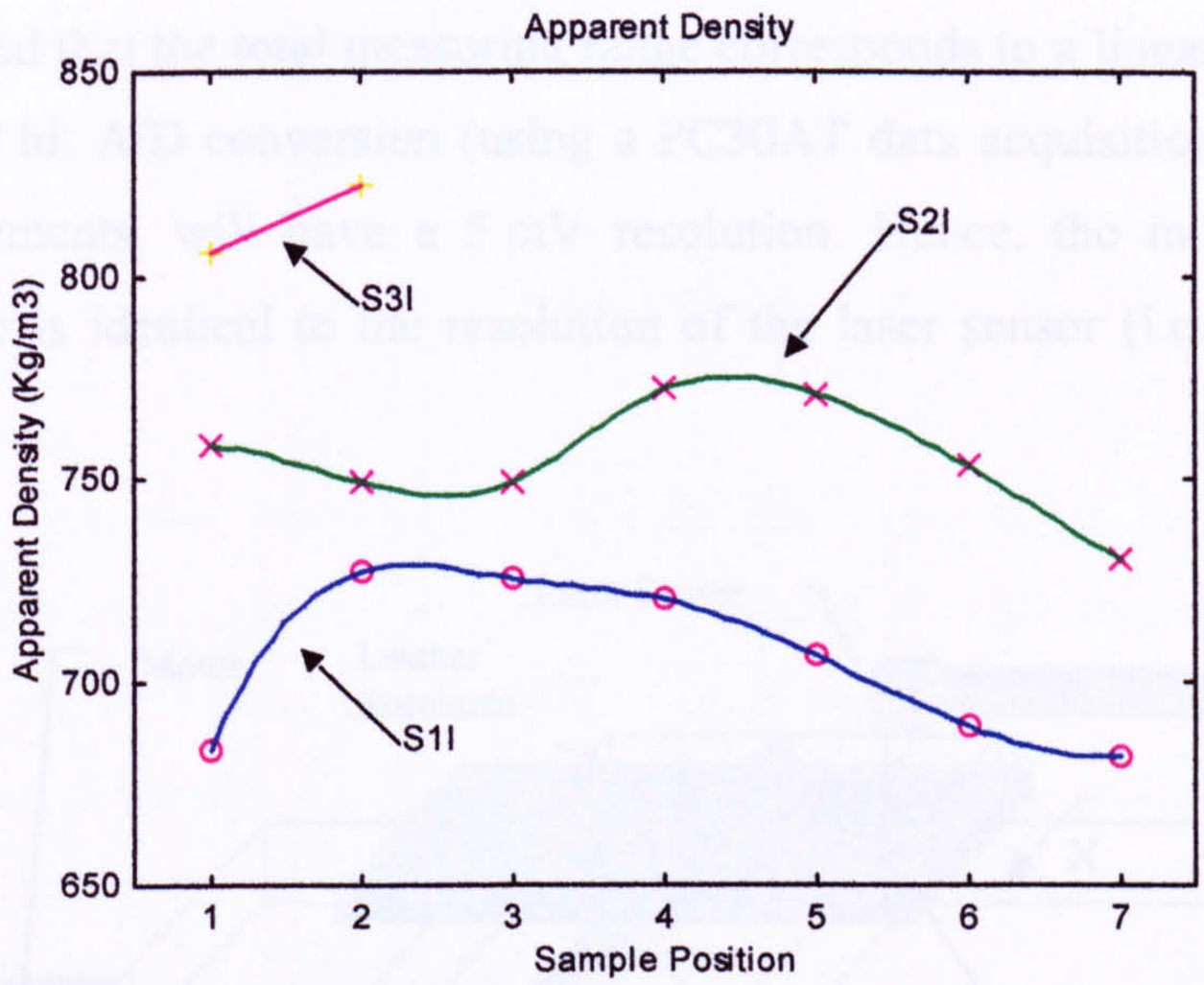

Figure 3.12-Apparent Density of "I" specimens.

3.7 Surface Roughness Tests

Surface roughness can be measured in two ways, either using a contacting method or a non-contacting method. A non-contact method based on laser has here been chosen to profile the surface because of the much higher accuracy and the fact that no pressure is applied on the specimen.

3.7.1 Instrumentation and Measuring Method

The test arrangement seen in Figure 3.13 consists of a laser sensor that is firmly attached to a fixed stand pointing downwards onto the slowly moving surface of a piece of leather which is placed on the X-Y table. The laser uses the triangulation technique (see Appendix B) to measure the distance between itself and the leather surface. Triangulation has the advantage of not being susceptible to colour changes or patterns providing that sufficient light is reflected back from the surface and is therefore well suited for leather testing. A beam of red light (675 nm) with a 300 μm diameter spot is projected from a laser diode onto the surface of the leather. Part of the emitted light is scattered back onto a photosensitive detector, which then signals the position of the image from it. As the reflected light strikes the detector at different locations depending on its distance from the fabric surface, the signal strength indicating the location of the reflected light is converted to distance. The sensor used for the present work (LD1605-4 by μ-Epsilon®) is capable of measuring a distance range of 4 mm with a resolution of 1 μm. Further technical specification of the laser sensor can be found in Appendix B.

Bearing in mind that the total measuring range corresponds to a linear voltage output of +/- 10 V, a 12 bit A/D conversion (using a PC30AT data acquisition card), as used in these measurements, will have a 5 mV resolution. Hence, the minimum detectable analog voltage is identical to the resolution of the laser sensor (i.e., 5 mV represents 1 μm).

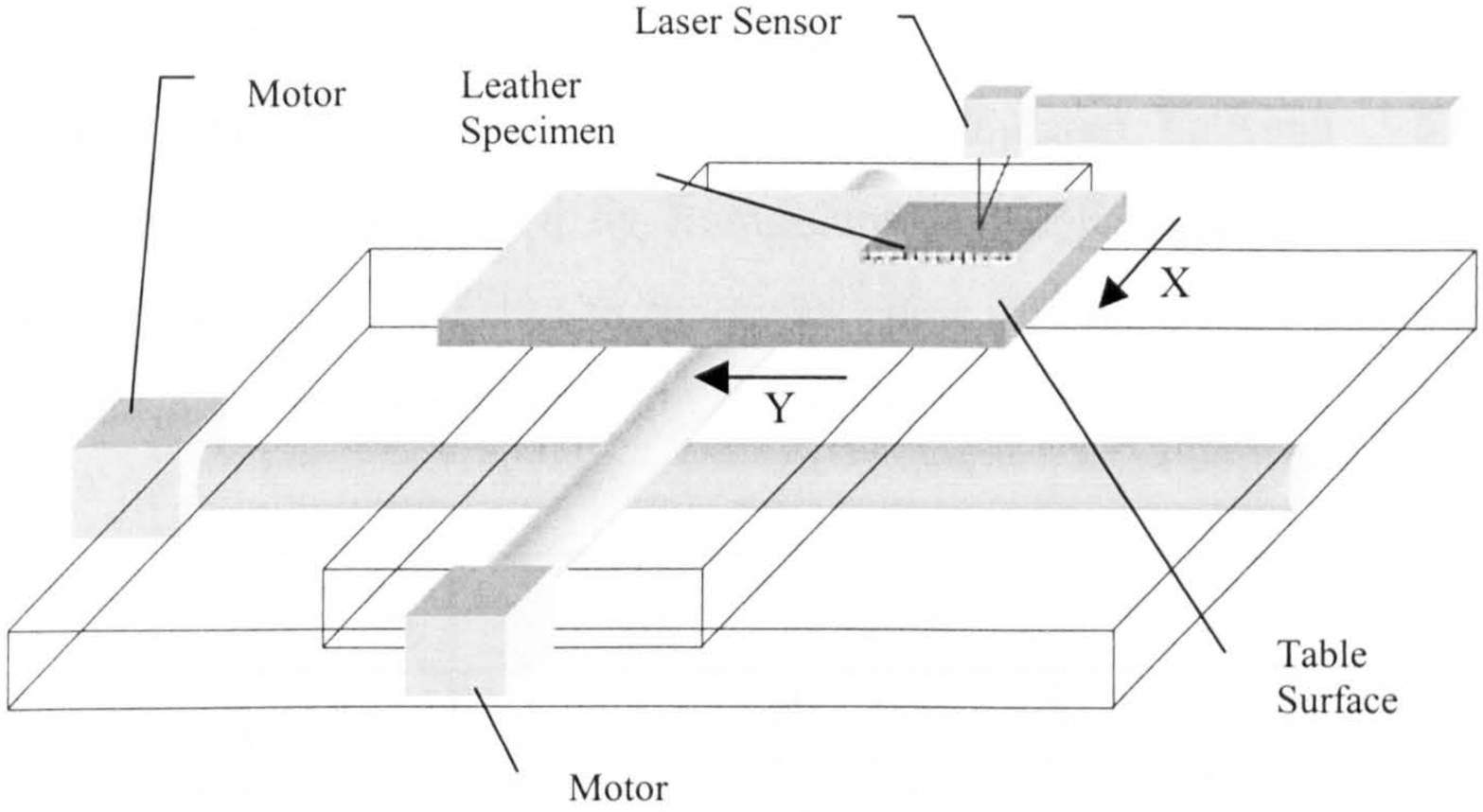

Figure 3.13-Sketch of the surface roughness test.

Leather specimens are measured eleven times in the forward X direction by the laser sensor over a 1 cm length, at Y step size of 0.1 mm. The specimens are placed stress free on the rubber surface of the X-Y table with the grain side of the leather upwards. The table is moved then at a velocity of 0.1 mms^{-1} while the voltage signal from the laser sensor is sampled at a rate of 500 Hz, giving 5000 samples in total for each pass in the X direction. Next, whilst keeping the leather untouched, the table moves back to its home position (in the X direction) and shifts 100 μm in the Y position ready for the next line scan. After a full test of eleven scans in one direction, the leather is turned 90° to face along the other principal direction. Thus, all leather specimens are tested eleven times in both directions (parallel and perpendicular to the backbone) covering a total area of 1 cm^2.

3.7.2 Roughness Testing Results

The surface roughness (SMD) of a leather specimen is calculated in accordance with the KES-FB4 test [Kawabata 80]. Here, a well established method from the textile area is used. The surface roughness is calculated from its height profile, h_i, obtained by the

laser sensor at *s* different points and is defined as the mean deviation, which is given as follows:

$$SMD = \frac{1}{S}\int_0^S \left| h_i - \bar{h} \right| ds \qquad (3.7)$$

with $\bar{h}$ representing the mean value of the heights. In order to compensate for any undulations of the leather, two mean heights and the local roughness based on them are calculated for 4 mm subdivisions; (SMD1) was calculated between 2-6 mm and (SMD2) between 6-10 mm as used by Ramgulam *et al.* [Ramgulam 93] (see Figure 3.14). The area in Figure 3.14 between the mean value and the actual roughness curve represents graphically the numerator of Equation 3.7.

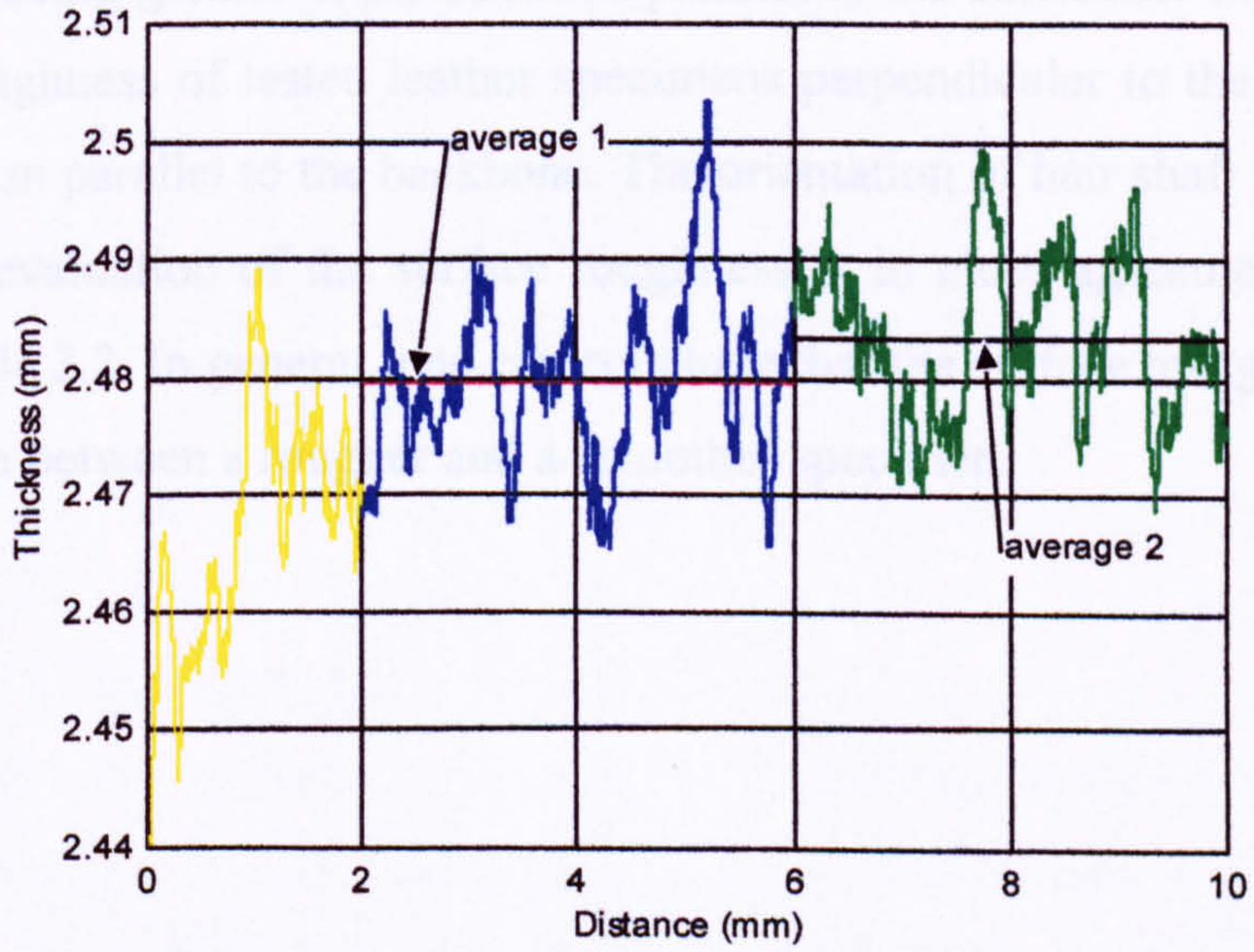

Figure 3.14-Profile scan perpendicular to the backbone.

Scanning the table, in an identical way as leather, produced an average surface roughness of 2.6 μm, indicating a smooth table surface. A two-dimension calibration matrix was also produced in order to eliminate the effects of eventual inclination of the X-Y table. Hence, the table will not superimpose any profile on the leather. As a comparison, the rubber surface has also been measured with a stylus, giving however, a ten fold lower surface roughness (0.2 μm). This shows, as has been detected for fabrics [Ramgulam 93], that a contact method gives a smaller roughness figure than a non-contacting method.

Six roughness values thus obtained from Equation 3.7 are averaged to give the mean roughness of the leather along each principal direction (see Table 3.2).

Table 3.2-Mean roughness values of the three standard specimens.

Leather Sample	Parallel to Backbone	Perpendicular to backbone
S14	8.6 μm	46.4 μm
S24	3.7 μm	20.2 μm
S32	14.5 μm	87.0 μm

A first glimpse at Table 3.2 shows that all SMD roughness values are in the same order of magnitude being greater in the direction parallel to the backbone. The mean deviation of surface roughness of tested leather specimens perpendicular to the backbone is five fold higher than parallel to the backbone. The orientation of hair shaft may explain such result. Hand evaluation of the surface roughness is in close agreement with the trend shown in Table 3.2. In general, one can conclude that the surface test gives a reasonable discrimination between a rougher and a smoother specimen.

4

4 Mechanical Scanning System

4.1 Introduction

This chapter presents the philosophy, design and implementation of a non-destructive leather testing cell designated Mechanical Scanning System (MSS). The results of experiments performed with the MSS are also presented.

The chapter begins with an overview of the concept of the MSS, followed by a detailed description of its mechanical and electronic hardware. The most relevant parts of the software specially written for this scanning system are described too. Finally, all results are shown as well as a small evaluation of these. This system was object of a European patent application that was published in September 1998 (see Appendix C).

4.2 Design Philosophy

The testing apparatus comprises two pairs of wheels, between which the leather passes. By adjusting the speeds and spacings of the wheels and by measuring the torques and positions of the wheels, various characteristics of the leather can be inferred, for example: Tensile Modulus for low strain regions along scanning lines, softness along scanning lines, compressibility across thickness and thickness. A laser sensor can be provided to measure surface profile (roughness).

A simple sketch of a sectional view of the Mechanical Scanning System is shown in Figure 4.1. A first nip is formed between wheel #1 & #2 (first pair of wheels) and a second nip between wheel #3 & #4 (second pair of wheels). A DC motor can drive each wheel. In order to measure the torque applied by the DC motors on wheels #3 & #4, two torque sensors are used. Wheels #2 & #4 are fixed, while the vertical position of wheel #1 is variable and spring loaded. The vertical position of wheel #3 is also adjustable and controlled by a stepper motor. A load cell is also provided for measuring

the compression force between wheel #3 & #4. The distance between wheel #3 & #4 is accurately measured with the aid of a very accurate displacement transducer.

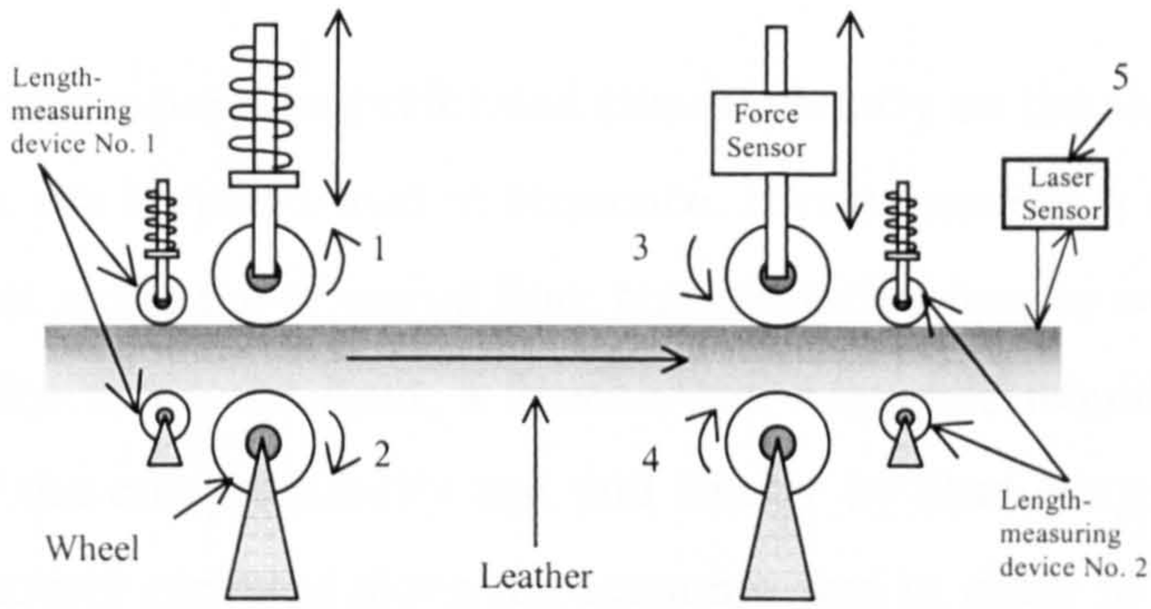

Figure 4.1-A sketch of the Mechanical Scanning System.

Using the available resources of the MSS it was then possible to perform several tests on a sample of leather in order to obtain the required information for leather characterisation.

The piece of leather to be tested is passed trough the nips at constant speed. In order to obtain data for inferring the Tensile Modulus for low strain regions along the scanning line, the speed of one pair of wheels is then modified with the purpose of stretching the sample. This stretching causes an increase of torque, which is measured by the torque sensors. It is this measurement that allows the computation of the above-mentioned physical property.

The compressibility across thickness of the leather can be determined by closing the nip between the wheels #3 & #4 of the second pair of wheels, measuring the reduction in the size of the nip and also measuring the force applied by the wheels #3 & #4. From this, the measuring system can produce a measurement of compressibility of the leather across its thickness and softness.

It follows, from the previous test, that the testing apparatus can also measure the thickness by measuring the distance between the wheels #3 & #4 at a predetermined compression force.

Shear stress across thickness is also possible to obtain. The leather sample is clamped between wheels #3 & #4 and these two wheels start to rotate in the same direction at the same speed. By measuring the torque applied by wheels #3 & #4, shear stress across thickness can be deducted.

A laser sensor can also be used in order to obtain the surface profile of the leather. This test is similar in every way to the surface roughness test described in the previous chapter, consequently no further reference is made to this test.

Obviously, these tests cannot be performed simultaneously on the same sample location, although the tests can be performed in sequence. If one assumes a smooth transition of physical properties along the scanning line, representative results would be expected. If an industrial device was to be built, a feasible test sequence would be the shear stress test, followed by the compressibility test and finally by stretching. This test sequence would be continuously repeated along the scanning line in order to obtain a map of the desired properties.

4.3 Detailed Implementation

4.3.1 Components of MSS

With the purpose of implementing the concept presented above, a mechanical device was built. The apparatus consists of a large aluminium framework (500 x 800 mm) comprising several mechanical and electronic components (see Figure 4.2).

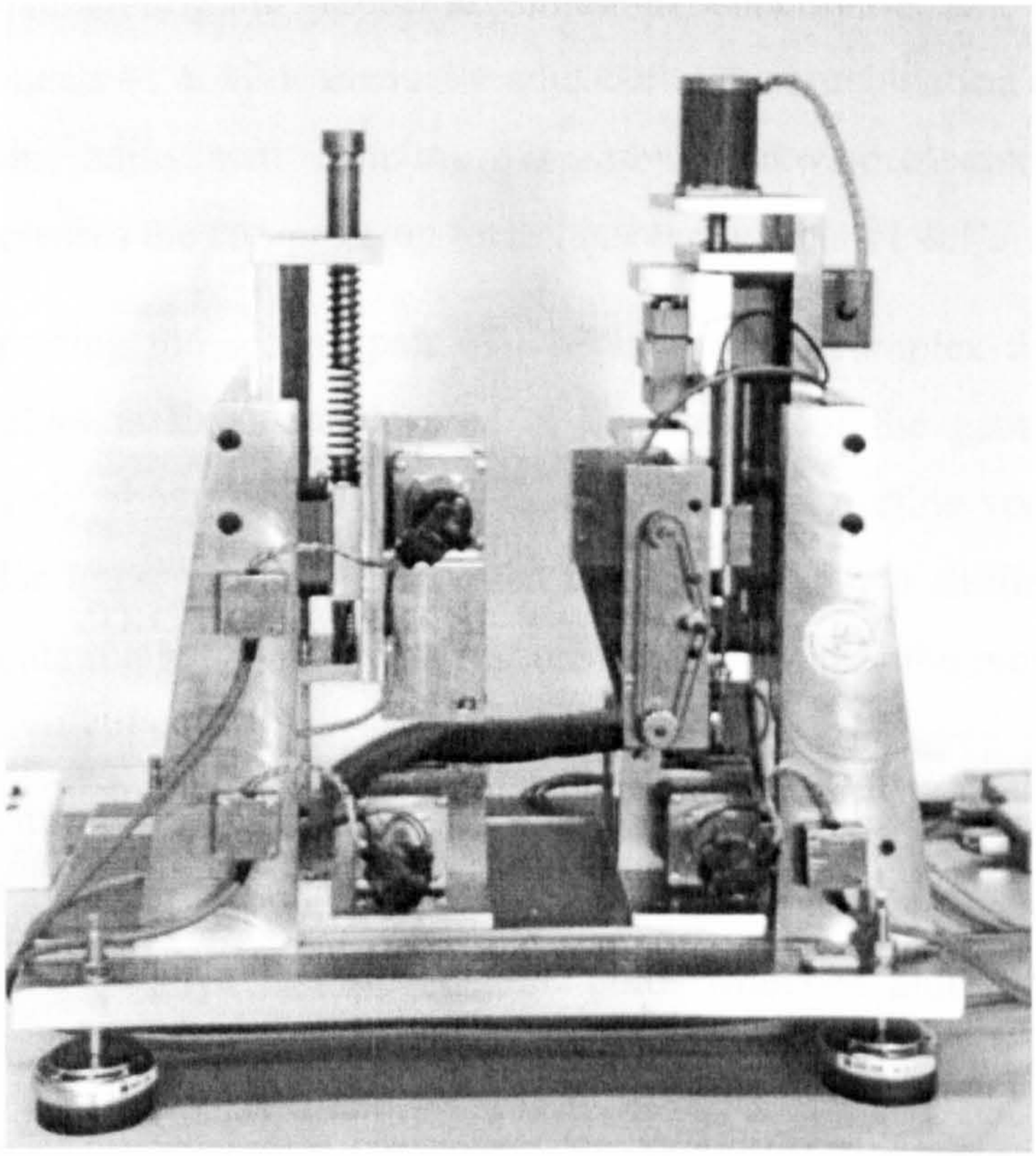

Figure 4.2-View of the Mechanical Scanning System.

The aluminium framework is composed of a base plate and two gantries holding the two pairs of wheels. The structure of the second pair of wheels is bolted to the aluminium base plate in a permanent position. On the other hand, the structure supporting the first pair of wheels is adjustable horizontally in order to enable the pre-setting of the distance between the two pairs of wheels (direction of the length of the leather sample). This distance ranges from 5 to 30 cm. The full system is mounted on rubber bobbins acting as damping units.

The gantry supporting the first pair of wheels includes a fixed wheel (wheel #2) located at the bottom. Wheel #1 is located immediately above wheel #2 and its position is adjustable vertically. For this purpose, a self-aligning, high load, low friction sliding system was adopted. A linear guide rail (LTH25-300 from NSK-RHP) is bolted to the gantry; a ball slide (LAH25ANZ from NSK-RHP), based on a recirculating ball system, is responsible for limiting the motion of wheel #1 and its driving system to one degree of freedom. The sliding system is particularly resistant to overturning loads. This characteristic is especially important in this application because when leather is stretched, a rotational moment is generated on wheel #1 unit. This sliding system also contributes for maintaining the vertical alignment of wheels #1 & #2. The compression force between wheels #1 & #2 is manually adjustable; the combination of a screw and a spring enables this adjustment. Rotating the screw clockwise compresses the spring, which in turn increases the compression force between wheels #1 & #2.

The gantry supporting the second pair of wheels is more complex than the one just described. Wheel #4 is fixed and located at the bottom of the gantry. Wheel #3 is located immediately above wheel #4 and its position is adjustable vertically. For this purpose, a similar linear guide rail is bolted to the gantry; two similar linear guides, based on a recirculating ball system, are responsible for limiting the motion of wheel #3 unit (driving system and compression force sensor) to one degree of freedom (see Figure 4.3). Because the compression force sensor (±50 lbs single axis load-cell) should not be subjected to out of line forces, the adopted solution was to use two linear guides sliding on the same rail. The first linear guide holds wheel #3 unit and one end of the load-cell, while the second linear guide holds the other end of the load-cell. The second linear guide is also attached to a lead screw through a rectangular nut. This 300 mm long lead screw in combination with a stepper motor enables precise computer controlled positioning of wheel #3. The combination of a 1.8° stepper motor, driven in

half-step mode, with a 2 mm lead screw pitch gives a theoretical linear displacement precision of 5 μm per step. Although, stepper motors can be run in open-loop mode with sufficient accuracy, an extra sensor for measuring this displacement is provided. To monitor the exact position of wheel #3 a displacement transducer (LVDT) is used, also providing the distance between wheel #3 and wheel #4 in a direction along a line normal to the axes of rotation of these wheels.

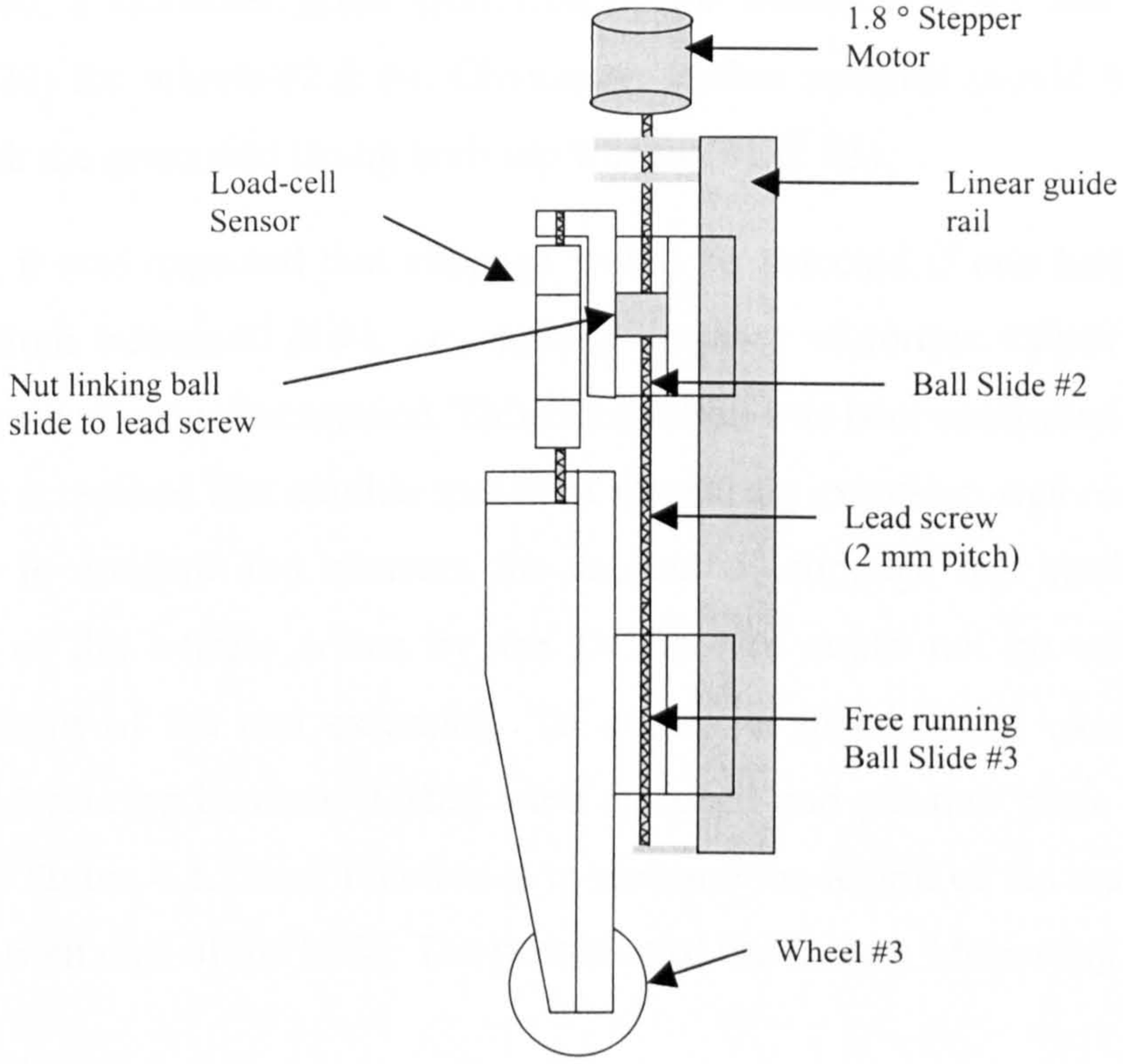

Figure 4.3-Skectch of a sectional view of Wheel #3 unit.

Each of the four wheels has its own driving system, which includes the following components: a DC motor, an encoder and a 500:1 ratio gearbox. In addition, each wheel of the second pair (wheel #3 & #4) has an associated torque sensor for monitoring the torque applied to the said wheel (see Figure 4.5). Furthermore, the position and velocity of each wheel is computer controlled. All four wheels have the same physical dimensions: 40.05 mm of diameter by 15 mm wide.

After performing some preliminary tests with the MSS, stretching leather in particular, it was found that the friction coefficient between the aluminium wheels and the leather specimens was too low. As soon as forces increased, slippage of the leather specimen between both pairs of wheels would occur even for high compression forces on both

nips. A solution had to be sought to increase the friction coefficient. The easiest way out would be to cover all four wheels with emery paper. Other options, such as wheels with small smoothed spikes and other kind of patterns, were also considered. However, emery paper proved to be an adequate solution for this study, because no relevant sample damage occurred even in extreme stretching conditions. Because friction coefficients of grain side and flesh side are very different, two grades of emery paper were used, a smoother grade (Ref. P1000) for wheels #1 & #3 and a rougher grade (Ref. P120) for wheels #2 & #4. Obviously, leather samples should be scanned in the MSS with the grain side facing both top wheels (#1 & #3).

Initially, it was expected that slippage would be detected if one looked at the torque signals from wheels #3 & #4, i.e., sudden decrease of torque values while stretching would mean slippage occurrence. This expectation was later confirmed in practice. Only then was it realised that another means of measuring extension was required and useful in order to confirm and measure the amount of slippage that really occurred. The position of the wheels driven by the DC motors could not be taken as a reliable measurement of the real extension. To overcome this initially overlooked problem, Length Measuring Devices (LMD) were designed and put into place as shown on the sketch of Figure 4.1. Their function is to measure the length of the material that travels between both nips of the MSS. The precision of the Length Measuring Devices is about 10 μm.

4.3.2 Electronics

The control of the whole Mechanical Scanning System is based on an ISA bus servo I/O card from ServoToGo, Inc as presented in Figure 4.4.

This card is a low cost, general purpose, motion control input/output board that can control up to eight motors simultaneously from an ISA-bus based computer such as an IBM compatible PC. This servo I/O control card includes resources for accepting signals from encoders, analog output, analog input, digital input/output and timers.

The ServoToGo servo I/O control board relies heavily on the processor of the host computer, in contrast to many other commercially available motion controller boards that sometimes possess two extra on-board processors to guarantee real-time control. However, the price of the latter type of board is several times higher than the ServoToGo board.

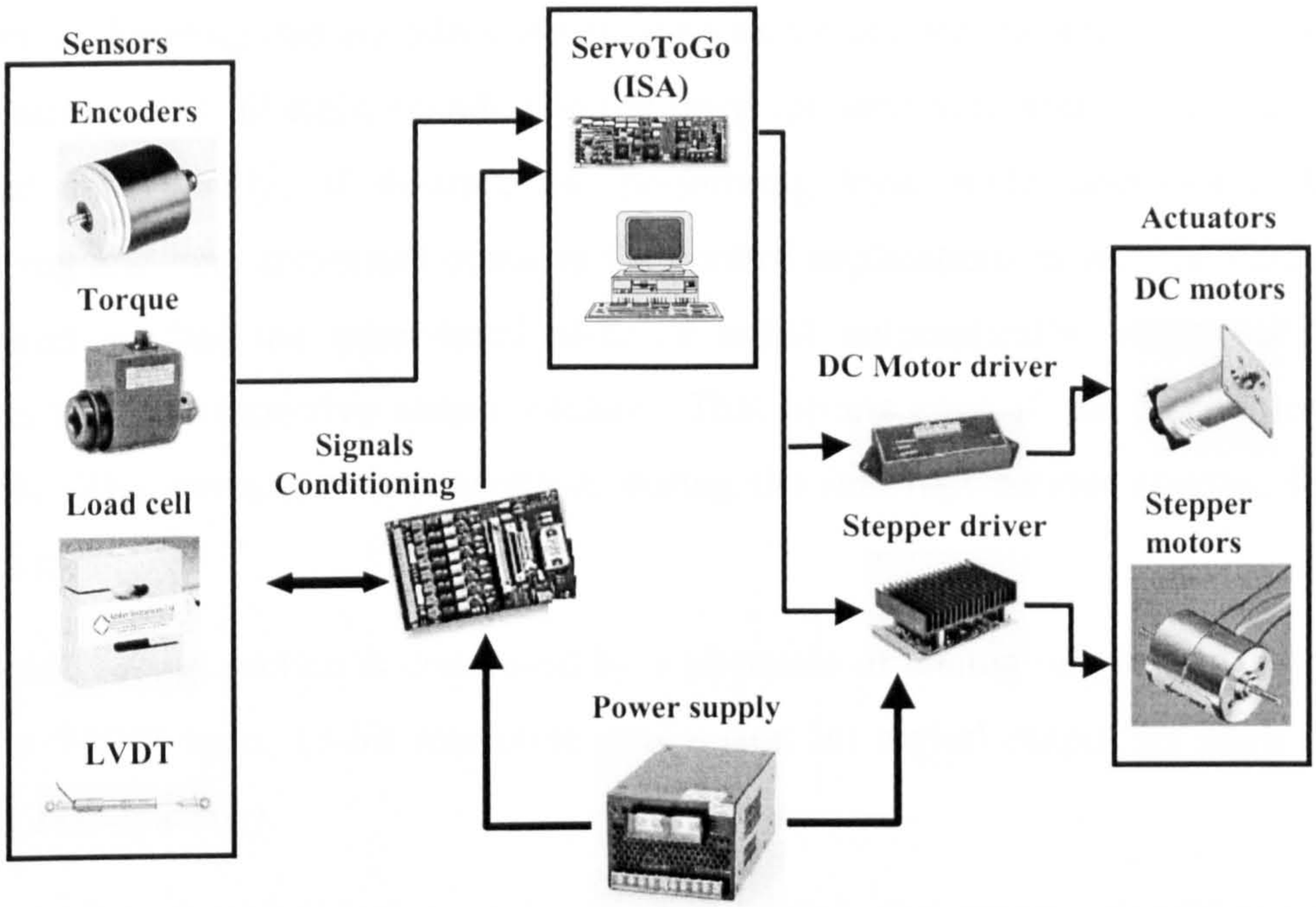

Figure 4.4-Mechanical Scanning System hardware architecture.

The ServoToGo board is accessed by the use of a set of registers located in the I/O addressing space of the PC. The board can be configured to generate periodic interrupts to the PC. This is necessary when the board is used in a control algorithm application. This servo control I/O board includes several features described below.

There are eight encoder input channels that can accept quadrature encoder inputs: "A", "B", and "I" (sometimes called "marker") input. From this input stream a 24-bit position count is generated. The hardware can be configured so that the count is multiplied by 1, 2, or 4. As a convenience, the count value is automatically latched to all counters for reading by a real-time interrupt.

The actual inputs are buffered using a RS-422 compatible receiver which accepts either differential or single ended inputs. For differential inputs, both inputs need to be connected for each channel. For single ended operation only the positive input (for example A+) is to be connected. If one of the encoder inputs becomes disconnected, the counter will increment and then decrement on each edge of the other pulse. This may be used to determine if the inputs are valid by detecting a count change of at least two. The maximum encoder input rate is 1.2 MHz.

The counter specific registers are arranged in memory so that two registers for two axes can be read or written simultaneously by performing word wide read and write

operations. Reading two encoders at a time saves a considerable amount of processing time when reading all eight encoders in the interrupt service routine. They can also be accessed individually, if desired, by performing byte wide operations. Another timesaving and very important measure for control applications is that the hardware is configured so that the timer-terminal-count event automatically latches all of the counters to their respective output latches. This occurs even if the timer interrupt is disabled. This saves a write operation, during the interrupt service routine, for each encoder input.

The analog output section is composed by 8 channels of analog output (DACs), with a -10 V to +10 V span, 13-bit resolution and a sign bit digital output for each channel (Opto-22 compatible).

In a control application during each sampling period, the control algorithm needs to read the encoders and write to the DACs. The encoders can be automatically latched when the periodic interrupt occurs. It is also possible to select whether or not the DACs are also simultaneously latched at the instant of the periodic interrupt. If both the encoders and DACs are latched by the hardware, the control algorithm can be performed at anytime during the window, with no change in performance from one sampling period to the next.

The digital I/O section provides 32 input or output signals. The signal levels and connectors are Opto-22 compatible for direct connection to industry standard isolation I/O modules. The signals come from an 82C55 integrated circuit, which will sink or source a maximum current of 5 mA. An internal 10KΩ resistor pulls up each line to +5 volts; so inputs will default to a known level if a line is broken or not connected. During initialisation, the control register should be set by the software to select which lines are inputs and which are outputs, then the output bits should be initialised by writing to the port registers.

The analog input section is composed by 8 channels of analog input (ADCs). The possible input voltage ranges are –10 to +10 V, and –5 to +5 V. The input resolution of the ADC will be 13 bits for these ranges. Obviously, the resolution would be 12 bits for 0 to 5 V and 0 to 10 V spans.

The timer section provides the possibility of generating a periodic real-time interrupt request that can be used for implementing control algorithm applications. The timing

control of the board is based on an 82C54 integrated circuit. The interrupt time interval is programmable from several microseconds up to ten minutes.

The board contains an optional battery connection. In the event that power should be lost to the card, the encoder counters will not loose their position count and will continue to operate if a battery is connected and the encoder counters are powered.

The board contains a "watchdog" timer that will be constantly watching writes to the card. If no writes occur within a specified time, the watchdog will time-out and "bark", thus signifying that something has gone wrong, for example, the processor may not be responding to interrupts as it should. When the watchdog times-out the output of the DACs are set to zero. This event can be used to trip a relay in order to take some external action such as applying breaks to the machine that is being controlled. The watchdog's time-out times are in the range 62.5 to 250 milliseconds.

The interrupt controller section manages all the interrupt sources within the board and their link to the computer such as an IBM compatible PC. The possible interrupt sources are: a real-time interrupt from the interval timer; index pulse interrupts from the encoder counters when overflow occurs; end-of-conversion interrupt from the analog-to-digital converter. The board uses an 82C59 interrupt controller, but only a few features of this chip are used. In this application, this integrated circuit only needs to be initialised and the interrupts need masking and unmasking.

Although the MSS base component is the ServoToGo board, there are many other important subsystems responsible for measuring torque, force, distance, displacement and driving motors.

One of the most important measurements performed by the MSS is the torque applied on wheels #3 & #4. For this purpose, wheels #3 & #4 units are instrumented with one torque sensor each. This sensor is an in-line rotating shaft sensor from Crane Electronics, Ltd (5 Nm IS CheckStar Hex Rotary Transducer) with a maximum capacity of 5 Nm. The measurement technique employed by these sensors is based on a strain gauge bridge glued to the rotating shaft whose connection to the sensor body is achieved using four silver slip rings. In Figure 4.5, wheel #4 unit is shown. The strain gauge bridge excitation is done with a precision voltage reference (Analog Devices AD586), while the torque sensor output amplification is based on a low power, high

accuracy instrumentation amplifier from Burr-Brown (INA102). The overall theoretical resolution of the torque measurement system is approximately 0.003 Nm.

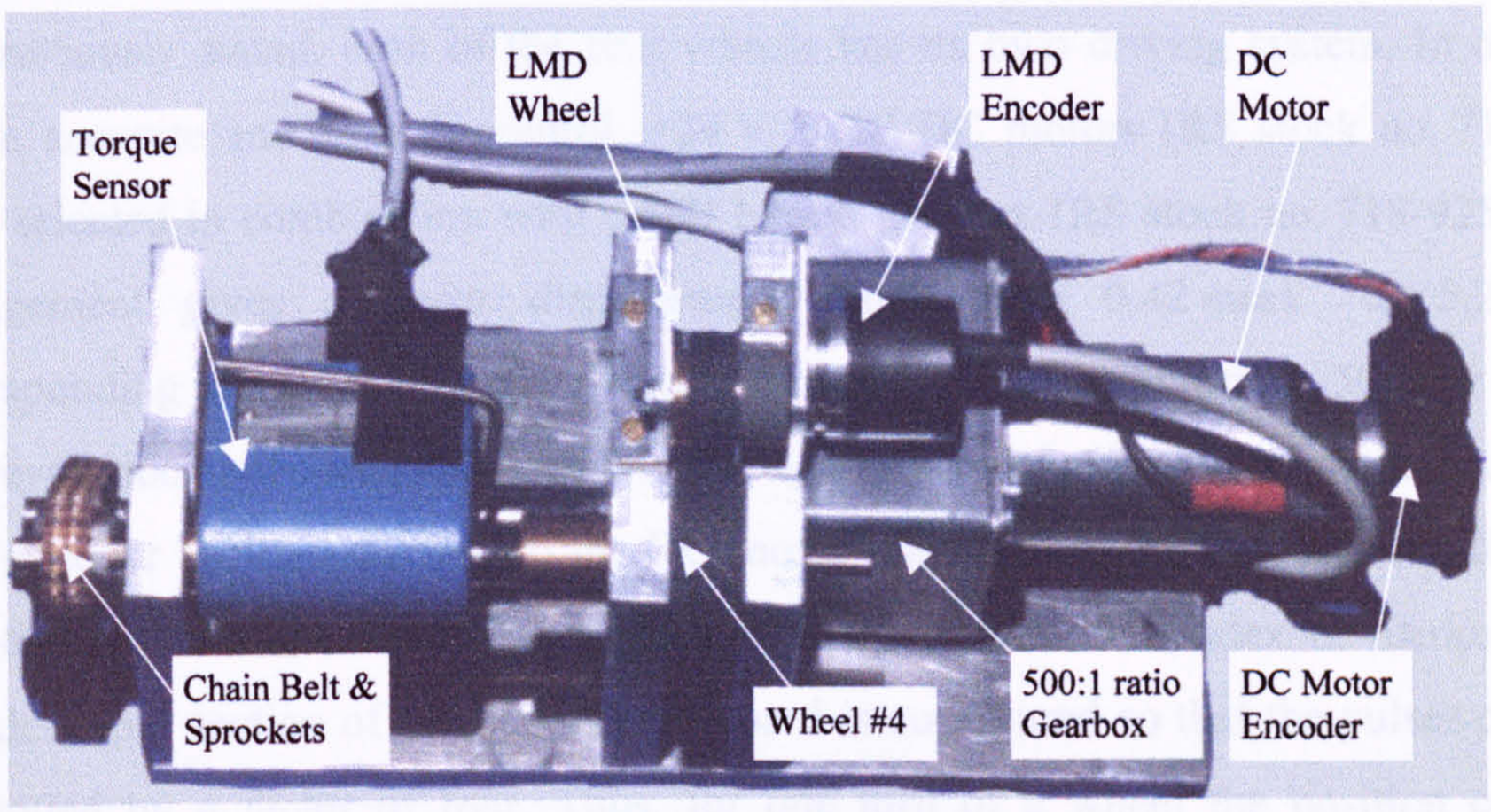

Figure 4.5-View of wheel #4 unit.

In order to measure the compression force between wheels #3 & #4, a general-purpose 50 lbs compression/tension load cell from Amber Instruments, Ltd was selected (Ref. 3185-50). The excitation and amplification of the load cell is performed by an Intelligent Load Cell Conditioning Amplifier (LCA 15), and was acquired to the same company. The LCA 15 proved to be very convenient as it allows the programming of the output range according to a desired input range. This characteristic enables the utilisation of the full input range of the analog to digital conversion section, thus providing maximum resolution. The overall resolution of the compression measurement system is approximately 3.7 g.

An LVDT (Linearly Variable Differential Transformer) displacement transducer is used for measuring the distance between wheels #3 & #4. This device consists of three coils, one for energisation, two for pick-up and a movable nickel iron core. The energisation coil is driven by a 5 KHz sine wave that produces an output and phase which is directly proportional to the position of the core with respect to the pick-up coils. A phase sensitive detector is required to demodulate the output signal. The main advantages of LVDTs in this particular application are: no friction introduced into the measured system, infinite resolution, high accuracy and linearity. In the MSS, a ±25 mm stroke LVDT is used (Schlumberger AC 25, RS stock no. 646-555) plus a single channel oscillator/demodulator (OD5, RS stock no. 285-908). The overall resolution of the

wheel #3 position measurement system is approximately 1.2 μm, being the full measurement range about 5 mm.

As previously stated, each of the four wheels has its own driving system. In order to obtain accurate and smooth control, +24 V 16 W DC motors (RS stock no. 715-112) were selected in combination with a 500:1 ratio gearbox (RS stock no. 718-925). This arrangement gives a linear displacement range from 0.42 mms^{-1} to 5.2 mms^{-1} corresponding to a DC motor speed range from 100 rpm to 1250 rpm. A 500 ppr (pulses per revolution) encoder (RS stock no. 205-6881) gives feedback for position control. This encoder is fitted directly to the DC motor rear shaft and provides resolution and direction information as well as a pulse once per revolution (index or marker). The encoder input section of the ServoToGo board is configured so that the pulses count is multiplied by a factor of four. Thus, for one turn of a wheel the position count is incremented by 1000000, for a wheel diameter of 40.05 mm, gives a theoretical resolution of 0.126 μm per count. Obviously, mechanical constraints such as gearbox backlash prevent this sort of resolution.

The two Length Measuring Devices are very simple devices and are based on an encoder (RS stock no. 341-597) plus a small gearbox providing a resolution of 11.76 μm per count.

The ServoToGo servo I/O control board is hosted by an ISA-bus based Pentium computer running at 100 MHz. This PC using software that runs on MS-DOS operating system controls all data acquisition and all hardware of the Mechanical Scanning System.

4.3.3 Software

The Pentium based personal computer is responsible for motion control of all five motors as well as controlling the data acquisition from sensors. Data acquisition, test and control routines have been implemented in "C" and "C++" programming language using Borland C++ v.3.1 compiler, under the Ms-Dos operating system. Analysis software, like curve fitting, data smoothing and other computations, have been implemented in scripts or functions ("m-files") for Matlab. These kinds of tasks are easily executed with Matlab scripts and functions, on the other hand if they had to be implemented in "C" programming language, it would demand a greater effort in writing

and debugging software. Another advantage of this approach is the graph capability and supported toolboxes variety of a software as Matlab.

Control algorithm applications, like this one, require precise timing control for sampling inputs, execute computations and update outputs. An interrupt-driven system is ideal for these applications and this is one of the reasons for working in Ms-Dos because the programmer has full control of all the PC resources. Despite Windows operating system being event-driven, it could also have been used but it would be necessary to develop software according to the Windows Driver Model (Windows 98 and Windows 2000) which would be considerably more complex and time consuming at the time the system was developed.

The control software architecture is based on interrupts generated by the timer section of the ServoToGo board. For the vast majority of the experiments carried out with MSS, the frequency of the interrupt request was 500 Hz. Despite being adjustable, this timing is an adequate compromise for this application in terms of quantity of data created and controllability. A sampling rate too high generates a high amount of data; a sampling rate too low prevents among other things a smoother motion control.

The positioning control of the four wheels is performed using a Proportional-Integral-Derivative (PID) controller. The tuning of the PID regulators, adjusting and optimising the system response, was performed according to Ziegler & Nicholas second method of adjusting gains of the PID controller.

All digital and analog data acquired in an experiment using the MSS are saved in a condensed binary format file, which is later read by a Matlab script function. The size of this data file is about 300 Kbytes for a 30 seconds long test. The analog data is saved in raw format, i.e., as acquired from the ADC (Analog to Digital Converter). The conversion to SI units is performed in Matlab, using calibration data previously recorded and applying cubic splines interpolation methods.

The user interface of the software which controls the Mechanical Scanning System is shown in Figure 4.6. This command line environment can be used for performing a variety of tasks, from reading a digital input to carrying out development process for debugging and configuration of many important control variables.

Three main areas compose the user interface screen, information frame on top, message frame just below and finally the last line for command line input.

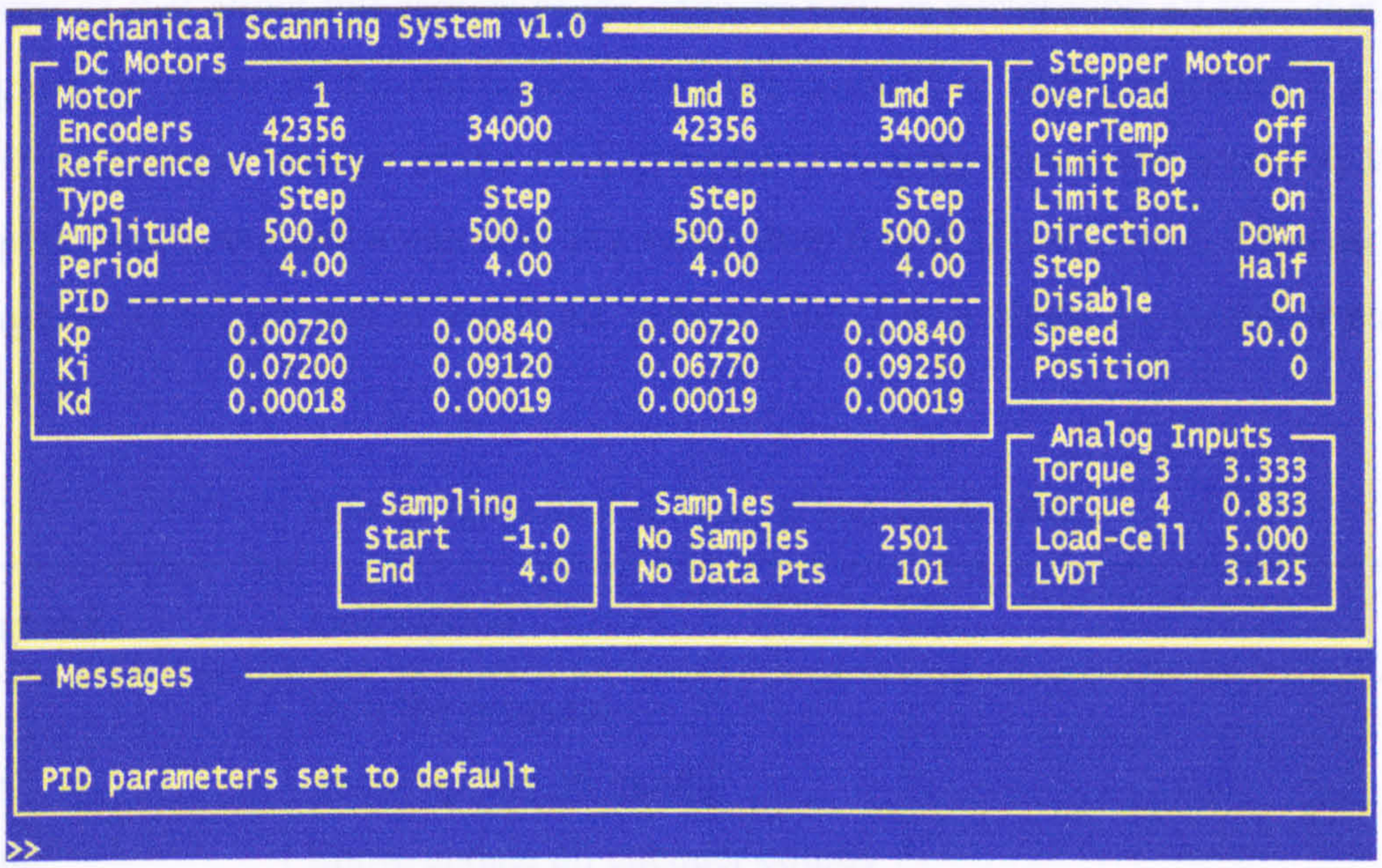

Figure 4.6-MSS control software user interface.

The information frame is divided in five sub frames: DC Motors, Stepper Motor, Analog Inputs, Sampling and Samples. The Samples sub frame shows the total number of samples to acquire during the sampling period, as well as the number of data points to be saved in a file. The Sampling sub frame presents the time to start and to end the sampling period in seconds, having in mind that motion always starts at time 0 seconds. The Analog Inputs sub frame gives the value in Volt for: the torque of wheel #3 (Torque 3), the torque of wheel #4 (Torque 4), the load-cell and finally the LVDT displacement transducer. The Stepper Motor sub frame shows relevant information about the stepper motor like: set speed, actual position in steps of wheel #3 unit, full or half step mode, direction of motion. The DC Motor sub frame presents all coefficients of the PID controller of each wheel; it also shows the reference velocity type, amplitude and period for each wheel; the number of counts of encoder of wheel #1, wheel #3 and both Length Measuring Devices.

The message frame objective is to display replies to command line inputs or warnings while running higher-level commands. This frame can show information such as, counts of all six encoders and all digital inputs.

On the last line of the screen is located the prompt where all commands are entered.

The commands defined for controlling the MSS carry out tasks of different level of complexity, as shown in Table 4.1. This table is just a partial list of all available commands that allow full control of the MSS as well as performing all tests that it was designed for. Some of the commands take extra numeric or text parameters, e.g., "vout *n*,-1.0" sets output voltage of the DAC (Digital to Analog Converter) *n* to -1.0 Volt. In this particular command *n* can take any value from 0 to 8, if $n = 7$ DAC 7 has an output voltage of -1.0 Volt and if $n = 0$ all DACs from 1 to 8 show an output voltage of -1.0 Volt.

Table 4.1-Partial list of commands of MSS control software.

Command	Description
"q"	Quit the program
"shin"	Show/update all inputs
"shenc"	Show/update all encoder counts
"p *n*"	Repeat last command *n* times
"out *n*,*value*"	Sets digital output *n* to *value*, if $n = 0$ sets all outputs
"vout *n*,*value*"	Sets DAC output *n* to *value*, if $n = 0$ sets all DACs ($0 \le n \le 8$)
"tachrst"	Resets all encoder counts to 0
"kp *n*,*value*"	Sets proportional gain of motor *n* to *value*, if $n = 0$ sets Kp for all DC motors ($0 \le n \le 4$). Similar commands for Kd and Ki
"wrpidconf"	Saves PID gains of four motors in a configuration text file named "confpar.txt", "rdpidconf" reads parameters from file
"ref *n,type,mag,t*"	Sets reference motion profile for each DC motor
"st"	Runs DC motors according to selected reference motion profile during time set by command "tend"
"step *n*"	Stepper motor gives *n* steps
"stspeed"	Sets stepper motor speed in steps per second
"stdir"	Toggles stepper direction making wheel #3 unit go up or down
"comp"	Performs a compressibility test according to set of parameters, like speed of stepper motor…
"tstart *value*"	Sets time to start collecting data to *value* in seconds
"tend *value*"	Sets time to stop collecting data to *value* in seconds and stop motion

The motion profile of each wheel (velocity profile) is set using the command "ref *n,type,mag,t*". This command sets the reference velocity profile of each motor or all motors if *n* is equal to 0. There are five types of reference waveforms that the user can select: step waveform (*type*=1), going from 0 rpm to *mag* rpm; square waveform (*type*=2) varying from 0 rpm to *mag* rpm with a period *t*; ramp waveform (*type*=3) varying from 0 rpm to *mag* rpm with a period *t*; sine waveform (*type*=4) varying from -*mag* rpm to *mag* rpm with a period *t*; arbitrary waveform (*type*=5) that is loaded from a stimulus file.

The stimulus file, created in Matlab, contains the velocity data for the four DC motors. This file contains four arrays of data, one for each wheel, where each value of the array is the instantaneous speed. The size of the array is dependent on the sampling rate and duration of the test, e.g., if the sampling rate is 500 Hz and the test is supposed to last 30 seconds then the array for each wheel must have 15000 elements. The construction of such array using Matlab is a straightforward task. Further, the author created a Matlab function, called "savewave", that saves the velocity profile of the four DC motors in a condensed binary format file, compatible with MSS reference file reading routine.

An example of an arbitrary velocity waveform is presented in Figure 4.7-a). Firstly, all four wheels accelerate for 1 second up to an instantaneous linear velocity of 2 mms^{-1}, followed by a period of constant speed for another second, and finally an increase of linear velocity to 2.5 mms^{-1}, at maximum acceleration, of wheels #3 & #4 during 8 seconds. This 4 by 5000 elements long velocity profile (sampling rate @500 Hz) is read by the MSS reference reading routine and is converted to a new array with instantaneous position (see Figure 4.7-b)). Because the variable controlled by the MSS software is the position of the wheels, this conversion is necessary.

When one wants to stretch a specimen with the MSS and measure the required torque to obtain such extension, the motion profile of Figure 4.7-a) could be used for that purpose. However, the extension of 4 mm shown in Figure 4.7-c) at time 10 seconds only happens if slippage does not occur between any wheel and the specimen being tested.

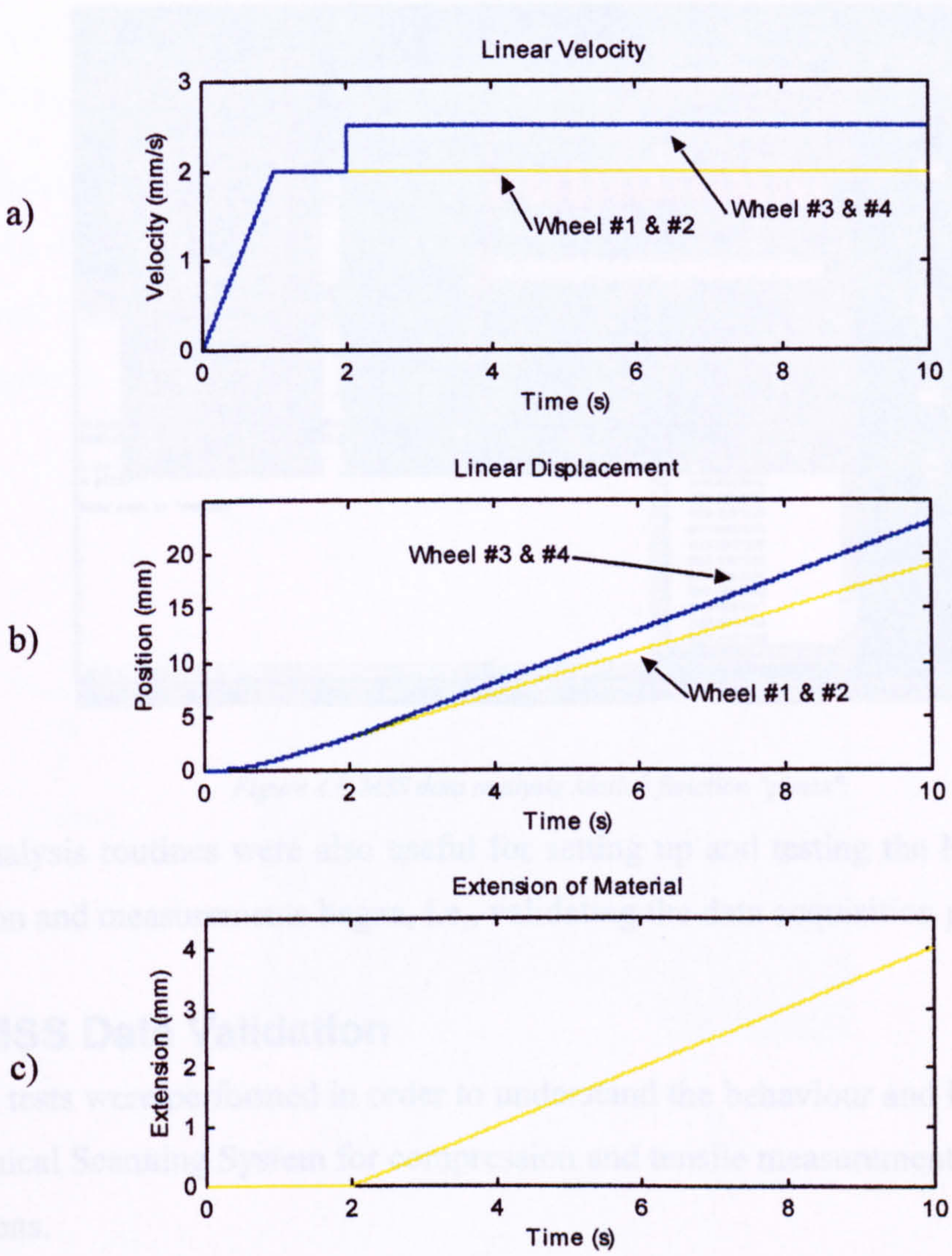

Figure 4.7-Arbitrary waveform example.

a) linear velocity profile of wheels b) linear displacement of material c) expected extension of material between both nips.

Data analysis was performed in Matlab. Among many scripts and functions developed for this purpose, the function "plmss" (plot MSS data), shown in Figure 4.8, allows a quick verification of the just acquired data for any obvious problem. It is possible to plot signals from sensors, real angular velocity, real linear velocity and real linear position, as well as plot an FFT (Fast Fourier Transform) of the torque signals.

The FFT option was very helpful during testing of the MSS, because it was possible to improve some mechanical parts to have a smoother torque signal when rotating wheels #3 & #4 without any load.

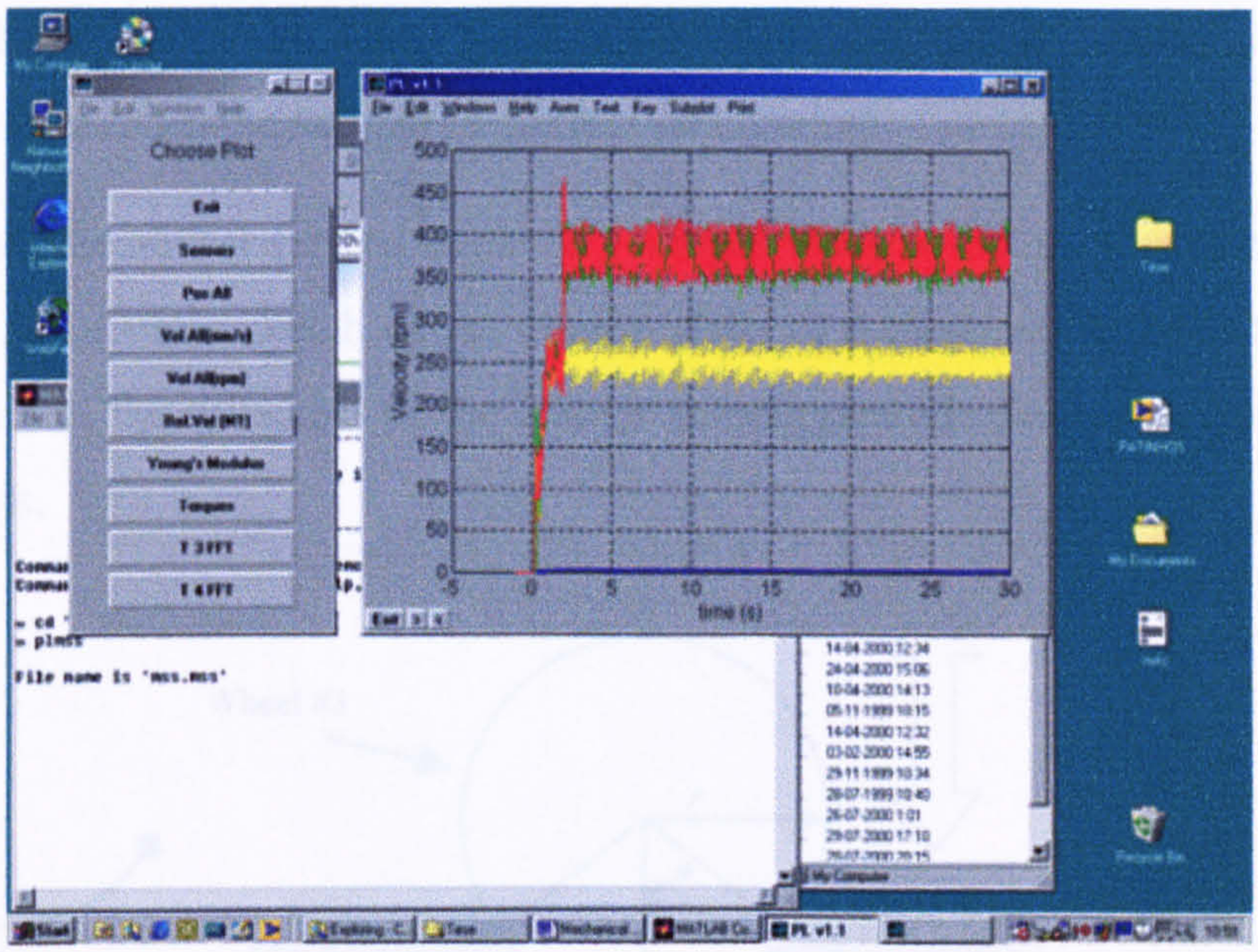

Figure 4.8-MSS data analysis Matlab function "plmss".

Data analysis routines were also useful for setting up and testing the MSS, before real operation and measurements began, i.e., validating the data acquisition process.

4.4 MSS Data Validation

Several tests were performed in order to understand the behaviour and limitations of the Mechanical Scanning System for compression and tensile measurements under different conditions.

4.4.1 Compression and Thickness Measurements

As already mentioned, a compression or thickness measurement is a dual parameter test in which a change in compression force or pressure corresponds to a change in distance between compressing surfaces.

For the determination of the pressure applied during a compressibility test, force and contact area must be known. In traditional compressibility tests, obtaining the real contact area is a straightforward task, however using the MSS that is not the case. Because in the MSS top and bottom pressure feet are actually wheels, the contact area is continuously changing with changing distance and compression between both wheels. Determination of the exact real contact area is not an easy task; Alexander [Alexander 72] studied thoroughly this subject applied to the situation of hot and cold rolling of materials. Also, he analysed the stresses involved in a situation where a

material is being compressed and displaced by rolling. Johnson [Johnson 85] is another excellent reference on the subject of contact mechanics.

Nevertheless, the author carried out a very simple study to better illustrate the problem. In Figure 4.9 a simple sketch of the compression of a material between two wheels is presented. Here, the thickness of the leather is exaggerated relatively to the dimensions of the wheels.

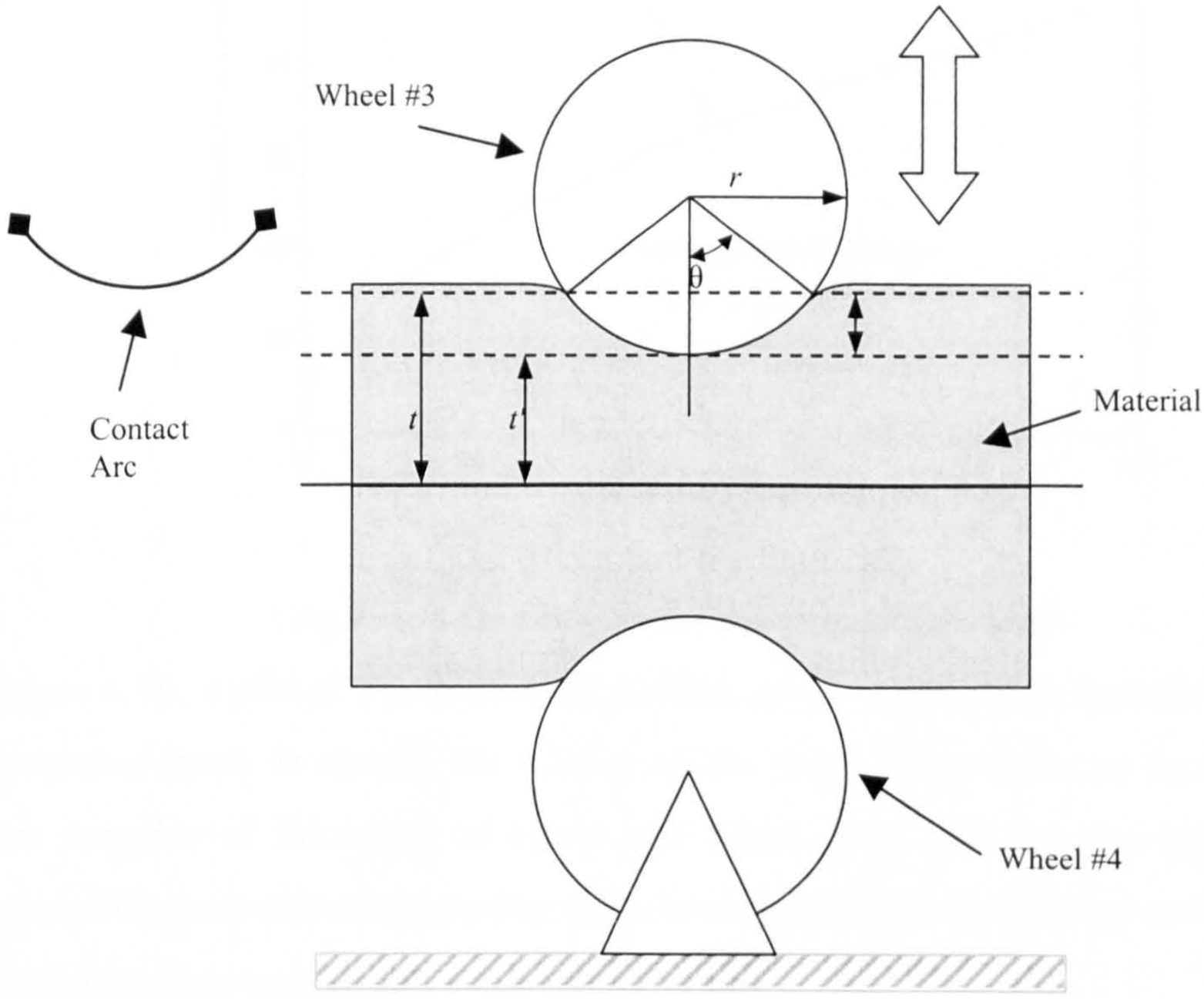

Figure 4.9-Sketch of a compressibility test using MSS.

The contact area is the product of the width of the wheels and the length of the contact arc. If t is half of the initial thickness of the leather, i.e., when the specimen starts to be compressed; if t' is half the thickness of the compressed leather; if r is the radius of the compression wheels; if θ is the angle (in radians) of half of the arc that is in contact with the leather sample; if w is the width of the wheels; the contact area is computed as follows:

$$\Theta = \arccos\left(1 + \frac{t'-t}{r}\right)$$
$$Area = 2 \cdot \Theta \cdot r \cdot w \qquad (4.1)$$

In practice, the real contact area is always smaller than the area obtained by applying Equation 4.1, because leather does not adjust to the shape of the wheel as illustrated in Figure 4.9.

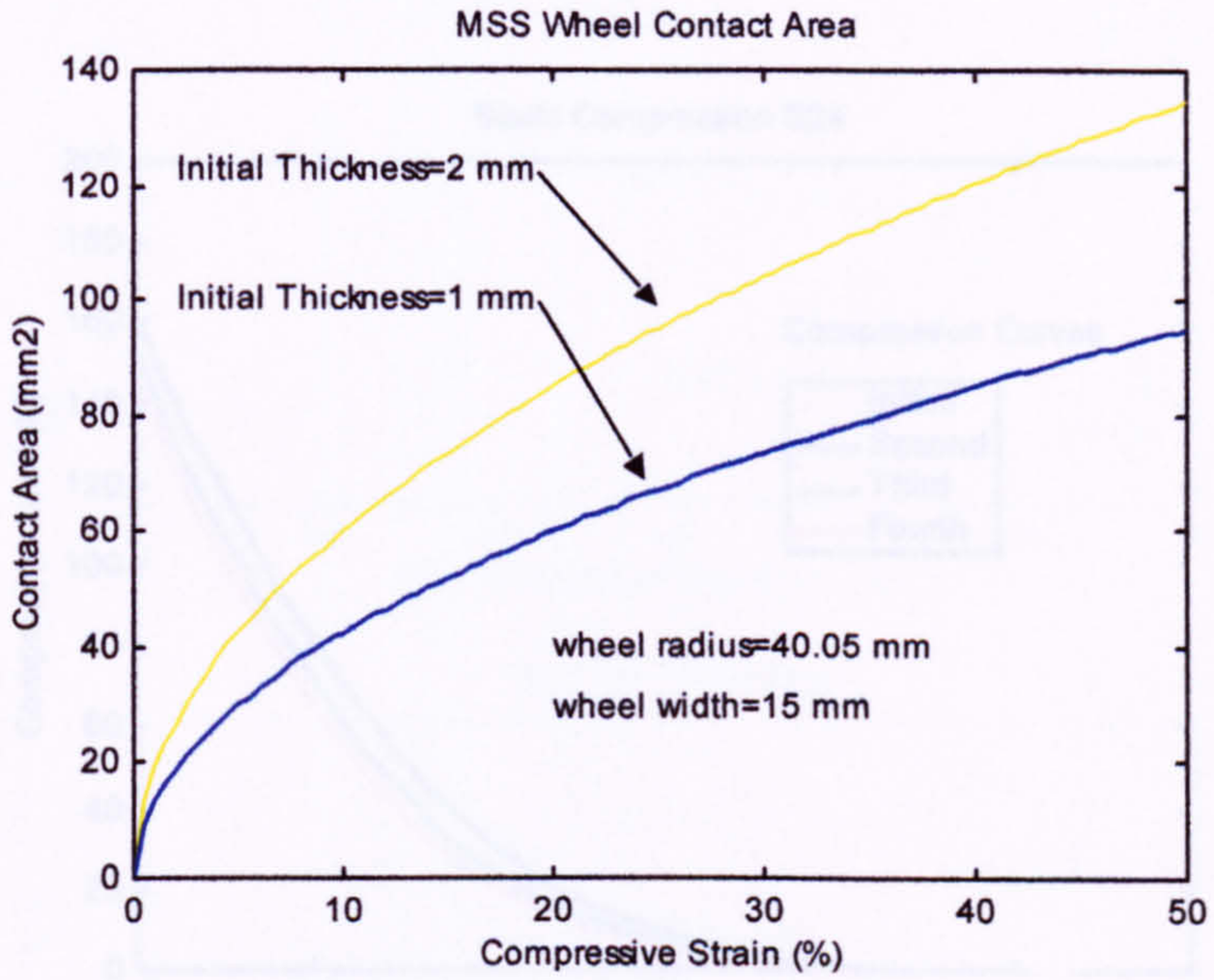

Figure 4.10-Theoretical contact area vs. compressive strain.

In Figure 4.10, a plot of the theoretical contact area, according to Equation 4.1, against compressive strain is shown for wheels of the same dimensions as in MSS for two leather samples of thickness of 1 mm and 2 mm. This fact has the implication that compressive stress also changes due to the increase of the contact area and it must taken into account when computing compressive stress.

The Mechanical Scanning System enables the implementation of static and dynamic compression tests, respectively with wheels #3 & #4 stopped and rotating.

Static compression tests in leather produce comparable results with those expected from conventional compression tests. Figure 4.11 shows the compression load vs. thickness of the leather specimen S24. Four compression curves are plotted, showing the amount of thickness not recovered between each compression and decompression cycle, in particular from the initial compression curve to the second compression curve.

Early dynamic compression tests showed unexpected results at the time, causing the building of the Length Measuring Devices. Initially, it was observed that the real displacement of a specimen being compressed was smaller than the expected displacement. In addition, different compression loads produced different displacements

of material. This behaviour was observed for leather and rubber, on wheels with an aluminium surface. After covering the wheel surface with emery paper, it was necessary to devise a test to measure the relationship between compression load and real displacement.

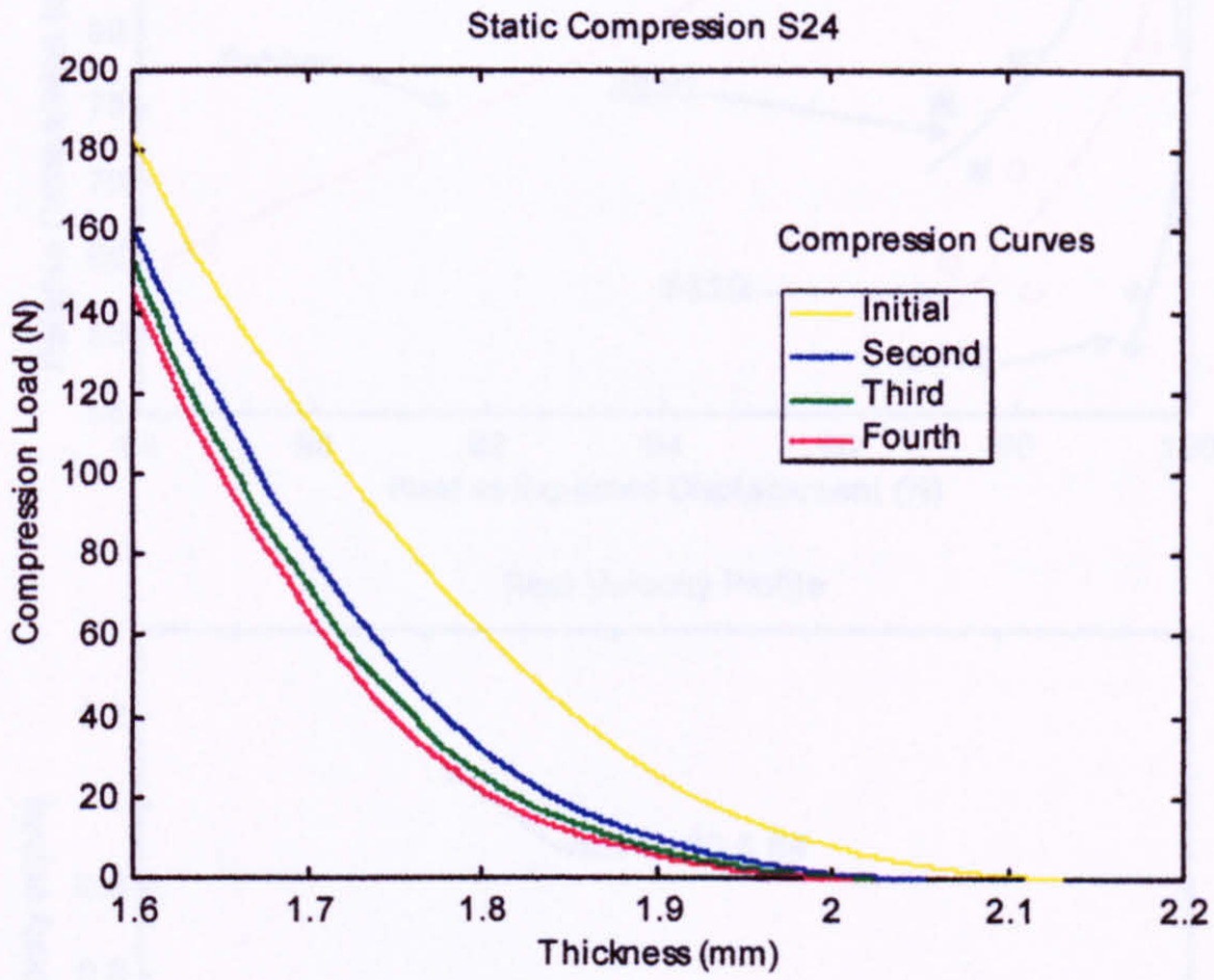

Figure 4.11-Static compression test.

Three samples of leather (S11, S22, S32) and a piece of soft rubber (like rubber of an inner tube car tire) were compressed at different compressive strains. Then the wheels were driven with the velocity profile displayed in Figure 4.12 b) and the real displacement recorded.

The total expected displacement for these tests was 38 mm, however the real displacement varied as shown in Figure 4.12 a). Rubber clearly shows the worst behaviour and the higher the compression loads the lower the real displacement. Leather shows a similar drift but in a much smaller scale. Such behaviour is explained by the occurrence of micro-slip and creep [Johnson 85], which is helped by the fact that rubber has two similar surfaces (same friction coefficient) but the top and bottom wheels of the MSS have different surfaces (different friction coefficients). Further, rubber is an example of an elastic material and that fact also contributes for the verified difference between real and expected displacement.

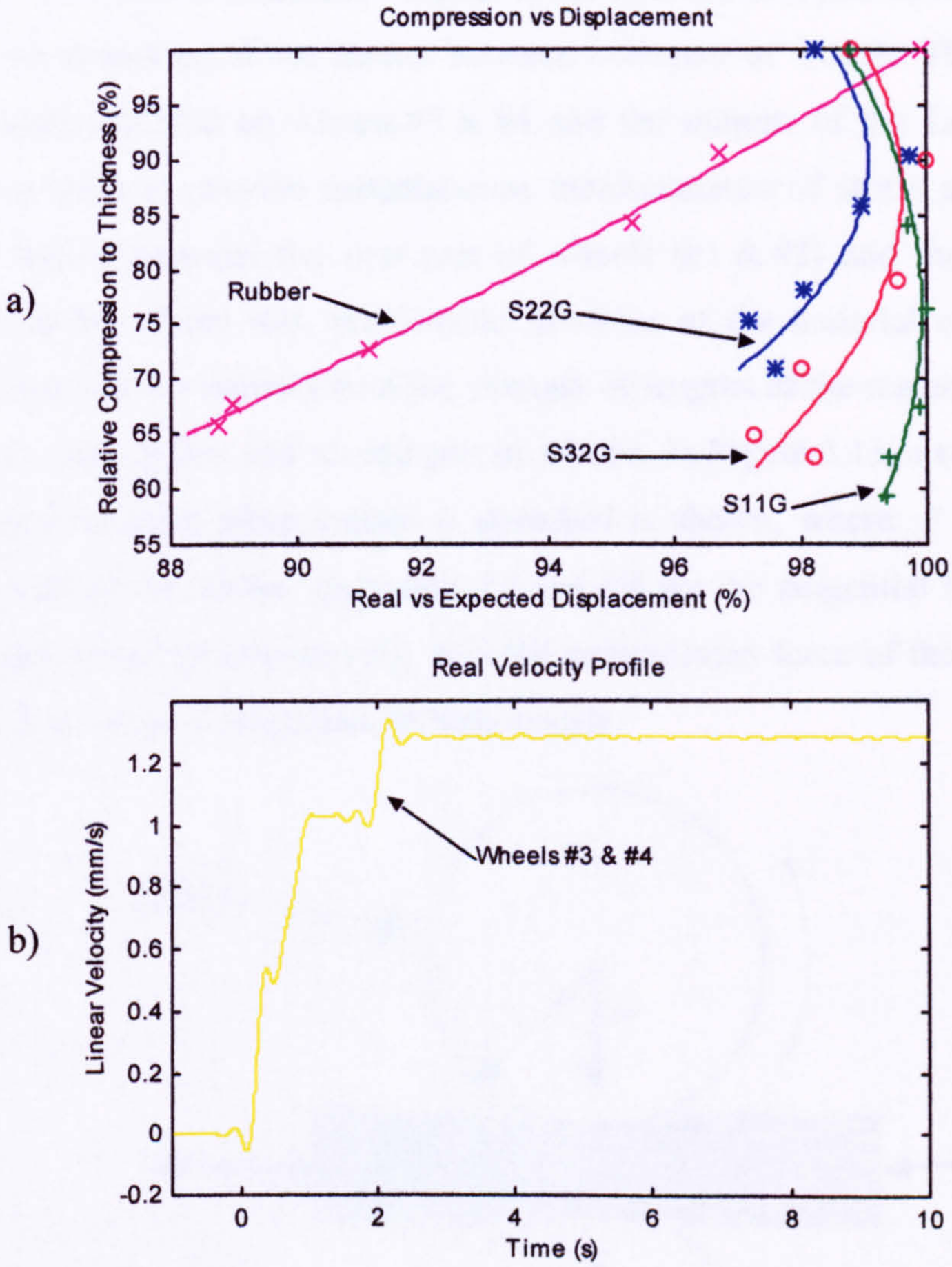

Figure 4.12-Compression vs. displacement of MSS.

a) Plot of relative compression against real vs. expected displacement; b) Linear velocity profile used during test.

The problem of compression vs. displacement needs further research as well as the most adequate wheel surface in order to obtain maximum friction and sample displacement without causing any noticeable sample damage.

4.4.2 Tensile and Elongation Measurements

The Mechanical Scanning System can be used to provide instantaneous measurements of tensile modulus of leather, in the direction of the length of the leather as the leather passes between the first and second pair of wheels. To do this, the leather is fed between the first and second pair of wheels, which are all driven at the same speed. Next, the

second pair of wheels is rotated at a higher speed than the first pair of wheels. The effect of this is the stretching of the leather between both pair of wheels. The outputs of the torque sensors installed on wheels #3 & #4 and the outputs of the Length Measuring Devices are used to provide instantaneous measurements of stress and strain of the length of leather between the first pair of wheels (#1 & #2) and the second pair of wheels (#3 & #4). From this, the Tensile Modulus of the material can be calculated which will provide an estimation of the strength of lengths of the material along the line passing between the first and second pair of wheels. In Figure 4.13, a simple illustration of the forces involved when leather is stretched is shown, where: F is the force that actually stretches the leather specimen, *F3* and *F4* are the tangential forces applied by wheel #3 and wheel #4 respectively, N is the compression force of the leather between wheels #3 & #4 and r is the radius of both wheels.

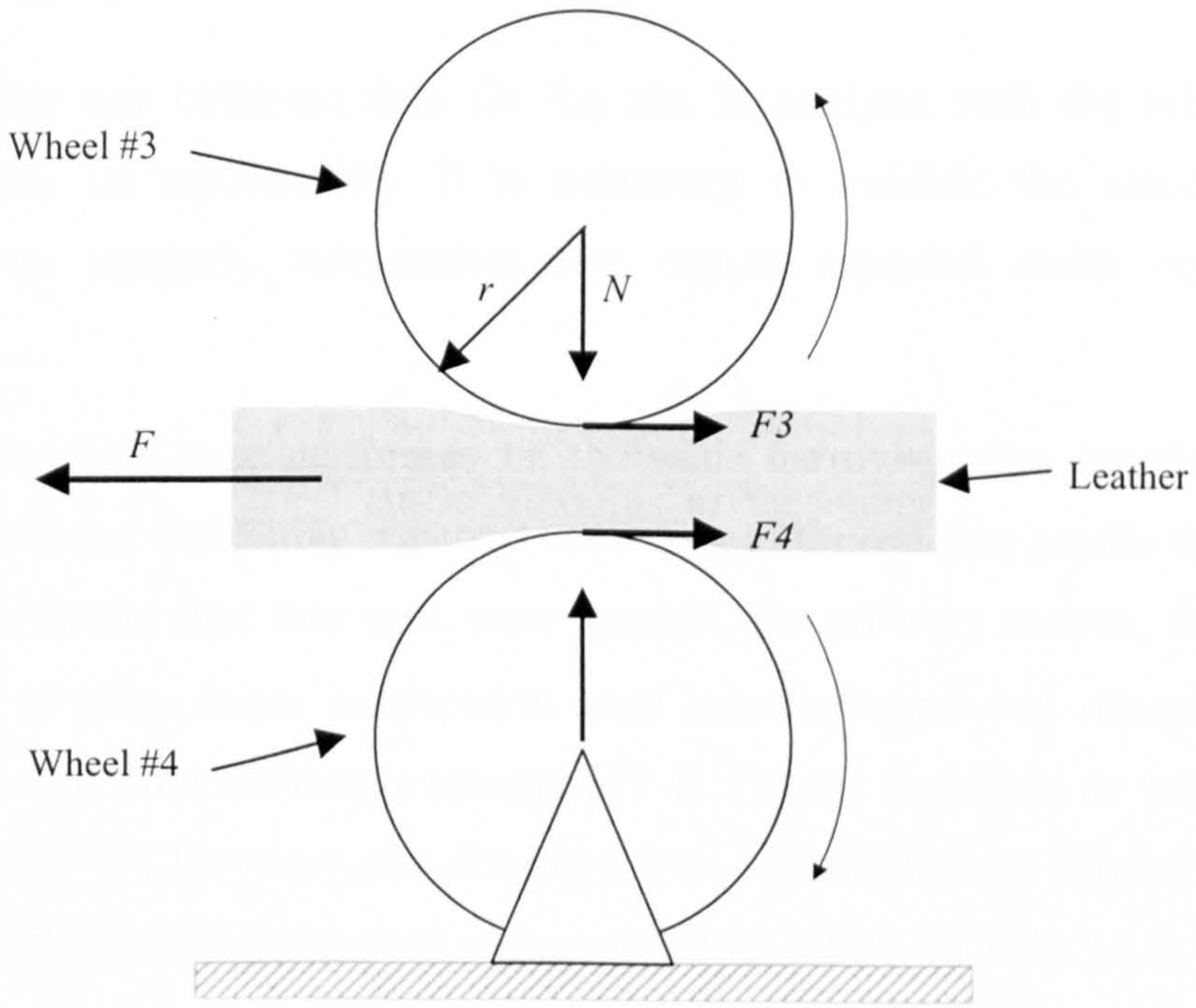

Figure 4.13-Sketch of stretching of leather.

Equation 4.2 is obtained from a simple analysis of the forces involved in this system, where *F3* and *F4* should have the same magnitude and half the magnitude of force *F*.

$$\begin{aligned} F &= F3 + F4 \\ T3 &= r \cdot F3 \\ T4 &= r \cdot F4 \end{aligned} \tag{4.2}$$

It must be noticed that stretching will only occur if the elongated material does not slip from the nip formed by wheels #3 & #4. This condition is verified as long as the compression load N is higher than the stretching force F divided by the friction coefficient between the wheels and both surfaces of the leather. If μ3 is the dynamic friction coefficient between wheel #3 and the grain side of the leather sample and if μ4 is the dynamic friction coefficient between wheel #4 and the flesh side of the leather, then Equation 4.3 must be verified at all times.

$$N > \frac{F3}{\mu 3} + \frac{F4}{\mu 4} \tag{4.3}$$

From the previous considerations, it can be concluded that the acquisition of the torque applied by the driving motors on wheels #3 & #4 is the most important and critical data that needs to be collected.

In order to validate any collected data for the test in analysis with the MSS, it is necessary to verify its repeatability. It is necessary to validate the closeness of agreement between mutually independent test results obtained under repeatable conditions.

Several consecutive tests were performed on the same narrow leather sample with a small compression force. Stretching occurred according to the velocity profile of Figure 4.7 b). The results of the first four runs were ignored, for obvious reasons. In Figure 4.14, the results of three more consecutive runs are displayed and designated as run 1,2 & 3. Raw data from the torque sensors (*F3 & F4*) are displayed as well as the sum of these two signals. However, the displayed sum signal has been filtered with an 8^{th} order Butterworth zero-phase forward and reverse digital filter in MATLAB.

Despite the small differences of force signals (*F3 & F4*) for runs 1 to 3, it can be seen that the sum of the forces (see Figure 4.14 c)) are in close agreement up to the approximate time of 5 seconds.

a)

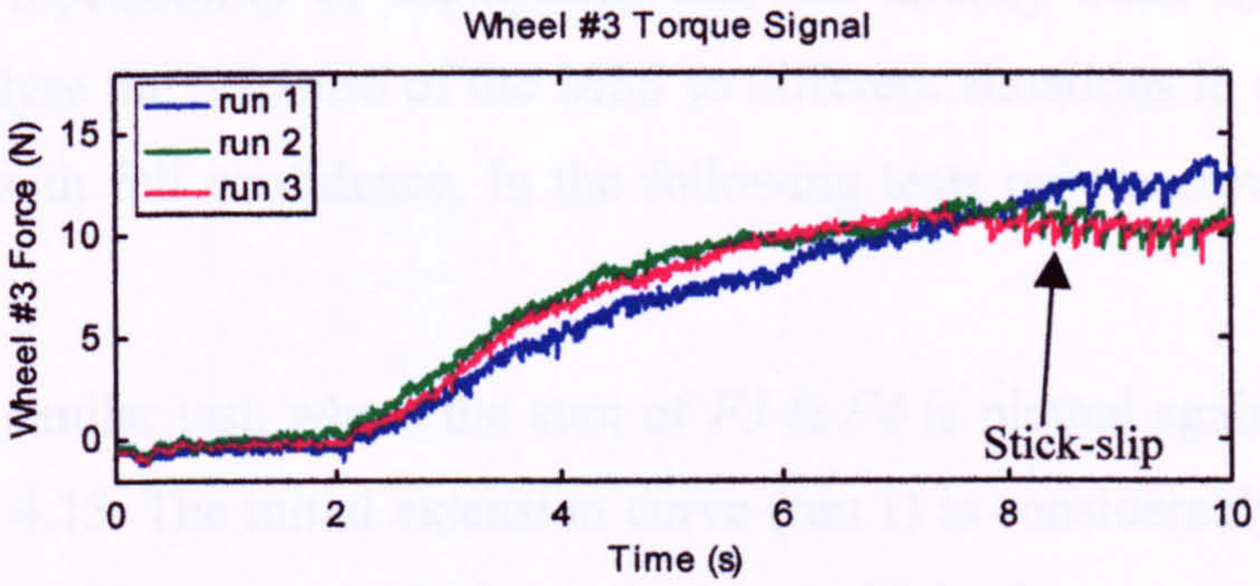

b)

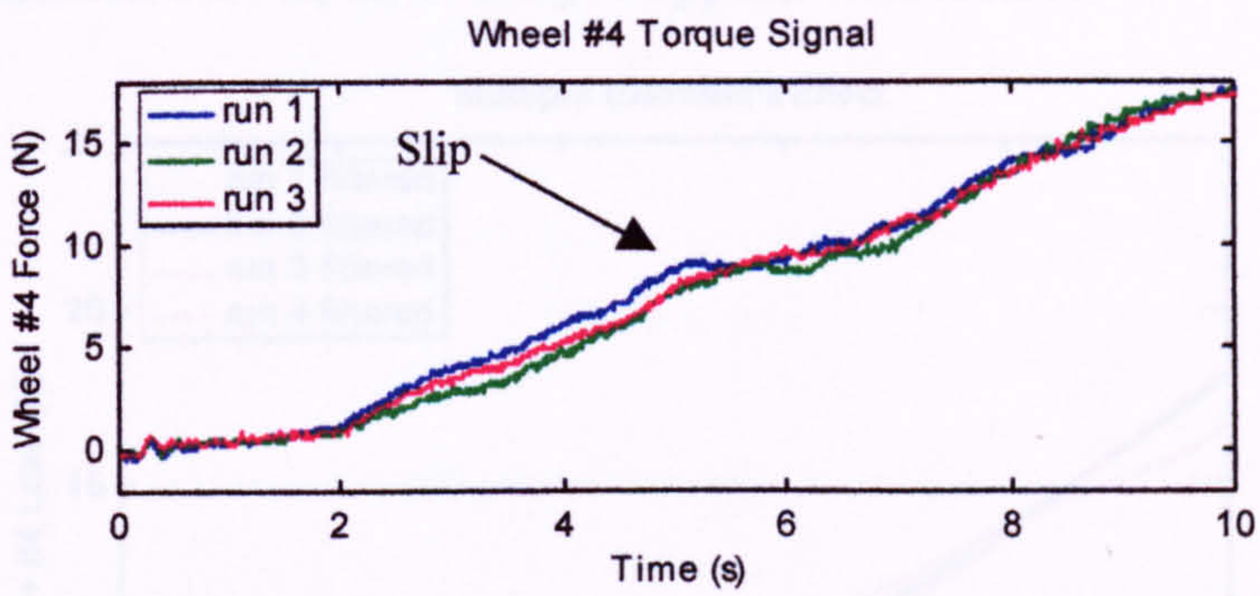

c)

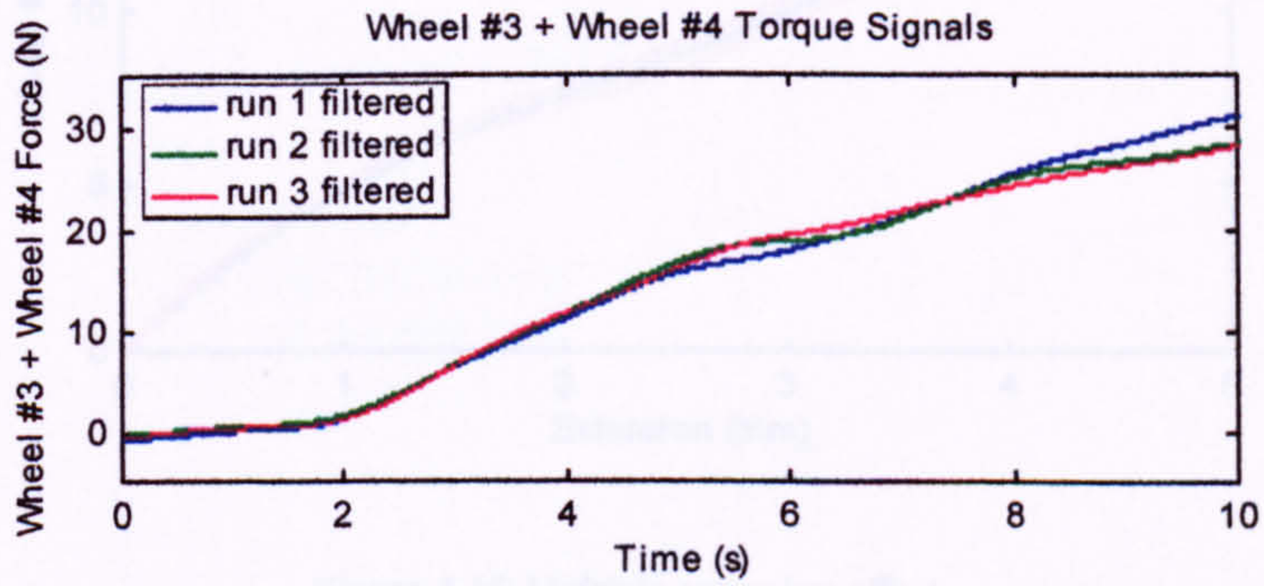

Figure 4.14-MSS torque signals repeatability.

a) Plot of raw torque signal of wheel #3. b) Plot of raw torque signal of wheel #4. c) Plot of the filtered sum of previous signals

The raw data from the torque sensors are very interesting and loaded with information. Looking at the period of time 8 to 10 seconds in Figure 4.14 a) a saw-tooth type waveform can be seen. This shape is caused by stick-slip occurrence between the grain side and the surface of wheel #3. The stick-slip is only visible on the grain side, such behaviour cannot be seen on the flesh side due to its rough surface nature. Observing Figure 4.14 b) at time 5 seconds, the occurrence of slip can be detected as a decrease in slope of the force signal. This event is also reflected on the sum of both forces.

Apart from the repeatability of the system that has already been shown, it is also important to analyse the response of the MSS to different situations in order to be able to acquire data with full confidence. In the following tests only narrow samples were used.

The results of a similar test, where the sum of *F3* & *F4* is plotted against extension, is shown in Figure 4.15. The initial extension curve (run 1) is considerably different from the following extension curves, as it always happens with leather.

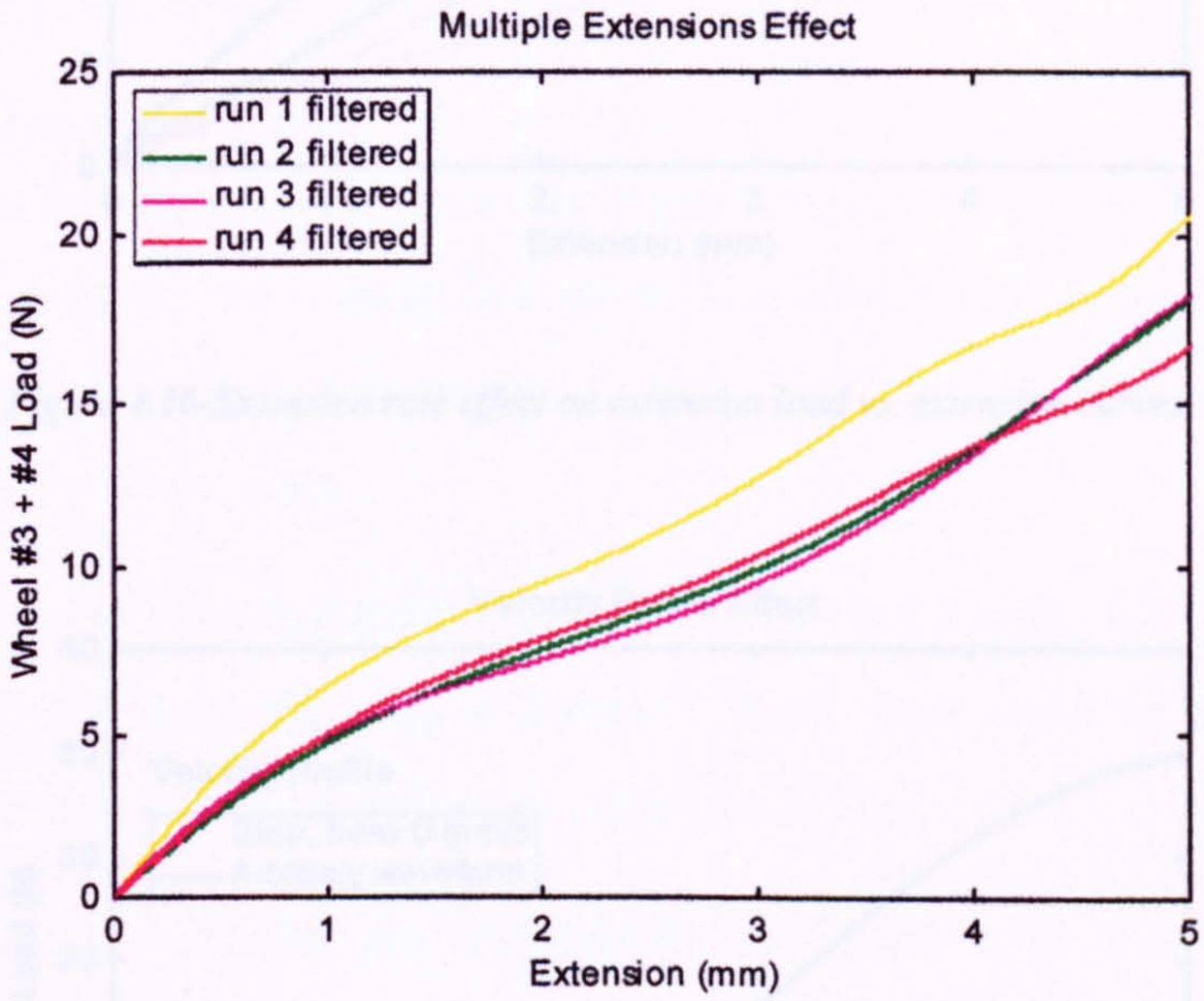

Figure 4.15-Multiple extension effect.

The results of another simple test to verify the behaviour of MSS are presented in Figure 4.16. Here a different velocity profile stimulus file is used, wheels #1 & #2 are locked while wheels #3 & #4 rotate at a predetermined velocity, i.e., velocity of wheels #1 & #2 is zero while a step reference velocity is applied to wheels #3 & #4. The plots of Figure 4.16 show the results of stretching leather with the MSS at extension rates of 0.26 mms^{-1}, 0.52 mms^{-1}, 1.05 mms^{-1}, 2.1 mms^{-1} and 4.20 mms^{-1}.

The stretching of leather at a constant extension rate (0.52 mms^{-1}) but with different velocity profiles was also performed (see Figure 4.17). A step reference velocity profile with a magnitude of 0.52 mms^{-1} was applied to wheels #3 & #4; while in the second experiment the arbitrary waveform of Figure 4.7 b) was applied. The results show a negligible difference that can be explained by the lack of quality of the gearboxes (high backlash) utilised in the MSS. Nevertheless, it can be concluded that the extension load vs. extension curves are quite immune to the type of extension waveforms.

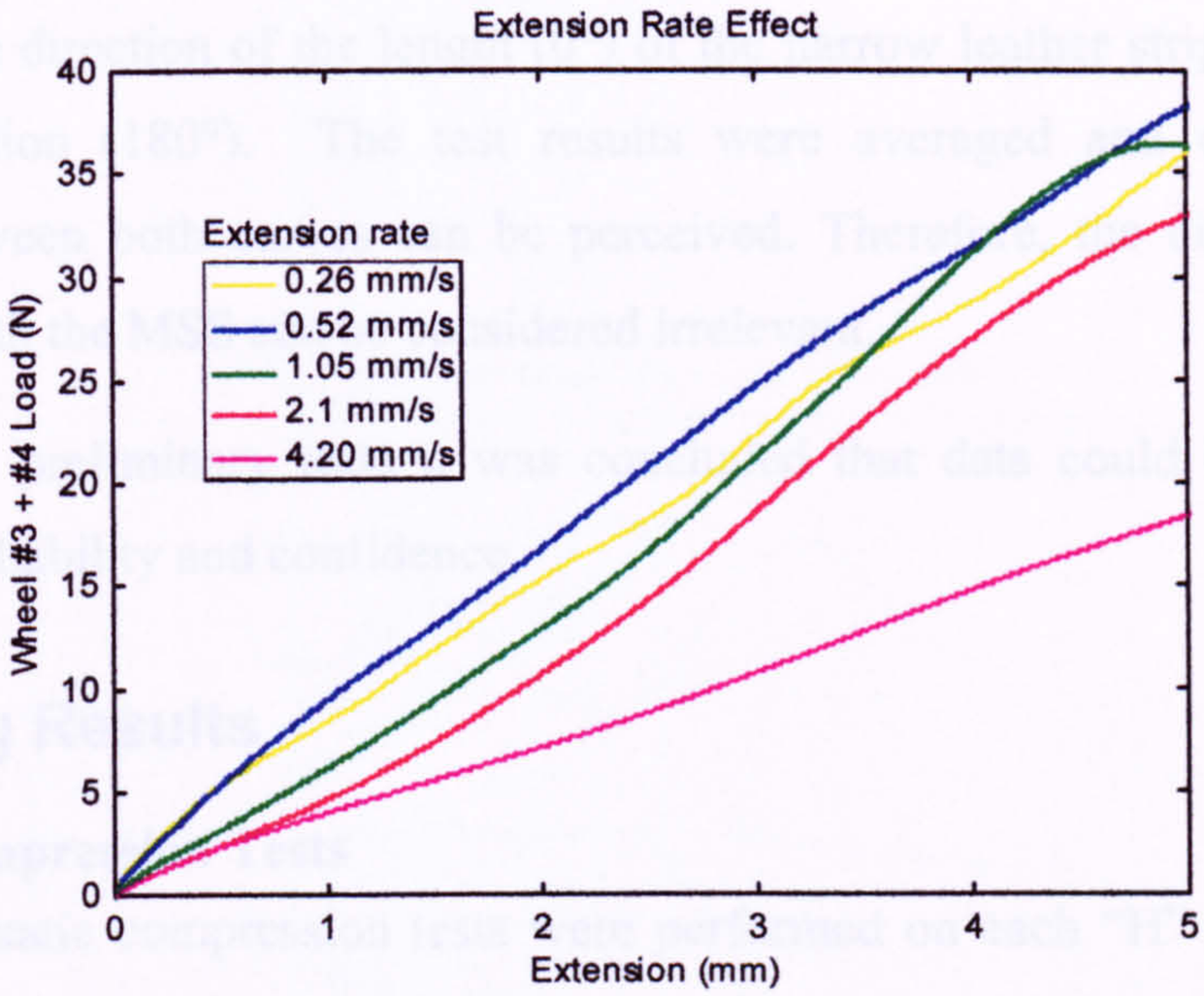

Figure 4.16-Extension rate effect on extension load vs. extension curves.

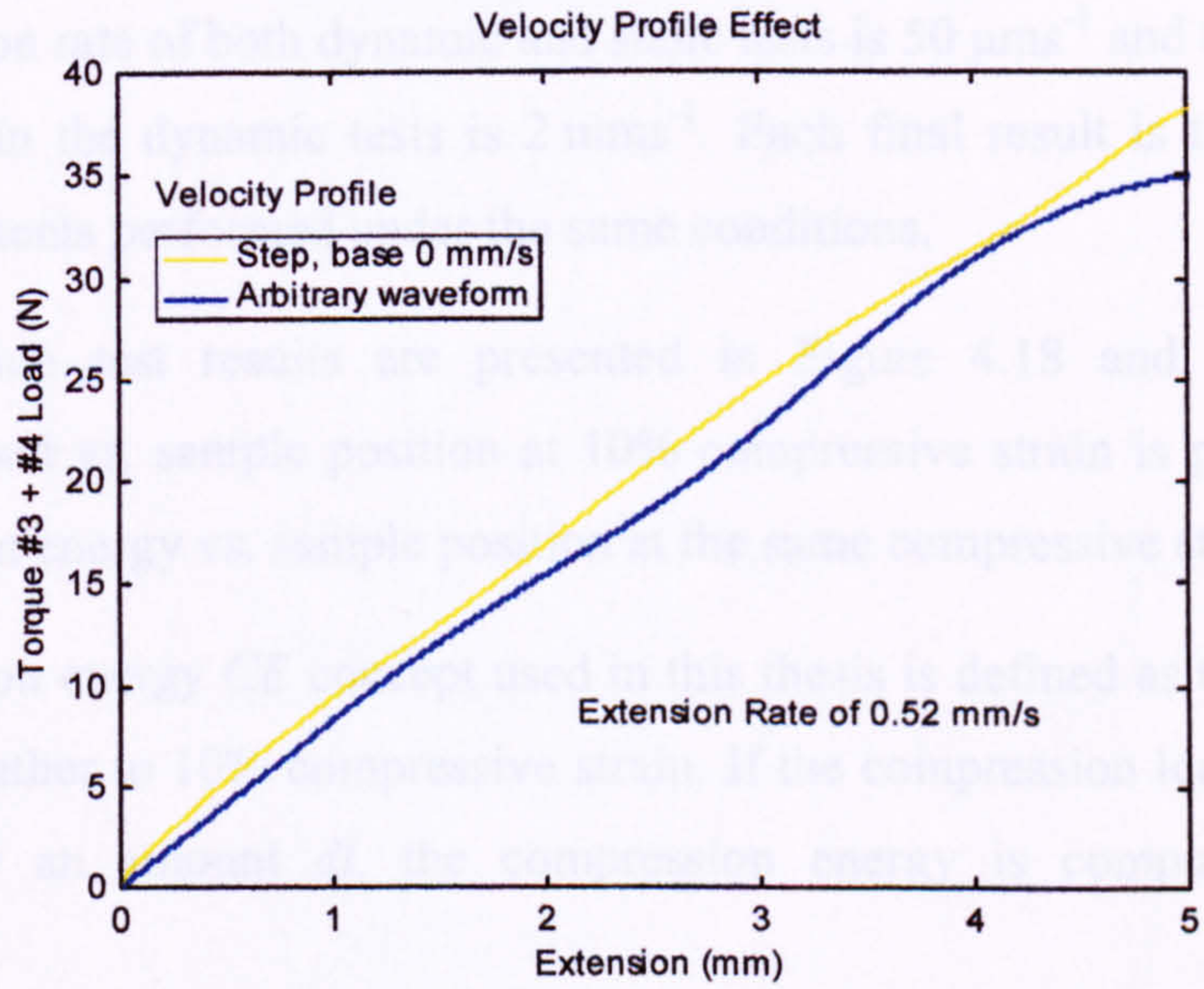

Figure 4.17-Velocity profile effect on extension. The arbitrary waveform is shown in Figure 4.7 b).

The stretching of leather at a constant extension rate (0.52 mms^{-1}) but at different base speeds was also performed. A step reference velocity profile was applied to both pairs of wheels, in a way that the wanted extension rate was always guaranteed. The results of extending the leather sample at base velocities of 0 mms^{-1}, 0.26 mms^{-1}, 1.05 mms^{-1} do not show any relevant difference.

Finally, another tested parameter was the influence of the direction of testing. For this matter, two similar narrow leather specimens were stretched six times, one specimen

stretched in the direction of the length (0°) of the narrow leather strip, the other in the opposite direction (180°). The test results were averaged and only a negligible difference between both curves can be perceived. Therefore, the direction of testing (0° or 180°) with the MSS can be considered irrelevant.

From all these preliminary tests it was concluded that data could be collected with considerable reliability and confidence.

4.5 Testing Results

4.5.1 Compression Tests

Dynamic and static compression tests were performed on each "H" specimen of each sampling location of the three available sides. The objectives of these tests are to draw conclusions and to compare the results of static and dynamic compression tests with conventional compression tests.

The compression rate of both dynamic and static tests is 50 μms^{-1} and the linear velocity of the wheels in the dynamic tests is 2 mms^{-1}. Each final result is the average of six similar experiments performed under the same conditions.

The compression test results are presented in Figure 4.18 and Figure 4.19, the compression load vs. sample position at 10% compressive strain is plotted, as well as the compression energy vs. sample position at the same compressive strain.

The compression energy *CE* concept used in this thesis is defined as the energy needed to compress leather to 10% compressive strain. If the compression load *CL* compresses the leather by an amount *dl*, the compression energy is computed according to Equation 3.3.

$$CE = \int_0^{10\%} CL \cdot dl \qquad (4.4)$$

Graphically, the compression energy *CE* represents the area under the curve compression load vs. compression length from 0 to 10 percent compressive strain. All data was calculated in MATLAB with functions developed by the author.

In Figure 4.18 and Figure 4.19 the compressive load of specimen S14H (side 1, position 4, specimen H) is read from the curve S1H "Sample Position" 4.

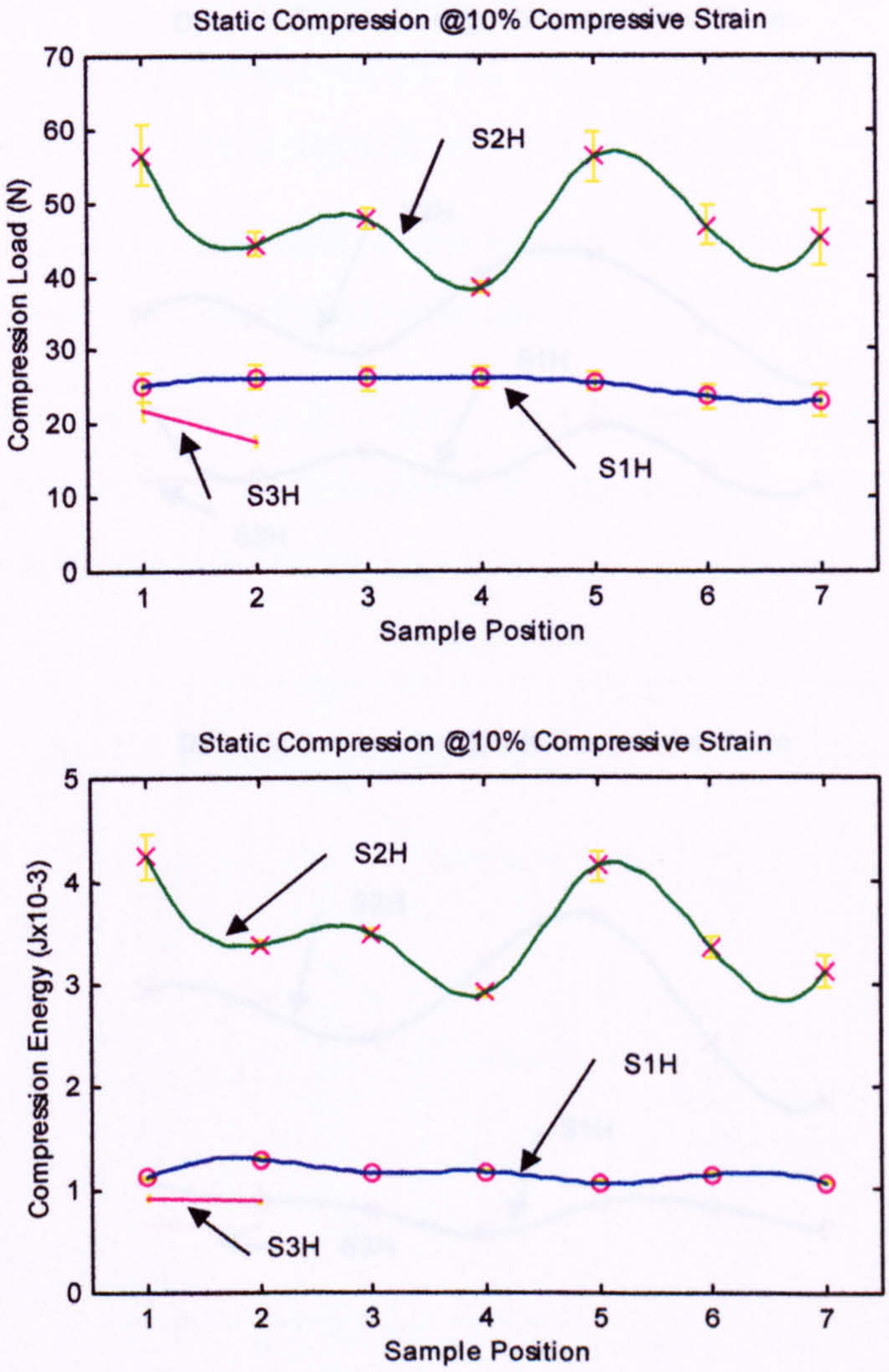

Figure 4.18-Static compression test results.

Tests performed under standard conditions, with a compression rate of 50 μms^{-1}, each result is the average of six runs.

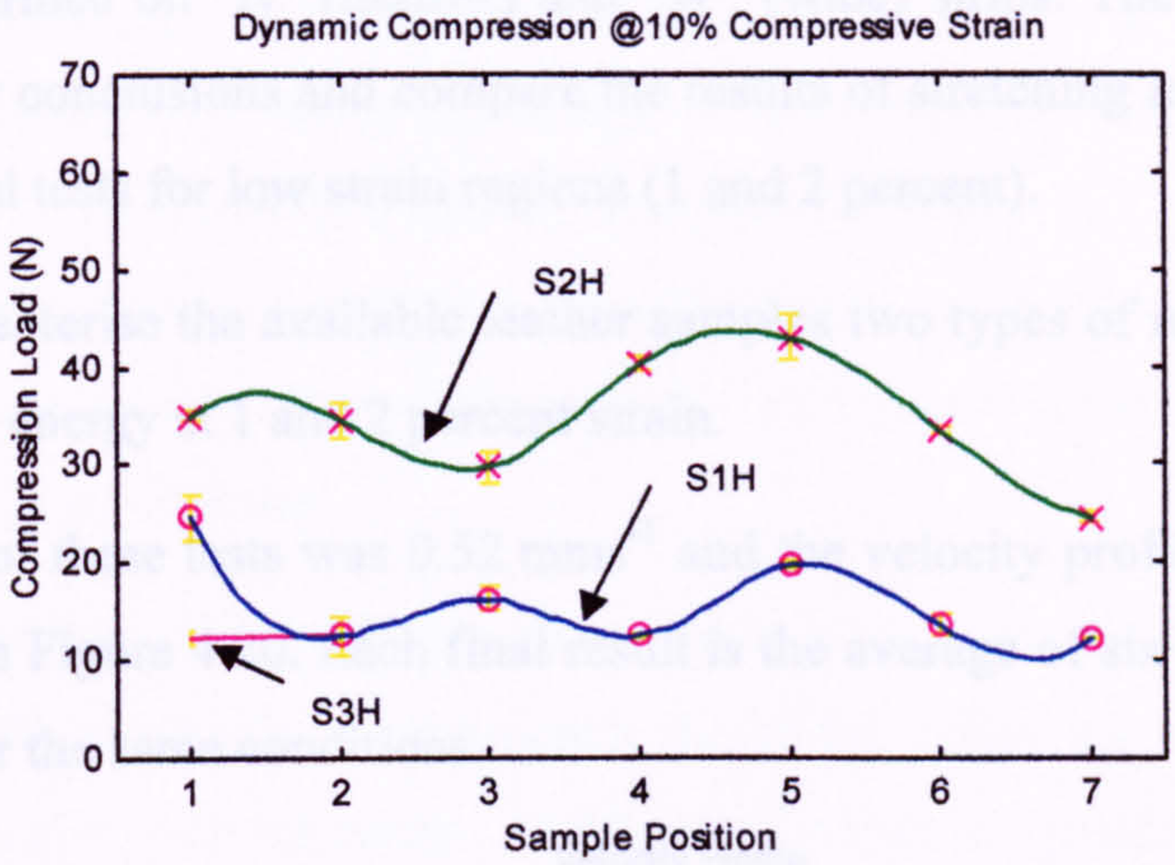

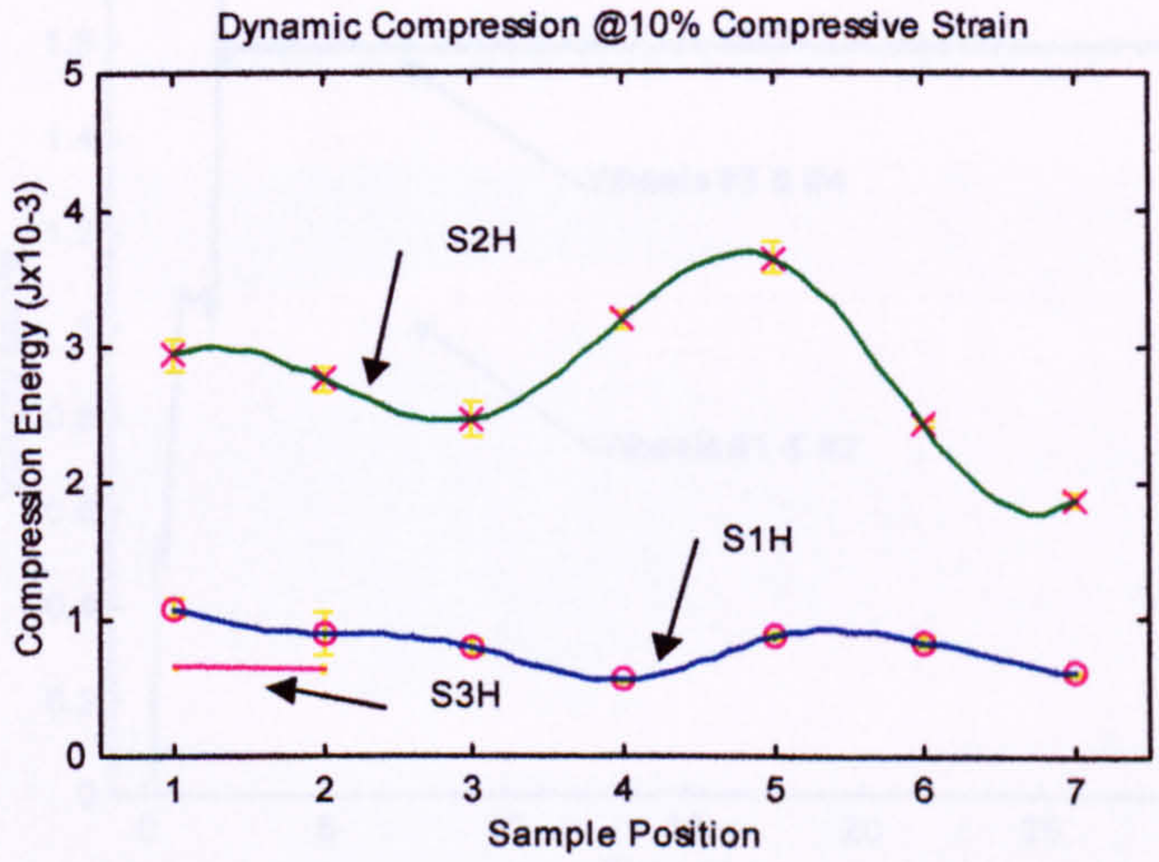

Figure 4.19-Dynamic compression test results.

Tests performed under standard conditions, displacement velocity of 2 mms^{-1} with a compression rate of 50 μms^{-1}, each result is the average of six runs.

4.5.2 Tensile Tests

Tensile tests were performed on each "G" (parallel to backbone) and "H" (perpendicular to backbone) specimens of each sampling location of the three available sides. These tests were performed on "N" (narrow) and "W" (wide) strips. The objectives of these tests are to draw conclusions and compare the results of stretching leather with the MSS and conventional tests for low strain regions (1 and 2 percent).

In order to characterise the available leather samples two types of results are presented, stress and strain energy at 1 and 2 percent strain.

The strain rate of these tests was 0.52 mms^{-1} and the velocity profile adopted for these tests is shown in Figure 4.20. Each final result is the average of six similar experiments performed under the same conditions.

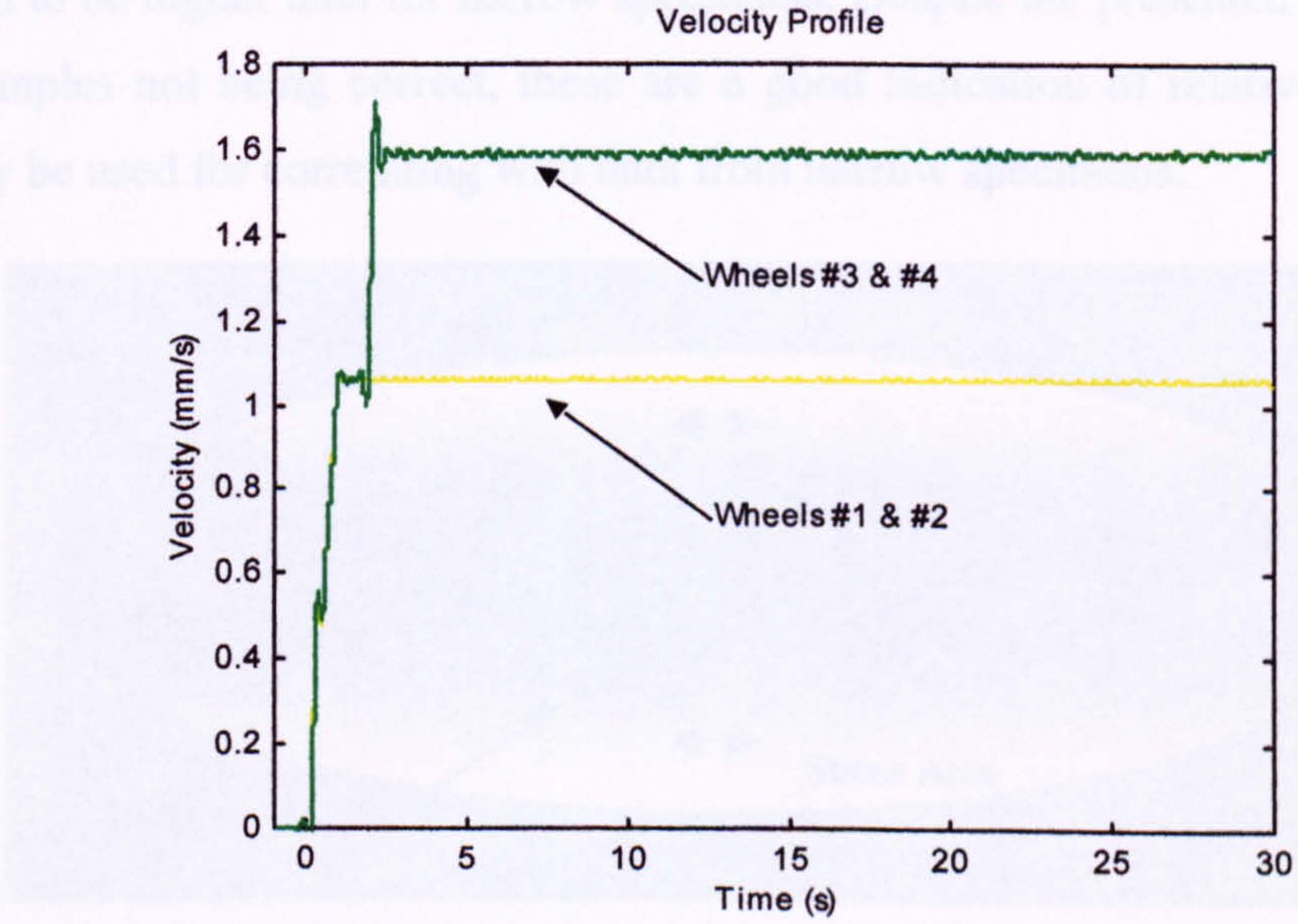

Figure 4.20-Velocity profile used throughout extension tests with MSS.

Stresses at 1 and 2 percent strain of all tested samples are shown in Figure 4.22 to Figure 4.25. In the first two figures the results of tests on parallel and perpendicular narrow samples are displayed, while in the last two figures the shown results correspond to wide samples. Stress is calculated according to Equation 3.4, however there is a problem with this calculation for wide samples.

$$Stress = \frac{Extension\ Load}{Thickness \cdot Width} \tag{4.5}$$

With narrow samples it is very easy to calculate the cross section area in order to obtain stress; the full width is being stretched, thus the full width is taken into account for computing stress.

When wide samples are stretched with the MSS, the calculation of cross section area is not a straightforward task. When the sample is wider than the wheels ("grippers") the extension load is distributed in a manner illustrated in Figure 4.21. Thus, the width of the zone where the load applied is wider than the width of the wheels. This is a problem that needs further research, an equivalent width figure should be found so an appropriate stress figure could be obtained.

The stress calculations for wide specimens were done with the thickness of narrow specimens (width of wheels), consequently the stress values for wider specimens are expected to be higher than for narrow specimens. Despite the presented stress values for wide samples not being correct, these are a good indication of relative stress and can certainly be used for correlating with data from narrow specimens.

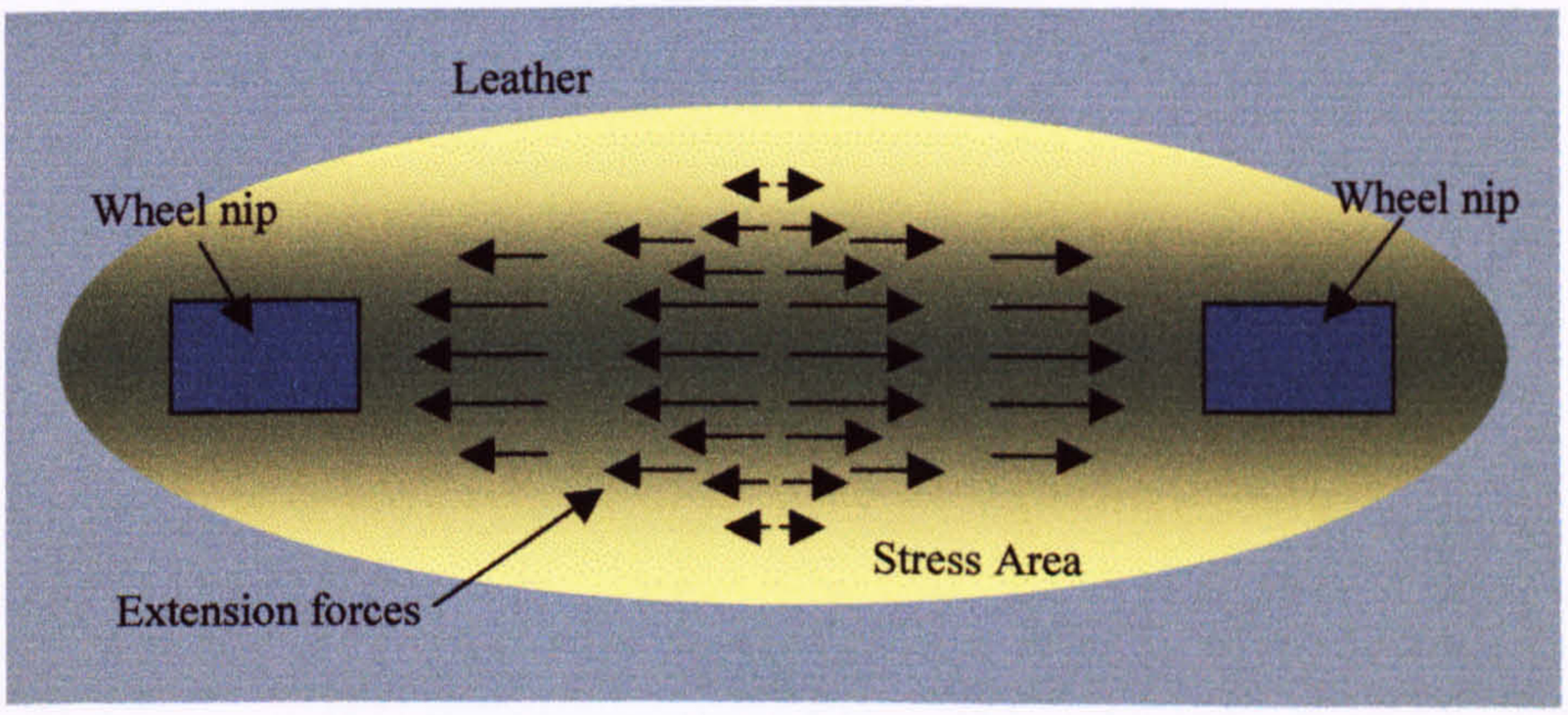

Figure 4.21-Extension load distribution on wide specimens (top view).

Stretching of wide specimens or even a hide creates some problems in particular for measuring the real amount of displaced material. When a large piece is stretched, there is a tendency for the leather specimen to curl around both nips. Consequently, the Length Measuring Devices readings are affected by this phenomenon. This is the main reason for the current location of the LMDs, however they could have been installed between both pair of wheels as it usually happens in extensometry. The measurement of the real displaced material of wide specimens when stretched with the MSS should be matter for further research.

Strain energy at 1 and 2 percent strain of all tested samples are shown in Figure 4.26 to Figure 4.29. In the first two figures the results of tests on parallel and perpendicular narrow samples are displayed, while in the last two figures the shown results correspond to wide samples. The strain energy *SE* concept used in this thesis is defined as the energy needed to extend leather to 1 or 2 percent strain. If the extension load *EL* extends the leather by an amount *dl*, the strain energy is computed according to Equation 4.6.

$$SE = \int_{0}^{1\% \text{ or } 2\%} EL \, dl \tag{4.6}$$

Graphically, the strain energy *SE*, represents the area under the curve extension load vs. extension length from 0 to 1 or 0 to 2 percent strain. All data was calculated in MATLAB with functions developed by the author.

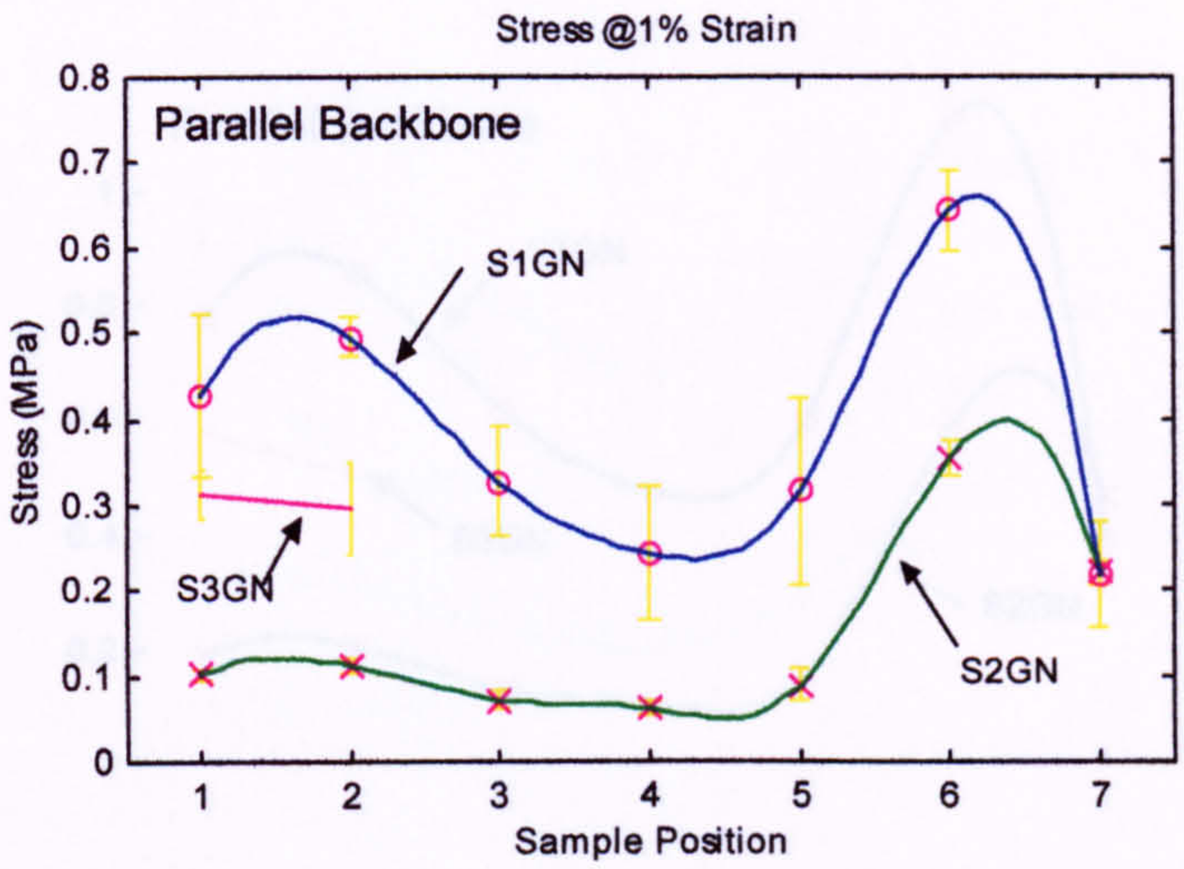

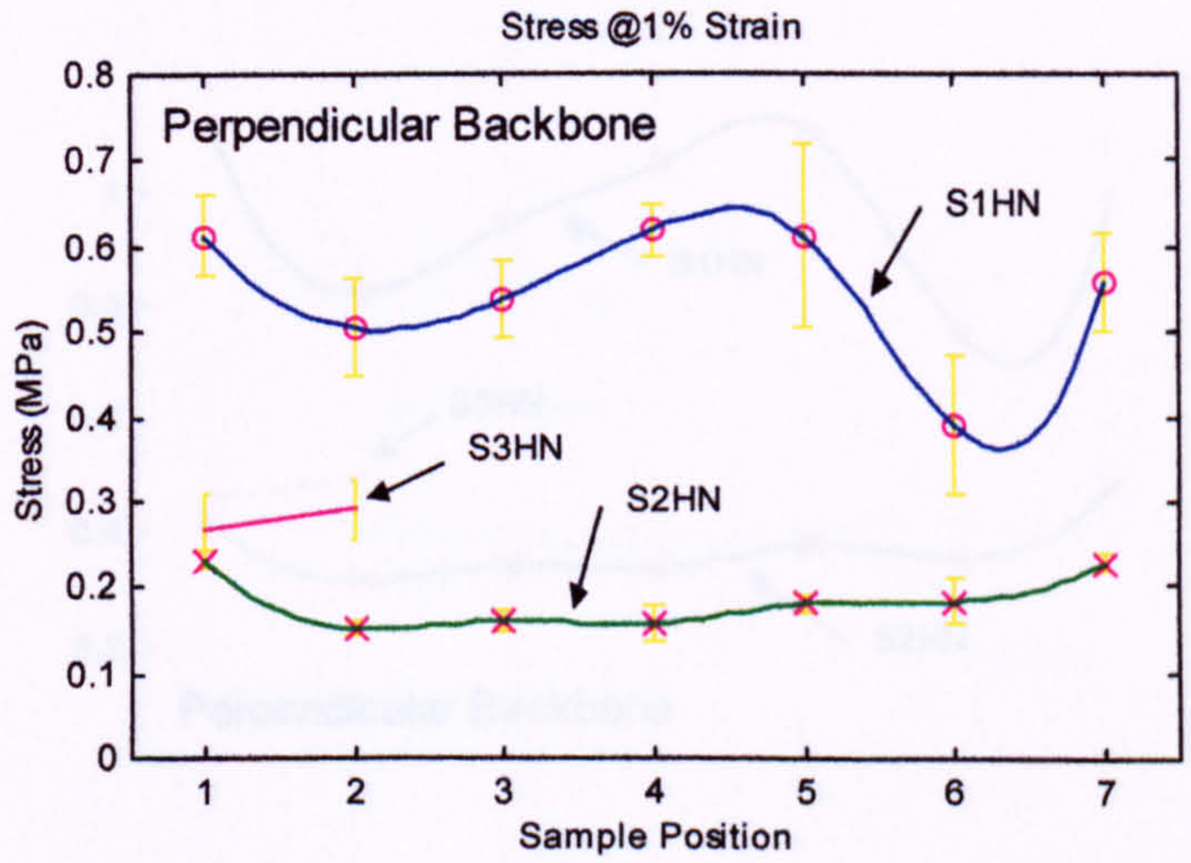

Figure 4.22-Plot of stress @1% strain for narrow samples parallel and perpendicular to backbone. Tests performed under standard conditions, extension rate of 0.52 mms^{-1} with the velocity profile of Figure 4.21, each result is the average of six runs.

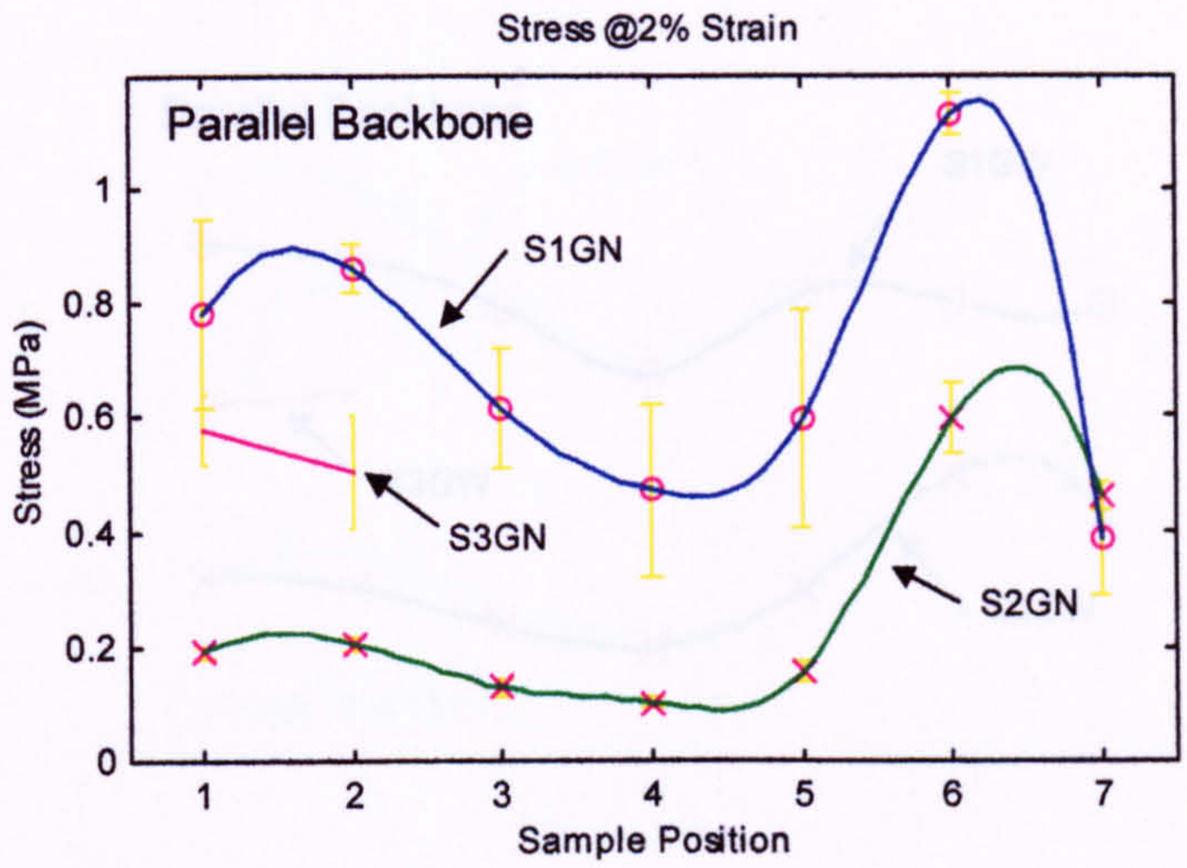

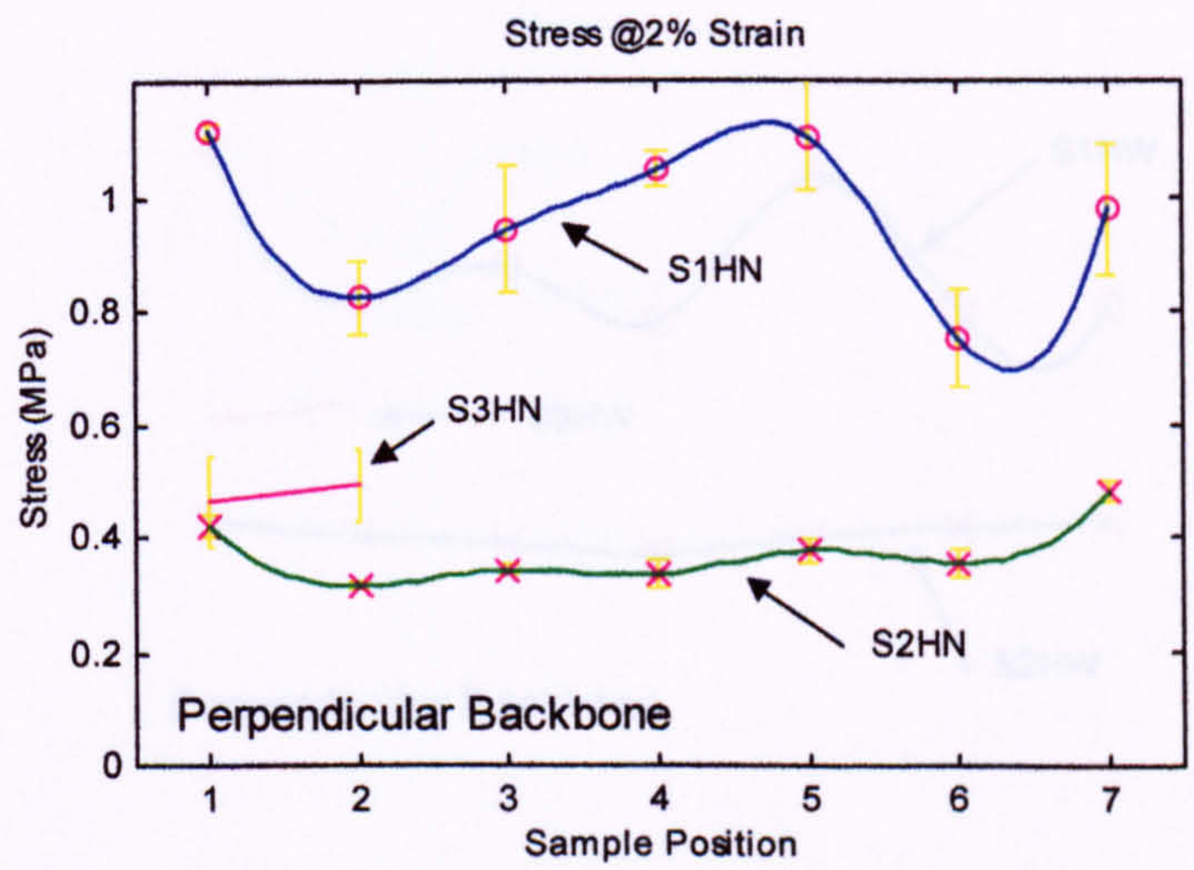

Figure 4.23-Plot of stress @2% strain for narrow samples parallel and perpendicular to backbone. Tests performed under standard conditions, extension rate of 0.52 mms^{-1} with the velocity profile of Figure 4.21, each result is the average of six runs.

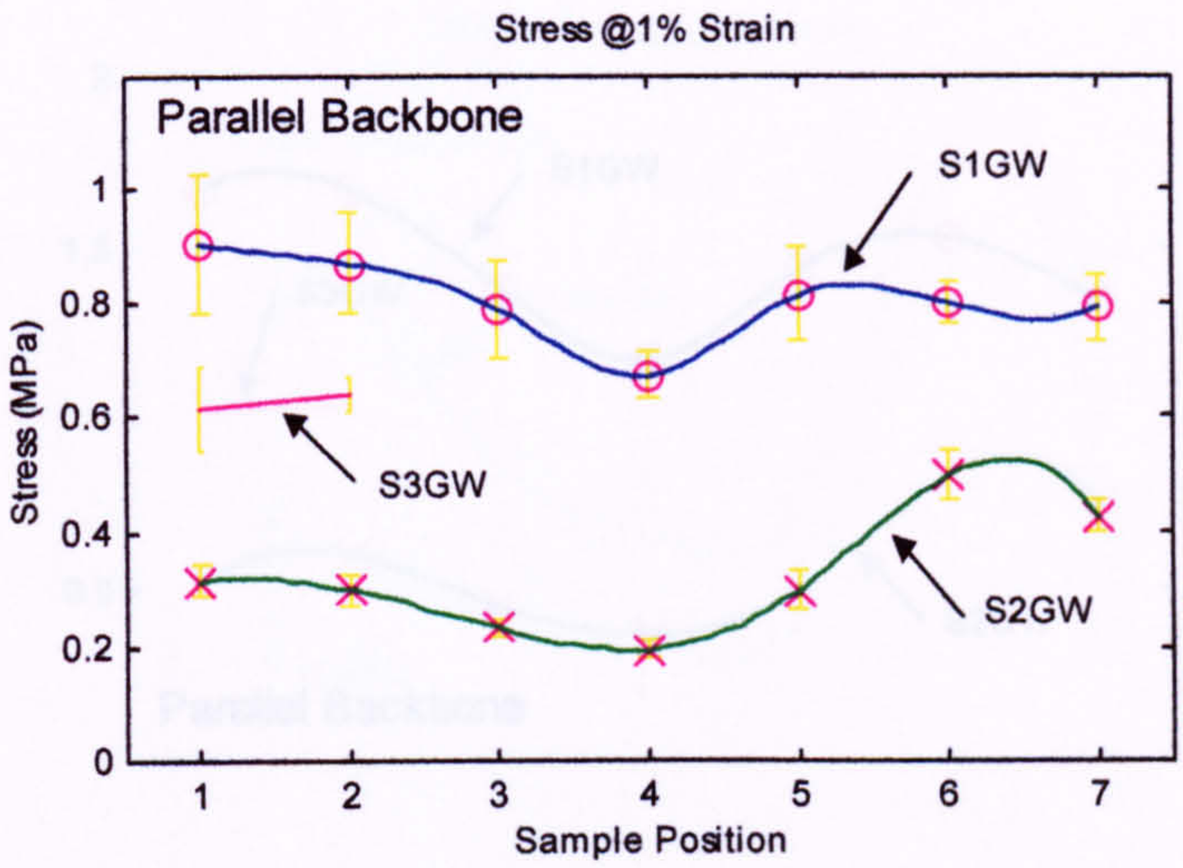

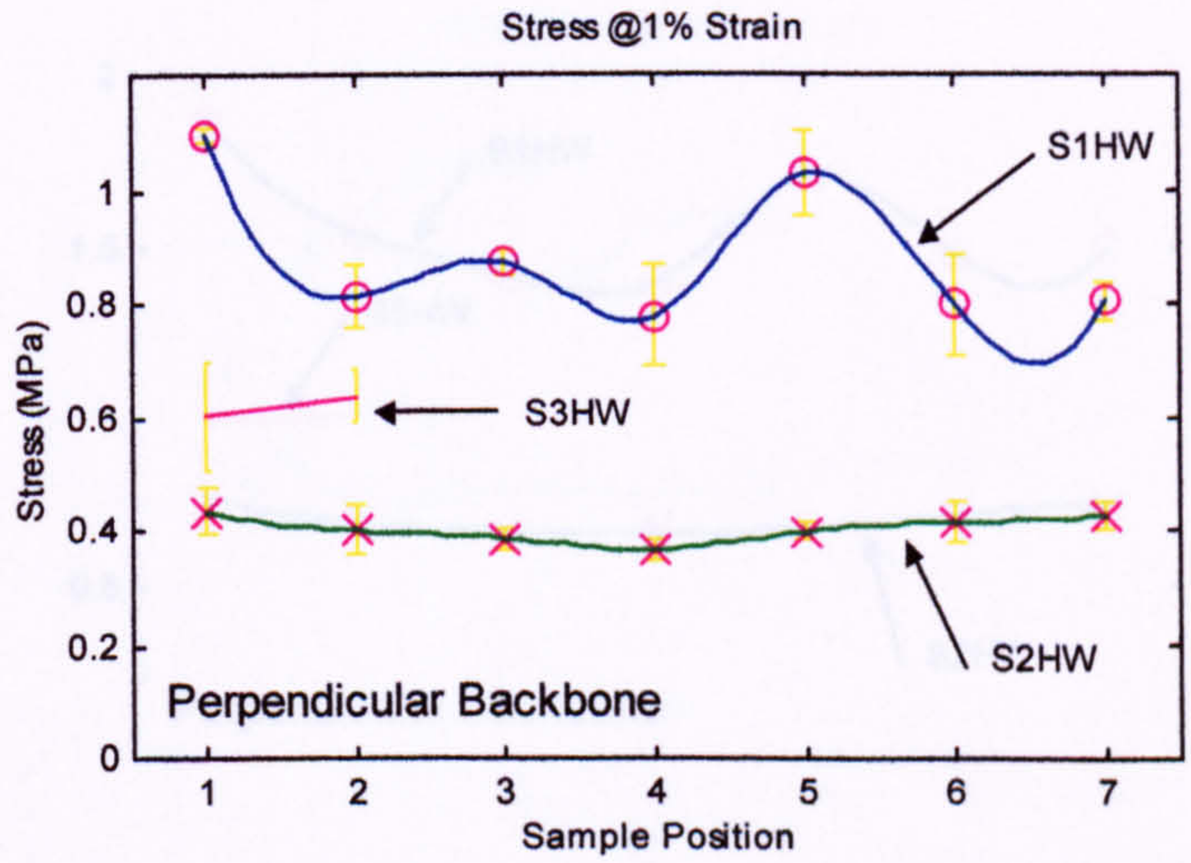

Figure 4.24-Plot of stress @1% strain for wide samples parallel and perpendicular to backbone. Tests performed under standard conditions, extension rate of 0.52 mms^{-1} with the velocity profile of Figure 4.21, each result is the average of six runs.

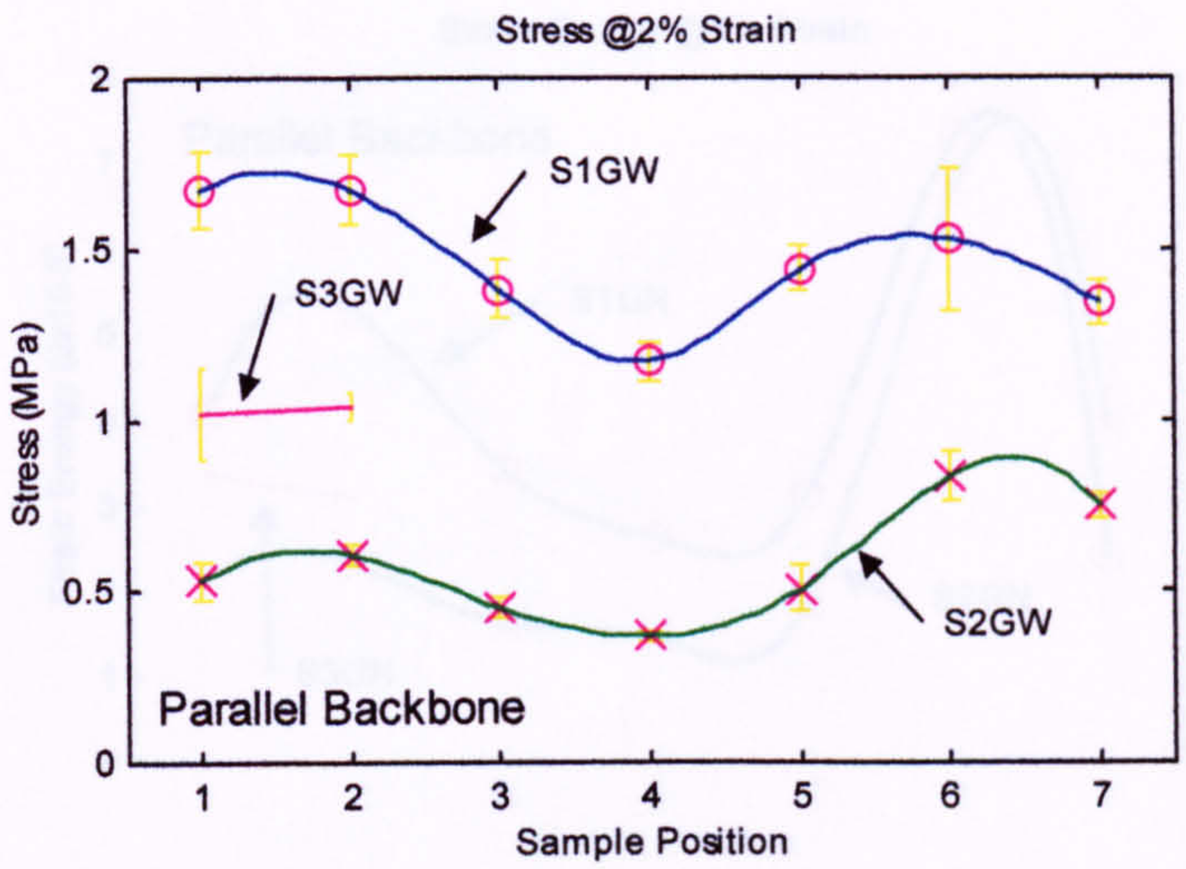

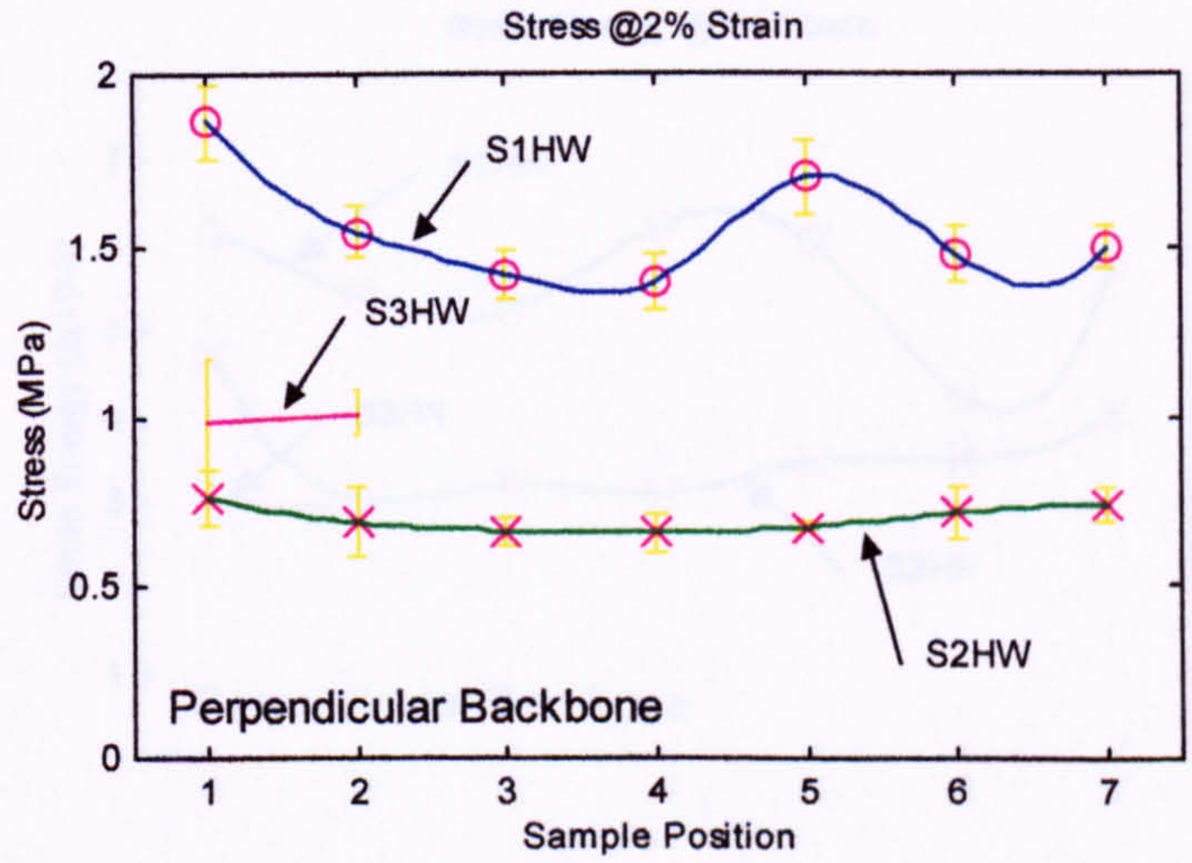

Figure 4.25-Plot of stress @2% strain for wide samples parallel and perpendicular to backbone. Tests performed under standard conditions, extension rate of 0.52 mms^{-1} with the velocity profile of Figure 4.21, each result is the average of six runs.

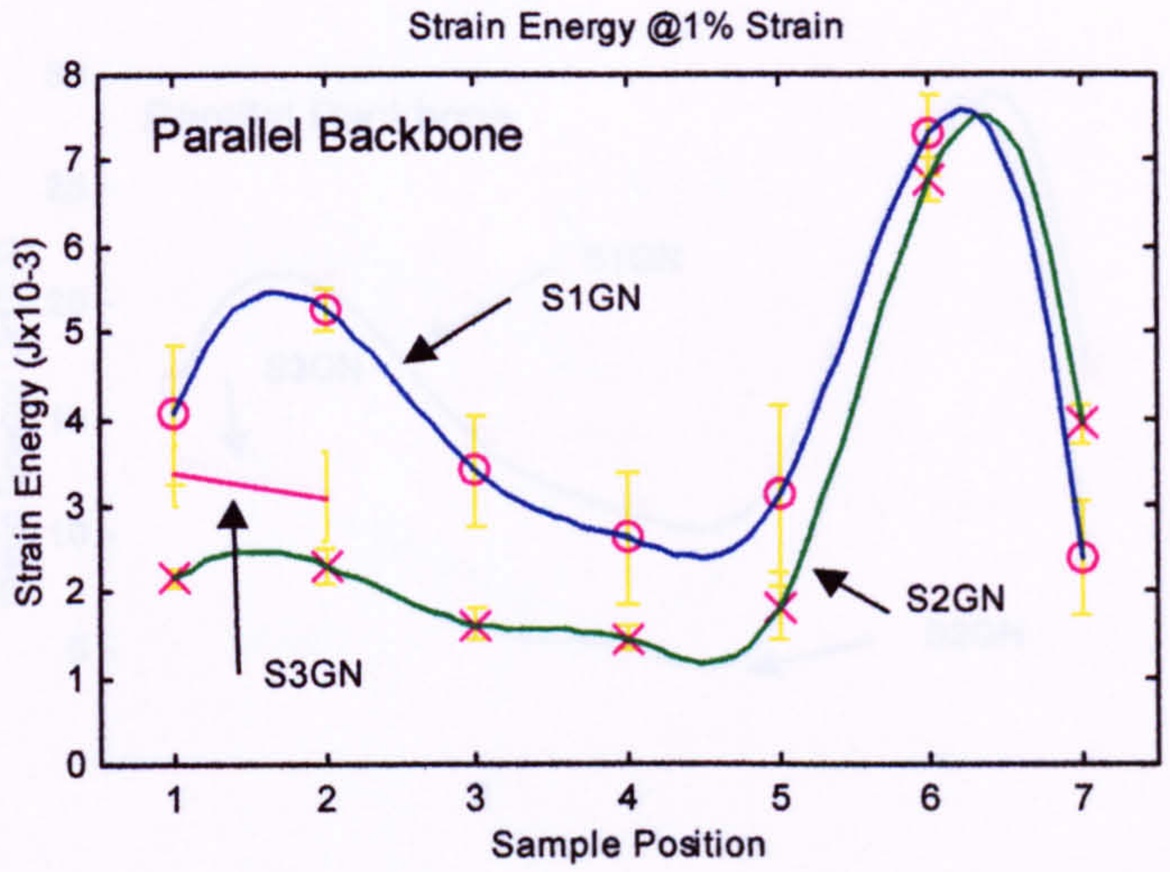

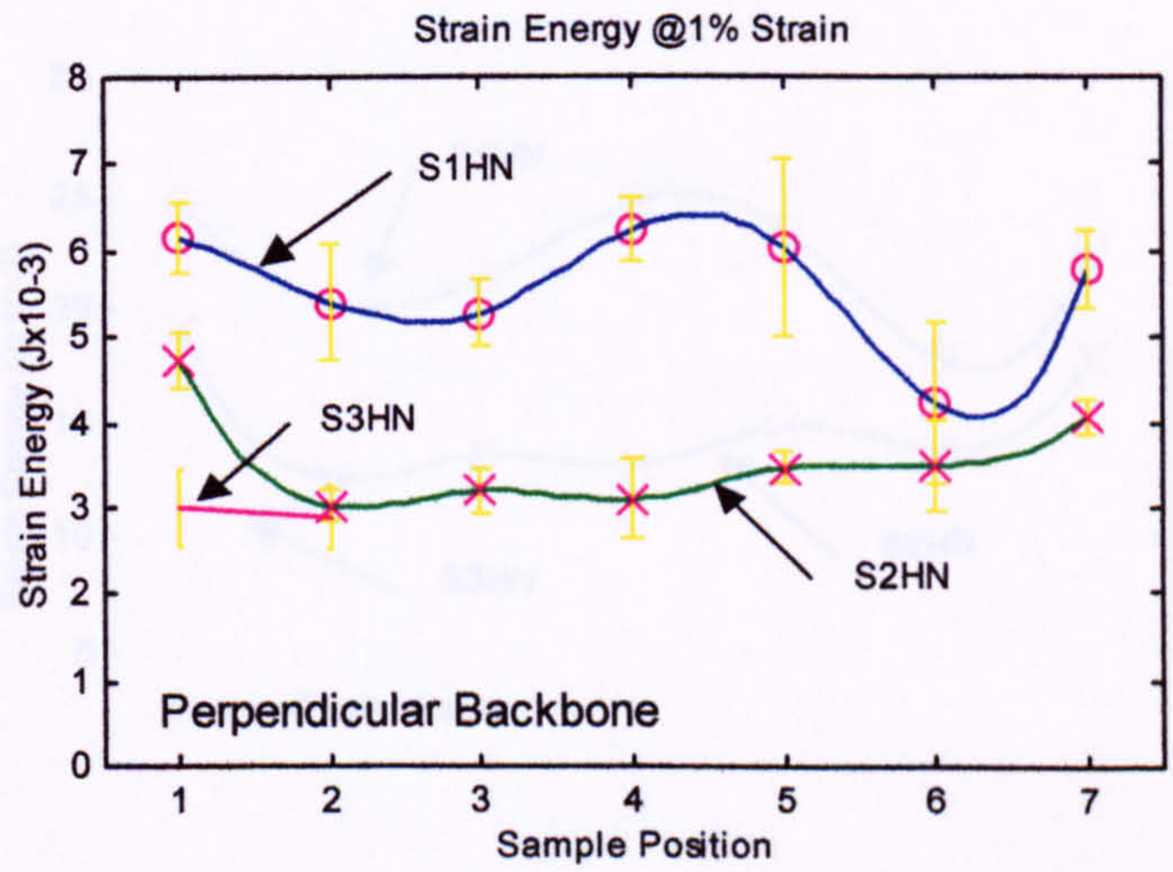

Figure 4.26-Plot of strain energy @1% strain for narrow samples parallel and perpendicular to backbone. Tests performed under standard conditions, extension rate of 0.52 mms^{-1} with the velocity profile of Figure 4.21, each result is the average of six runs.

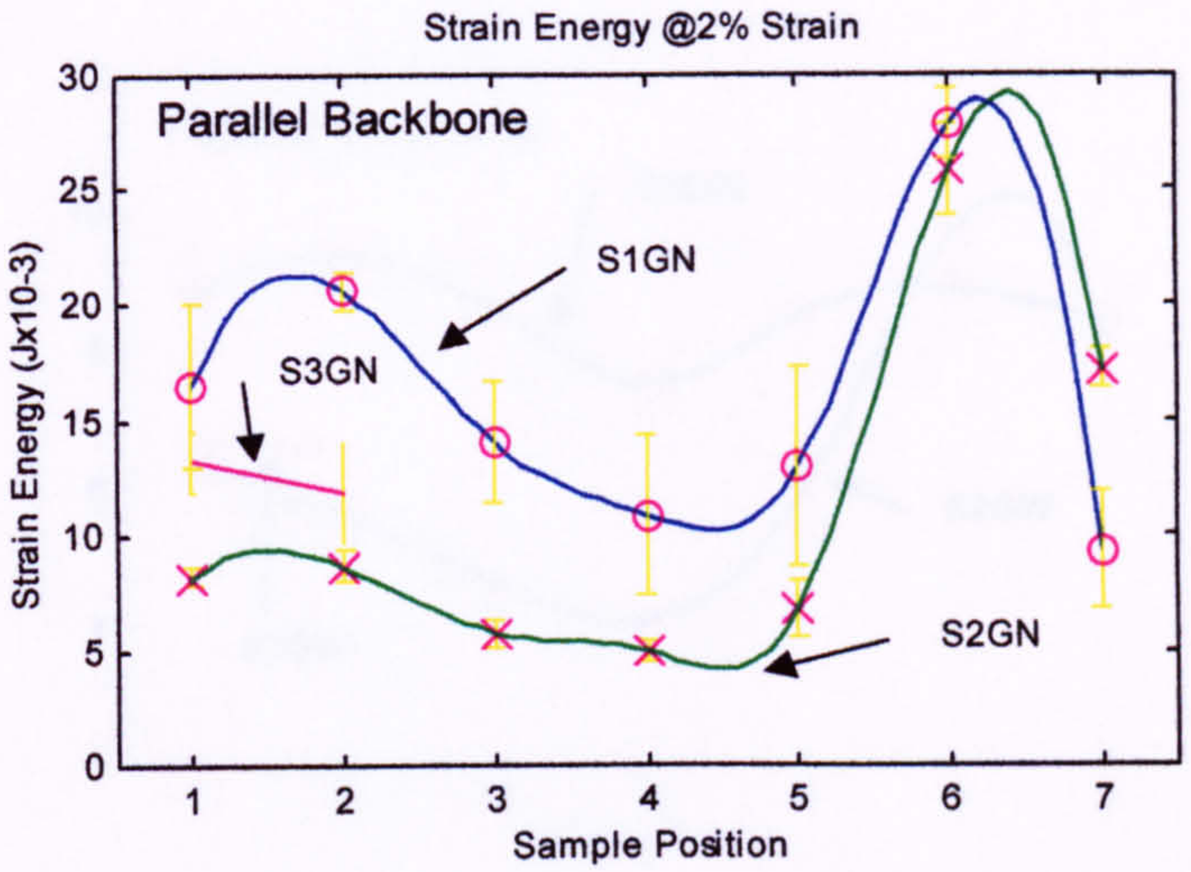

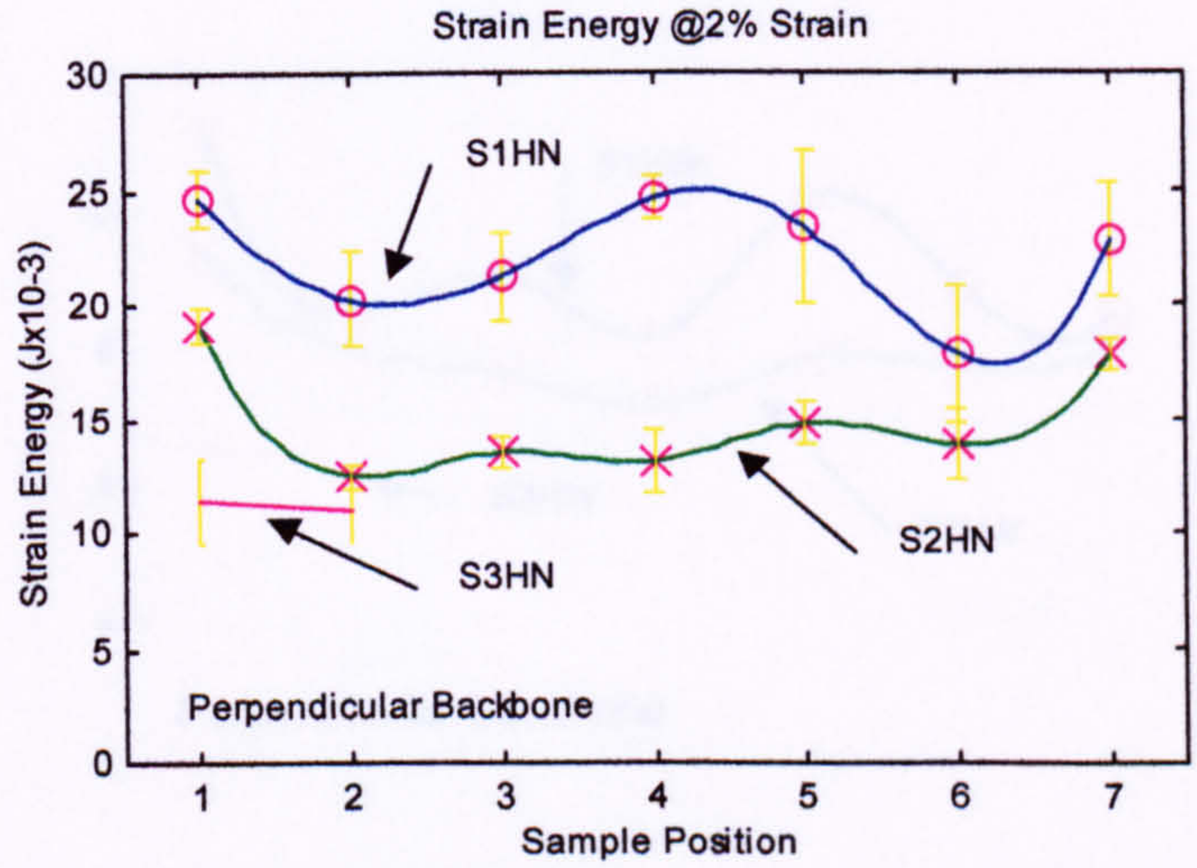

Figure 4.27-Plot of strain energy @2% strain for narrow samples parallel and perpendicular to backbone. Tests performed under standard conditions, extension rate of 0.52 mms^{-1} with the velocity profile of Figure 4.21, each result is the average of six runs.

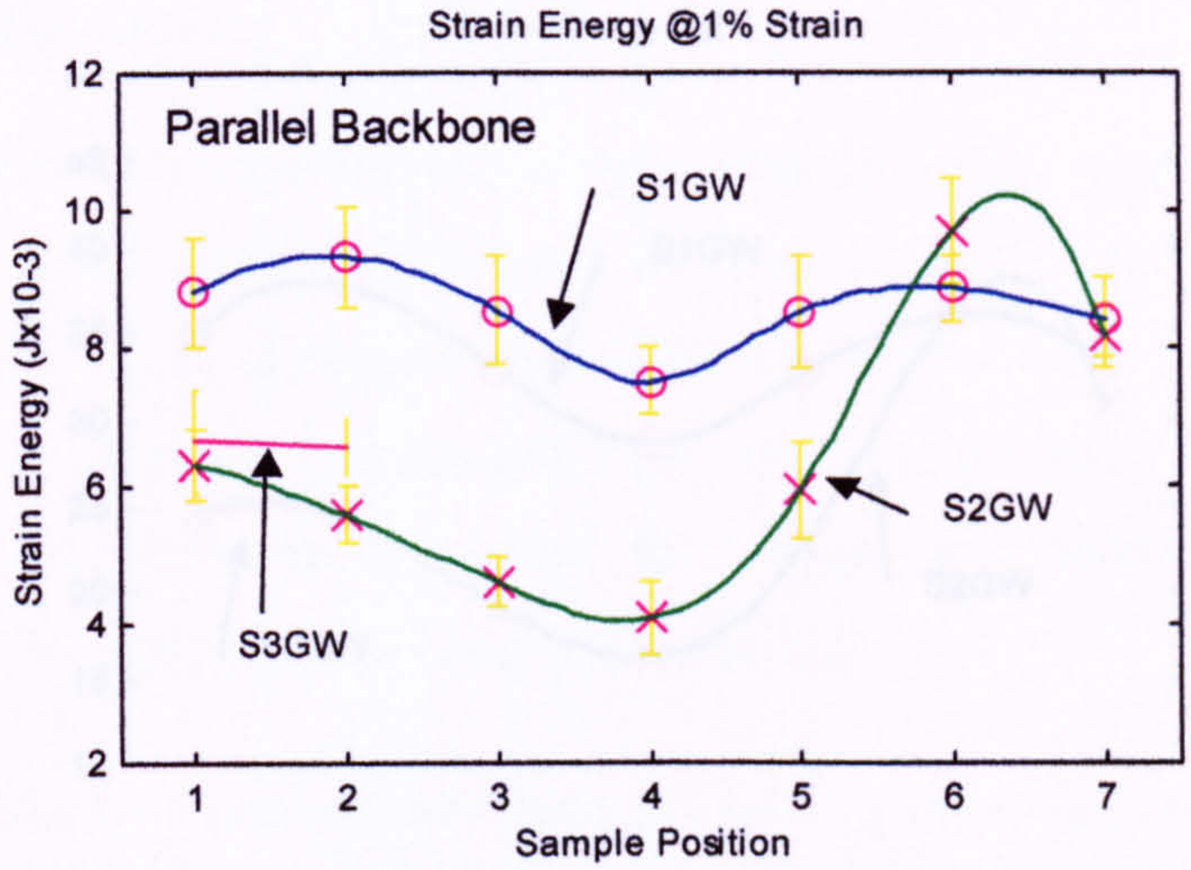

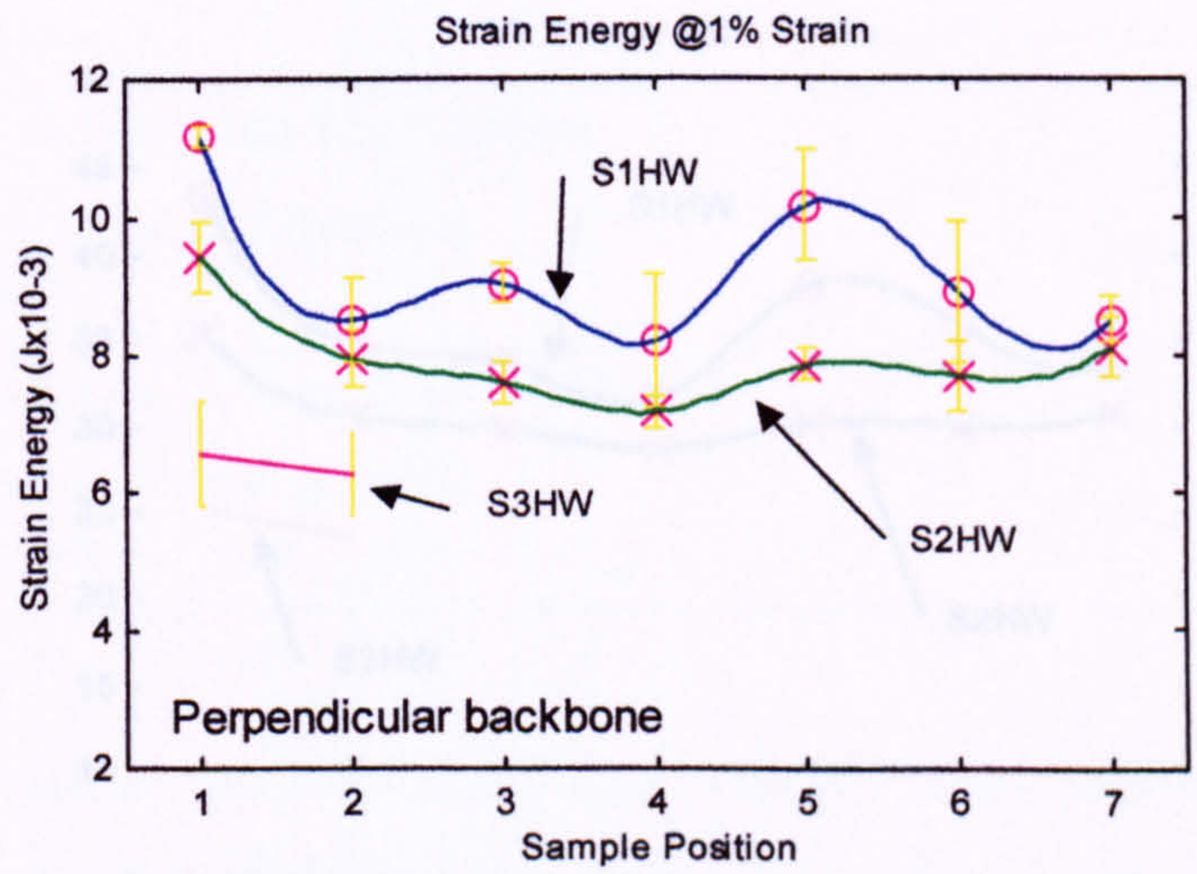

Figure 4.28-Plot of strain energy @1% strain for wide samples parallel and perpendicular to backbone. Tests performed under standard conditions, extension rate of 0.52 mms^{-1} with the velocity profile of Figure 4.21, each result is the average of six runs.

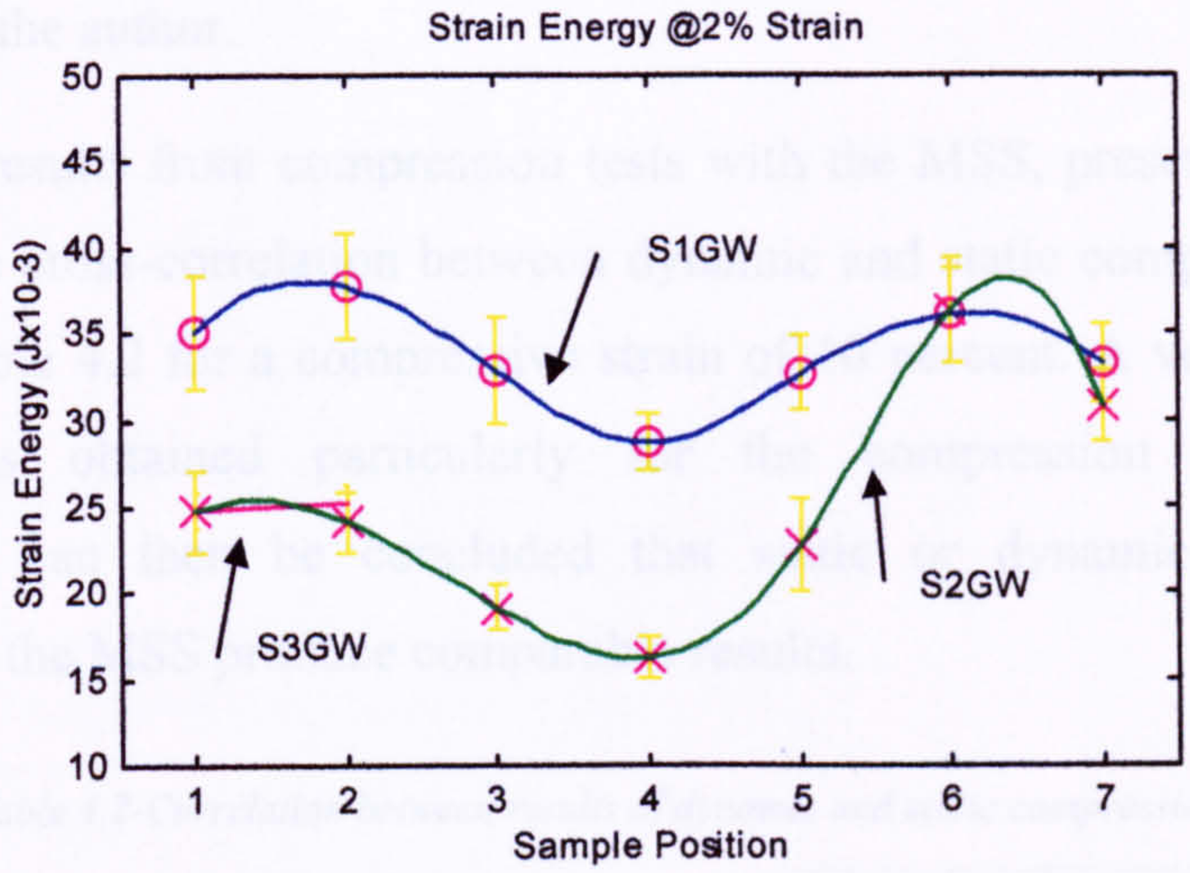

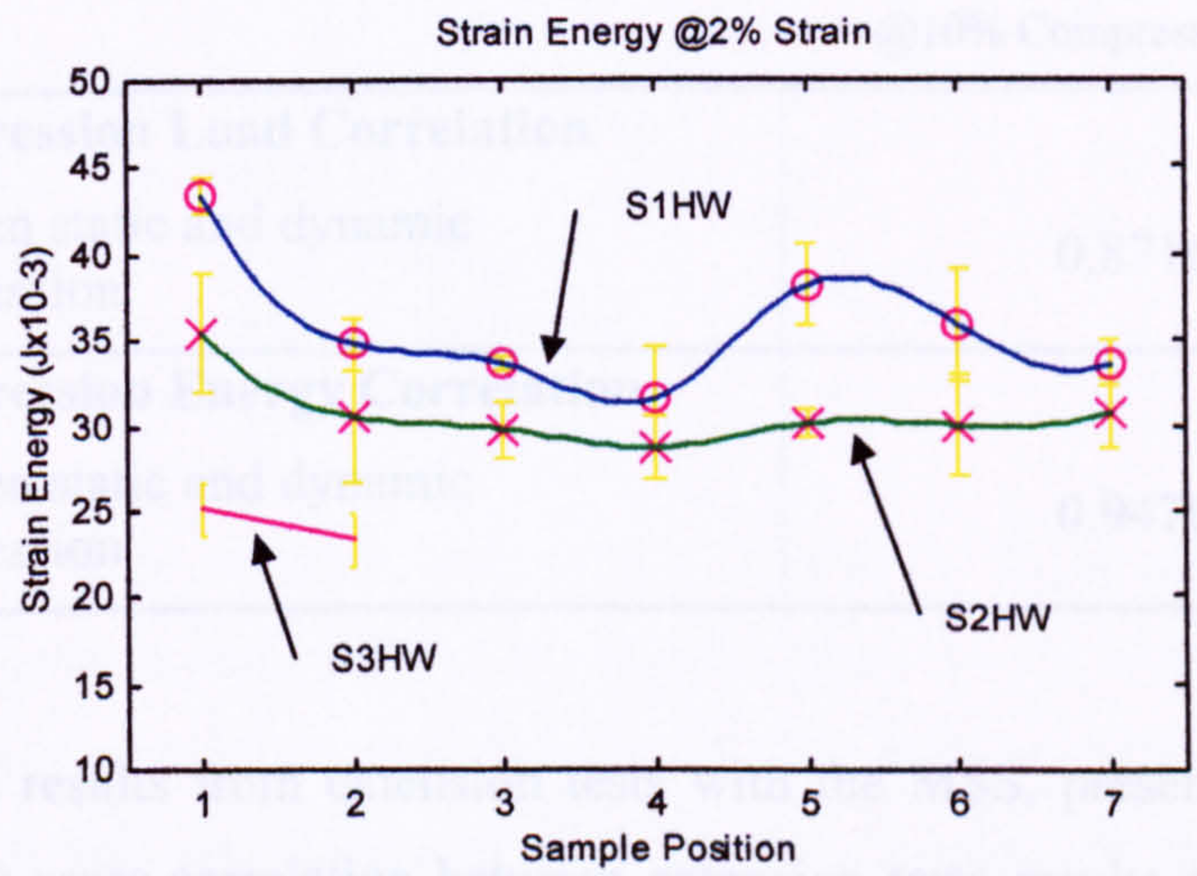

Figure 4.29-Plot of strain energy @2% strain for wide samples parallel and perpendicular to backbone. Tests performed under standard conditions, extension rate of 0.52 mms^{-1} with the velocity profile of Figure 4.21, each result is the average of six runs.

4.6 Evaluation of Results

The results of tests carried out with the Mechanical Scanning System to check the ability of the system to reliably collect data from testing leather confirmed the expectations of the author.

Regarding the results from compression tests with the MSS, presented in the previous sub-chapter, the cross-correlation between dynamic and static compression tests results is shown in Table 4.2 for a compressive strain of 10 percent. A very good correlation coefficient was obtained particularly for the compression energy correlation (r^2=0.9476). It can then be concluded that static or dynamic compression tests performed with the MSS produce comparable results.

Table 4.2-Correlation between results of dynamic and static compression tests.

	Correlation Coefficients @10% Compressive Strain
Compression Load Correlation	
Between static and dynamic compression	0.8716
Compression Energy Correlation	
Between static and dynamic compression	0.9476

Concerning the results from extension tests with the MSS, presented in the previous sub-chapter, the cross-correlation between extension tests results on narrow and wide samples is shown in Table 4.3 for a strain of 1 and 2 percent. A very good coefficient was obtained for stress and strain energy correlation between narrow and wide specimens. However, better correlations were found for samples perpendicular to the backbone. Thus, it can then be concluded that alike results are obtained for extension tests performed with the MSS for a strain of 1 and 2 percent.

In this work, only compression and extension experiments were performed, due to lack of time, shear stress experiments were not carried out. Other kind of tests could have been carried out if the mechanical characteristics of the MSS would allow it. The backlash of the utilised gearboxes and poor performance of the DC motors were serious limitations, because only tests in tension could be performed. In addition, from a test

where leather is initially stretched followed by a period of retraction (relaxation) more information could have been obtained about the viscoelasticity of the tested specimen.

Table 4.3-Correlation between extension tests results on narrow and wide samples.

	Correlation Coefficients	
	@1% Strain	@2% Strain
Stress Correlation		
Between narrow (N) and wide (W) samples	0.8826	0.8990
Between narrow (N) and wide (W) samples, parallel to backbone	0.8199	0.8618
Between narrow (N) and wide (W) samples, perpendicular to backbone	0.9445	0.9561
Strain Energy Correlation		
Between narrow (N) and wide (W) samples	0.8827	0.8967
Between narrow (N) and wide (W) samples, parallel to backbone	0.8019	0.8413
Between narrow (N) and wide (W) samples, perpendicular to backbone	0.9572	0.9574

Nevertheless, further work is needed to fully evaluate the MSS concept potential, such as, implement torque control instead of position control of the wheels. A better method for measuring real material displacement is a subject that should also be looked at. The stress calculation of wide samples also requires additional research. Finally, an investigation of the effect of using wheels with bigger diameter should be carried out regarding compression and extension tests. Obviously, bigger wheels have several other implications, for instance: more powerful motors are required, as more torque is needed; more compression force is necessary, as compression contact area is larger.

5

5 Infrared Thermography

5.1 Introduction

This chapter is concerned with leather inspection and characterization using infrared thermography. All tests were performed at the Department of Materials Science of Bath University, using the available system for transient thermography, with the permission and help of Professor D. Almond.

A description of the full transient thermography system is given, followed by considerations about infrared image restoration. Here, radiometric and spatial correction procedures are explained, as well as noise suppression techniques and effects of thermal stimulation methods in image restoration.

The characterisation results of infrared thermography, thermal diffusivity measurements and effect of leather anisotropy, precedes the divulgation of inspection results.

Man-made defects, with different diameters at different depths, were assessed by infrared thermography in different observation modes (reflection and transmission). Defect sizing was also carried out, followed by a brief analysis of the results.

5.2 Experimental Set-up for Thermal Analysis

The experimental set-up for thermal analysis by infrared thermography on its active approach is composed by four main components: a thermal stimulating source, an infrared camera, a recording system and an image analysis system.

As thermal stimulating source, two common floodlight lamps of 500 Watts each are mounted horizontally left and right of the centre line of the specimen as shown in Figure 5.1. These floodlight lamps are controlled by a personal computer, which is also connected to the recording system. However, to precisely control the heating time of the sample, two shutters are used to block the infrared radiation still emanating from the hot

lamp filaments after power removal. These shutters are like two guillotines that are controlled by the same personal computer.

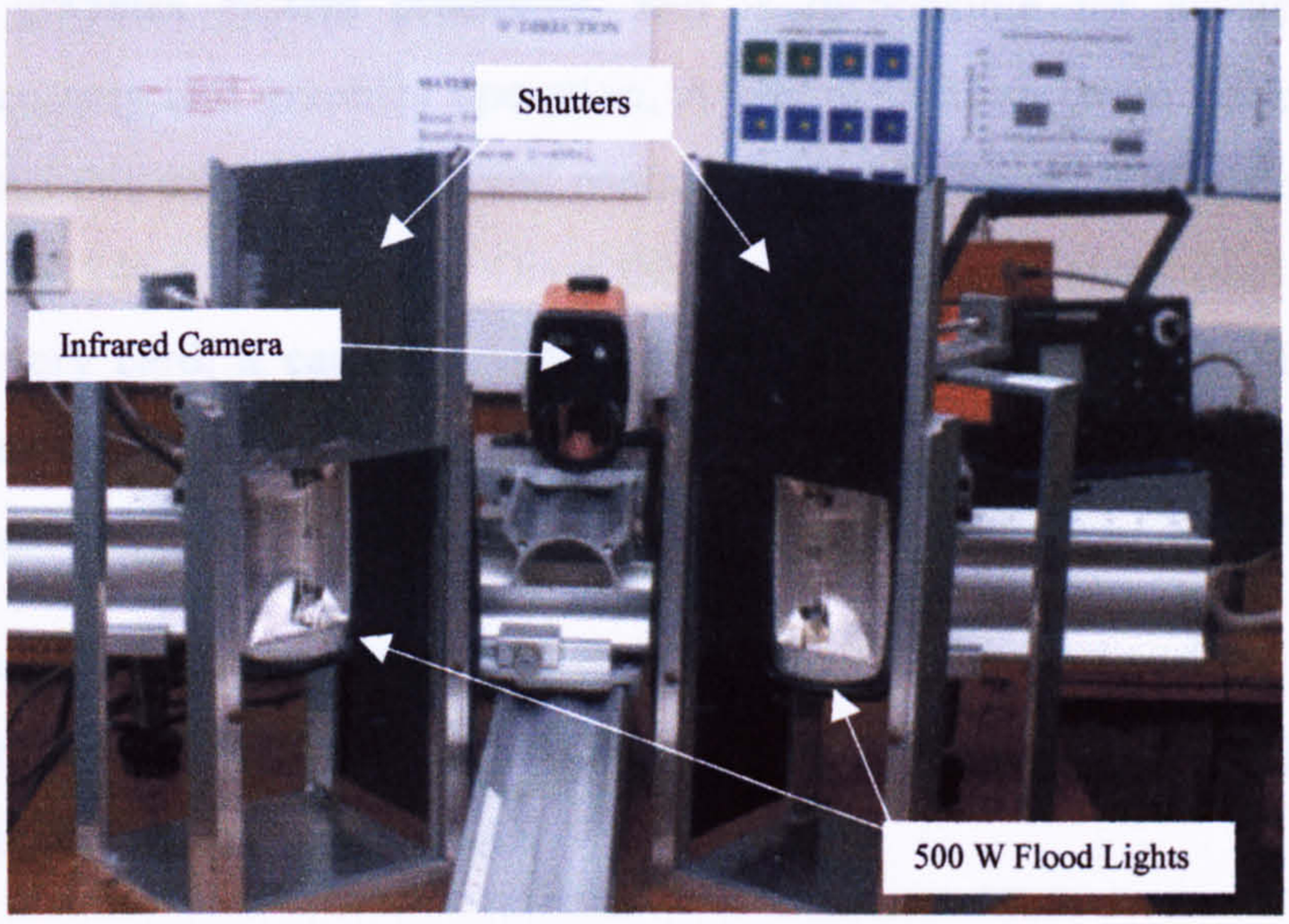

Figure 5.1-Infrared thermography set-up for active reflection mode approach.

The infrared camera used in this study is an IR camera Thermovision 750, manufactured by BG Agema Infrared Systems AB, Sweden [AGA 76]. The camera has a single Indium Antimonide (InSb) photovoltaic infrared detector, which is sensitive to the spectral range from 2 to 5.6 μm and is cooled by a liquid nitrogen dewar. According to its specifications, the minimum detectable temperature difference is 0.2 °C at 30 °C object temperature. Because a single infrared detector is employed, two polygon prisms are used in order to scan horizontally and vertically the field of view. These two prisms are continuously rotating at high speed (18000 rpm) in a synchronised way, resulting an image of four interlaced frames of 100 lines by 256 columns each. However, only 62 lines per frame contain useful data, consequently, an image composed of 248 lines by 256 columns is obtained. The scanning rate is 25 frames per second, producing a new complete image at a rate of 6.25 Hz. During these experiments, two proprietary lenses were utilised with a field of view of 12.5 ° and 40 ° respectively, both with a maximum aperture of f/1.8 and minimum focus distance of 700 mm. For close-up viewing an extension ring of 11 mm is also used.

A computer fitted with a modular frame grabber composes the recording system, which is capable of storing in memory a maximum of 24 images of data, approximately 3.84 seconds of continuous data from the camera. Data collection over longer periods

requires discarding many grabbed images and keeping only every Nth image up to the card maximum capacity. The frame grabber card is based on a Digital Signal Processor, TMS34020 graphics system processor, and is responsible for accelerating image display, processing and graphics operation. A commercial software library package is used to control this card [MFG 93] and produces an eight-bit resolution image (0 to 255 grey levels) of 246 by 256 pixels. Once the data is digitised and stored in the frame grabber memory card, it can be saved to disk for subsequent analysis. Each frame is stored in a single file named with the frame number in a specific proprietary format; a utility program converts these image files to Tag Image File Format (tiff) format.

The image analysis system available at Bath University is limited and not very flexible. Therefore, the author developed a small set of routines (functions and scripts) dedicated to infrared thermography in MATLAB.

Initial tests with the infrared imaging system available at Bath University performed by the author showed that this system, as it is, should not be used for absolute quantitative temperature measurements. A continuous slow drift of the output values for the same image under the same conditions over a relatively short period was observed, making it very difficult to perform experiments without occasional adjustments to the infrared camera settings (offset adjustments). Perhaps, the fact that the single infrared radiation detector of the camera is cooled by liquid nitrogen and each refill of the cooling dewar lasts for two hours, in combination with the age of the camera explains the observed drift. Unless two reference temperature targets are included in the field of view of every single thermogram, proper calibration for converting to absolute temperature is very difficult if not impossible. With these temperature references, one at room temperature while the other at a higher temperature (ideally equal to the maximum input range of the camera), conversion from arbitrary temperature units (eight bit value) to absolute temperature units would be easily achieved, as long as the emissivity of the material being analysed is known.

Nevertheless, qualitative and quantitative measurements in arbitrary units can be carried out with the infrared imaging system of Bath University, with the usual difficulties associated with thermal image processing.

5.3 Infrared Image Restoration

5.3.1 Radiometric Correction

A former researcher at Bath University, Hamzah, characterised experimentally the infrared imaging system used in this work and concluded that no significant improvements were achieved if radiometric distortion corrections were applied [Hamzah 96a]. If quantitative measurements of absolute temperature are not to be carried out, then radiometric correction may be avoided.

Nevertheless, the author performed several tests and concluded that some correction should be applied to the raw thermal data as shown below, unless it is used a contrast method for image analysis that is immune to emissivity (e.g., standard contrast).

In Figure 5.2, each curve corresponds to the average of all rows of an image, i.e., the value of column one is the average of the values of same column of all 246 rows of the image. It is clear that there is a trend for the right hand side of the image to be always hotter than the rest. This is not caused by non-uniform heating as suggested by Hamzah, but by radiometric distortion.

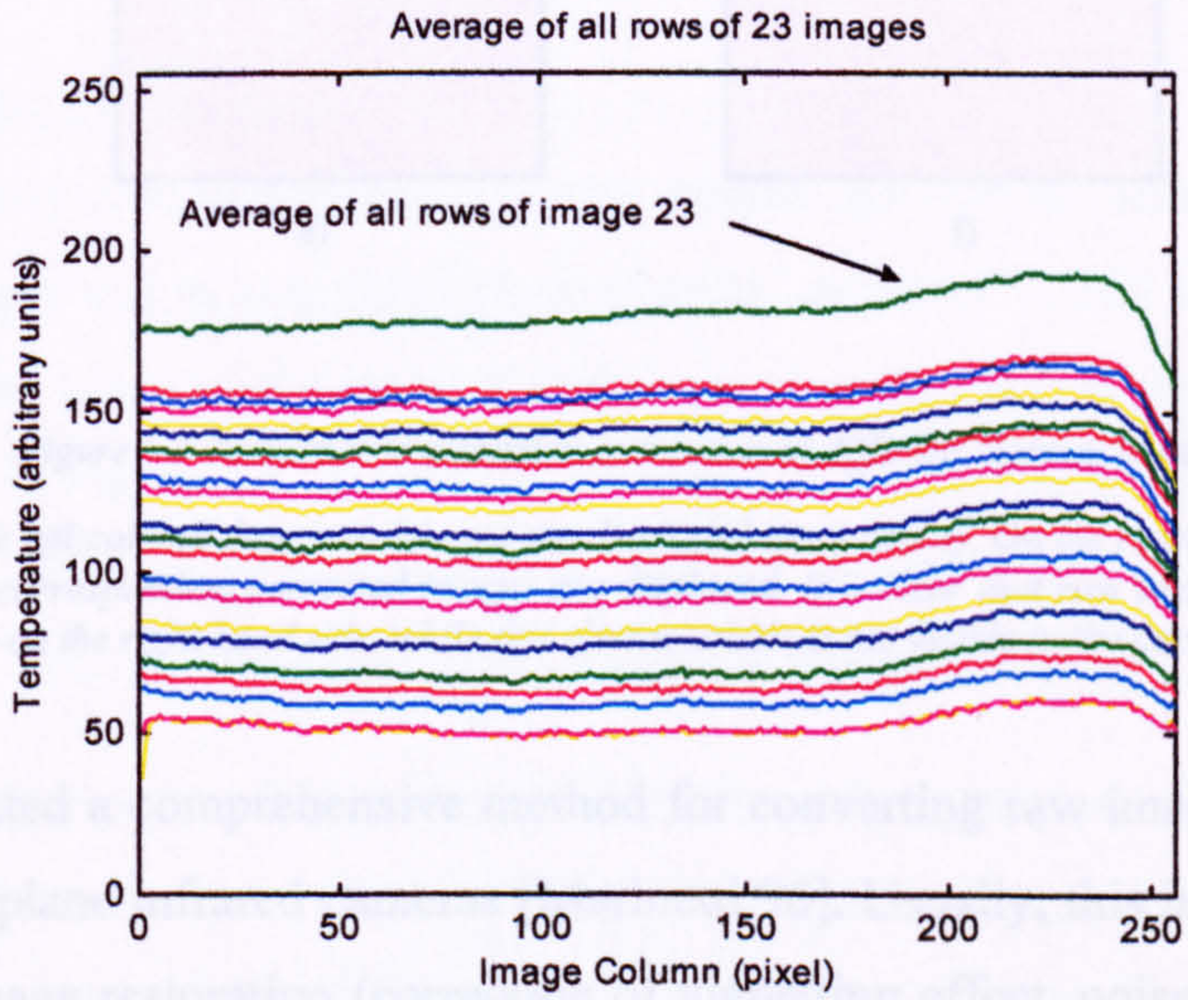

Figure 5.2-Side view frame representation of 23 images at different temperatures.

Each curve corresponds to the average of all rows of an image. The raw thermograms represent the temperature of a copper plate ("blackbody"), covered with black paint for maximum and homogenous emissivity. The temperature of the copper plate was controlled by a water bath in a set-up built by the author. The black paint is a special heat dispersant matt black paint with added graphite with emissivity about 0.99.

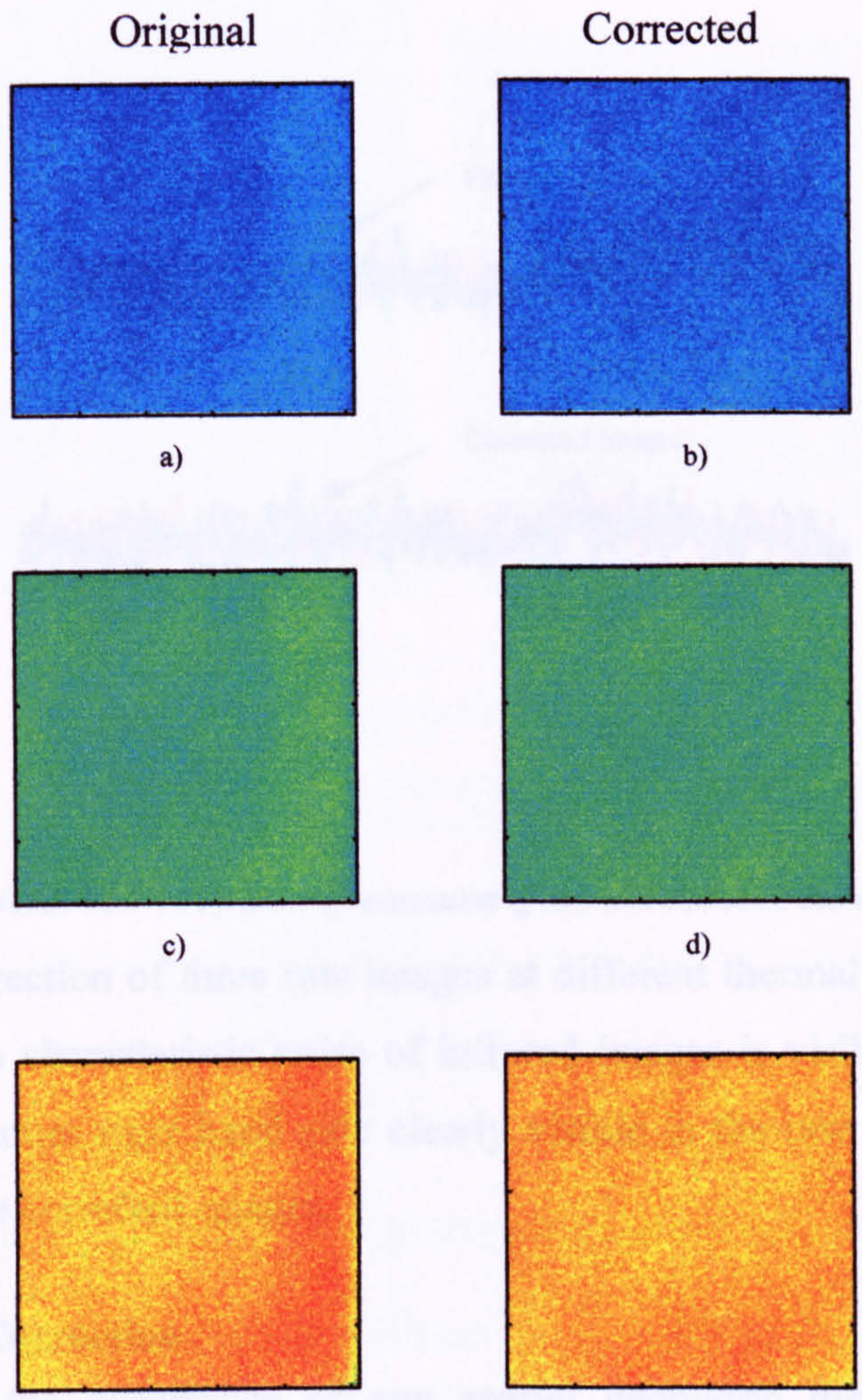

Figure 5.3-Radiometric distortion correction at different thermal levels.

On the left column three raw images are displayed a), c) and e). On the right hand side the three correspondent corrected images are displayed. It is clear that raw images tend to be hotter on the right hand side, while this characteristic is not visible in the corrected images.

Marinetti presented a comprehensive method for converting raw images to temperature images of focal plane infrared cameras [Marinetti 96]. Usually, this involves one or two steps such as image restoration (correction of vignetting effect, noise suppression), and conversion of raw pixel values to temperature, following a calibration procedure.

In Figure 5.4, a side view wire frame representation of a few rows of a raw image is shown, as well as the same rows after correction for radiometric distortion.

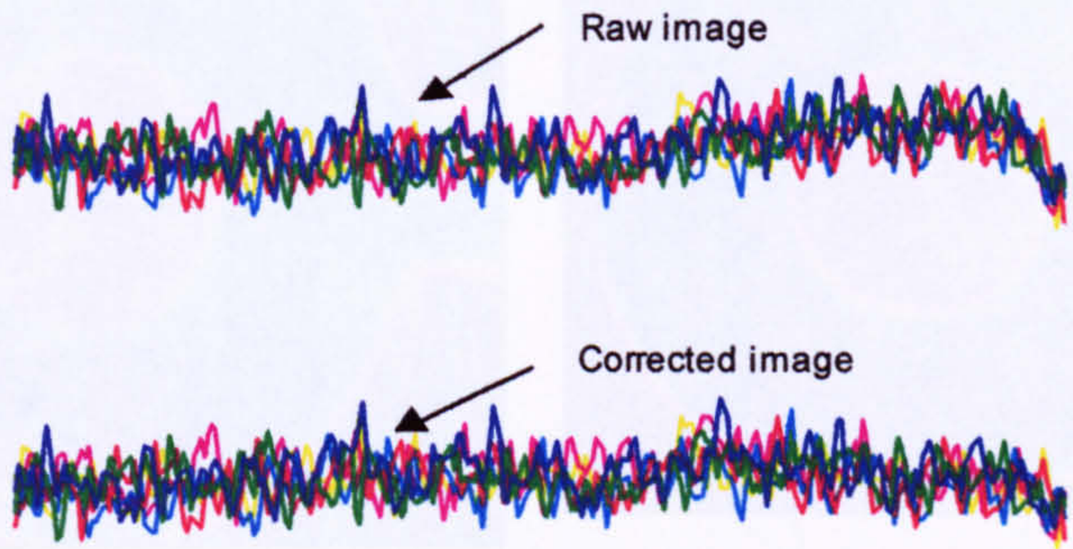

Figure 5.4-Side view wire frame representation of raw and corrected thermogram.

The radiometric correction of three raw images at different thermal levels in shown in Figure 5.3. Only the characteristic noise of infrared images is visible in the corrected thermograms. The hotter right hand side clearly visible in the raw thermograms is no longer relevant in the corrected images.

5.3.2 Spatial Correction

In order to verify the occurrence of any spatial geometric distortion, the author performed a simple test with a round piece of metal as target. A full sequence of images (24 images) of the scene of the piece of metal was acquired and averaged. The resulting image is shown in Figure 5.5 a). Clearly, the vertical to horizontal ratio is distorted and this affects this infrared imaging system. The ellipsoidal shape in the centre of the image should be circular, as shown in the corrected image in Figure 5.5 b).

The geometrical correction factor was obtained from the spatial resolution of the image (pixel.mm^{-1}), dimensions of the circle in the original image (pixel) and the real dimension of the inner circle of the piece of metal (mm). It was found that the vertical axis was oversized by a factor of 1.112; to correct the original image it is necessary to resize the vertical axis. The overall spatial resolution of the camera for this set-up (lens, extension rig, distance object-focal plane) is about 4.5 pixel.mm^{-1}.

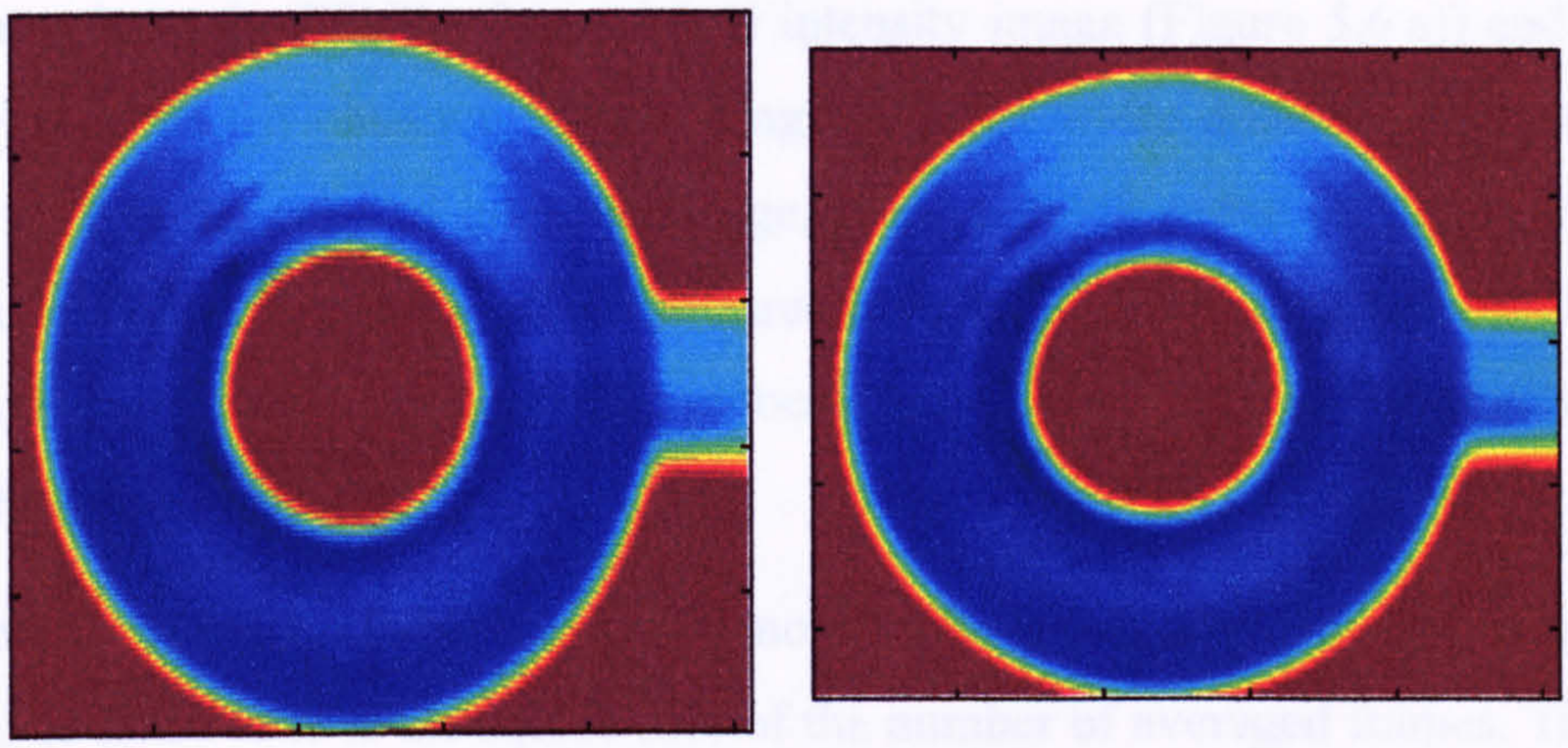

a) b)

Figure 5.5-Spatial distortion correction.

a) original infrared image b) infrared image after geometric correction; Set-up: lens of 12.5° FOV plus 11 mm extension ring; distance object focal plane 370 mm.

The same amount of geometrical distortion was observed for any combination of lens and extension ring.

5.3.3 Noise Suppression

It is of interest to quantify the noise content present in infrared images.

Following a technique proposed by Fisher *et al.* [Fisher 95], and presented in Section 2.5.4, the peak signal-to-noise ratio (PSNR) of images acquired with the infrared imaging system of Bath University was computed.

Several infrared images of a specimen of leather (grain side), under the same conditions at room temperature, were recorded. PSNR calculations for three different level settings of the infrared camera are shown on Table 5.1, these values result from averaging six PSNR. Before performing PSNR calculations, all infrared images were obviously scaled down to the range [0..1].

These results show that noise is independent of the selected thermal level, thus the intensity of the image, which is certainly desirable.

Table 5.1-PSNR calculations for three different level settings.

Thermal Level	PSNR (dB)
Low Level (30)	+22.08
Medium Level (128)	+21.93
High Level (220)	+21.87

As a comparison, the PSNR of an original intensity image (Figure 5.6 a)) and another image (Figure 5.6 b)) obtained from adding Gaussian white noise of zero mean and variance 0.01 to the original intensity image, gives a PSNR value of 20.79 dB. Figure 5.6 gives an idea of how noise affects infrared images. If broadcasted television images had such a poor PSNR, certainly the number of people addicted to the television sets would be much lower.

The simplest and most reliable method for noise reduction is temporal averaging, where the signal-to-noise ratio is the square root of the number of averaged frames. The edges and spatial resolution are not affected as long as repeatability of the experiments is adequate. In this work, all image sequences were acquired at least four times for averaging and consequent noise reduction.

a) b)

Figure 5.6-Effects of noise in a normal image on the same scale of infrared image noise.

PSNR of these images is +20.79 dB. a) original image; b) original image with added Gaussian noise type of zero mean and variance 0.01.

Other noise suppression techniques, used in normal vision image processing, can also be used, for instance, median filtering techniques. However, great care is needed to preserve the edges and to minimize the characteristic high frequency noise of infrared images.

Table 5.2-PSNR calculations for grain and flesh side.

Specimen	PSNR (dB)	
	Grain Side	Flesh Side
S14I	+22.09	+23.83
S24I	+21.98	+23.93
S32I	+21.94	+23.97

Nonetheless, there are approaches that can further contribute to minimise the noise content of infrared images. In infrared thermography, rougher surfaces tend to give higher noise content images. A small experiment was designed to find out if infrared image acquisition should be accomplished from the grain side or the flesh side. Three sets of twenty-four infrared images of the grain side of specimens S14I, S24I and S32I were acquired. Another three sets of twenty-four infrared images of the flesh side of the same specimens were also taken. These images represent the same stationary scene either of the grain side or the flesh side without any kind of thermal stimulation. Peak signal-to-noise ratio (PSNR) of every two subsequent images was calculated and averaged and Table 5.2 presents the final results.

5.3.4 Stimulation Methods

The stimulation method available at Bath University is restricted to pulse thermography or transient thermography, with the stimulation sources previously described in section 5.2 and a heat gun/hot-air jet. Thus, the assessment of other stimulation methods and sources for leather testing was not possible.

A PC controls the thermal stimulation system, composed by two common floodlight lamps of 500 Watts and respective shutters. The heating timing is the product of heating time units by 0.16 seconds. The system does not allow control over the heating power of the lamps; they are either on or off.

The major problem associated with thermal stimulation by surface heating is that a certain degree of non-uniform heat flux on the specimen is always present. For small inspection areas that effect may be ignored. However, for large inspection areas the non-uniformity of the heat flux must be considered and the correspondent correction should be applied. In lock-in thermography, the non-homogeneity of the heating source is not a concern, as this method is completely immune to it, which is a great advantage when compared with transient thermography.

In Figure 5.7, two thermograms of a sequence of twenty-four are displayed and the effect of non-homogenous heating is clearly visible, where the centre of the specimen gets hotter than peripheral areas.

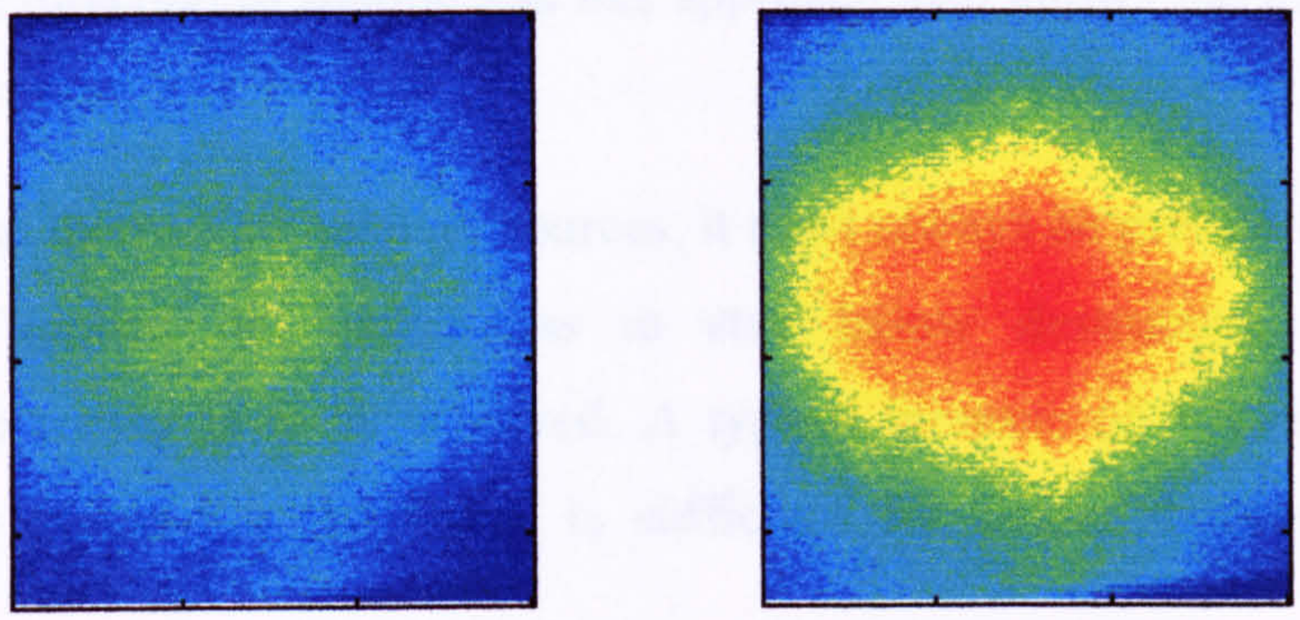

a) b)

Figure 5.7-Effect of non-uniform surface heating.

a) infrared image at t=1 s b) infrared image at t=3 s; Transmission observation mode; heating time 4 units; frame acquisition delay 250 ms; lens of 40° FOV; distance object focal plane 550 mm.

In Figure 5.8, a three-dimensional plot of Figure 5.7 b) gives a better perception of the distribution of heat on the surface of the specimen. The test was performed on a defect free specimen, so no subsurface flaws cause any relevant perturbation in the captured images. These thermograms are only affected by noise and non-uniform heating.

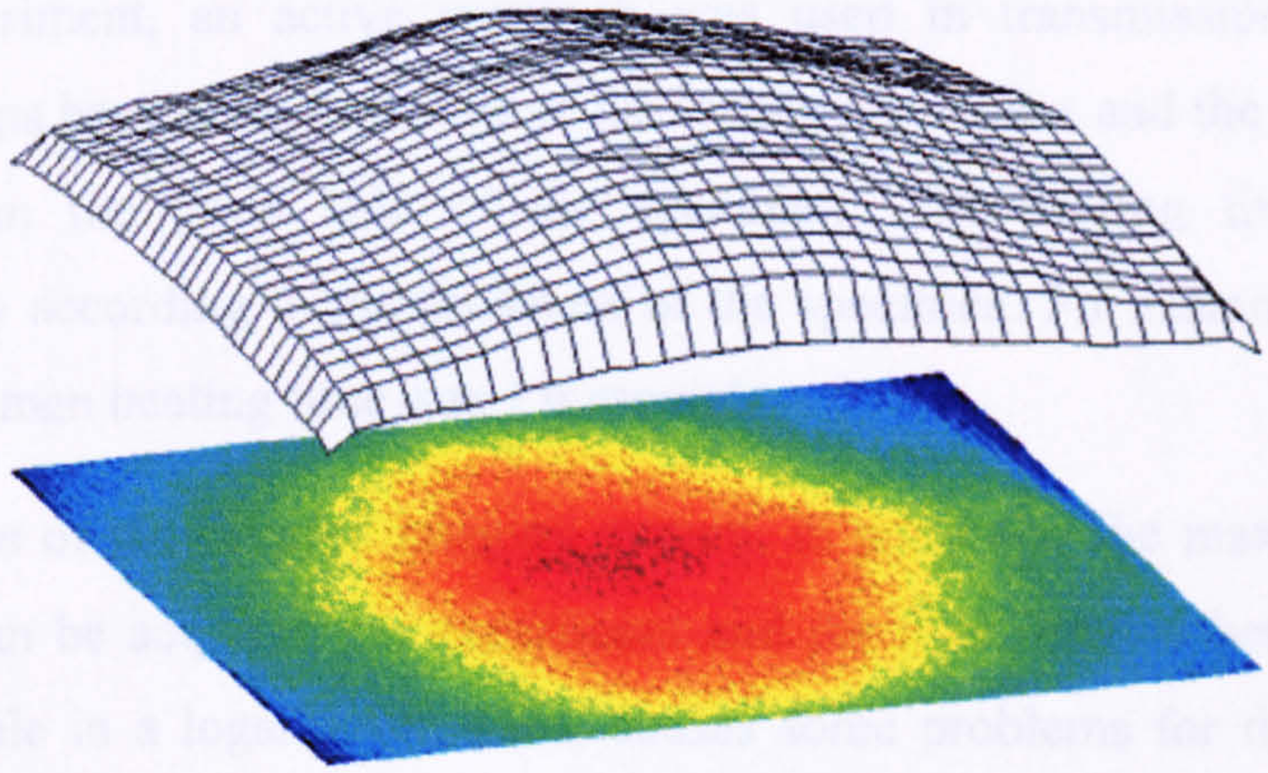

Figure 5.8-Non-uniform heating.

Infrared image at t=3 s; Transmission observation mode; heating time 4 units; frame acquisition delay 250 ms; lens of 40° FOV; distance object focal plane 550 mm.

With line heating, two configurations are possible: either the specimen is static and the inspection head (heating element and camera) moves to cover the specimen surface; or the inspection head is static and the specimen moves. Heating uniformity is easily

achieved in the direction of motion and this approach also allows the utilisation of line scan cameras.

When setting up thermal stimulation sources, it must always be present that the amount of heat flux applied on leather has to stay below destructive levels, if real non-destructive testing is to be achieved. A typical increase of 5 °C to 10 °C on the surface of the material to be tested is sufficient for defect detection by infrared thermography.

5.4 Characterisation results

Leather characterisation by infrared thermography in this thesis is limited to thermal diffusivity measurements in arbitrary temperature units and verification of the effects of leather anisotropy in heat flow.

5.4.1 Thermal Diffusivity measurements

In this particular measurement, the fact of not knowing the absolute temperature is irrelevant because the measurement of interest is the time required for the specimen to reach its half maximum, thus a relative measurement.

For this experiment, an active approach was used in transmission mode, i.e., the floodlight lamps heated the flesh side of the leather specimens and the infrared radiation measured from the grain side of the specimen. The heating time was adjusted experimentally according to the thickness of the specimen. For instance, in the case of the thick specimen heating time was 1.6 seconds.

The limitations of the infrared imaging system, in particular the maximum number of images that can be acquired per experiment and the time interval between images not being adjustable in a logarithmic scale, causes some problems for thermal diffusivity measurements. The measurement of temperature increase is much more critical than measuring temperature decay because the first phenomenon is much faster than the second. In Figure 5.9, a plot of a thermal diffusivity measurement, with a linear and logarithmic time scale, are shown. The curve of Figure 5.9 is a composition of two image sequences, the first and second acquired with a frame time interval respectively of 250 milliseconds and 2.75 seconds. This approach allowed the accurate recording of 60 seconds of data.

To take into account the initial temperature of the specimens, thermograms of the specimens before heating were recorded, enabling later offset correction of errors.

Each datum displayed in Figure 5.9 results from averaging a small 10 by 10 pixel matrix on the same relative location of each thermogram.

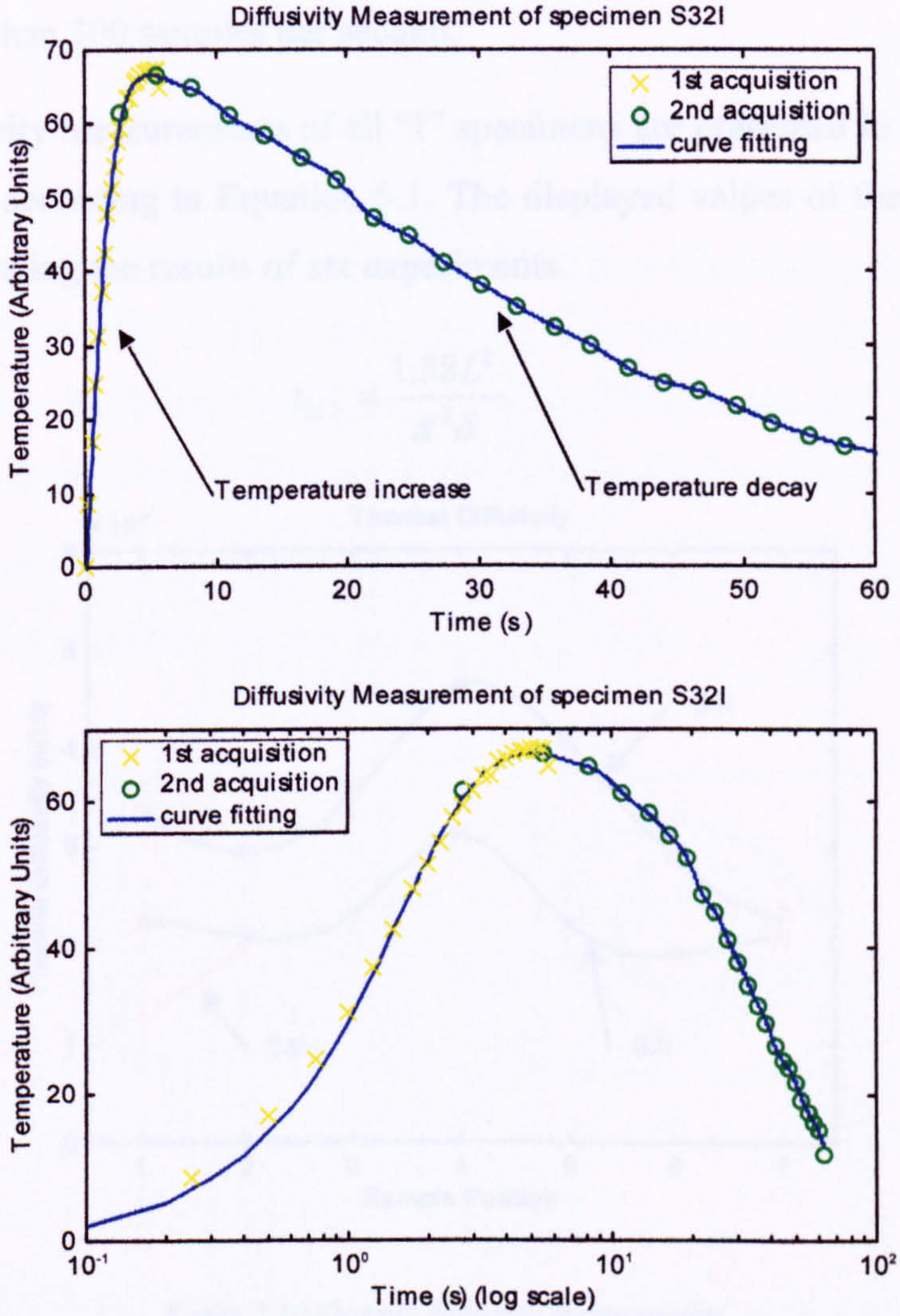

Figure 5.9-Thermal diffusivity measurement of specimen S32I.

Transmission observation mode; heating time of 1.6 s; frame acquisition delay for 1st acquisition and 2nd acquisition of respectively 250 ms and 2.75 s; lens of 12.5° FOV plus 11 mm extension ring; specimen distance from camera 370 mm.

Thermal diffusivity measurements of the thin specimens turned out to be quite difficult because the temperature increase phenomenon was too quick for the maximum frame

acquisition rate allowed by the infrared camera. A compromise between heating time, temperature amplitude variation and frame capturing interval had to be found.

Obviously, the procedure described above for measuring thermal diffusivity would have been unnecessary if a more up to date system was available, especially with a focal plane array based infrared camera. In these cameras, high sampling rates can be achieved, more than 300 samples per second.

Thermal diffusivity measurements of all "I" specimens are presented in Figure 5.10 and were calculated according to Equation 5.1. The displayed values of thermal diffusivity result from averaging the results of six experiments.

$$t_{1/2} = \frac{1.38L^2}{\pi^2 \delta} \tag{5.1}$$

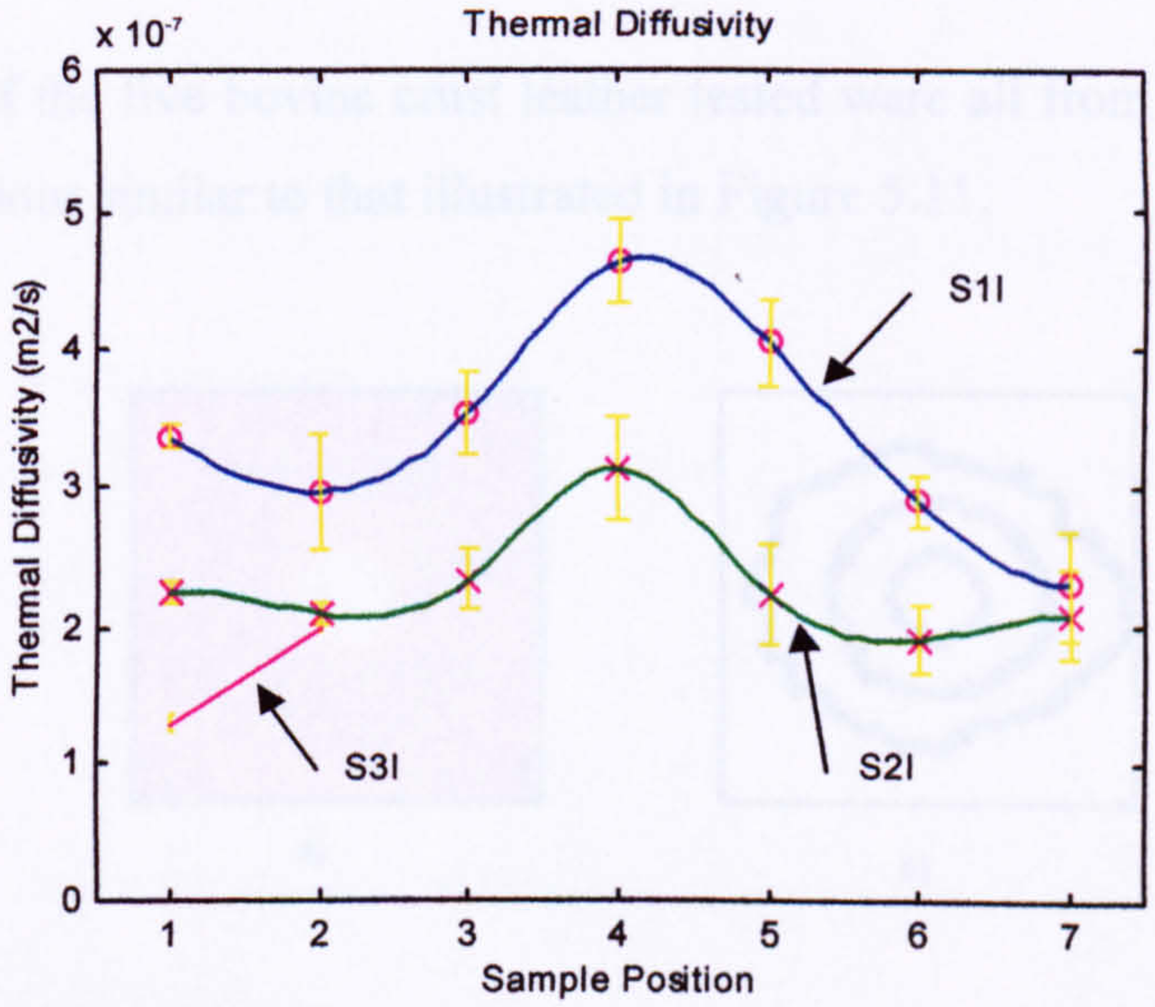

Figure 5.10-Thermal diffusivity measurements.

The values obtained for thermal diffusivity of leather are not mentioned in literature, however glass has a thermal diffusivity of 4.2×10^{-7} $m^2 s^{-1}$ [Maldague 93b].

5.4.2 Effects of leather anisotropy in heat flow

Composite materials, for instance graphite epoxy, consist of a matrix of carbon fibres embedded in epoxy resin. Material properties and anisotropy of these materials are easily controllable by orienting the individual plies of the matrix. Infrared thermography can be used for evaluating the fibre-resin ratio of such materials as well as orientation of plies; when a specimen is point heated by a laser beam, the observation of the thermal

pattern provides that information. For an isotropic material a circular heating pattern is obtained while an ellipsoidal pattern is observed for an orthotropic material [Maldague 93c].

The fact that fibre bundles oriented in a particular direction compose the structure of leather, it could be hypothesised that heat flow within leather would reflect its structural characteristics.

In order to verify this hypothesis, a laser beam heated five leather specimens and the thermal pattern was recorded by an infrared camera. These tests were kindly performed by Professor Xavier Maldague of the University of Laval (Canada) during his sabbatical leave at IKP (University of Stuttgart, Germany) by request of the author. For this reason, only a few specimens were tested in transmission mode with a FLIR infrared camera and a pulsed Nd-YAG laser was used as a point heating source.

The specimens of the five bovine crust leather tested were all from the butt region and revealed a behaviour similar to that illustrated in Figure 5.11.

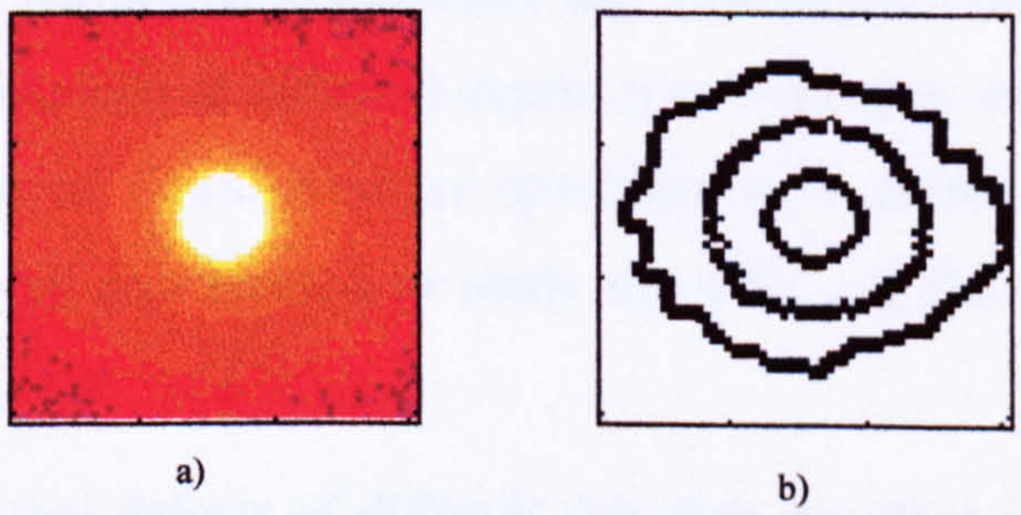

Figure 5.11-Leather heated with a laser.

Test performed in transmission mode with a pulsed Nd-YAG laser as point heating source a) original infrared image; b) three isothermal lines. These tests were kindly performed by Professor Xavier Maldague of University of Laval (Canada) during his sabbatical leave in Germany at IKP (Stuttgart University), by request of the author.

In Figure 5.11 a) an infrared image two seconds after removing the heating source is shown. Figure 5.11 b) presents a plot of three isothermal areas. It is very interesting to observe that the two inner curves (higher temperature) possess a quasi-perfect circular shape, while the outer curve (lower temperature) reveals an ellipsoidal shape. Perhaps, the low thermal diffusivity of leather explains this behaviour, why the ellipsoidal shape

is obtained only in the regions that start to get heated. In anisotropic composite materials the ellipsoidal shape is found in all heated areas.

No definitive conclusions can be taken from this data, but a good indication is given by these results that a relation between fibre bundles orientation (lines of tightness) and shape might exist.

Further research is needed to better comprehend this behaviour and, for instance to find out if there is any link between the ratio of the ellipsoidal shape axes and any thermal or physical property of leather.

5.5 Inspection Results

Artificial defects were made in the leather specimens by drilling circular holes on the flesh side for a range of diameters and depths relatively to the grain surface. The inspection of well-characterised defects is the first step in the validation of this technique. Similar approaches have been taken for other materials by other researchers [Vavilov 94] and in other techniques like ultrasonic flaw detection [Krautkramer 90].

Inspection tests were performed in reflective and transmission mode. A specimen with defects of the same diameter at different depths was created in order to study the effect of depth in detection of flaws. Another specimen with defects at same depth with different diameters was also created to study the effect of the size of flaws in their detection.

Inspections of a few real defects of difficult detection by other inspection systems are also presented in this section.

Thermal image processing was performed in MATLAB, with scripts and functions specially written by the author, as well as functions included in the Image Processing Toolbox for use with MATLAB [Matlab 95].

5.5.1 Same diameter defects at different depth

On the flesh side of the specimen S27C three 10 mm diameter holes were drilled with different depths. The average thickness of this specimen is about 1.95 mm and the thickness of leather where the three defects are located is 0.59 mm, 1.05 mm and 1.55 mm with a layout shown in Figure 5.12.

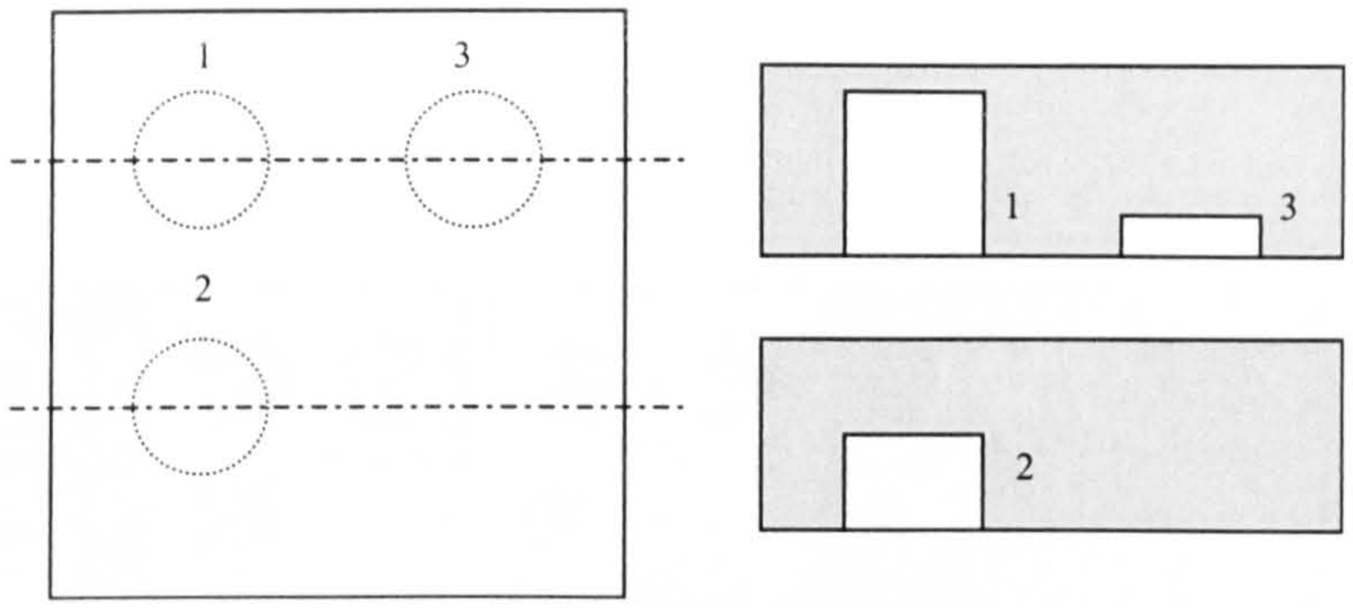

Figure 5.12-Layout of defects of same diameter different depth.

Difficulty of detection of these artificial defects increases from defect 1 to 3. Defect 3 is a very weak defect (difficult detection) that is located very deep with regard to the grain side surface. Defect 3 possesses a difference in thickness of just 0.40 mm when compared with full thickness.

The specimen was mounted vertically in front of the infrared camera at 370 mm distance, and heated uniformly during 35 heating units (approximately 5.6 seconds) by the two flash lamps of 500 W each in reflection mode. The heating time was obtained experimentally in order to cope with the three defects. A compromise had to be achieved so defect 3 was noticeable without saturating the output of the other defects. The specimen was heated four times with a fifteen minutes interval to allow the cooling of the specimen to room temperature and the results were averaged in order to improve the signal-to-noise ratio. The raw thermograms were corrected for radiometric and geometric distortion. The overall spatial resolution of the camera for this set-up (lens, extension rig, distance object-focal plane) is about 4.5 pixels per millimetre.

Figure 5.13 displays the sequence of raw thermograms from time 1 second to 23 seconds because frame acquisition interval was set to 1 second. This is a typical result for pulse thermography in which a "hot spot" above the defects becomes hotter on flash heating and cools slower than the adjacent material. In case of defect 2, its temperature changes from orange (t = 1 s) to light green (t = 16 s) still with reasonable visibility. The temperature of defect 1 stays saturated up to time 6 seconds, this fact is caused by the low input range of the infrared camera (8 bit system).

In the montage of Figure 5.14, the corrected thermograms of the montage of Figure 5.13 are displayed. The hotter right hand side of each frame shown in the latter montage is not as visible in Figure 5.14 and noise is better distributed across each frame.

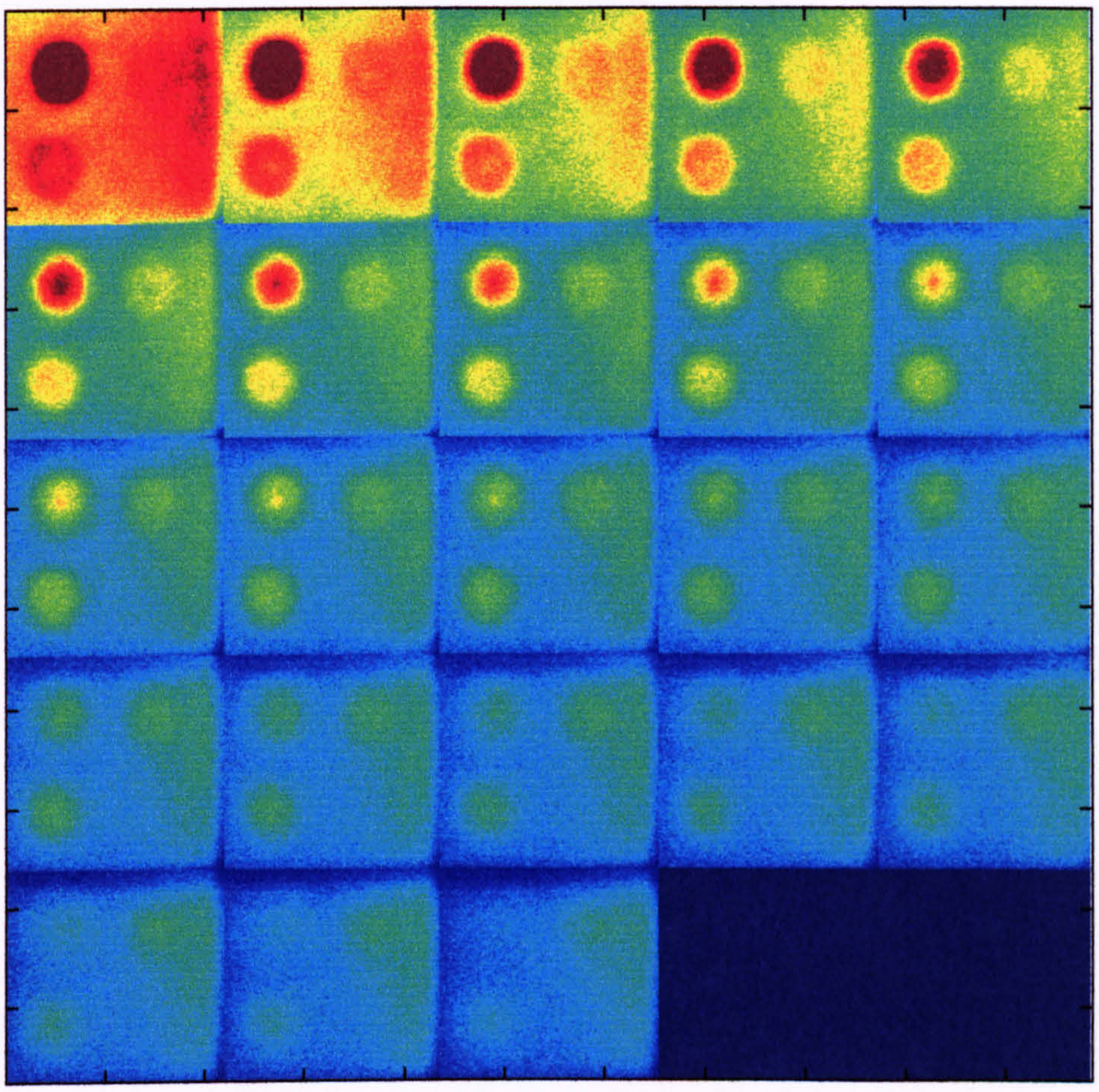

Figure 5.13-Montage of raw thermograms of defects of same size different depth.

From left to right, top to bottom sequence of raw thermograms at time 1 s to 23 s. Set-up: Reflection observation mode; heating time 35 units; frame acquisition delay 1000 ms; lens of 12.5° FOV plus 11 mm extension ring; distance object focal plane 370 mm.

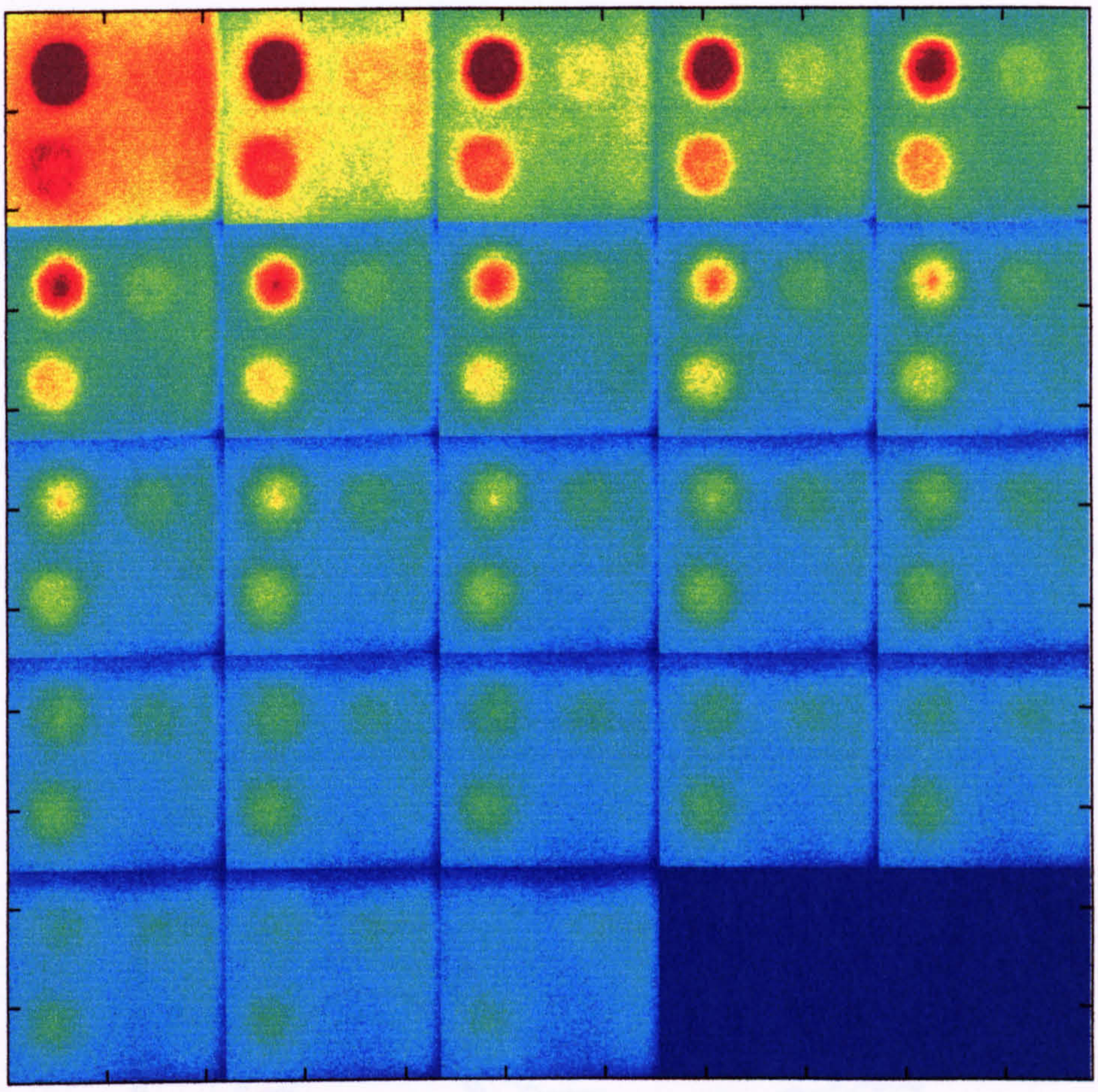

Figure 5.14-Montage of corrected thermograms of defects of same size different depth.

From left to right, top to bottom sequence of corrected thermograms at time 1 s to 23 s. Set-up: Reflection observation mode; heating time 35 units; frame acquisition delay 1000 ms; lens of 12.5° FOV plus 11 mm extension ring; distance object focal plane 370 mm.

a)

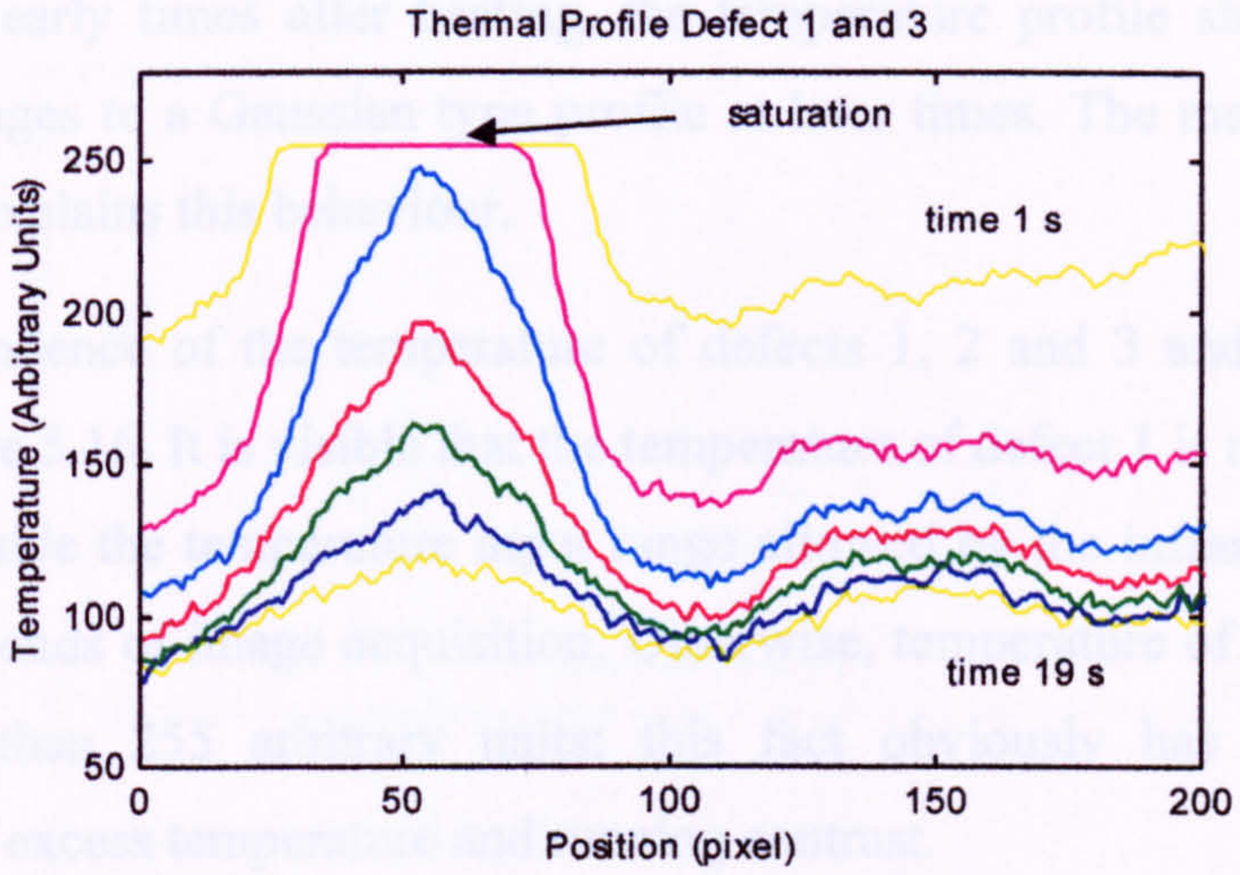

b)

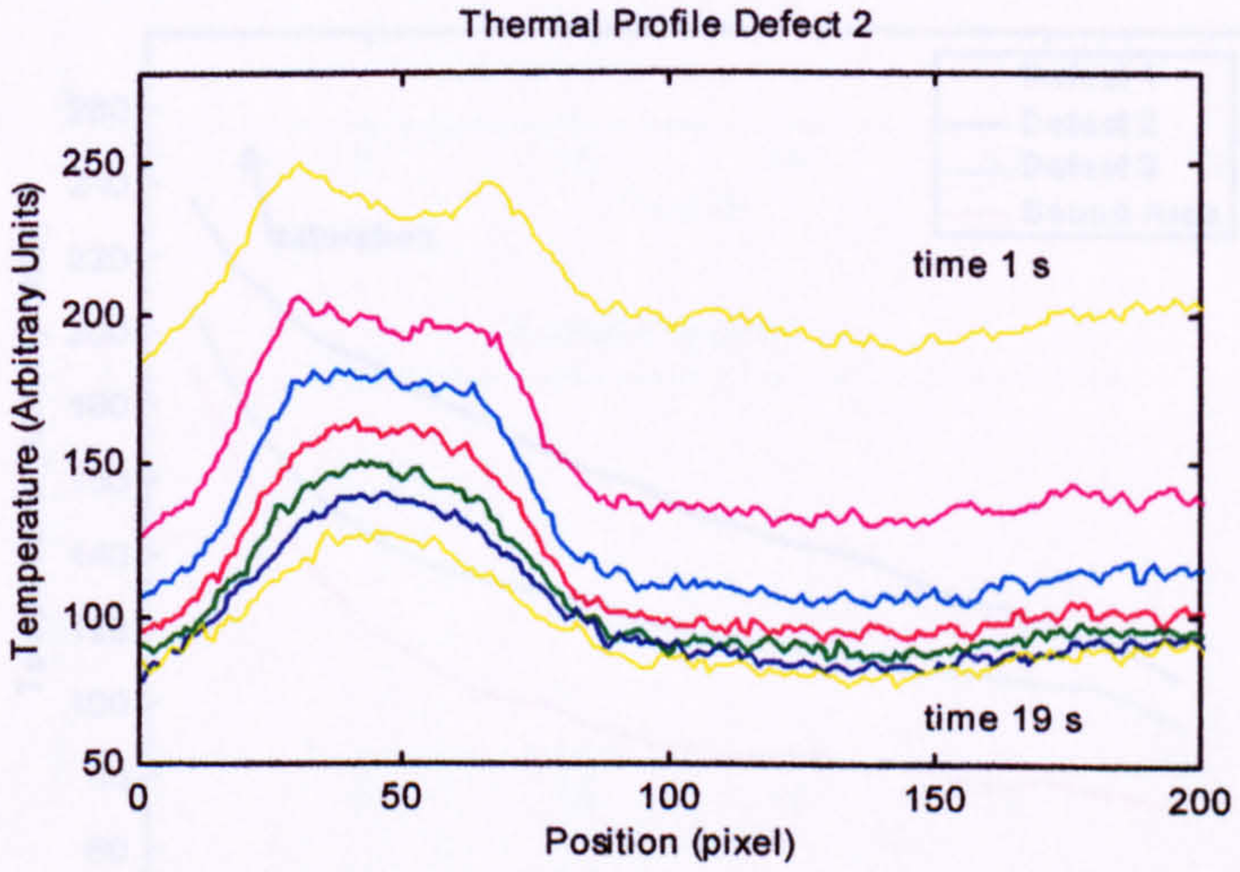

Figure 5.15-Thermal profiles of 10 mm defects.

Thermal profiles of thermograms corresponding to time 1, 4, 7, 10, 13, 16 and 19 seconds. These profiles are rows of the infrared images that cross defects 1 and 3 (Figure 5.15 a)), and defect 2 (Figure 5.15 b)).

Temperature profiles of thermograms corresponding to time 1, 4, 7, 10, 13, 16 and 19 seconds are displayed. These profiles represent rows of the infrared images that cross defects 1 and 3 in Figure 5.15 a), and defect 2 in Figure 5.15 b).

In defect 2 at early times after heating, the temperature profile shows a trapezoidal shape that changes to a Gaussian type profile at later times. The mechanism of lateral heat diffusion explains this behaviour.

The time dependence of the temperature of defects 1, 2 and 3 and a sound area are plotted in Figure 5.16. It is visible that the temperature of defect 1 is not correct because its value is outside the temperature input range allowed by the infrared camera, during the first six seconds of image acquisition. Otherwise, temperature of defect 1 would be much greater than 255 arbitrary units; this fact obviously has its effect on the computation of excess temperature and running contrast.

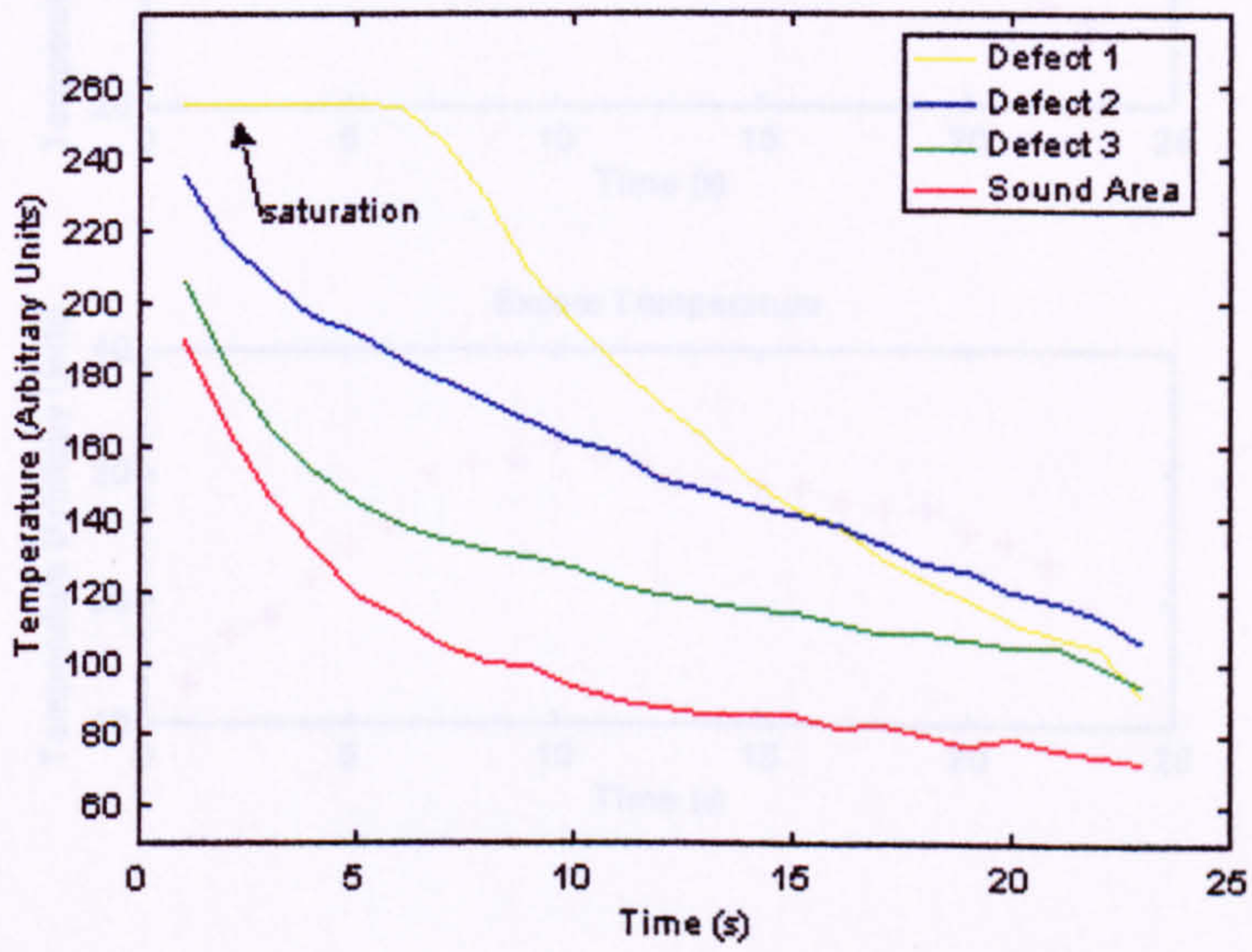

Figure 5.16-Plot of temperature vs. time of defects 1,2 and 3 and a sound area.

The increased or excess temperature signal of each defect is presented in Figure 5.17, while their running contrast is presented in Figure 5.18.

As expected, excess temperature and running contrast decrease significantly from defect 1 to 3. Better visibility of defect is achieved at maximum excess temperature or contrast; this instant only depends on the depth of the defect. Deeper defects have a peak excess temperature and running contrast at later times. The area of the defect does not affect the instant of peak contrast.

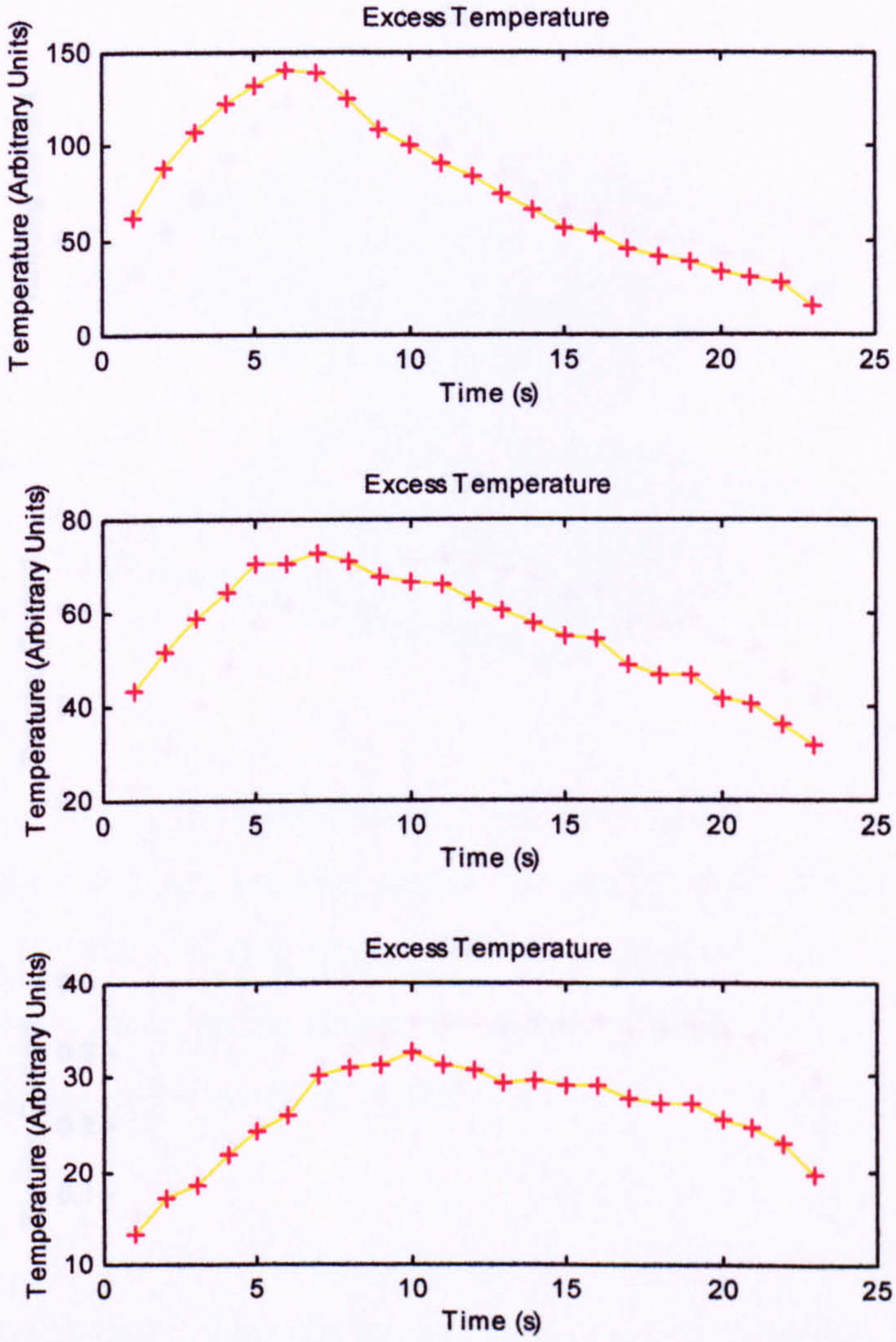

Figure 5.17-Excess temperature of defect 1,2 and 3 vs. time.

(The first 5 s of the curve of defect 1 do not represent the correct excess temperature).

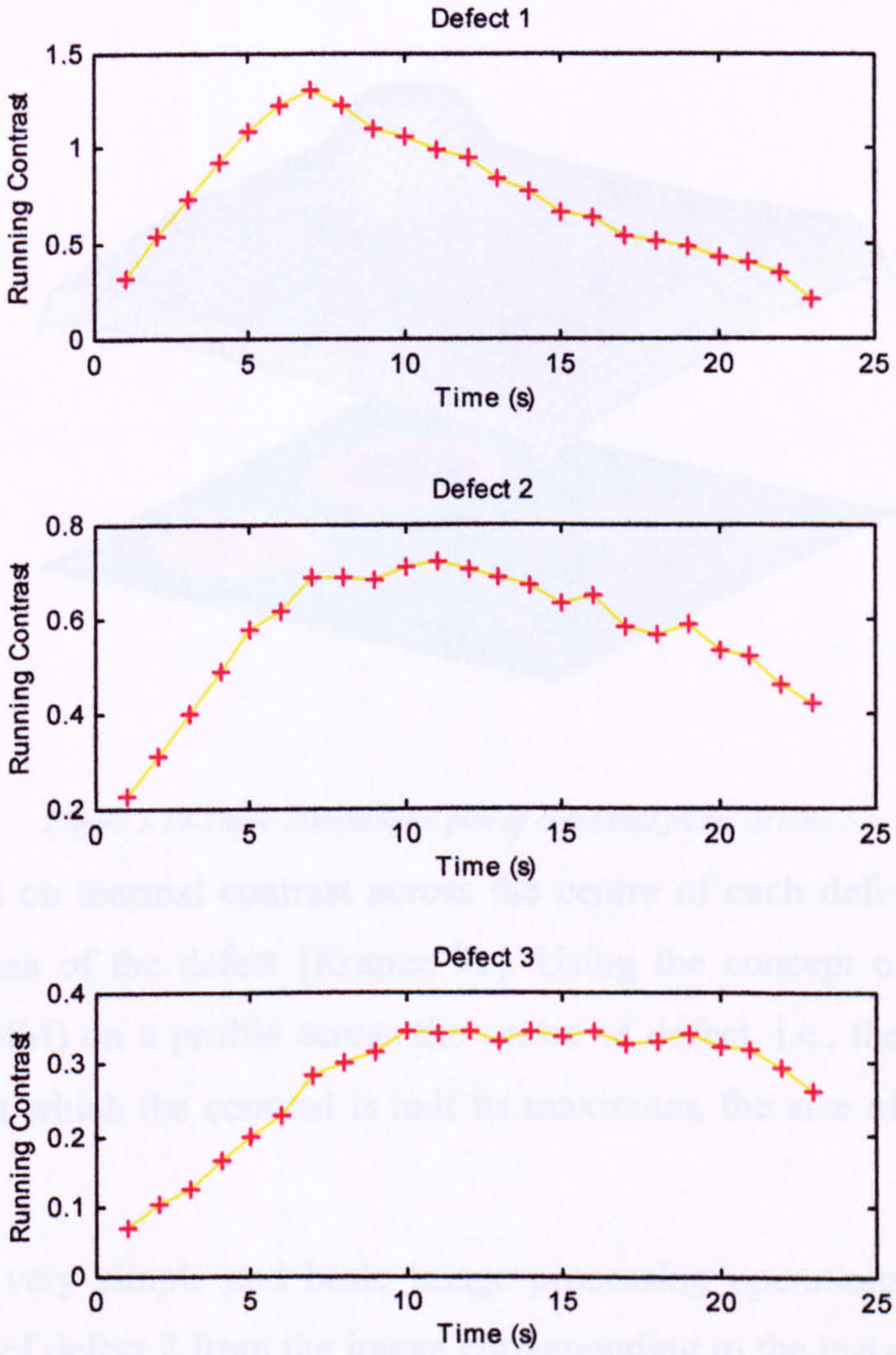

Figure 5.18-Running contrast of defect 1,2 and 3 vs. time.

(The first 5 s of the curve of defect 1 do not represent the correct running contrast).

Although the resulting thermal contrast image clearly identifies the presence of defects (see Figure 5.19), it is not clear how an accurate measure of defect size may be obtained.

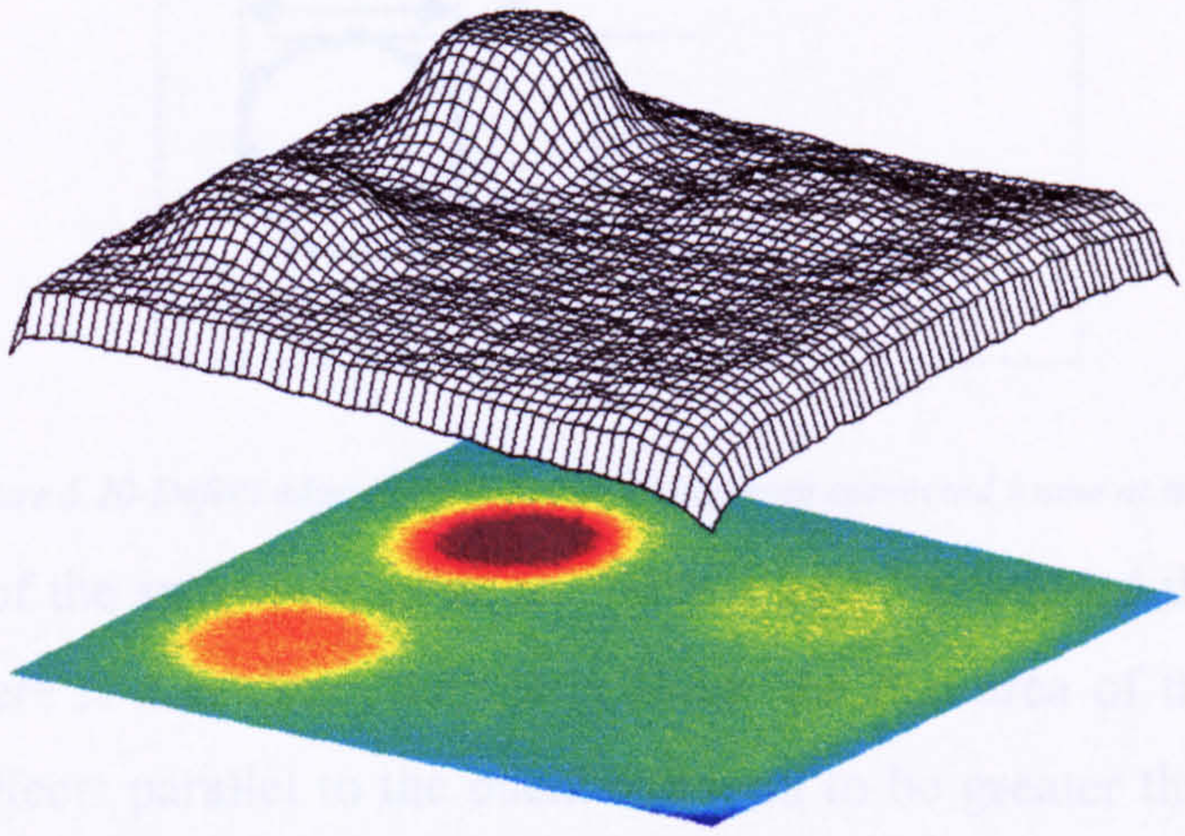

Figure 5.19-Three-dimensional plot of corrected frame at time 5 s.

A method based on thermal contrast across the centre of each defect may be used to determine the size of the defect [Krapez 91]. Using the concept of Full Width Half Maximum (FWHM) on a profile across the centre of defect, i.e., the distance between the two points at which the contrast is half its maximum, the size of the defect can be estimated.

Applying some very simple and basic image processing operations, it is possible to extract the edge of defect 2 from the image corresponding to the instant of its maximum contrast. After segmentation of the contrast image corresponding to time 5 seconds with a threshold level of half the maximum contrast of defect 2, an edge extraction routine was applied and the resulting image is displayed in Figure 5.20. The edge extraction routine uses the Marr-Hildreth method, which returns edges at the zero crossings of the Laplacian of the Gaussian filtered image.

With the edge image or a segmented image, defect sizing is possible. In case of a circular defect, the diameter of the defect is measured in pixels and converted to SI units, dividing the number of pixels by the spatial resolution of the camera. Using this method, resulted a defect 2 of 10.4 mm and 10.6 mm, perpendicular and parallel to the backbone respectively, as shown in Figure 5.20.

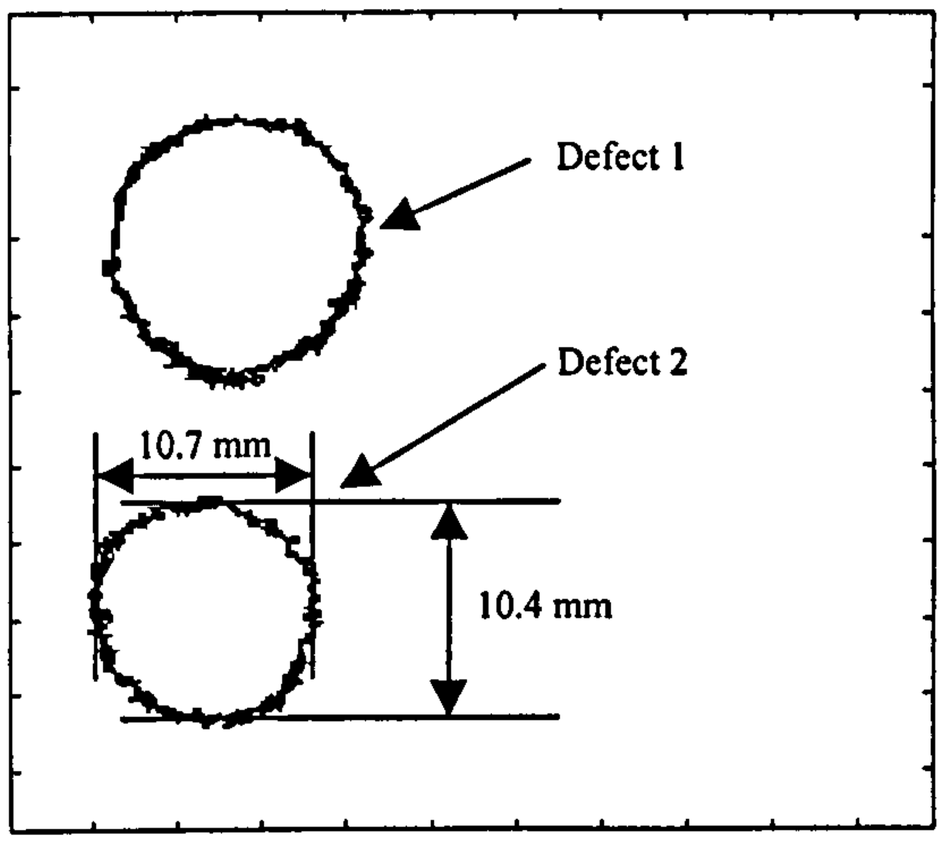

Figure 5.20-Defect edge extraction and sizing from corrected frame at time 5 s.

The application of the same procedure to defect 1 and 3 produced the results presented in Table 5.3. There is a tendency to overestimate the real area of the defect. Also, the dimensions of defects parallel to the backbone tend to be greater than perpendicular to the backbone.

Table 5.3-Defect sizing at peak contrast of 10 mm defects at three different depths.

Defect	Diameter	
	Parallel to backbone	Perpendicular to backbone
Defect 1	10.4 mm	9.8 mm
Defect 2	10.7 mm	10.4 mm
Defect 3	10.9 mm	10.7 mm

The experiment just described was repeated but in transmission mode, i.e., heating was applied at the back of the specimen (flesh side) while observation was achieved from the grain side.

The specimen was mounted vertically in front of the infrared camera at 370 mm distance, and heated uniformly during 30 heating units (approximately 4.8 seconds) by the two flash lamps of 500 W each in transmission mode. Heating time was obtained experimentally in order to cope with the three defects. A compromise had to be found so defect 3 was noticeable without saturating the output of the other defects.

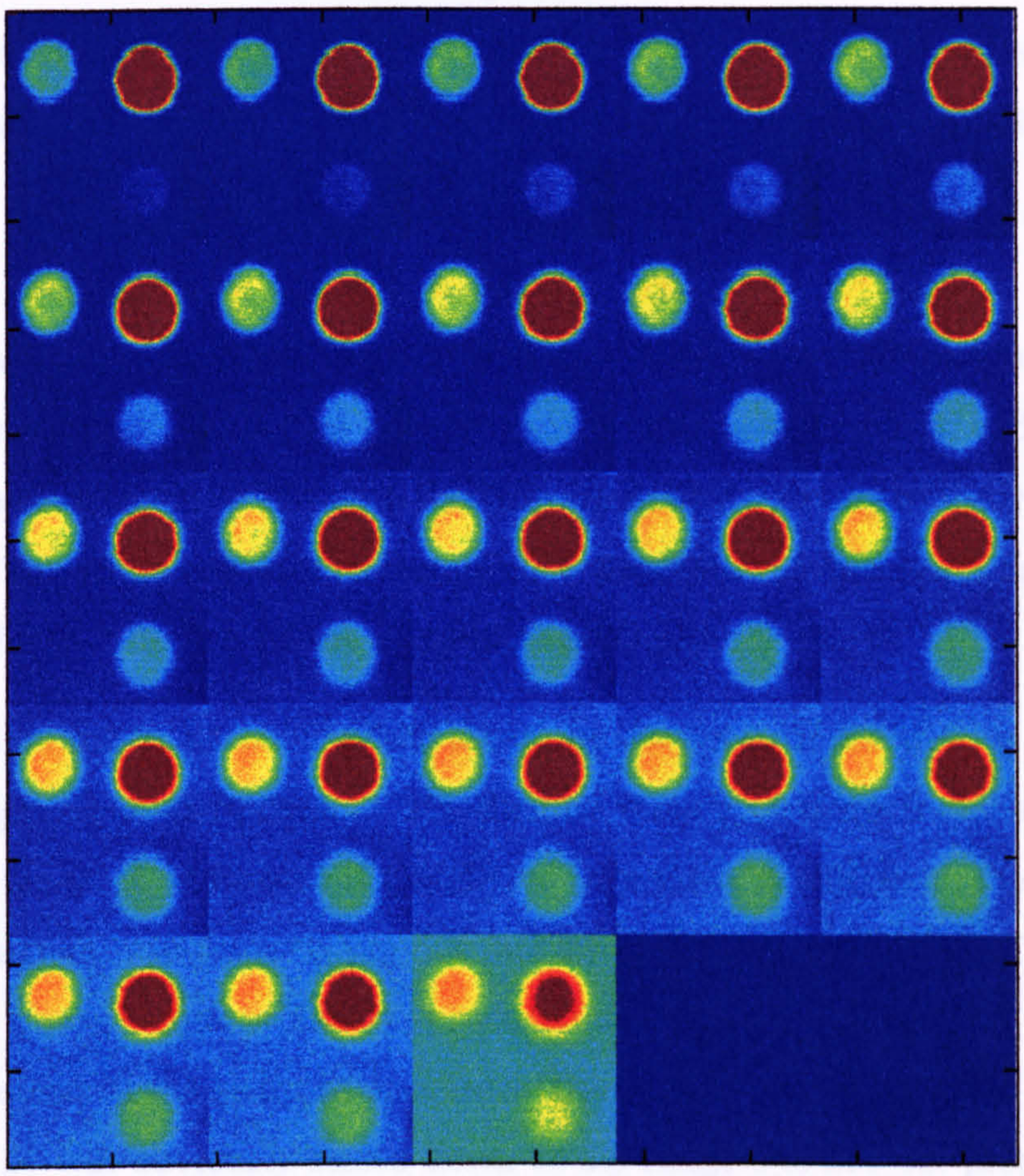

Figure 5.21-Montage of corrected thermograms of defects of same size and different depth.

From left to right, top to bottom sequence of corrected thermograms at time 0.1 s to 2.3 s. Set-up: Transmission observation mode; heating time 30 units; frame acquisition delay 100 ms; lens of 12.5° FOV plus 11 mm extension ring; distance object focal plane 370 mm.

The specimen was heated four times with a fifteen-minute interval to allow cooling of the specimen to room temperature and the results were averaged in order to improve the signal-to-noise ratio. The raw thermograms were corrected for radiometric and geometric distortion. The overall spatial resolution of the camera for this set-up (lens, extension rig, distance object-focal plane) is about 4.5 pixels per millimetre.

Figure 5.21 displays the sequence of corrected thermograms from time 0.1 second to 2.3 seconds because frame acquisition interval was set to 0.1 second. Here, deeper defects show up as a "hot spot" later than defects closer to the observation surface and with smaller contrast. The sound material temperature also increases with time and at time 16 seconds lateral heat diffusion has taken over and visibility of the three defects is very weak. The temperature of defect 1 stays saturated the full time, but on the last frame lateral heat diffusion effects are already noticeable.

In transmission mode, no conclusions about the deepness of the defects can be taken from the sequence of thermograms. The thermal wave propagates simultaneously from the back to the front. However, if qualitative inspection is sufficient, the transmission mode thermograms can certainly provide that information. The addition of all images of Figure 5.21, a very simple procedure, produced the image of Figure 5.22, which clearly shows the defects of the analysed specimen. The sum of the twenty-three thermograms of Figure 5.21 was obviously scaled down to the range 0 to 255 for proper display in MATLAB with the same map of colours of previous image displays.

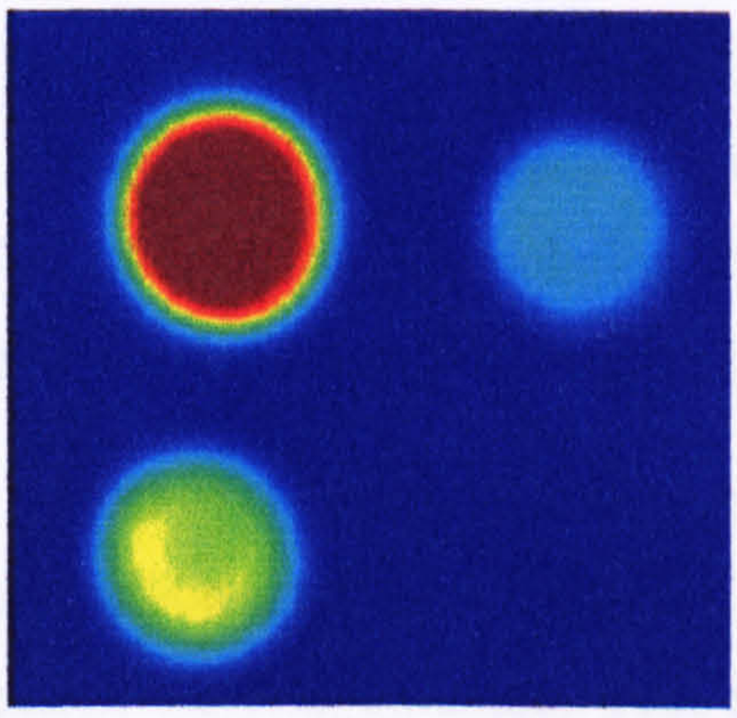

Figure 5.22-Image of the sum of all thermograms of Figure 5.21.

5.5.2 Different diameter defects at same depth

On the flesh side of the specimen S24D three 0.74 mm deep holes were drilled with different diameters. The average thickness of this specimen is about 2.08 mm and the diameter of the three defects is 10 mm, 5 mm and 2 mm with a layout shown in Figure 5.23.

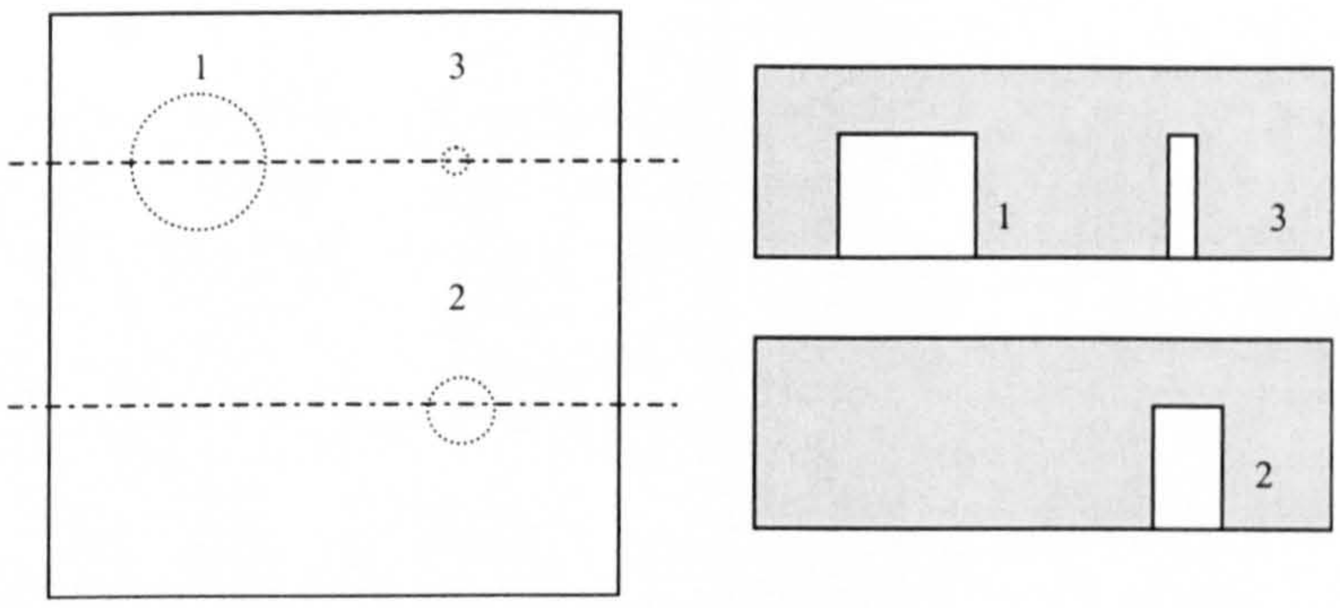

Figure 5.23-Layout of defects of same depth different diameter.

Difficulty of detection of these artificial defects increases from defect 1 to 3. Defect 3 is a narrow defect of difficult detection, due to lateral heat diffusion.

The specimen was mounted vertically in front of the infrared camera at 370 mm distance, and heated uniformly during 35 heating units (approximately 5.6 seconds) by the two flash lamps of 500 W each in reflection mode. Heating time was obtained experimentally in order to cope with the three defects. A compromise had to be achieved so defect 3 was noticeable without saturating the output of the other two defects. The specimen was heated four times with a fifteen-minute interval to allow cooling of the specimen to room temperature and the results were averaged in order to improve the signal-to-noise ratio. The raw thermograms were corrected for radiometric and geometric distortion. The overall spatial resolution of the camera for this set-up (lens, extension rig, distance object-focal plane) is about 4.5 pixels per millimetre.

Figure 5.24 displays the sequence of raw thermograms from time 1 second to 23 seconds because frame acquisition interval was set to 1 second. A similar behaviour to the case described in section 5.5.1 is obtained. This is a typical result for pulse thermography in which a "hot spot" above the defects becomes hotter on flash heating and cools slower than the adjacent material. The contrast of the temperature of defect 3 decreases very rapidly, at time 6 seconds it is already difficult to distinguish this defect from the background.

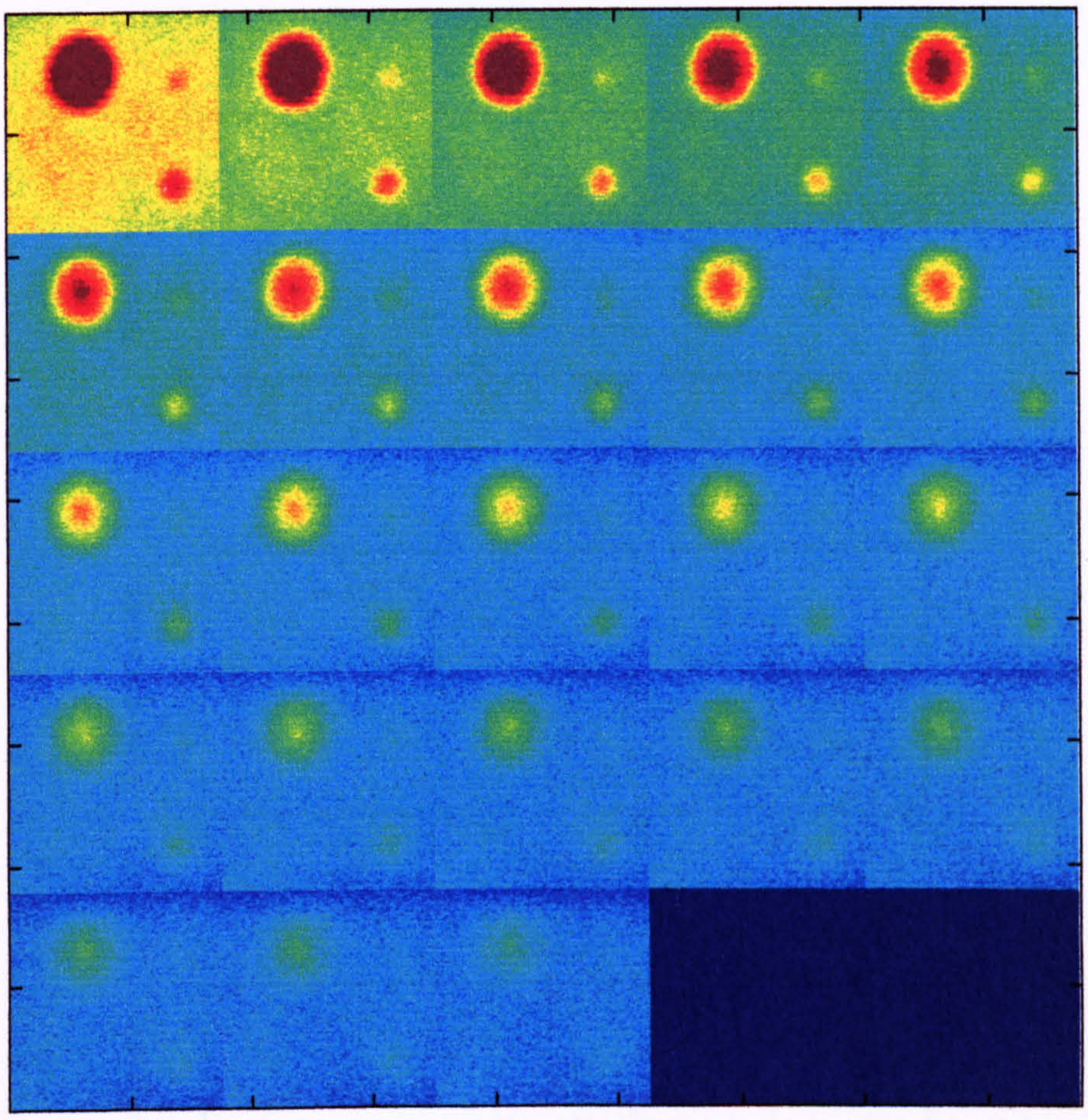

Figure 5.24-Montage of corrected thermograms of defects of same depth different size.

From left to right, top to bottom sequence of corrected thermograms at time 1 s to 23 s. Set-up: Reflection observation mode; heating time 35 units; frame acquisition delay 1000 ms; lens of 12.5° FOV plus 11 mm extension ring; distance object focal plane 370 mm.

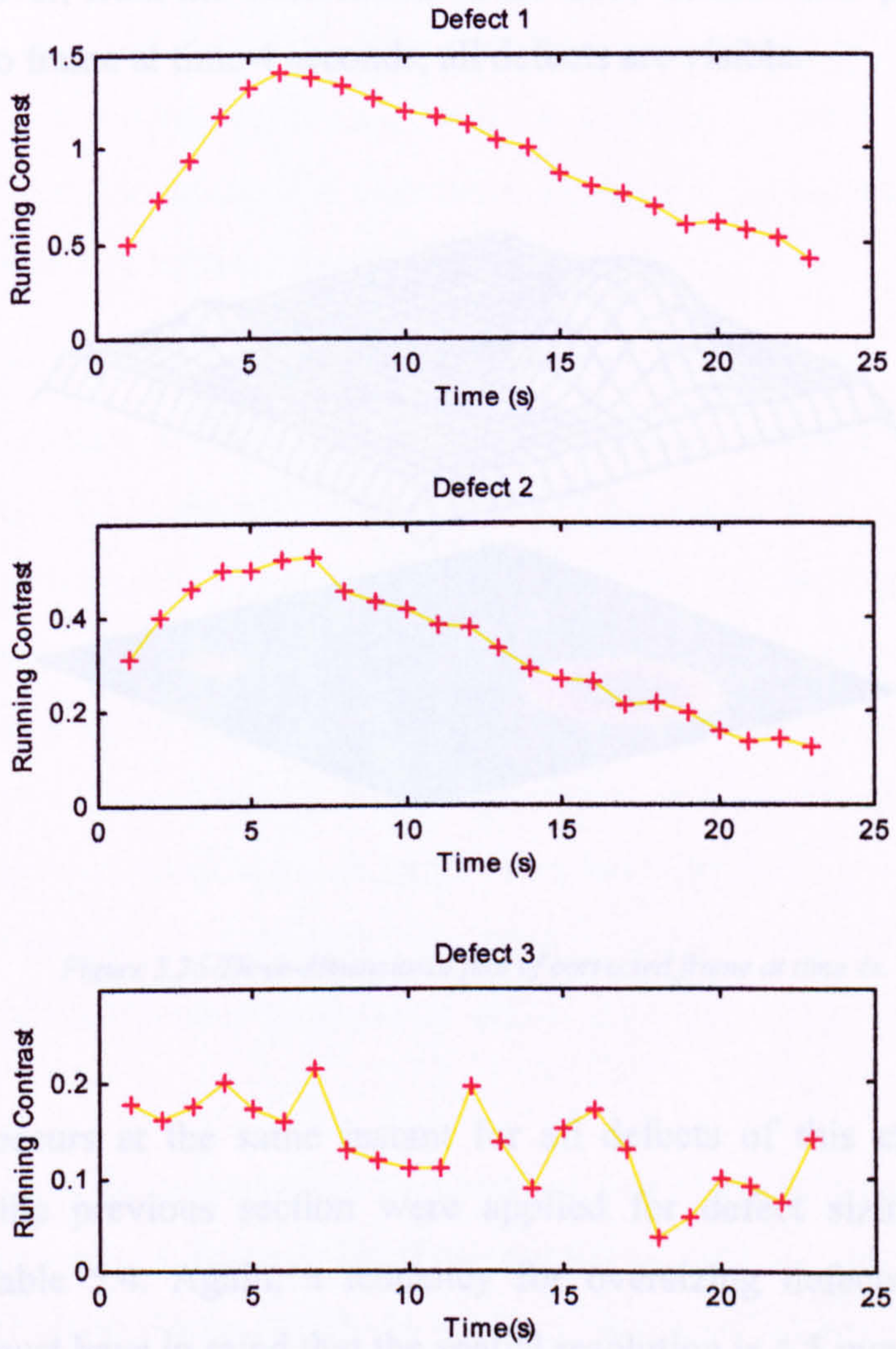

Figure 5.25-Running contrast of defect 1,2 and 3 vs. time.

(The first 5 s of the curve of defect 1 do not represent the correct running contrast).

The running contrast of the defects 1, 2 and 3 is shown in Figure 5.25. If detecting peak contrast for defect 1 and 2 is an easy task, the same cannot be said for defect 3. Peak contrast of this last defect is very faint and it can be said that it is almost on the limit of detection. However, from the observation of the three-dimensional plot of Figure 5.26, corresponding to frame at time 4 seconds, all defects are visible.

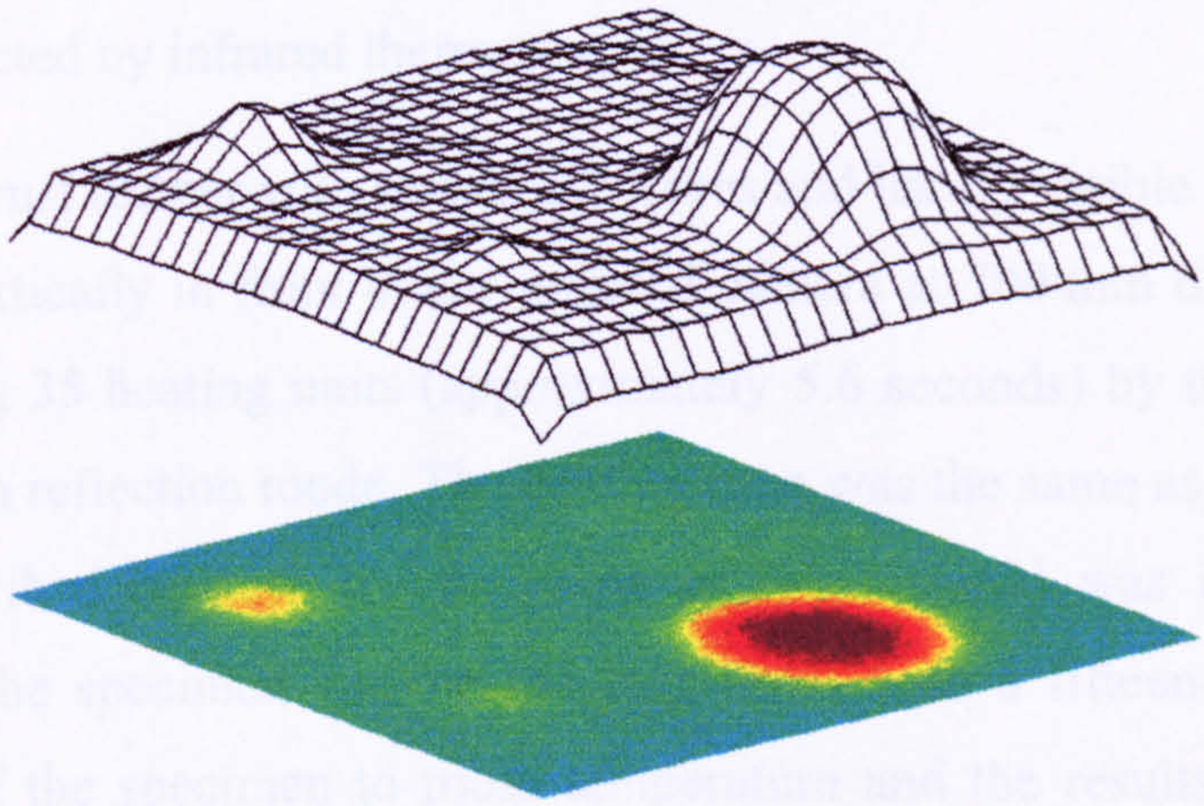

Figure 5.26-Three-dimensional plot of corrected frame at time 4s.

Peak contrast occurs at the same instant for all defects of this experiment. Similar procedures to the previous section were applied for defect sizing and results are presented in Table 5.4. Again, a tendency for oversizing defects may be verified. However, one must have in mind that the spatial resolution is 4.5 mms^{-1}, thus to a length of about 2 mm corresponds a length of just 9 pixels.

Table 5.4-Defect sizing at peak contrast of three 0.74 mm deep defects with different sizes.

Defect	Diameter	
	Parallel to backbone	Perpendicular to backbone
Defect 1	2.4 mm	2.6 mm
Defect 2	5.3 mm	10.6 mm
Defect 3	10.7 mm	10.4 mm

5.5.3 Real Defects

In order to assess the real impact of infrared thermography as an inspection tool for leather, a few real defects were put to test. The type of defects chosen represents defects that are very difficult to detect by normal vision systems, because they are hardly visible from the grain side and detection from the flesh side is not advisable due to noise considerations. Grain wrinkles, areas of smaller substance, scores, putrefaction, brand marks and any flaws that also cause significant changes in emissivity are typical defects that may be detected by infrared thermography.

A specimen of crust leather with two small scores and hardly visible from the grain side was mounted vertically in front of the infrared camera at 700 mm distance, and heated uniformly during 35 heating units (approximately 5.6 seconds) by the two flash lamps of 500 W each in reflection mode. The heating time was the same as in the experiments previously described because the thickness of the material was in the same range (about 2 mm). The specimen was heated four times with a fifteen-minute interval to allow cooling of the specimen to room temperature and the results were averaged in order to improve the signal-to-noise ratio. The raw thermograms were corrected for radiometric and geometric distortion. The overall spatial resolution of the camera for this set-up (lens, extension rig, distance object-focal plane) is about 2.4 pixels per millimetre.

Figure 5.27 displays the sequence of raw thermograms of a single experiment from time 1 second to 23 seconds as frame acquisition interval was set to 1 second. Again, this is a typical result for pulse thermography in which a "hot spot" above the defects becomes hotter on flash heating and cools slower than the adjacent material. In this case, non-uniform heating affects all thermograms. Figure 5.28 and Figure 5.29 illustrate further the effect of non-uniform heating and allow better visualisation of defects.

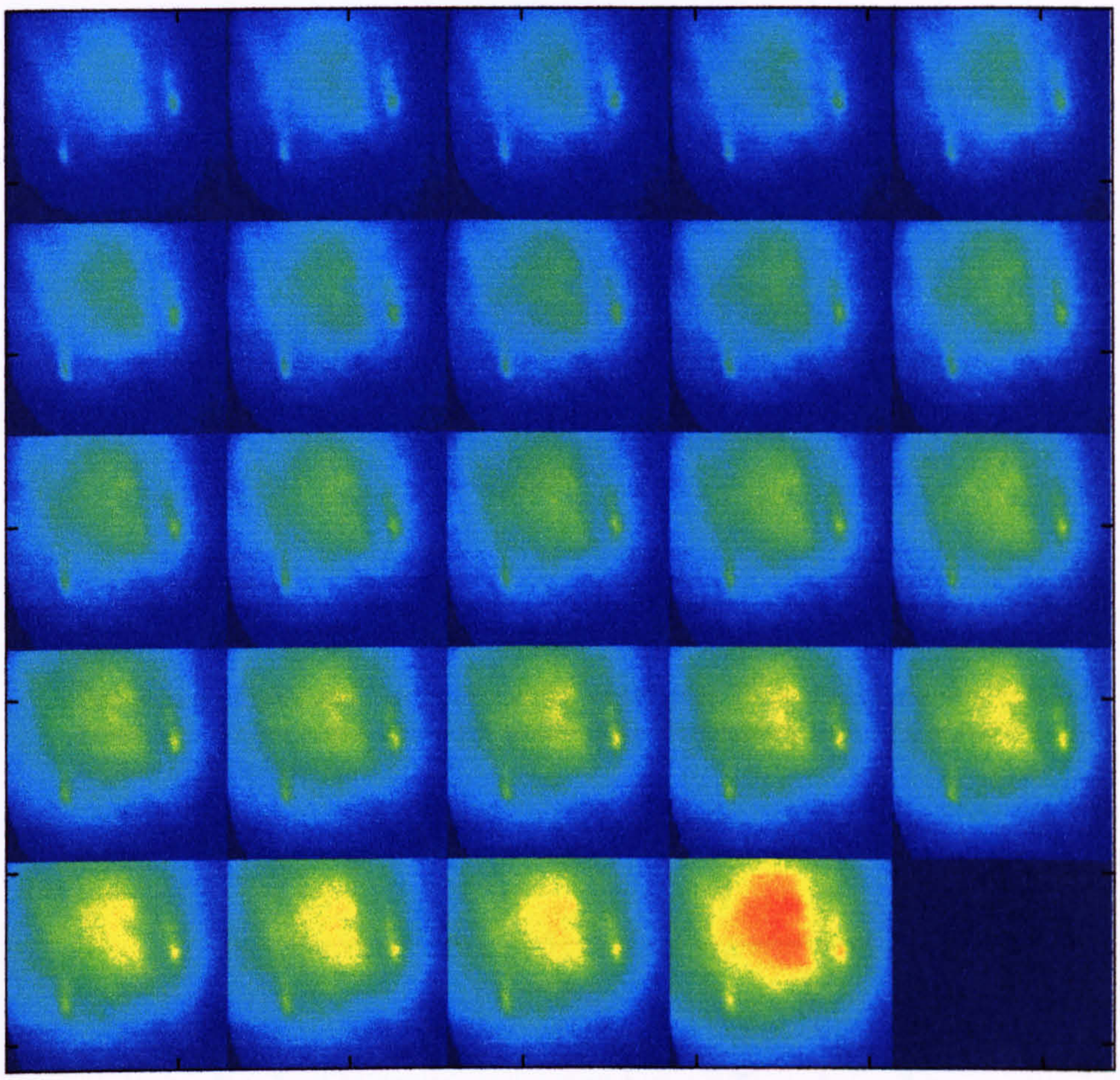

Figure 5.27-Montage of corrected thermograms of real defects (flaying cuts).

From left to right, top to bottom sequence of corrected thermograms at time 1 s to 23 s. Set-up: Reflection observation mode; heating time 35 units; frame acquisition delay 1000 ms; lens of 12.5° FOV; distance object focal plane 700 mm.

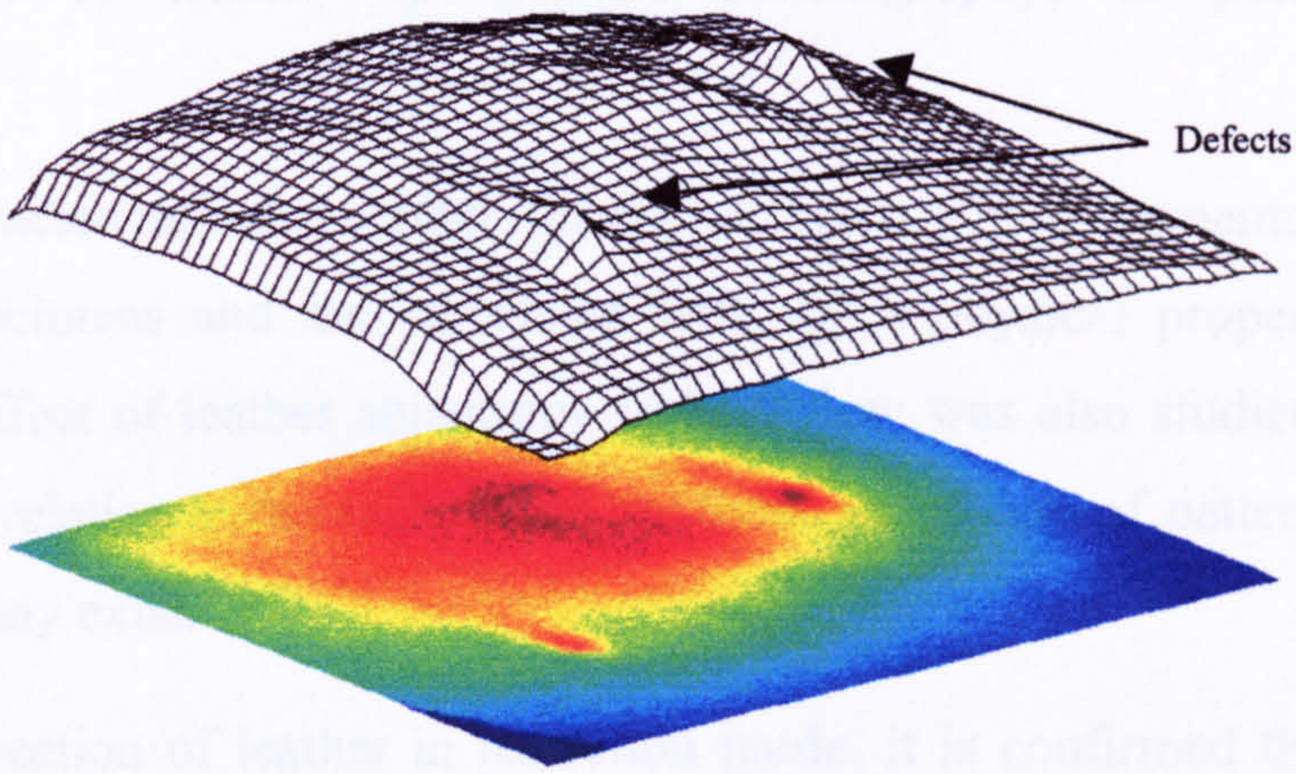

Figure 5.28-Three-dimensional plot o f two real defects.

Two defects (flaying cuts) are clearly visible in this plot. These defects are very difficult to detect by a normal vision inspection system. This thermogram, time 18 s, is not corrected for non-uniform heating.

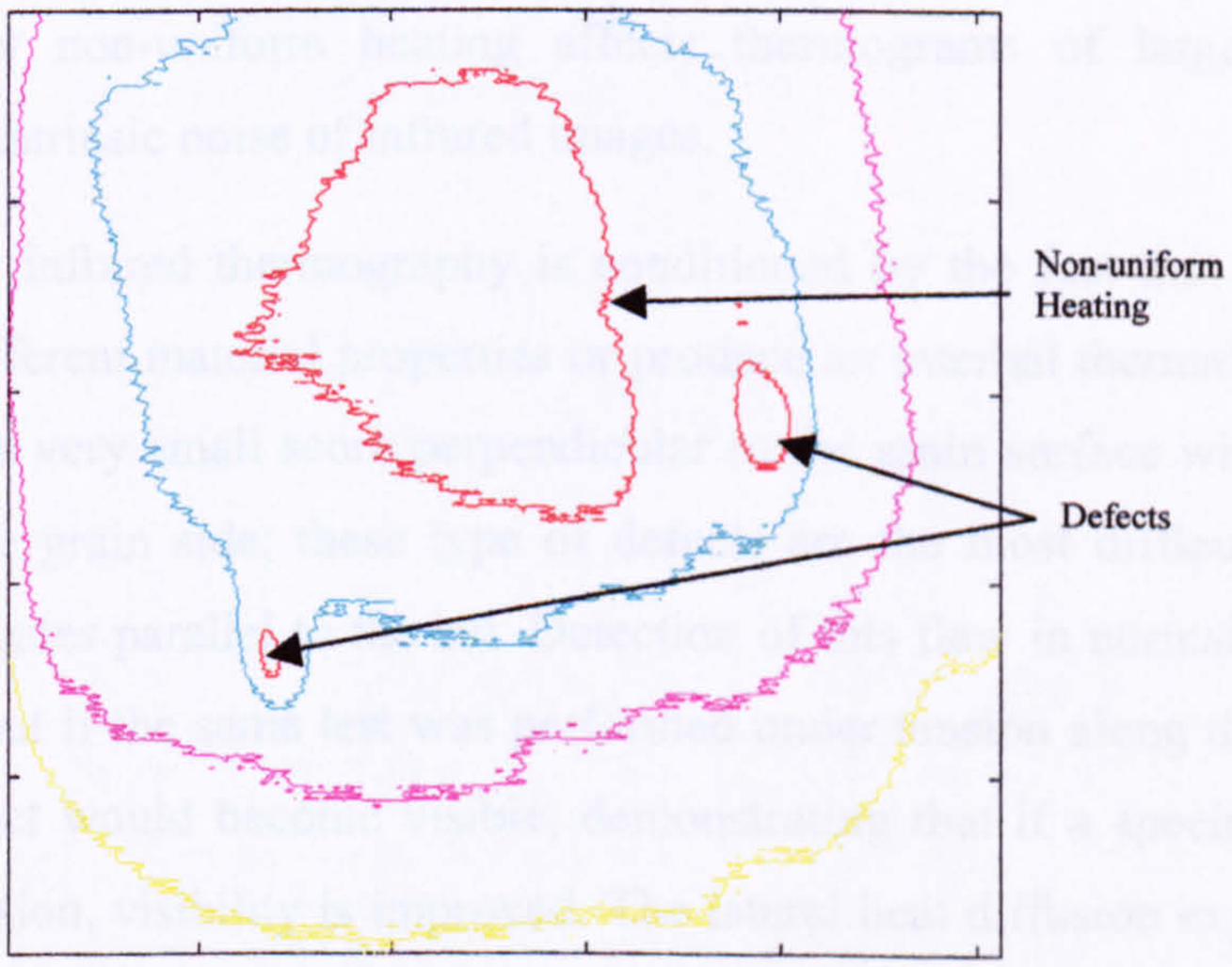

Figure 5.29-Isothermal lines of infrared image.

Two defects (flaying cuts) are clearly visible in this plot. This contour plot of thermogram at time 18 s, shows the two defects and non-uniform heating.

5.6 Evaluation

The results presented in this chapter are divided in the categories of inspection and characterization of leather by infrared thermography, in particular transient thermography.

Regarding characterization of leather, thermal diffusivity measurements were performed for all "I" specimens and are correlated with other physical properties in the next chapter. The effect of leather anisotropy in heat flow was also studied and the results suggest that a relation between lines of tightness and shape of pattern resulting from point heating may exist.

Regarding inspection of leather in reflection mode, it is confirmed that the instant of peak contrast of defects depends on their deepness. Shallower defects reach maximum contrast earlier than deeper defects. Deeper defects maximum contrast is weaker than maximum contrast of shallower defects. The area of a defect does not affect the instant of maximum contrast, but smaller defects have lower contrast because of the effects of lateral heat diffusion, thus diminishing their visibility. It is also shown that approximate defect sizing is also possible.

It was shown how non-uniform heating affects thermograms of larger areas of inspection, and the intrinsic noise of infrared images.

Defect visibility by infrared thermography is conditioned by the fact that a defective area has to have different material properties or produce an internal thermal resistance. The author caused a very small score perpendicular to the grain surface with a scalpel not visible from the grain side; these type of defects are the most difficult to detect because heat propagates parallel to the cut. Detection of this flaw in normal conditions was not achieved, but if the same test was performed under tension along the length of the leather the defect would become visible, demonstrating that if a specimen can be inspected under tension, visibility is improved. The lateral heat diffusion explains these results.

The author regrets that line heating thermal stimulation on leather could not be tested, as well as lock-in thermography. Lock-in thermography is immune to emissivity and to non-uniformity of heating and is by far the best method for subsurface flaw detection.

6

6 Evaluation of Results

6.1 Introduction

This chapter is concerned with the evaluation of results of conventional physical testing and results obtained with the Mechanical Scanning System (MSS). The agreement of the results is verified in order to assess if the MSS is a reliable and correct method of characterising leather non-destructively. Compression and tensile test results are compared.

A physical property and a thermal property, respectively apparent density and thermal diffusivity are analysed to verify any possible link between them.

6.2 Conventional Physical Testing vs. MSS Testing

The results of two very important physical tests in leather characterisation are evaluated. Compression results obtained with the compressibility and softness tester are correlated with the results from compression measured by the MSS. In Table 6.1, the correlation coefficients of results of compression tests at a 10 percent compressive strain are shown.

The correlation coefficients of the compression load for static compressibility and static compression by the MSS demonstrate the non-existence of a link between these measurements. A similar result is observed for the correlation coefficients of the compression load for static compressibility and dynamic compression by the MSS. These findings are explained by the shape of the pressure foot; in one case, there is a flat surface with constant contact area; while in the other, there is a curved surface with a contact area changing with the compression load.

Table 6.1-Correlation between results of conventional and MSS compression tests.

	Correlation Coefficients @10% Compressive Strain
Compression Load Correlation	
Between static and MSS static compression	-0.2847
Between static and MSS dynamic compression	-0.4339
Compression Energy Correlation	
Between static and MSS static compression	0.9703
Between static and MSS dynamic compression	0.9176

However, when the entity analysed is the compression energy required to compress leather to a 10 percent compressive strain, the results are positively surprising. A correlation coefficient of 0.9703 is observed for the compression energy results of tests carried out with the static compressibility tester and the MSS. A correlation coefficient of 0.9176 is observed for the compression energy results of tests carried out with the static compressibility tester and the MSS with the wheels rotating and obviously displacing material.

These last findings confirm that the MSS can be reliably used to execute compressibility tests of leather. Nevertheless, further research is needed if the results of the Mechanical Scanning System are to be expressed in terms of compressive stress.

In Table 6.2, the author compares the results of conventional tensile tests performed in specimens "A" and "B" with the results of tensile tests carried out in specimens "GN" and "HN" with the MSS. In Table 6.3, the author compares the results of conventional tensile tests performed in specimens "A" and "B" with the results of tensile tests carried out in specimens "GW" and "HW" with the MSS. Stress correlation coefficients and strain energy correlation coefficients at a strain of 1 and 2 percent are shown in these tables.

Table 6.2-Correlation between tensile test results (narrow specimens GN, HN & A, B).

	Correlation Coefficients	
	@1% Strain	@2% Strain
Stress Correlation		
Between MSS and conventional tensile testing	0.7687	0.8226
Between MSS and conventional tensile testing, parallel to backbone	0.7571	0.7783
Between MSS and conventional tensile testing, perpendicular to backbone	0.8402	0.9022
Strain Energy Correlation		
Between MSS and conventional tensile testing	0.7982	0.8641
Between MSS and conventional tensile testing, parallel to backbone	0.7480	0.8545
Between MSS and conventional tensile testing, perpendicular to backbone	0.8250	0.8662

Table 6.3- Correlation between tensile test results (wide specimens GW, HW & A, B).

	Correlation Coefficients	
	@1% Strain	@2% Strain
Stress Correlation		
Between MSS and conventional tensile testing	0.8427	0.9272
Between MSS and conventional tensile testing, parallel to backbone	0.9009	0.9374
Between MSS and conventional tensile testing, perpendicular to backbone	0.8010	0.9202
Strain Energy Correlation		
Between MSS and conventional tensile testing	0.7014	0.8493
Between MSS and conventional tensile testing, parallel to backbone	0.7114	0.8199
Between MSS and conventional tensile testing, perpendicular to backbone	0.7208	0.8775

The first conclusion to be drawn from the data of Table 6.2 and Table 6.3 is that higher correlation coefficients are achieved for stress and strain energy computations at 2 percent strain (it is very likely that this trend would be confirmed for tests at higher strains, for example 5 or 10 percent strain). For this reason, only correlation coefficients at 2 percent are looked at.

In Table 6.2, the stress correlation coefficient between specimens perpendicular to the backbone, specimens "B" and "HN", is to some extent higher than for specimens parallel to the backbone, specimens "A" and "GN". A similar trend is observed for the strain energy correlation coefficients. Further, higher correlation coefficients are found for strain energy than for stress. The overall correlation coefficient for stress results of 0.8226, and for strain energy results of 0.8641, give confidence that measurements taken by the MSS of narrow strips of leather can be trusted.

In Table 6.3, the stress correlation coefficient between specimens perpendicular to the backbone, specimens "B" and "HW", is slightly lower than for specimens parallel to the backbone, specimens "A" and "GW". The opposite trend is observed for the strain energy correlation coefficients. Further, higher correlation coefficients are found for stress than for strain energy. The overall correlation coefficient for stress results of 0.9272, and for strain energy results of 0.8493, give confidence that measurements taken by the MSS of wide strips of leather can be trusted.

Surprisingly, correlation coefficients of the same order for wider strips and narrower strips ("GN", "HN", "GW" and "HW") were achieved, which is very convenient. However, one must have in mind that calculated stress values for wide specimens ("GW" and "HW") are not correct (see section 4.5.2).

6.3 Physical Properties vs. Thermal Properties

In section 2.6.1, it was hypothesized that a relationship could exist between thermal diffusivity and tensile strength of leather.

Leather thermal diffusivity measurements were taken from all sampling positions and correlated with measurements of their respective apparent density. Apparently, no good correlation can be found between thermal diffusivity and apparent density of leather. Thus, no link can be established between thermal diffusivity and the tensile strength of

leather through its apparent density. In Figure 6.1, a plot of the thermal diffusivity function of apparent density is presented.

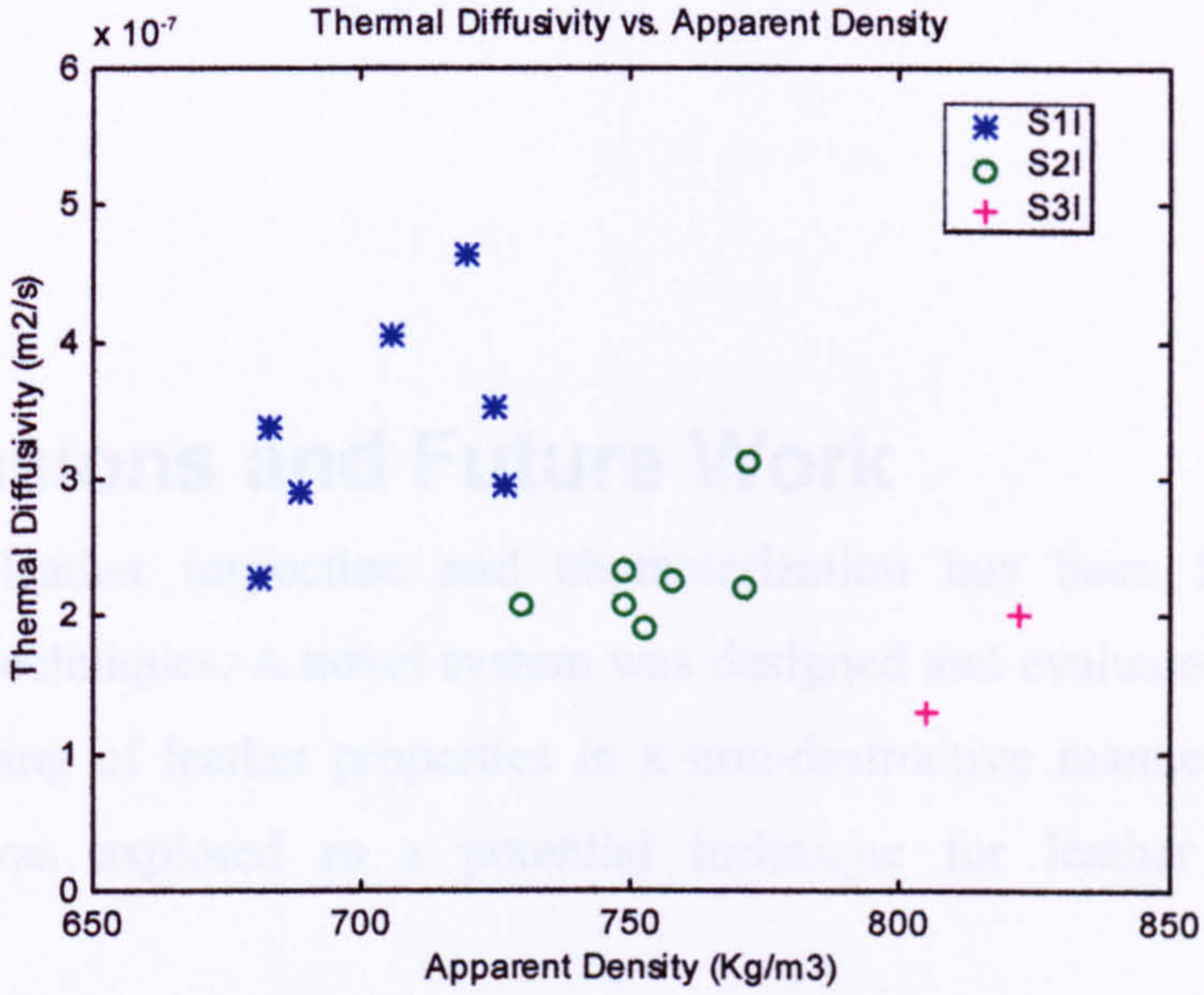

Figure 6.1-Thermal diffusivity vs. apparent density.

The good correlation between porosity and thermal diffusivity observed by other researchers for other materials needs more attention in the case of leather. If a material is more porous, then its apparent density should be smaller. A more porous material should have a smaller thermal conductivity and consequently a smaller thermal diffusivity. These thoughts support the idea that higher porosity should cause smaller thermal diffusivity, but definitely more research is required to fully understand the relationship between thermal diffusivity, thermal conductivity and apparent density of leather and only then draw final conclusions on this matter.

7

7 Conclusions and Future Work

In this thesis, leather inspection and characterization has been looked at using non-destructive techniques. A novel system was designed and evaluated for performing mechanical probing of leather properties in a non-destructive manner. Also, infrared thermography was explored as a potential technique for leather inspection and characterisation.

With respect to the Mechanical Scanning System (MSS), the investigation was focused on two of the most important physical leather properties, static compressibility across thickness and tensile properties for low strain regions. The results of static compression energy measurements carried out by the MSS for a compressive strain of 10 percent, showed a close agreement with the results of tests performed by a conventional compressibility tester. The results of strain energy and stress measurements performed by the MSS for a strain of 2 percent, revealed a very good correlation (about 0.90) with the results of conventional tensile tests for a similar strain.

Some suggested future research topics are now listed for the MSS:

- Shear stress tests across thickness still need to be carried out and the results analysed in order to find out which information can be extracted from the referred test and how it correlates with other leather physical properties.
- For the determination of the compressive stress, further research is needed to fully understand the mechanics of compressing leather with a curved surface and how the contact area between leather and wheels changes with compressive strain.
- Despite the good results obtained for the correlation coefficients of stress and strain energy computations at 2 percent strain, confirmation of these results is needed for higher strains, for example 5 and 10 percent strain.

- Stress strain cycling should be performed with the MSS and the recovery part of these tests should be looked at in detail in order to find out which relevant information can be extracted.

- The best surface for the wheels of the MSS needs to be investigated so grip is maximised without causing any damage to the surface.

Despite the limitations of the work completed to date, the findings demonstrate that this scanning system can be used reliably to test leather for its compressibility and tensile properties for low strain regions, in a non-destructive manner with no need for sample removal from the whole skin or hide.

If a device, based on the MSS concept, was to be built for industrial application, it could be used as a useful quality control tool in the laboratory of the tanner or leather goods industry. Also, it could be used as an in-line instrument to characterise leather and produce a map of the physical properties referred above. In this case, the device could consist of several scanning heads placed, for instance 25 cm apart, so a hide could be scanned in both directions, parallel and perpendicular to the backbone. Every single hide would have to be scanned, so decisions regarding fitness for purpose could be made with a higher accuracy and consistency than when assessed manually. Further, it is also recommended that wheels with higher radius should be used, as more contact area between wheels and leather would be achieved. Obviously, bigger wheels have several other implications, for instance: more powerful motors are required, as more torque is needed; more compression force is necessary, as compression contact area is larger. The speed of testing could be increased in order to achieve sufficient productivity.

Considering now the infrared thermography technique. Measurements of the thermal diffusivity of leather were correlated with measurements of their respective apparent density; unfortunately, no positive relationship was found between these two properties. Thus, no link could be established between thermal diffusivity and the tensile strength of leather as initially hypothesised.

The effect of leather anisotropy in heat flow was also studied and the results suggested that a relation between lines of tightness and shape of pattern resulting from point heating might exist.

Regarding inspection of leather, it was shown that transient thermography could be used for detecting defects in leather, as well as for estimating their size and deepness with regard to the observed surface. However, defect visibility by infrared thermography is conditioned by the fact that a defective area has to cause different material properties or produce an internal thermal resistance.

Currently, the application of infrared thermography for leather characterisation and inspection is limited by the prohibitive cost of infrared thermography cameras. Another limitation of infrared thermography is the typical slowness of an infrared thermography testing procedure.

Further research on infrared thermography for leather characterisation and inspection is suggested as follows:

- The idea of characterising leather non-destructively in a contact less manner requires further work, in particular the effect of porosity on the thermal diffusivity and thermal conductivity of leather and their relationship with apparent density and tensile strength.
- The effect of leather anisotropy in heat flow needs further studying to confirm if a relationship between lines of tightness and shape of pattern resulting from point heating really exists.
- It will be also important to evaluate lock-in thermography for leather defect detection, as well as other heat stimulation sources and methods like line heating. The development of algorithms for automatic leather defects detection using infrared thermography is still a vast field of research.

Finally, if an effective automatic system for characterisation and inspection of leather were to be built, it would have to result from the combination of several methods of characterisation and inspection. The author believes that the ideal solution would be based on the combination of mechanical scanning, normal computer vision and infrared thermography. Here, the weaknesses of a method would be compensated by the strengths of another method. The normal computer vision part of this system would be responsible for measuring area and detecting defects that are visible in nature. The infrared thermography part of the system would be responsible for detecting defects of difficult detection by a normal computer vision as well as some thermo-physical

parameters. Finally, the Mechanical Scanning System would provide the physical properties of leather, like compressibility, tensile modulus, shear stress and softness that the vision based inspection systems are incapable of providing. In this way, every single skin could be completely characterised in terms of defects and physical properties. This information should then be passed to CAD systems in order to maximise the yield of every single skin and achieve maximum fitness for purpose.

References

[Aga 76] AGA Thermovision 750 Operating Manual, AGA Infrared System, 1976.

[Alexander 72] Alexander, J.M., "On the theory of rolling", Proceedings of the Royal Society of London, A. 326, pp. 535-563, 1972.

[Alexander 93] Alexander, K.T.W.,Stosic, R.G., "A Non-Destructive Leather Softness Test", Journal of International Society Leather Trades' Chemists, vol.77, pp.139-142, 1993.

[Allport 88] Allport, J., McHugh, J., "Quantitative Evaluation of Transient Video Thermography", Review of progress in Quantitative Non Destructive Evaluation, Plenum Press, New York, vol.7A, pp.253-262, 1988.

[Almond 94] Almond, D., Lau, S., "Defect sizing by transient thermography: an analytical treatment", Journal Physics D: Applied Physics, vol.27, pp.1063-1069, 1994.

[Attenburrow 93] Attenburrow, G.E., "The Rheology of Leather-A Review", Journal of International Society Leather Trades' Chemists, vol.77, pp.107-114, 1993.

[Bailey 89] Bailey, D., "Leather, Encyclopaedia of Polymer Science and Engineering", supplement volume, John Wiley & Sons, Inc., New York, pp. 362-379, 1989.

[Boccone 77] Boccone, R.L., Fontana, J. and Kamp, G., "Topographic Distribution of Properties in Softy Shoe Upper Leathers", Journal of International Society Leather Trades' Chemists, vol.61, pp.106-111, 1977.

[Busse 92] Busse, G., Wu, D., Karpen, W., "Thermal Wave Imaging with phase sensitive modulated thermography", Journal of Applied Physics, vol.78, pp.3962-3965, 1992.

[Butlin 63] Butlin, J., "The Plasticity and Related Properties of Upper Leather: Part I", Journal of International Society Leather Trades' Chemists, vol. 47, pp. 3-38, 1963.

[Carslaw 59] Carslaw, H., Jaeger, J., "Conduction of Heat in Solids", Claredon Press, Oxford, 1959.

[Casado 95] Casado, F., "Termografia Infraroja, Principios Básicos", Alava Ingenieros, Division Electro-Óptica, pp.5-10, 1995.

[Castleman 96] Castleman, K., "Digital image processing", Prentice-Hall, Englewood Cliffs, NJ 07632, pp.112, 1996.

[Cielo 87] Cielo, P., Maldague, X., Déom, A.A., Lewak, R., "Thermographic Nondestructive Evaluation of Industrial Materials and Structures", Materials Evaluation, vol.45, pp.452-460, 1987.

[Connolly 92] Connolly, M., P., "The Measurement of Porosity in Composite Materials using Infrared Thermography", Journal of Reinforced Plastics and Composites, vol. 11, No. 12, pp. 1367-1375, 1992.

[de Jong 86] de Jong, S., Snaith, J. W., and Michie, N. A., "A Mechanical Model for the Lateral Compression of Woven Fabrics", Textile Research Journal, Vol. 56, No. 12, pp. 759-767, 1986.

[Favro 95] Favro, L., Han, P., Kuo, R., "Image of early time behaviour of reflected thermal-wave pulses", Thermosense XIV, Proceedings SPIE, vol.2473, pp.162-166, 1995.

[Fisher 95] Fisher, Yuval, "Fractal Image Compression: Theory and applications", New York, Springer Verlag, pp. 43-44, 1995.

[Gaffron 94] Gaffron, I., Cory, N.J., Wood, C.B., "Automatic Inspection by Image", Journal of American Leather Chemists Association, vol.89, pp. 283-288, 1994.

[Gaussorgues 94a] Gaussorgues, G., "Infrared Thermography", Microwave Technology Series 5, Chapman & Hall, London, pp. 181-184, 1994.

[Grinzato 95] Grinzato, E., Vavilov, V., Bison, P., Marineti, S., Bressan, C., "Methodology of processing experimental data in transient thermal NDT", Thermosense XIII, Proceedings SPIE, vol.2473, pp.167-178, 1995.

[Guy 74] Guy, R. and Marriott, A.G., "The Choice of Experimental Error in the Determination of Some Tensile Parameters of Leather", Journal of International Society Leather Trades' Chemists, vol.58, pp.145-146, 1974.

[Guy 74a] Guy, R. and Marriott, A.G., "The Measurement of Elongation at Break in Leather Testing", Journal of International Society Leather Trades' Chemists, vol.58, pp.137-143, 1974.

[Guy 75] Guy, R. and Marriott, A.G., "A Comparison of Two Tear Tests for Leather", Journal of International Society Leather Trades' Chemists, vol.59, pp.30-40, 1975.

[Halmshaw 91] Halmshaw, R., "Non-Destructive Testing", Second Edition, Edward Arnold, London, 1991.

[Hamzah 96] Hamzah, A.R., "The application of transient thermography to defect detection", PhD Thesis, University of Bath, pp.194, 1996.

[Hamzah 96a] Hamzah, A.R., "The application of transient thermography to defect detection", PhD Thesis, University of Bath, pp.79, 1996.

[Hayden 87] Hayden, H.C., "Data smoothing routine", Computing Physics, vol.1, pp.74-75, 1987.

[Hilton95] Hilton, P. Gabric R., "Multiple image acquisition for Inspection of Natural Products", Proceedings of SPIE - The International Society for Optical Engineering, vol. 2345, pp. 10-19, 1995.

[Hoang 97] Hoang, K., Wen, W., Nachimuthu, A., Jiang, X., "Achieving Automation in Leather surface Inspection", Computers in Industry, Elsevier, vol. 34, No 1, pp. 43-54, 1997.

[Hobbs 91] Hobbs, C.P., Kenway-Johnson, D, Milne, J., "Quantitative Measurement of thermal parameters over large areas using Pulse Video Thermography", Thermosense XIII, Proceedins SPIE, vol.1467, pp.264-277, 1991.

[Hudson 69] Hudson, R.D., "Infrared Systems Engineering", Wiley Interscience, New York, pp. 642, 1969.

[Johnson 85] Johnson, K.L., "Contact mechanics", Cambridge University Press, 1985.

[Kanagy 55] Kanagy, J.R., "Significance of the Results of Some Physical Tests on Upper Leather", Journal of American Leather Chemists Association, vol.50, pp.112-148, 1955.

[Kanagy 65] Kanagy, J.R., "Physical and Performance Properties of Leather", American Chemical Society Monograph 134, vol. 1, chap. 64, Reinhold Publishing Corp., New York, pp. 369-416, 1965.

[Kawabata 80] Kawabata, S., "The Standardization and Analysis of Hand Evaluation", 2nd ed., Textile Machinery Society of Japan, Osaka, 1980.

[Kawabata 82] Kawabata, S., "Objective Specification of Fabric Quality, Mechanical Properties and Performance", Proceedings of the Japan Autralia Joint symposium on Objective specification og Fabric Quality, Kyoto, 1980.

[Krapez 91] Krapez, J., Maldague, X., Cielo, P., "Thermographic NDE: Data inversion procedure, Part 2: 2D Analysis and Experimental Results", Research in Nondestructive Evaluation, vol.3 (2), pp.101-106, 1991.

[Krapez 94] Krapez, J., Balageas, D, "Early detection of thermal contrast in pulsed stimulated infrared thermography", Proceedings of QIRT 94, Eurotherm Seminar 42, pp.260-266, 1994.

[Krautkramer 90] Krautkramer, J., Krautkramer, H., "Ultrasonic Testing of Materials", 4th edition, Springer-Verlag, London, 1990.

[Kronick 92] Kronick, P., Maleef, B., "Nondestructive Failure Testing of Bovine Leather by Acoustic Emission", Journal of American Leather Chemists Association, vol.87, pp.259-265, 1992.

[Landmann 94] Landmann, A., Stosic, R.G., Vaculik, J., Hanson, M., "Softness- an international comparison of manual assessment against instrumental methods", Journal of International Society Leather Trades' Chemists, vol.78, pp.88-92, 1994.

[Liu 97] Liu, C., McClintick, M., "Measurements of the Initial Strain Energy of Leather", Journal of American Leather Chemists Association, vol.92, pp.157-171, 1997.

[Lokanadam 89] Lokanadam, B., Subramaniam, V. and Nayar, R.C., "Compressibility Measurement and the Objective Assessment of Softness of Light Leathers", Journal of International Society Leather Trades' Chemists, vol.73, pp.115-119, 1989.

[Maeser 54] Maeser, M., Dion, O., "The effect of splitting on the tensile properties of leather", Journal of American Leather Chemists Association, vol. 49, pp. 262, 1952.

[Maeser 65] Maeser, M., "Dynamics and Nondestructive Testing", American Chemical Society Monograph 134, vol. 1, chap. 62, Reinhold Publishing Corp., New York, pp. 310-332, 1965.

[Maldague 93] Maldague, X.P.V., "Nondestructive Evaluation of Materials by Infrared Thermography", Springer Verlag London Ltd, London, 1993.

[Maldague 93a] Maldague, X.P.V., "Nondestructive Evaluation of Materials by Infrared Thermography", Springer Verlag London Ltd, London, pp.83, 1993.

[Maldague 93b] Maldague, X.P.V., "Nondestructive Evaluation of Materials by Infrared Thermography", Springer Verlag London Ltd, London, pp.7, 1993.

[Kronick 92] Kronick, P., Maleef, B., "Nondestructive Failure Testing of Bovine Leather by Acoustic Emission", Journal of American Leather Chemists Association, vol.87, pp.259-265, 1992.

[Landmann 94] Landmann, A., Stosic, R.G., Vaculik, J., Hanson, M., "Softness- an international comparison of manual assessment against instrumental methods", Journal of International Society Leather Trades' Chemists, vol.78, pp.88-92, 1994.

[Liu 97] Liu, C., McClintick, M., "Measurements of the Initial Strain Energy of Leather", Journal of American Leather Chemists Association, vol.92, pp.157-171, 1997.

[Lokanadam 89] Lokanadam, B., Subramaniam, V. and Nayar, R.C., "Compressibility Measurement and the Objective Assessment of Softness of Light Leathers", Journal of International Society Leather Trades' Chemists, vol.73, pp.115-119, 1989.

[Maeser 54] Maeser, M., Dion, O., "The effect of splitting on the tensile properties of leather", Journal of American Leather Chemists Association, vol. 49, pp. 262, 1952.

[Maeser 65] Maeser, M., "Dynamics and Nondestructive Testing", American Chemical Society Monograph 134, vol. 1, chap. 62, Reinhold Publishing Corp., New York, pp. 310-332, 1965.

[Maldague 93] Maldague, X.P.V., "Nondestructive Evaluation of Materials by Infrared Thermography", Springer Verlag London Ltd, London, 1993.

[Maldague 93a] Maldague, X.P.V., "Nondestructive Evaluation of Materials by Infrared Thermography", Springer Verlag London Ltd, London, pp.83, 1993.

[Maldague 93b] Maldague, X.P.V., "Nondestructive Evaluation of Materials by Infrared Thermography", Springer Verlag London Ltd, London, pp.7, 1993.

[Maldague 93c] Maldague, X.P.V., "Nondestructive Evaluation of Materials by Infrared Thermography", Springer Verlag London Ltd, London, pp.76, 1993.

[Maldague 94] Maldague, X.P.V., "Infrared Methodology and Technology" Nondestructive Testing Monographs and Tracts, vol. 7, Gordon and Breach Science Publishers, Illinois, 1994.

[Marinetti 96] Marinetti, S., Maldague, X., Prystay, M., "Calibration procedure for focal plane arrays cameras and noise equivalent material loss for quantitative thermographic NDT", Materials Evaluation, vol.54, pp.281-286, 1996.

[Matlab 95] Thompson, C.M., Shure, L., "Image Processing Toolbox User's guide", The Mathworks, 1995.

[Matsudaira 95] Matsudaira, M., and Qin, H., "Features and Mechanical Parameters of a Fabric's Compressional Property", *Journal of the Textile Institute*, Vol. 86, No. 3, pp. 476-486, 1995.

[MFG 93] MFG Hardware Reference Manual, Imaging Technology Inc., February 1993.

[Micro-Epsilon 94] "optoNCDT 1605 Non-contact Optical Displacement Measuring System, Instruction Manual", Micro-Epsilon Messtechnik GmbH, Ortenburg, Germany, 1994.

[Mitton 45] Mitton, R., "Mechanical Properties of Leather Fibres", Journal of International Society Leather Trades' Chemists, vol. 29, No. 8, pp. 69-194, 1945.

[Mitton 48] Mitton, R., "Tensile Properties and their Variability in Chrome-tanned Calf-skins", Journal of International Society Leather Trades' Chemists, vol. 32, No. X, pp. 310-323, 1948.

[Muthiah 76] Muthiah, P.L., Ramanathan, N., "Locational Differences in the Physical Properties of Upper Leather", Journal of International Society Leather Trades' Chemists, vol.60, pp.77-85, 1976.

[O'Leary 96] O'Leary, D, "Differences in Strength between the grain and corium layers of bovine leather", PhD Thesis, University of Leicester, 1996.

[Onions 67] Onions, *et al.*, "", Journal of Textile Institute, vol. 58, pp. 296, 1967.

[Parker 61] Parker, W.J., Jenkins, R.J., Butler, C.P., "Flash Method of Determining Thermal Diffusivity, Heat capacity, and Thermal Conductivity", Journal of Applied Physics, vol.32, No.9, pp.1679-1684, 1961.

[Parker 94] *PDX Series Drive, User Guide*, Unimatic Engineers Ltd., London, UK, 1994.

[Peralta 91] Peralta, S.B., "Photopyroelectric measurement of the thermal diffusivity of recrystallized high purity aluminum", Research in NonDestructive Evaluation, vol.3, No.2, pp.69-80, 1991.

[Pölzleitner 95] Pölzleitner, W., Schwingshakl, G., Paar, G., "ARGUS - a flexible real-time system for 2D defect and texture classification of wooden materials", Proceedings of SPIE - The International Society for Optical Engineering, vol. 2345, pp. 50-58, 1995.

[Postle 71] Postle, R., "The Thickness and Bulk Density of Plain-Knitted Fabrics", Journal of the Textile Institute, Vol. 62, No. 4, pp. 219-231, 1971.

[Randall 52] Randall, E., Kanagy, J.R., "", Journal of American Leather Chemists Association, vol. 47, pp. 404, 1952.

[Rangulam 93] Rangulam, R., Porat, I., "Measurement of Fabric Roughness by a Non-Contact Method", Journal of Textile Institute, vol. 84, No. 1, pp. 99-106, 1993.

[Roddy 56] Roddy, W, O'Flaherty, F., "Chemistry and Technology of Leather", American Chemical Society Monograph 134, vol. 1, chap. 2, Reinhold Publishing Corp., New York, pp. 1956.

[SATRA 92] Rose, S., "Modern Shoemaking, Shoemaking with Leather", SATRA Footwear Technology Centre, No. 11 (revised) December, 1992.

[Sayers 84] Sayers, C.M., "Detectability of Defects by Thermal Non-Destructive Testing", British Journal of NDT, January, pp.28-33, 1984.

[Sigma 90] *Stepping Motors, Sigma Motion Control*, Unimatic Engineers Ltd., London, UK, 1990.

[Smith 91] Smith, D.L., "The Manipulation of Leather Workpieces for the Assembly of Shoe Uppers", PhD Thesis, Department of Electronic Engineering, The University of Hull, 1991.

[Spicer 91] Spicer, J.W., Kerns, W.D., Aamodt, L.C., Murphy, J.C., "Time Resolved Infrared Radiometry (TRIR) of multiplayer organic coatings using a surface and subsurface heating", Thermosense XIII, Proceedings SPIE, vol.1467, pp.308-314, 1991.

[Taylor 98] Taylor, Paul M., Mendes, José A., "Testing Apparatus", Patent Application No. EPO866327 published on September 23rd 1998.

[Timoshenko 73] Timoshenko, S. P., and Gere, J. M., *Mechanics of Materials*, Van Nostrand Reinhold Company, New York, pp. 34-37, 1973.

[Vavilov 94] Vavilov, V.P., Maldague, X.P.V., "Infrared Methodology and Technology" Nondestructive Testing Monographs and Tracts, vol. 7, Gordon and Breach Science Publishers, Illinois, pp.156, 1994.

[Vavilov 82] Vavilov, V., Taylor, R., "Theoretical and Practical Aspects of the Thermal Nondestructive Testing of Bonded Structures", Research Tecniques in NDT, Academic Press, vol.V, pp.238-279, 1982.

[Vibro-meter 95] *Proximity Transducer Type TQ-402/412, Data sheet 265-042*, Vibro-meter Ltd., Hazel Grove, Cheshire, UK, 1995.

[Vos 73] Vos, A., Vlimmeren, P.J., "Topographic Differences in Physical Properties", Journal of International Society Leather Trades' Chemists, vol.57, pp.93-98, 1973.

[Wang 92] Wang, Y., "Characteristics of Brazilian Goat and Sheep Skin and Leather", MPhil Thesis, Nene College, University of Leicester, 1992.

[Wang 92a] Wang, Y., "Characteristics of Brazilian Goat and Sheep Skin and Leather", MPhil Thesis, Nene College, University of Leicester, pp.88-91, 1992.

[Williams 92] Williams, T.L., "The MTF of Thermal Imaging Cameras – Its Relevance and Measurement", Proceedings of Quantitative Infrared Thermography (QIRT 92), Eurotherm Seminar 27, pp 51-56, 1992.

Secondary Sources:

Barlow, J.R., A Simple Apparatus for Measuring the Tensile and Tear Strength Properties of Leathers, Journal of International Society Leather Trades' Chemists, vol.61, pp.112-113, 1977.

Barlow, J.R., A Simple Lastometer, Journal of International Society Leather Trades' Chemists, vol.62, pp.114-115, 1977.

Carvalho-Rodrigues, F., Carvalho, D.F., Peixoto, J.P., Silva, M.S. and Silvestre, V., Application of Information Entropy to Defect Characterisation in Leather, Journal of International Society Leather Trades' Chemists, vol.75, pp.10-14, 1991.

Chow, K.M., "Various Sensing Methods for Inspecting Leather", Final Year Report, Dep of Electronic Engineering, The University of Hull, 1993.

Dulio, S., An Application of Automation Technology to Leather Cutting, Advanced Automotive Manufacturing Procedings, pp.83-96, Dec. 1990.

Gratacos, E., Costa,R., Sans and J., Portavella, M., Grain Strain in Sheepskins Produced During Flaying: Part 1, Journal of International Society Leather Trades' Chemists, 19..., vol.74, pp.174-184.

Gratacos, E., Costa,R., Sans and J., Portavella, M., Grain Strain in Sheepskins Produced During Flaying: Part 2, Journal of International Society Leather Trades' Chemists, vol.75, pp.1-9, 1990.

Gulik, T.M. and Klopper, P.J., The Mechanical Properties of Sheepskin Splits as Determined by an Experimental Method, Journal of International Society Leather Trades' Chemists, vol.71, pp.38-42, 1991.

Heidemann, E., "Fundamentals of Leather Manufacturing", Eduard Roether KG, Darmstadt, 1993.

Holst, P.J., Peters, D.E., Allan, C.J. and Pervez, M., Properties of Leather Produced from a Sample of Australian Feral Goats, Journal of International Society Leather Trades' Chemists, vol.71, pp.134-137, 1987.

Jarret, R.M. and Sykes, R.L., Analysis of Video Recordings to Investigate Mechanical Operations, Journal of International Society Leather Trades' Chemists, vol.72, pp.94-96, 1988.

Kanagy, J.R. and Robinson, M., Studies on Leather by Means of a Sonic Technique, Journal of International Society Leather Trades' Chemists, vol.51, pp.174-197, 1956.

Koeppen, R., Quantification of Hide Defects on Today's Leather, Journal of American Leather Chemists Association, vol.86, pp.9-13, 1991.

Kronick, P. and Buechler, R.P., Fibre Orientation in Calfskin by Laser Light Scattering or X-Ray Diffraction and Quantitative Relation to Mechanical Properties, Journal of American Leather Chemists Association, vol.81, pp.221-230, 1986.

Kronick, P. and Maleef, B., Nondestructive Failure Testing of Bovine Leather by Acoustic Emission, Journal of American Leather Chemists Association, vol.87, pp.259-265, 1992.

Kronick, P., Page, A. and Komanowsky, M., An Acoustic Emission Study of Staking and Fatliquor, Journal of American Leather Chemists Association, vol.88, pp.179-186, 1993.

Kronick, P.L. and Buechler, P.R., Fibre Orientation and Small-Deformation Modulus of Stretched, Partially-Dried Hide, Journal of American Leather Chemists Association, vol.83, pp.115-124, 1988.

Landman, A.W., Repeatability and Reproducibility of Test Methods, Journal of International Society Leather Trades' Chemists, vol.73, pp.144-145, 1989.

Landman, A.W., Stosic, R.G. and Deadman, T.J., A Test for Bagginess and Computer Lastometer Test, Journal of International Society Leather Trades' Chemists, vol.78, pp.105-108, 1994.

Landman, A.W., Stosic, R.G., Vaculik, J. and Hanson, M., Journal of International Society Leather Trades' Chemists, vol.78, pp.88-92, 1994.

Landman, A.W., The Role of Instrumental Testing in the 90s, Journal of International Society Leather Trades' Chemists, vol.74, pp.39-40, 1990.

Landman, A.W., Within and Between Skin Variation of Physical Properties in Bovine Leather Journal of International Society Leather Trades' Chemists, vol.63, pp.45-48, 1979.

Lin, J. and Hayhurst, D.R., Constitutive Equations for Multi-Axial Straining of Leather Under Uni-Axial Stress, Eur. J. Mech., A/Solids, vol.12, no.4, pp.471-492, 1993.

Lin, J., "Computer Aided Modelling of The Lasting of Leather Shoes", PhD Thesis, Dep. of Mechanical and Process Engineering, University of Sheffield, 1991.

Mantysalo, E., Marjoniemi, M. and Kemppinen, Anisotropy of Physical-Characteristic Functions of Fur Leather, Journal of American Leather Chemists Association, vol.86, pp.133-140, 1991.

McGonnagle, W.J., "Automated Nondestructive Testing - Nondestructive Testing Monographs and Tracts", vol. 4, Gordon and Breach Science Publishers, Illinois, 1986.

Miller, R., "Manual of Shoemaking", Clarks Ltd., 2nd edition, 6th impression, Bristol, 1989.

Monastyrska-Przybylak, R., Anomalies of Pigskin Structure, Part I. Differences in Basic Strength Properties, Journal of International Society Leather Trades' Chemists, vol.66, pp.61-65, 1982.

Monastyrska-Przybylak, R., Anomalies of Pigskin Structure, Part III. Analysis of Leather Structure Through Fatigue and Density Tests, Journal of International Society Leather Trades' Chemists, vol.66, pp.74-78, 1982.

Peters, D.E. and Stephens, L.J., The Physical Properties of Leather from Kangaroo Skins I. Comparison Between Species and Sexes, Journal of American Leather Chemists Association, vol.84, pp.133-142, 1989.

Peters, D.E. and Stephens, L.J., The Physical Properties of Leather from Kangaroo Skins II. Variation in Properties with Sampling Position, Journal of American Leather Chemists Association, vol.84, pp.143-149, 1989.

Russel, A.E., Stress-Strain Relationships in Leather and the role of Fibre Structure, Journal of International Society Leather Trades' Chemists, vol.72, pp.121-134, 1988.

Ryan, A. and Postle, R., Application of Sonic Wave Theory to the Measurement of the Dynamic Elastic Moduli of Woven and Knitted Fabrics, Textile Research Journal, pp.732-740, Nov.1981.

Scott, I.G., "Basic Acoustic Emission - Nondestructive Testing Monographs and Tracts", vol. 6, Gordon and Breach Science Publishers, Illinois, 1991.

Sharphouse, J.H., "Leather Technician's Handbook", Leather Producers' Association, London, 1983.

Stylios, G., "Textile Objective Meausurement and Automation in Garment Manufacture", Ellis Horwood Ltd., 1991.

Sykes, R.L., Leather Research-Where now?, Journal of International Society Leather Trades' Chemists, vol.76, pp.149-156, 1992.

Tancous, J.J., "Skin, Hide and Leather Defects", 2nd edition, Lee Corporation, Ohio, 1986.

Vavilov V. Maldague, X.P.V., "Research in NonDestructive Evaluation", vol. 6, No 1, pp 1-18, 1994.

Wang, Y.-L., Attenburrow, G. E., Factors Influencing the Softness of Brazilian Goatskin Leathers, Journal of International Society Leather Trades' Chemists, vol.78, pp.85-87.

Wang, Y.-L., Attenburrow, G. E., Strength of Brazilian Goatskin Leathers in Relation to Skin and Animal Characteristics, Journal of International Society Leather Trades' Chemists, vol.78, pp.55-60, 1994.

Whittaker, R.E., The Viscoelastic properties of Leather and Poromerics, Journal of International Society Leather Trades' Chemists, vol.59, pp.172-180, 1975.

Witnauer, L.P. and Palm, W.E., The Flexibility of Leather, Journal of American Leather Chemists Association, vol.57, pp.246-258, 1963.

Yahiaoui, G., Borocco, B., Leather Texture Classification for car Industry Using a Neutral Networks Development Methodology, SPIE Computer Vision for Industry, vol.1989, pp.257-266, 1993.

"System for Automated Fault Detection and Digitisation of Leather Skins and Fabrics", BRITE EURAM Programme, contract: RI1B-266, proposal: P-2195, 1989.

Collett, N.J., Hobbs, C.P., Kenway-Jackson, D., "Adapting Transient Thermography to Industrial Problems", Insight, vol 38, No. 3, pp 163 166, 1996.

Hamzah, A.R., Delpech, P., Saintey, M., Almond, D., "An Experimental Investigation of Defect Sizing by Transient Thermography", Insight, vol.38, No. 3, pp 167 170, 1996.

Milne, J., Reynolds, W., "Applications of Thermal Pulses and Infrared Thermal Images for Observing Subsurface Structures in Metals and Composites", SPIE, vol 590, pp 293 302, 1985.

Appendix A Leather Details

A.1 Specimen dimensions

Specimen "A1", "A2", "A3", "B1", "B2" and "B3" have the dimensions shown in Figure A.1, according to Guy [Guy 74a]. Specimens "A" are parallel to the backbone, while "B" specimens are perpendicular to the backbone.

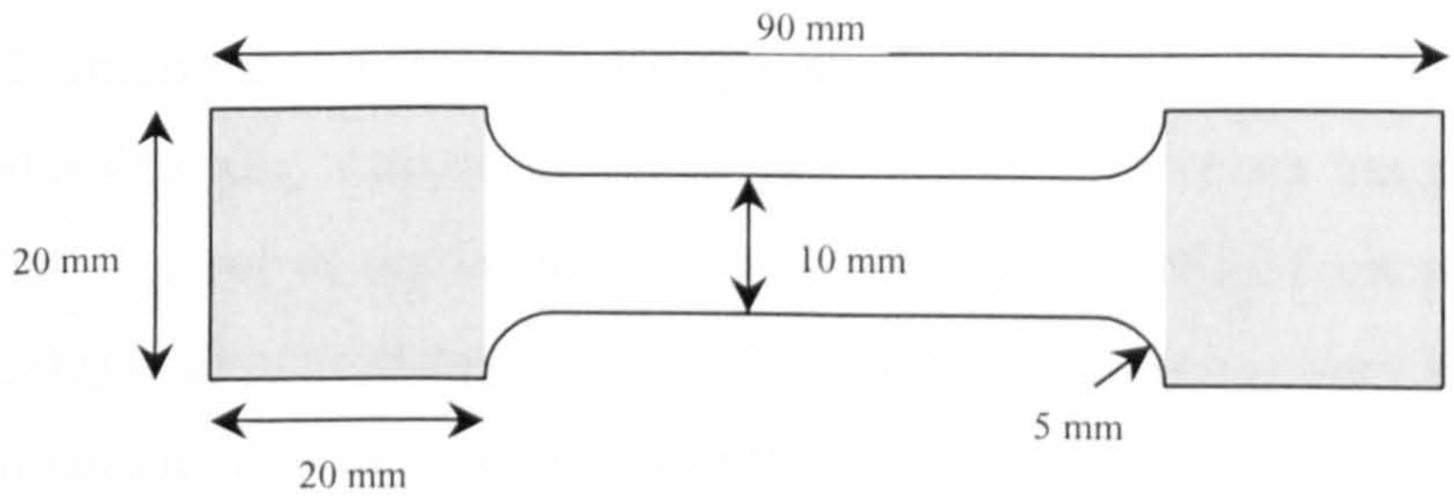

Figure A.1-Tensile testing specimen dimensions.

Specimens "C" and "D" have a rectangular shape of 75 mm by 50 mm, specimen "D" length is parallel to the backbone and specimen "C" length is perpendicular to the backbone.

Specimens "E1", "E2" and "E3" have a circular shape with a diameter of 30 mm.

Specimen "F" also has a circular shape, but with a diameter of 60 mm.

Specimen "I" also has a circular shape, but with a diameter of 100 mm.

Specimens "GN" and "HN" have a rectangular shape of 15 mm by 230 mm, specimen "GN" length is parallel to the backbone and specimen "HN" length is perpendicular to the backbone.

Specimens "GW" and "HW" have a rectangular shape of 60 mm by 230 mm, specimen "GW" length is parallel to the backbone and specimen "HW" length is perpendicular to the backbone.

Appendix B Test Equipment

B.1 X-Y Table

The X-Y table, pictured in Figure B.1, comprises a rectangular base (250 x 350-mm) to which different surfaces can be attached. The table slides on camroller guides and is directly connected to a permanent magnet stepper motor (see Table B.1 for details) via a 4 mm pitch leadscrew. To reduce potential vibrations, generated by the steppers and mechanical misalignments, a bi-directional shaft coupling isolates the steppers from the leadscrews. Furthermore, a rubber pad physically decouples the motor from the X-Y table and a damping mass in the form of a 12.6 kg brass plate has been added to the surface. The control of the steppers is provided by a MOSFET chopper regulated drive (PDX15-D) with micro stepping options, which gives, even at very low velocities, a relatively smooth motion as seen in Figure B.2.

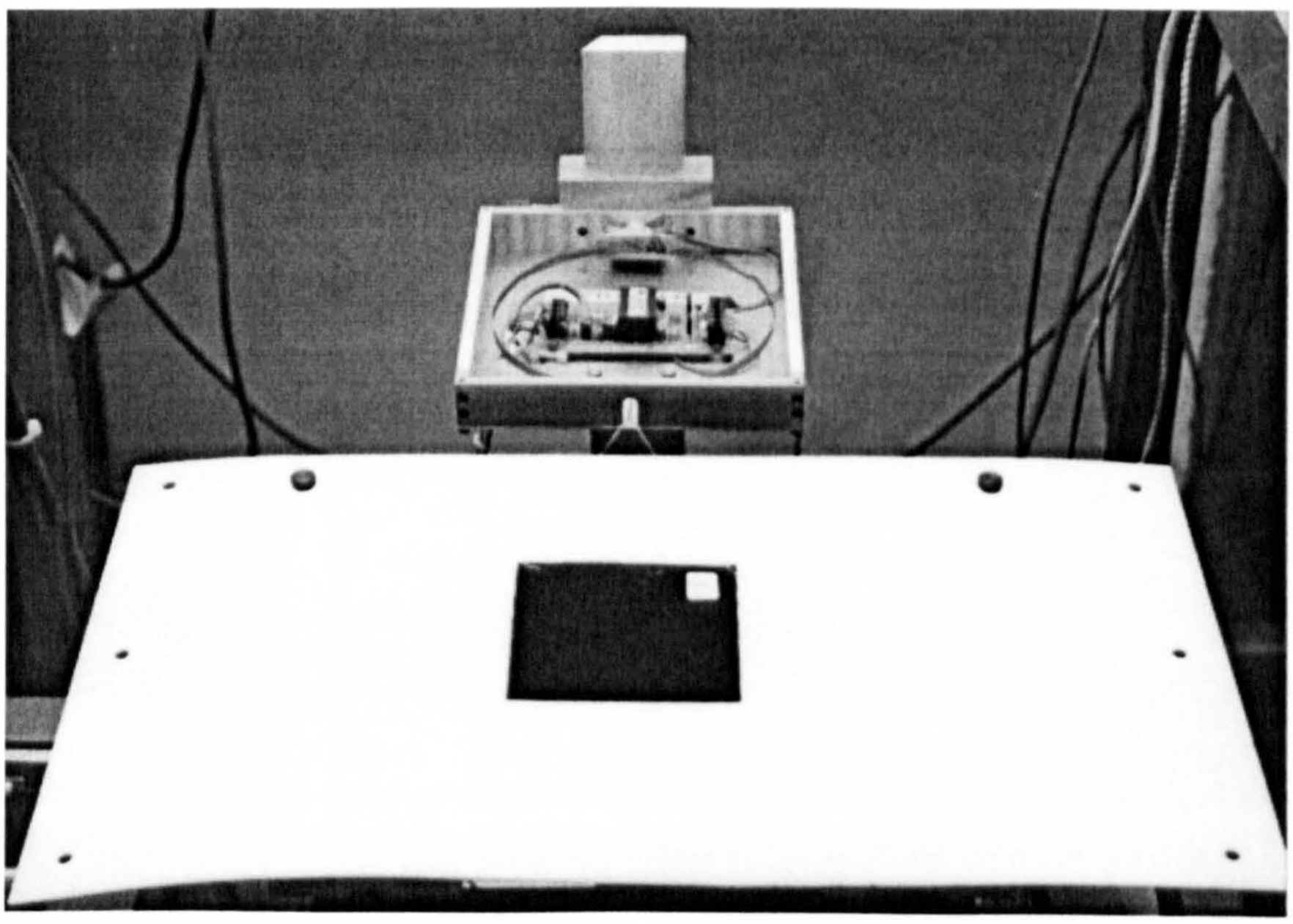

Figure B.1-Picture of the X-Y table and a load-cell for friction tests.

Table B.1-Specifications of the stepper motor (20-3437D200-F075) [Sigma 90].

Parameter	Range
Phases	2
Step angle	1.8°
Windings	4 independent
2 stack rotor	

Table B.2-Specifications of the PDX15-D series mini-stepping drives [Parker 94].

Parameter	Range
Motor resolution (selectable)	4000 steps/rev
Nominal output current	5 A/phase
Mapximum stepping rate	200 kHz at 4000 steps/rev
Nominal chopping frequency	20 kHz
Communication	RS232C

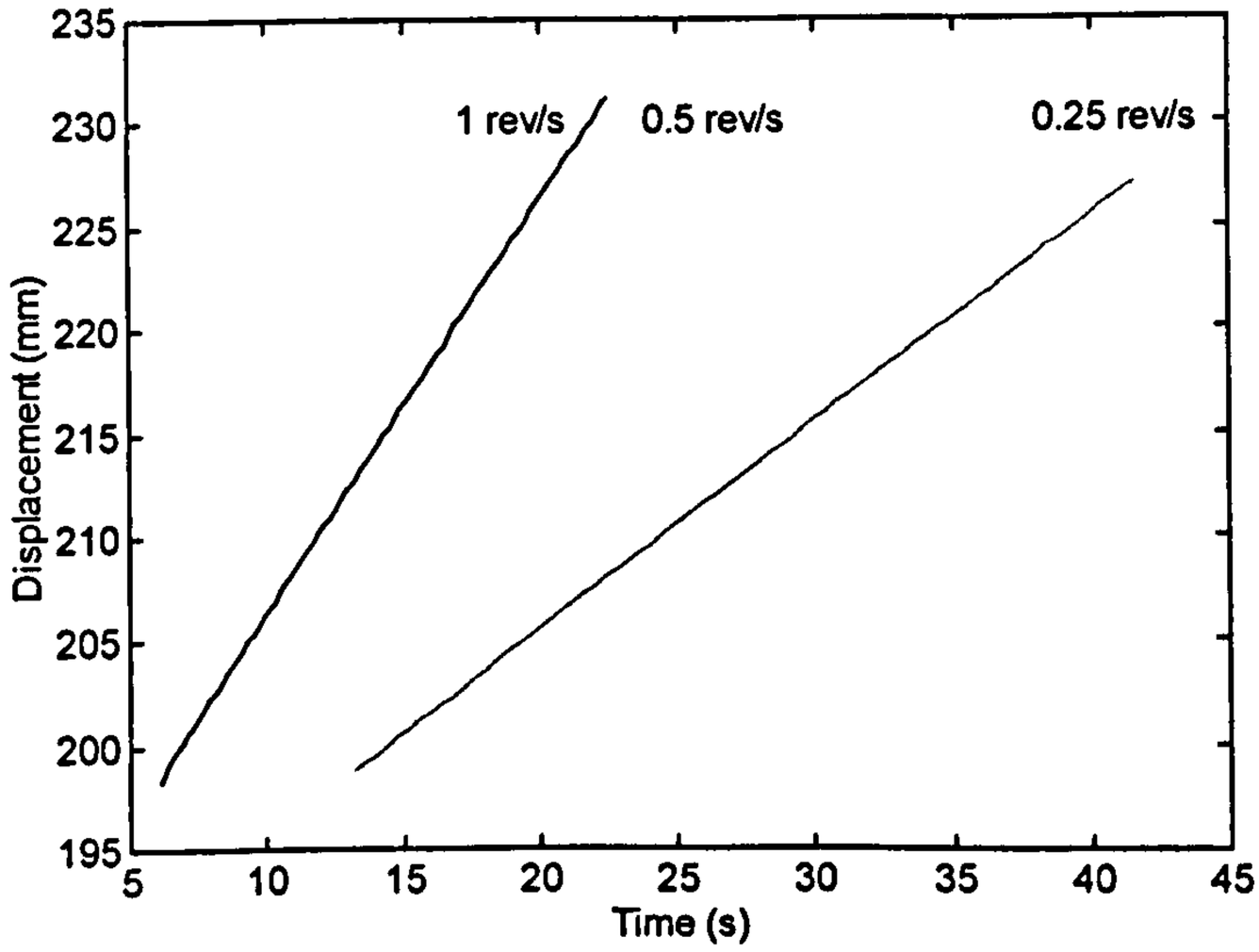

Figure B.2-Displacement of the friction table at various velocities

The table movement has been captured with a video camera, which monitored the table passing over a precision ruler

B.2 Specifications of the Micro-Epsilon® Laser Sensor (LD1605-4)

The laser sensor uses triangulation as a non-contacting measuring technique and has a measuring range of 4 mm at a 1 μm resolution. As depicted in Figure B.3, a beam of red light projected onto the target, scatters back onto a certain position in the detector and so determines the position of the target. The laser light is modulated and therefore practically independent of constant ambient light or light fluorescent tubes. Further, the incident light intensity is automatically matched to the reflectivity of the target, which makes the sensor able to cope with colour changes or patterns. Error messages displayed by LED indicators on the signal conditioning unit monitor the light reflection and indicate whether the target is in measuring range. A summary of the most important technical details is given in Table B.3.

Table B.3-Technical summary of the LD1605-4 [Micro-Epsilon 94].

Parameter	Range
Measuring range (mm)	± 2
Stand-off midrange (mm)	24
Non-linearity < ± 0.3% (μm)	12
Resolution (noise) static (μm)	1
Measuring spot diameter (mm)	0.3
Laser source (class 2)	1 mW, λ 675 nm
Sampling frequency	40 kHz
Analogue output	± 10 V
Output impedance	0 Ω (10 mA
Rise time (selectable)	0.1/0.2/2 or 20 ms
Temperature stability	0.03%/°K

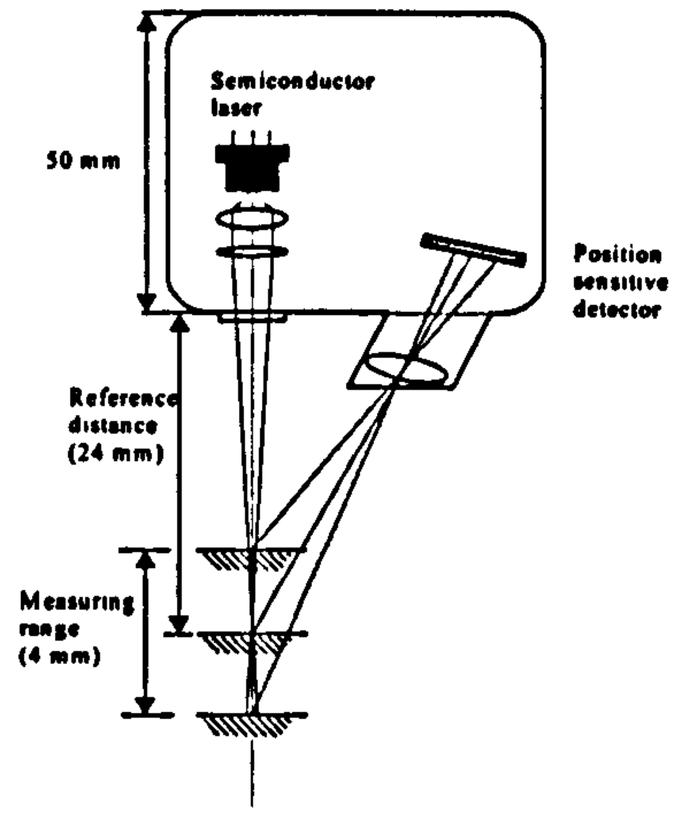

Figure B.3-Triangulation measuring principle [Micro-Epsilon 94].

B.3 Static Compression and Softness Tester

The static compression and softness tester is mechanical device that can be adapted for performing either automated static compressibility tests or automated softness tests (see Figure B.4). For each kind of test a specific presser foot and base are available, being interchangeable as can be confirmed from the observation of Figure B.5 and Figure B.6.

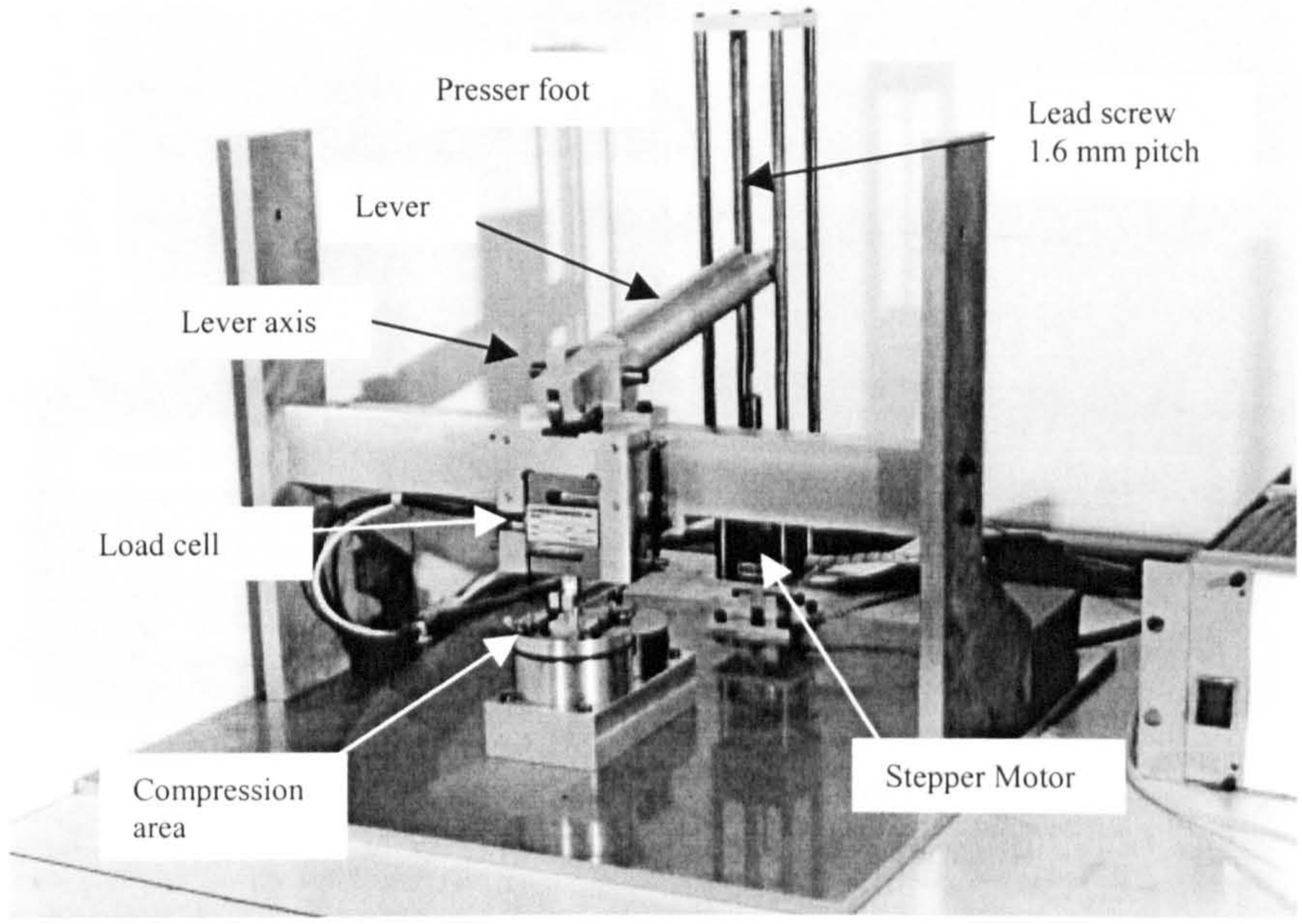

Figure B.4-View of the static compressibility test and softness test.

The compression tester has been built in-house according to the ASTM D1813-89 (thickness measurement standard) specifications with slight modifications of the pressure foot and anvil diameters. The new anvil and pressure foot characteristics are: a flat anvil with 7.8 mm diameter projecting 2.5 mm from the surface of a flat circular platform about 50 mm; a flat pressure foot with 7.8 mm diameter having an effective compression area of 48 mm^2 (see Figure B.5).

The parallelism between compression surfaces is maintained through two linear slides that support the structure containing the load cell and presser foot, assuring a smooth displacement and accurate positioning. Both compression surfaces are mirror finished and give an airtight match of less than 10 μm when compressed empty.

Further, the compression cell comprises a 4 mm range inductive displacement sensor (probe TQ 402/412 and correspondent signal conditioner) and a load cell (LCCA-50) of which the specifications are listed in Table B.4 and Table B.5 respectively. The load cell output and excitation is based on a strain gage signal conditioner from Analog Devices, 1B32, which feeds an analog input of a data acquisition card (PC30AT). This

multipurpose data acquisition card is also responsible for sampling the output from the inductive sensor, which measures the distance between both compressing surfaces, as well as the state of the limit switches of the device.

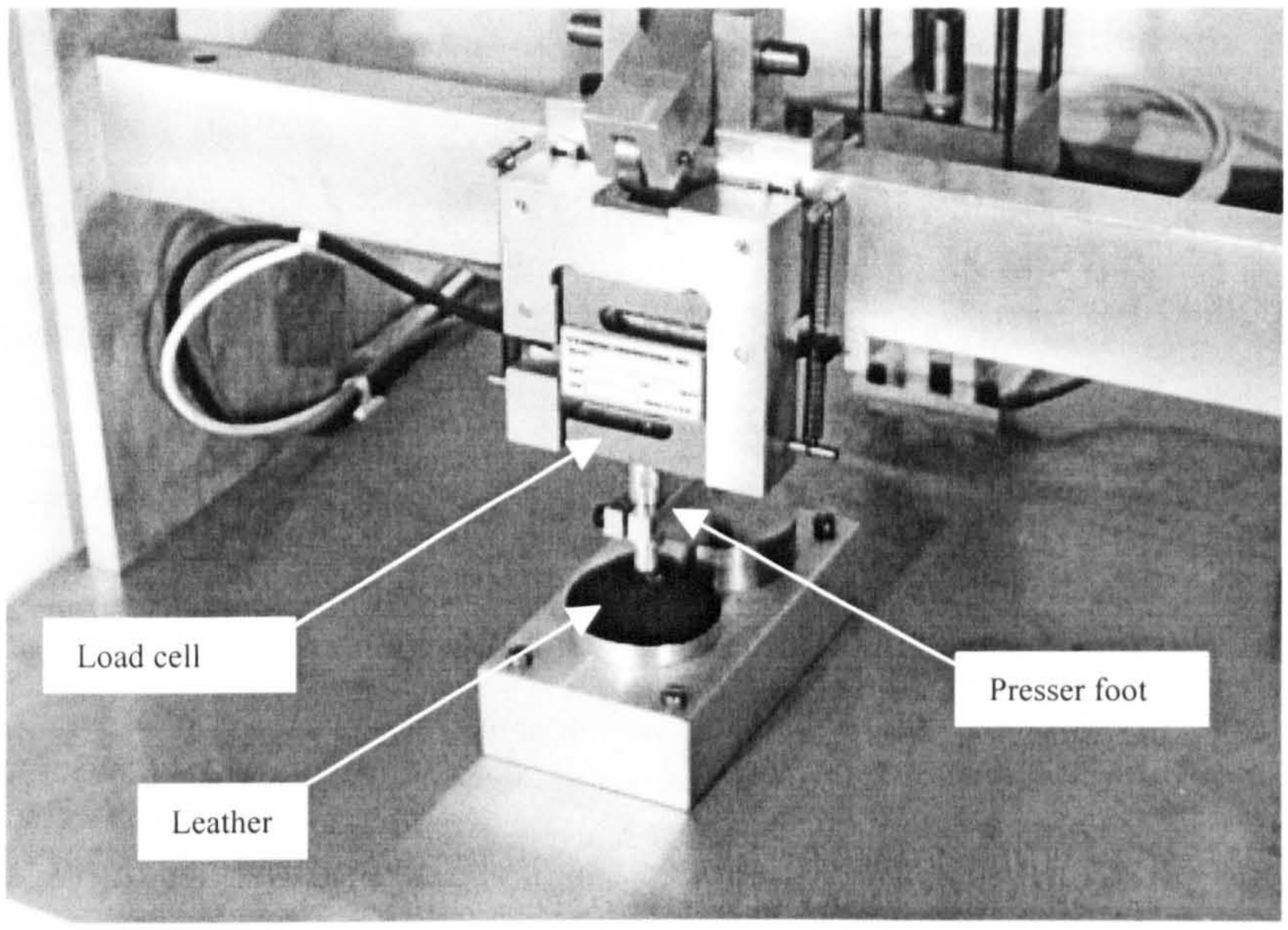

Figure B.5-Static compression tester.

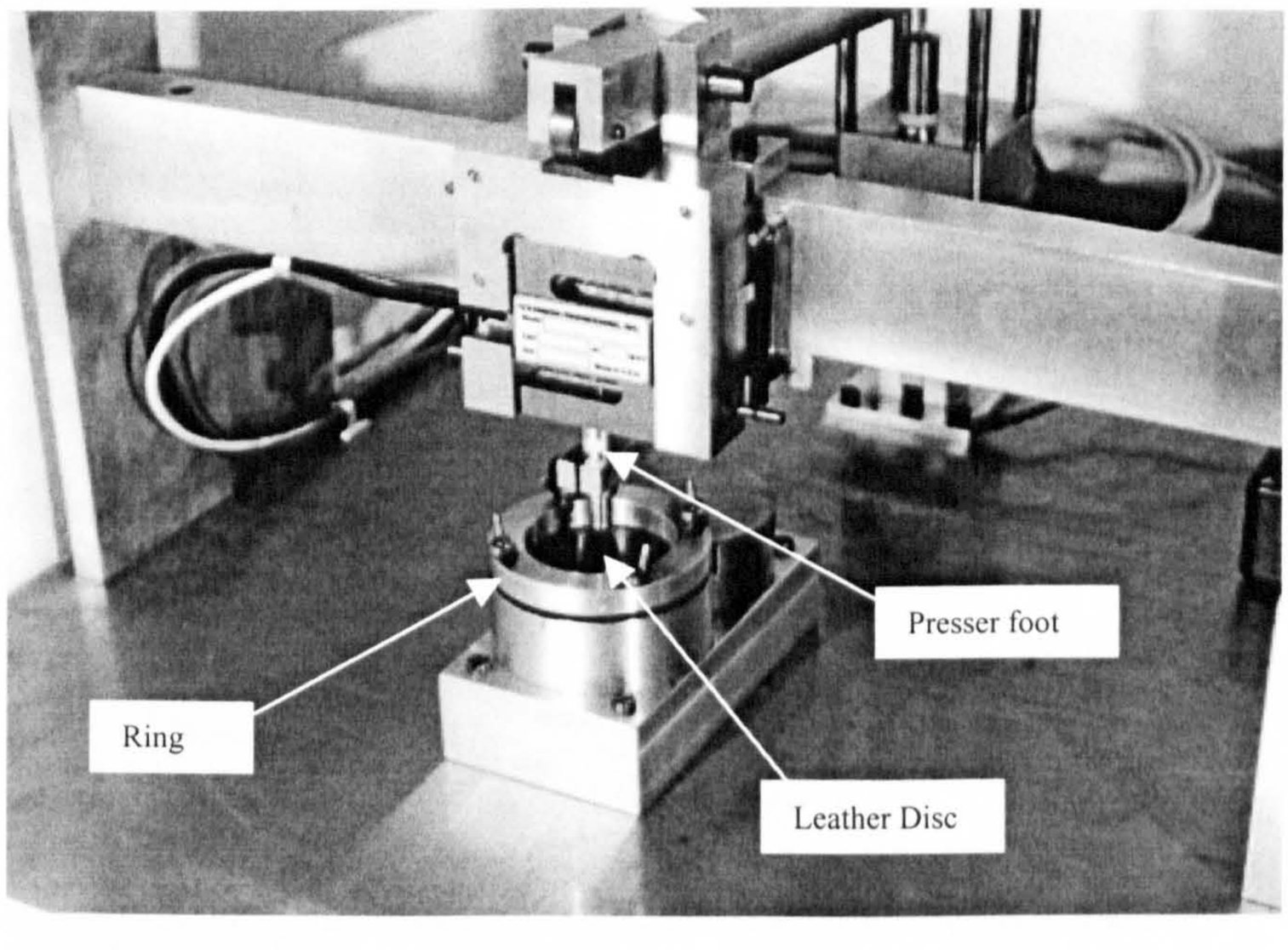

Figure B.6-View of the softness tester.

For compressing a material, a force is applied by a lever on top of the structure containing the load cell and inductive sensor (see Figure B.6 for a better view of this detail). This lever has a relation of 8:1 and is driven by a combination of a stepper motor, gearbox and a lead screw with a 1.6 mm pitch. Despite the linear displacement of

the compression head not being linear with the rotation of the lead screw, the resolution is approximately 200 μm per turn of the lead screw.

Tests can be controlled manually using the control buttons on the front panel of the power driving rack, or controlled by software specially written in programming language C for this device. All the outputs, including distance between compression surfaces and force, are saved in a MATLAB format file.

The softness tester is based on the same principle of the BLC ST300 softness tester [Alexander 93] [Landmann 94], with a presser foot with 8 mm diameter ending with a spherical shape 4 mm radius, at the bottom a 50 mm diameter ring holds the specimen to be tested.

Table B.4-Specifications of the TQ-402/412 [Vibro-meter 95].

Parameter	Range
Measuring range (mm)	4
Linear measuring range (mm)	0.3-4.3
Sensitivity (mV/μm)	4
Frequency response	DC to 20 kHz (-3 dB)

Testing conditions are 23°C ± 5% on a steel target VCL 140 (1.7225). Different alloys will need re-calibration. The compression tester had an unknown steel target but has been calibrated with the laser sensor (LD1605-4).

Table B.5-Specifications of the LCCA-50 [Omega 95].

Parameter	Range
Measuring range (lbs)	± 50
Signal output (mV/V)	2.05
Linearity and hysteresis	± 0.15% full scale
Zero balance	± 2% max.
Repeatability	± 0.05% full scale
Input resistance (Ω)	385
Output resistance (Ω)	350
Safe overload	150% full scale

B.4 Impact Pendulum Tester

The impact tester, shown in Figure B.7, consists of a pendulum arm (overall length 1315 mm) with mirror finished pressure foot (10 cm^2), which is centred in a rod at the top of a large aluminium framework. The rod is suspended on precision bearings for a smooth rotation and can be released from an adjustable angle with a computer controlled solenoid mechanism. In addition, a dead weight of 1550 gram on the pendulum arm giving an overall weight of 4.5 kg can be balanced to give variable impact forces on the fabric sample, which is clamped on the impact table. Further, the impact table is adjustable relative to the pressure foot and houses the laser sensor (LD1605-4), which points to a metal indicator at the side of the pressure foot.

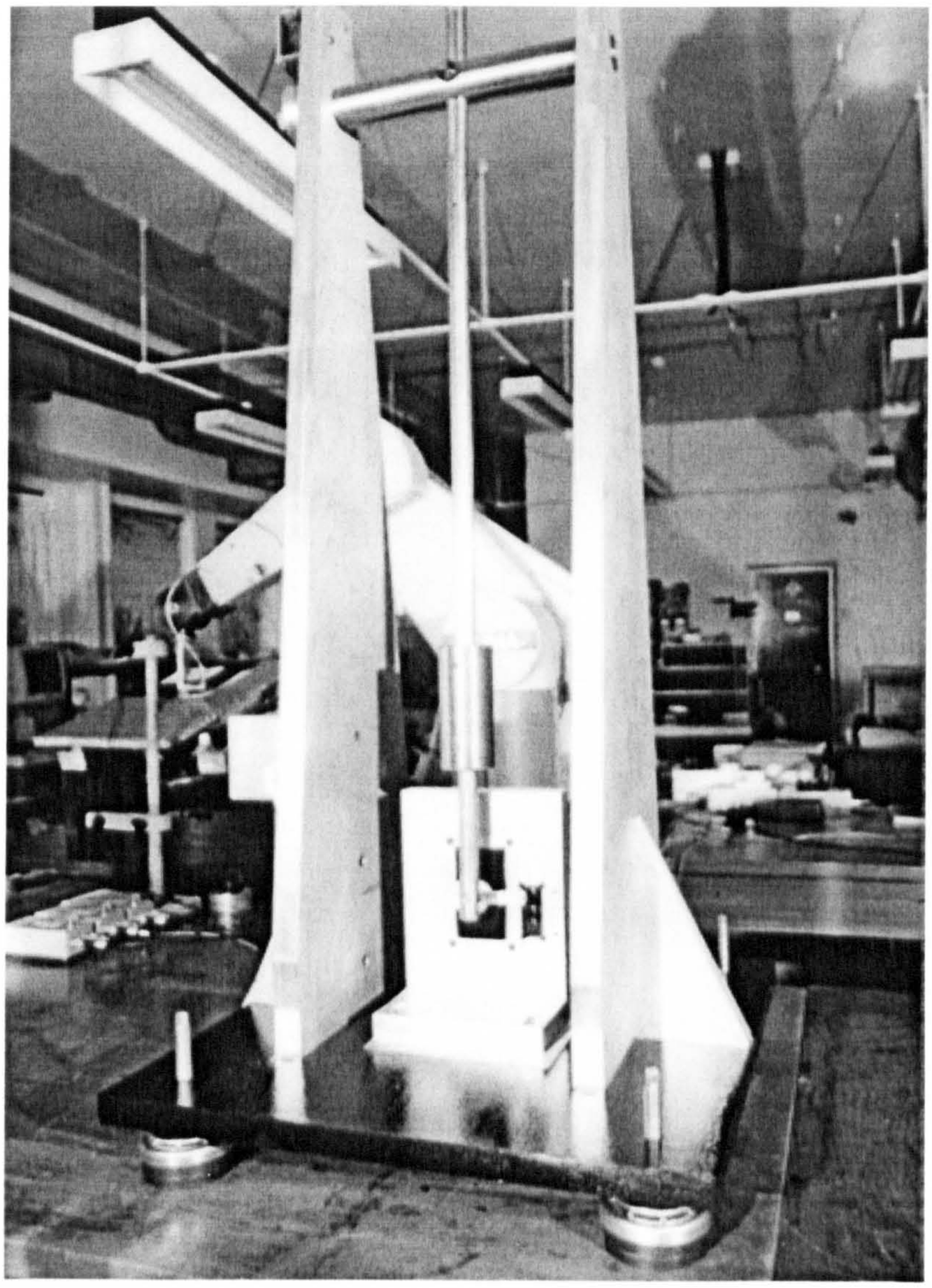

Figure B.7-Full view of the impact tester.

Appendix C MSS Patent

In this appendix, a copy of the application for a European patent of the Mechanical Scanning System is reproduced.

The patent application was published on the 23rd of September 1998, bulletin of 1998/39.

(19) Europäisches Patentamt
European Patent Office
Office européen des brevets

(11) EP 0 866 327 A2

(12) EUROPEAN PATENT APPLICATION

(43) Date of publication:
23.09.1998 Bulletin 1998/39

(21) Application number: **98302145.2**

(22) Date of filing: **23.03.1998**

(51) Int. Cl.[6]: **G01N 3/08**, G01N 33/44, G01B 11/30

(84) Designated Contracting States:
AT BE CH DE DK ES FI FR GB GR IE IT LI LU MC NL PT SE
Designated Extension States:
AL LT LV MK RO SI

(30) Priority: **21.03.1997 GB 9705946**

(71) Applicant:
The University of Hull
Kingston-upon-Hull HU6 7RX (GB)

(72) Inventors:
- **Taylor, Paul Michael**
  Goxhill, North Lincs. (GB)
- **Mendes, Jose de Araujo**
  4730 Vila Verde (PT)

(74) Representative:
Knott, Stephen Gilbert et al
MATHISEN, MACARA & CO.
The Coach House
6-8 Swakeleys Road
Ickenham Uxbridge UB10 8BZ (GB)

(54) Testing apparatus

(57) A testing apparatus which is particularly suitable for leather comprises two pairs of rollers between which the leather passes. By adjusting the speeds and spacings of the rollers and by measuring the torques and positions of the rollers, various characteristics of the leather can be determined. For example, the Young's Modulus can be determined to find low strain regions, a measure of softness can be obtained, shear stress across the thickness can be determined, as can compressiblity and thickness. A laser sensor can be provided to measure surface profile (roughness).

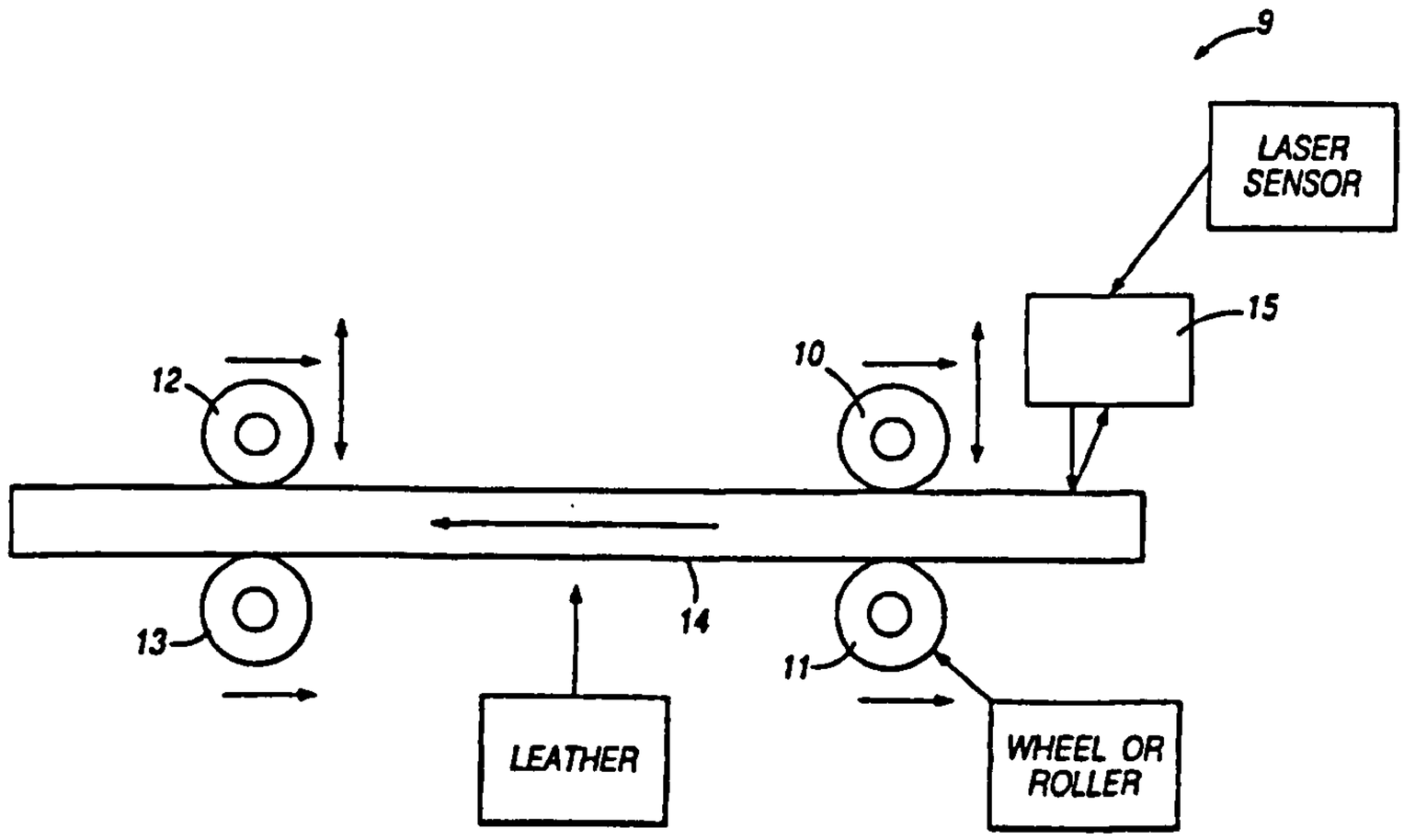

Fig.1

EP 0 866 327 A2

Printed by Xerox (UK) Business Services
2.16.3/3.4

Description

The invention relates to testing apparatus and in particular to testing apparatus for elastic materials.

An example of an elastic material is leather. Leather is an expensive component of many products such as shoes, furniture, car seats, garments and bags. Since it is a natural material, a tanned leather hide will contain visual and hidden flaws. In addition, its mechanical properties vary over the hide so that certain pieces must be cut from certain parts of the skin and in certain orientations to make the product easy to manufacture and comfortable to wear or use.

At present, hides are tested by visual and tactile inspection by skilled operatives at tanneries and at places of manufacture, with faulty regions being cut out or avoided. Mechanical testing requires the removal of samples and thus gives information only about the sample and not about the rest of the hide. Further, some current testing is destructive. For this reason, testing gives little useful information.

According to a first aspect of the invention, there is provided apparatus for testing a piece of elastic material such as leather comprising first and second pairs of rollers forming respective nips for receiving the material, the rollers being rotatable to advance the material, the second pair of rollers being located after the first pair of rollers in the direction of advance of the material and being rotatable at a faster speed than the first pair of rollers to stretch the material between the pairs of rollers and a measuring system for providing a measure of the respective lengths of the material that have passed through each pair of rollers and a measure of the torque on at least one of the rollers, and for deriving therefrom instantaneous measures of the Young's Modulus of material between the pairs of rollers.

According to a second aspect of the invention, there is provided apparatus for testing a piece of elastic material such as leather comprising first and second pairs of rollers forming respective nips for receiving the material, the rollers being rotatable to advance the material, the second pair of rollers being located after the first pair of rollers in the direction of advance of the material and being rotatable at a faster speed than the first pair of rollers to stretch the material between the pairs of rollers, a measuring system being provided for sensing the rotational positions of the rollers and the torque on the rollers and deriving therefrom instantaneous measures of the Young's Modulus of material between the pairs of rollers.

In this way, an idea can be provided of the strength of the material along the whole length or the whole breadth of the piece of the material. This can allow accurate cutting of the material to give desired qualities.

The following is a more detailed description of embodiments of the invention, by way of example, reference being made to the accompanying drawings in which:-

Figure 1 is a schematic view of a first testing apparatus for testing leather; and

Figure 2 is a schematic view of a second testing apparatus for testing leather.

Referring to Figure 1, the first testing apparatus 9 comprises a first pair of rollers 10,11 and a second pair of rollers 12,13. Each pair of rollers, 10,11; 12,13, forms a nip between which passes a piece of leather 14 to be tested.

The distance between the first pair of rollers 10,11 and the second pair of rollers 12,13 is adjustable. In addition, the spacing between the axes of the rollers in the first pair of rollers 10,11 and the spacing between the axes of the rollers in the second pair of rollers 12,13 are also adjustable to adjust the width of the nip between each pair of rollers 10,11 or 12,13.

Each roller 10,11; 12,13, is driven by a motor and the speed and acceleration of each motor is controlled.

In addition, each roller 12,13, of the second pair of rollers has an associated torque sensor for monitoring the torque applied to the associated roller 12,13. Each roller also has an associated position sensor for sensing the rotational position of the associated roller. Further, a displacement sensor senses the distance between the axis of one roller 12 of the second pair of rollers and the axis of the other roller 13 of the second pair of rollers in a direction along a line normal to said axes and passing through said axes. A fourth sensor determines the force applied between one roller 12 of the second pair of rollers and the other roller 13 of the second pair of rollers.

In addition, as seen in the drawing, a laser sensor 15 gives the surface profile of the leather.

The testing apparatus described above with reference to the drawings can be used to test a number of characteristics of the leather 14.

First, it can be used to provide instantaneous measurements of Young's Modulus of the leather in a direction lying in the plane of the leather as the leather passes between the first and second pairs of rollers, 10,11 to determine the location of low strain regions. To do this, the leather is fed between the first and second pairs of rollers 10,11 and 12,13 and the rollers 10,11; 12,13 are all driven at the same speed. As seen in Figure 1, the second pair of rollers 12,13 are located after the first pair of rollers 10,11 in the direction of advance of the leather 19. Next, the second pair of rollers, 12,13 are rotated at a slightly higher speed than the first pair of rollers, 10,11. The effect of this is to stretch the leather 14 between the pairs of rollers.

While the second pair of rollers 12,13 are rotated faster than the first pair 10,11, the length of leather 14 that passes through the second pair of rollers 12,13 in any period is longer than the length of leather 14 that passes through the first pair of rollers 10,12 in that period, the leather 14 passing through the second pair of rollers being stretched compared to the leather pass-

ing through the first pair of rollers 10,11. The difference between the lengths of leather passing between the two pairs of rollers 10,11;12,13 is indicative of the extent to which the leather 14 is stretched.

The outputs of the torque sensors on the rollers 12,13 of the second pair of rollers and the outputs of the position sensors on all the rollers 10,11; 12,13 (which give a measure of the lengths of leather that have passed through the pairs of rollers 10,11;12,13) can be used by a measuring system (not shown) to provide an instantaneous measure of the stress and strain on the region of leather 14 extending between the first pair of rollers, 10,11 and the second pair of rollers 12,13. From this can be calculated the Young's Modulus of the region which will provide an idea of the strength of the region. Thus the testing apparatus can give a number of Young's Modulus values corresponding to such regions spaced over the leather 14.

These measurements can also be used to assess the hysteresis of the leather 14.

The stress and strain determined as described above can also be used to produce a measure of softness. Although softness is in general considered a subjective measurement, the results produced from the apparatus described above with reference to the drawing produces an acceptable indication of softness.

The apparatus can also be used to determine shear stress across the thickness of the leather 14. This is achieved by holding the first pair of rollers 10,11 stationary and rotating the rollers 12,13 of the second pair in opposite directions. The measuring system monitors the torque applied to the rollers 12,13 and from this, and the relative rotational positions of the rollers 12,13, the stress and strain in the leather 14 across its thickness can be determined.

This can help identify low strain regions.

The compressibility across the thickness of the leather 14 can be determined by closing the nip between the rollers 12,13 of the second pair of rollers, measuring the reduction in the size of the nip and also measuring the force applied by the rollers 12,13. From this, the measuring system can produce a measurement of compressibility of the leather across its thickness. It follows, from the previous test, that the apparatus can also measure the thickness by measuring the distance between the axes of the rollers 12,13 (i.e. the width of the nip) at a predetermined compression force.

As described above, the laser sensor 15 can be used to measure the surface profile or roughness of the specimen of the leather 14 while it is moving.

A second testing apparatus 16 is shown in Figure 2. Features of the second apparatus 16 common to the first apparatus 9 are given the same reference numerals and are not described in detail.

The second apparatus 16 has first and second pairs of rollers 17,18;19,20 that are the same as the first and second pairs of rollers 10,11;12,13 of the first apparatus 9, but which are not provided with sensors for detecting the rotational positions of the rollers 17-20.

Instead the second apparatus 16 is provided with a first measuring wheel 21 located adjacent the first pair of rollers 17,18, before the first pair in the direction of advance of the leather, and a second measuring wheel 22 located adjacent the second pair of rollers 19,20 after the second pair in the direction of advance of the leather 14. Each measuring wheel 21,11 is provided with a respective position sensor (not shown) for sensing the rotational positions of the wheels 21,22.

Additionally, the second apparatus is provided with first and second spring-loaded wheels 23,24. Each spring-loaded wheel 23,24 is located opposite a respective one of the measuring wheels 21,22 and serves to press the leather 14 into contact with the associated measuring wheel 21,22.

The second apparatus 16 is used with a measuring system (not shown) as described for the first apparatus 9.

The second apparatus 16 operates in a similar manner to the first apparatus 9. However, the measuring system uses the outputs of the position sensors on the measuring wheels 21,22 (together with the outputs of the torque sensors on the rollers 17,18;19,20) to provide instantaneous measures of the stress and strain on regions of the leather 14 extending between the pairs of rollers. Young's Modulus values are calculated from these measures as for the first apparatus 9. As the first and second measuring wheels 21,22 are located adjacent the first and second pairs of rollers 17,18;19,20 respectively, the position sensors on the measuring wheels give a measure of the lengths of leather 14 that have passed through the two pairs of rollers 17,18;19,20.

The second apparatus 16 can also be used to determine the softness, compressibility and thickness at a predetermined compression force, as described above for the first apparatus 9. Additionally, if the rollers 17,18;19,20 are provided with rotational position sensors (in addition to those provided on the measuring wheels 21,22) the second apparatus 16 can also be used to determine shear stress across the thickness of the leather 14, as described for the first apparatus 9.

It will be appreciated that the first and second testing apparatus described above need not be used to determine all the characteristics described above; they could be used to determine only any one of them. The systems need not be used with leather; they could be used with other elastic materials.

It will also be appreciated that the first and second testing apparatus described above can be used as "on-line" devices monitoring continuously a piece of leather as the leather is fed to processing machinery.

Claims

1. Apparatus for testing a piece of elastic material

such as leather comprising first and second pairs of rollers forming respective nips for receiving the material, the rollers being rotatable to advance the material, the second pair of rollers being located after the first pair of rollers in the direction of advance of the material and being rotatable at a faster speed than the first pair of rollers to stretch the material between the pairs of rollers, and a measuring system for providing a measure of the respective lengths of the material that have passed through each pair of rollers and a measure of the torque on at least one of the rollers, and for deriving therefrom instantaneous measures of the Young's Modulus of material between the pairs of rollers.

2. Apparatus according to claim 1, wherein the measure of the respective lengths comprises information about the respective rotational positions of at least one of the rollers of each pair, the measuring system sensing said rotational positions.

3. Apparatus according to claim 1, wherein the measuring system comprises a first wheel located adjacent the first pair of rollers and a second wheel located adjacent the second pair of rollers, the wheels rotating in contact with the material as the material advances, the measure of the respective lengths comprising information about the respective rotational positions of the wheels, the measuring system sensing said rotational positions.

4. Apparatus according to claim 3, wherein the first wheel is located before the first pair of rollers in the direction of advance and the second wheel is located after the second pair of rollers in the direction of advance.

5. Apparatus according to claim 3 or claim 4, wherein the material is pressed against the first and second wheels by respective spring loaded wheels, each spring located wheel being located at the opposite side of the material to the corresponding one of the first and second wheels.

6. Apparatus according to any preceding claim, wherein the measuring system derives from said measure of the respective lengths and said measure of the torque, a measure of the softness of the material.

7. Apparatus for testing a piece of elastic material such as leather comprising first and second pairs of rollers forming respective nips for receiving the material, the rollers being rotatable to advance the material, the second pair of rollers being located after the first pair of rollers in the direction of advance of the material and being rotatable at a faster speed than the first pair of rollers to stretch the material between the pairs of rollers, a measuring system being provided for sensing the rotational positions of the rollers and the torque on the rollers and deriving therefrom instantaneous measures of the Young's Modulus of material between the pairs of rollers.

8. Apparatus according to claim 7, wherein said measuring system derives from said rotational positions and said torque on the rollers, a measure of the softness of the material.

9. Apparatus according to any one of claims 2, 6 or 7, wherein, with the first and second pairs of rollers halted, one of said pairs of rollers are rotatable in respective opposite directions, the measuring system sensing the torque on the oppositely rotated rollers and the relative rotational positions of the oppositely rotated rollers and deriving therefrom a measure of the Young's Modulus of the material in a direction extending generally along a line normal to the axes of the oppositely rotated rollers and passing through the axes.

10. Apparatus according to any preceding claim, wherein the rollers of one of said pairs of rollers are operable to adjust the size of the nip between the rollers to compress the material between the rollers of said pair, the measuring system sensing the size of the nip and the compressive force and deriving therefrom the compressibility of the material.

11. Apparatus according to claim 10, wherein the measuring system derives a measurement of the thickness of the material from the size of the nip between said pair of rollers at a predetermined compressive force.

12. Apparatus according to any preceding claim and including a sensor for measuring the surface profile of the material to provide an indication of roughness.

13. Apparatus according to claim 12 wherein said sensor is a laser sensor.

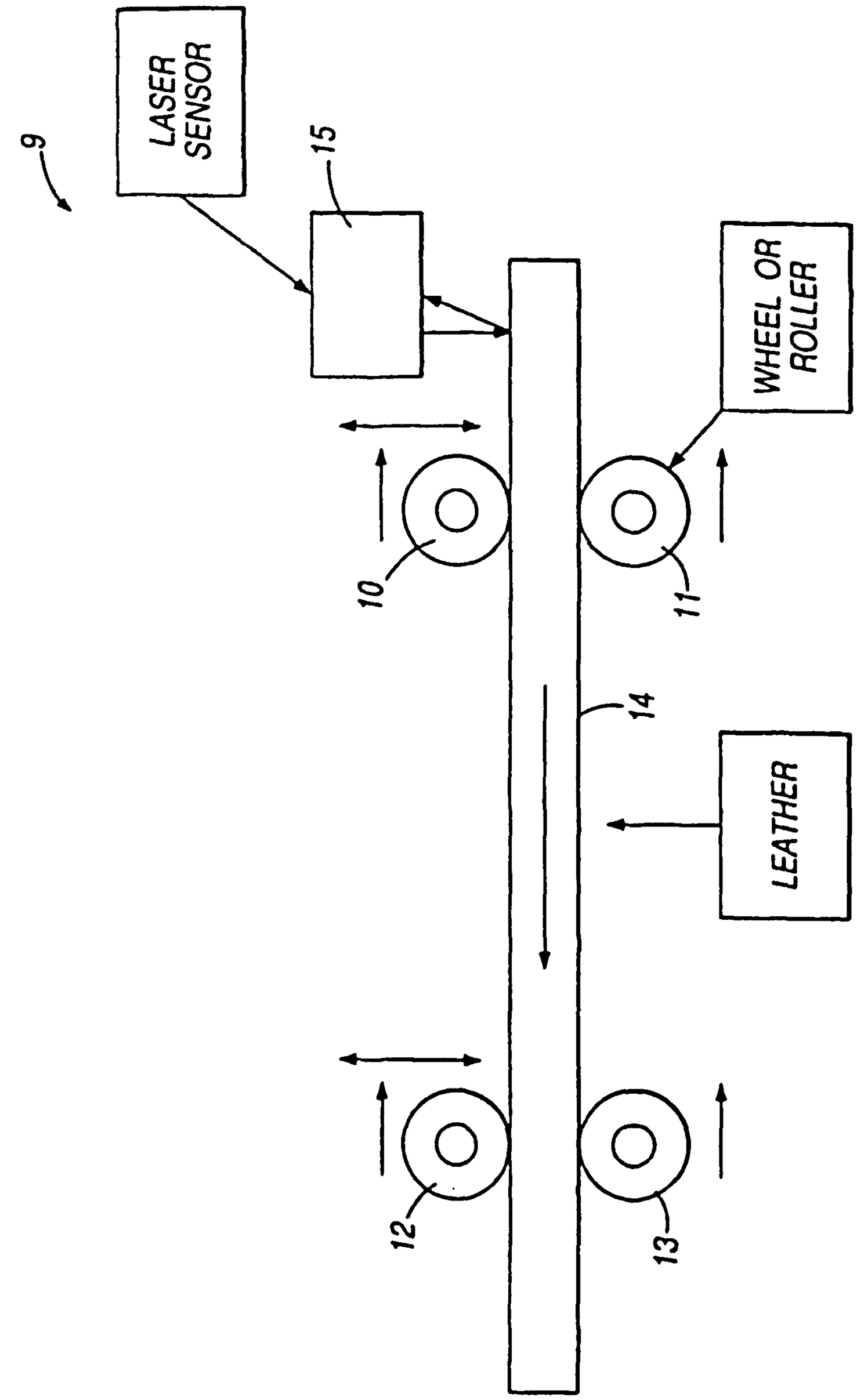

Fig. 1

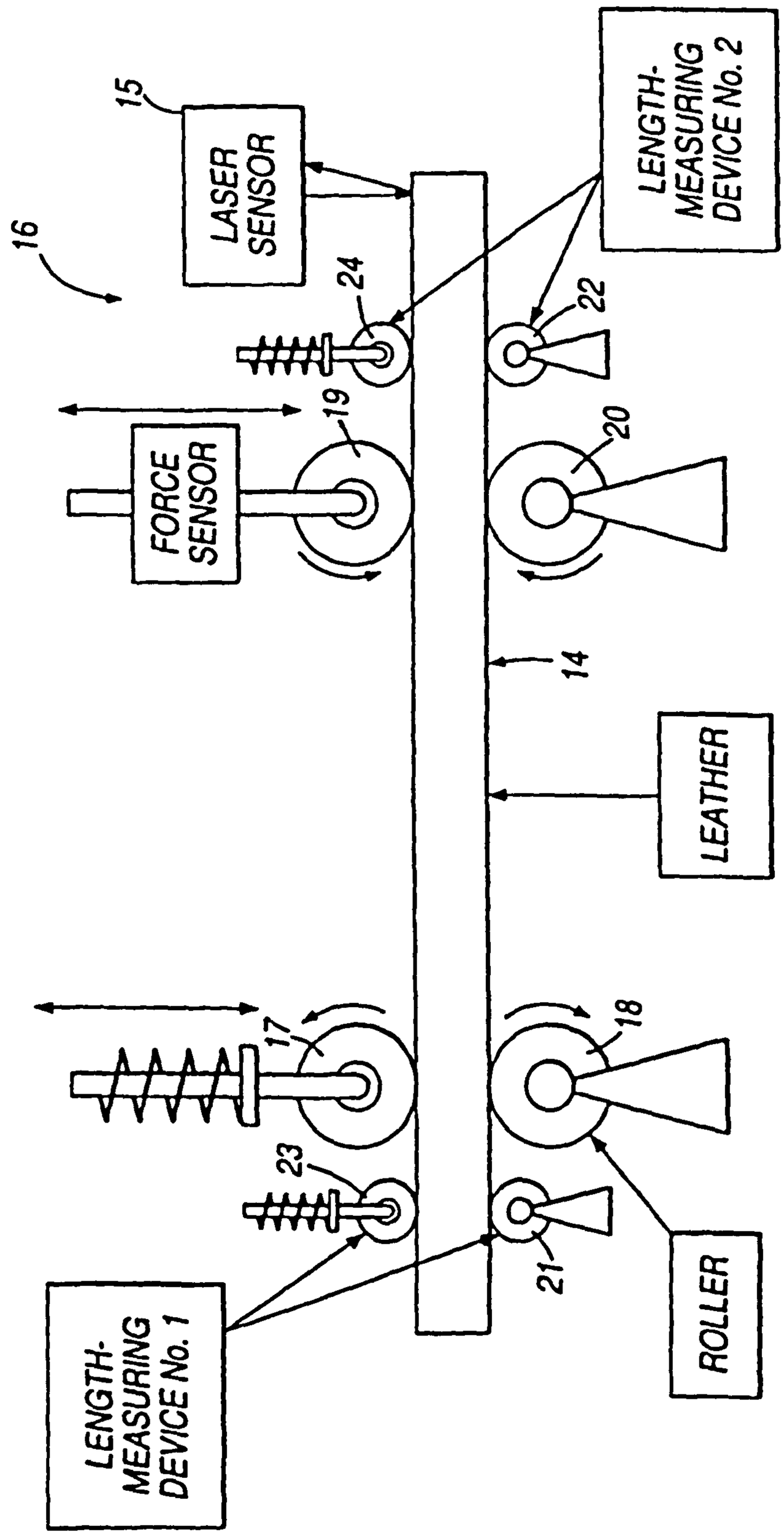
LENGTH-MEASURING DEVICE No. 2
15
LASER SENSOR
16
24
22
19
FORCE SENSOR
20
14
LEATHER
17
18
23
21
LENGTH-MEASURING DEVICE No. 1
ROLLER

Fig.2

(19) Europäisches Patentamt
European Patent Office
Office européen des brevets

(11) EP 0 866 327 A3

(12) EUROPEAN PATENT APPLICATION

(88) Date of publication A3:
28.07.1999 Bulletin 1999/30

(43) Date of publication A2:
23.09.1998 Bulletin 1998/39

(21) Application number: 98302145.2

(22) Date of filing: 23.03.1998

(51) Int. Cl.[6]: G01N 3/08, G01N 33/44, G01B 11/30

(84) Designated Contracting States:
AT BE CH DE DK ES FI FR GB GR IE IT LI LU MC NL PT SE
Designated Extension States:
AL LT LV MK RO SI

(30) Priority: 21.03.1997 GB 9705946

(71) Applicant:
The University of Hull
Kingston-upon-Hull HU6 7RX (GB)

(72) Inventors:
- Taylor, Paul Michael
  Goxhill, North Lincs. (GB)
- Mendes, Jose de Araujo
  4730 Vila Verde (PT)

(74) Representative:
Knott, Stephen Gilbert et al
MATHISEN, MACARA & CO.
The Coach House
6-8 Swakeleys Road
Ickenham Uxbridge UB10 8BZ (GB)

(54) Testing apparatus

(57) A testing apparatus which is particularly suitable for leather comprises two pairs of rollers between which the leather passes. By adjusting the speeds and spacings of the rollers and by measuring the torques and positions of the rollers, various characteristics of the leather can be determined. For example, the Young's Modulus can be determined to find low strain regions, a measure of softness can be obtained, shear stress across the thickness can be determined, as can compressiblity and thickness. A laser sensor can be provided to measure surface profile (roughness).

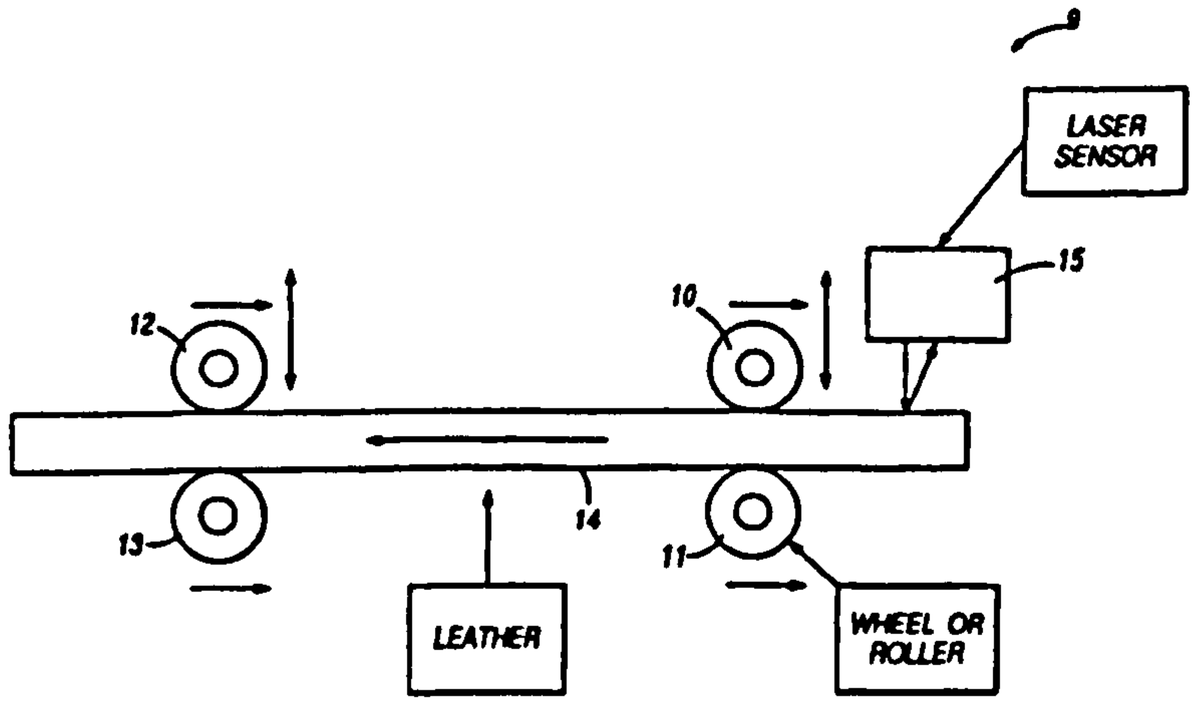

Fig.1

EP 0 866 327 A3

Printed by Xerox (UK) Business Services

EP 0 866 327 A3

European Patent Office

EUROPEAN SEARCH REPORT

Application Number
EP 98 30 2145

DOCUMENTS CONSIDERED TO BE RELEVANT

Category	Citation of document with indication, where appropriate, of relevant passages	Relevant to claim	CLASSIFICATION OF THE APPLICATION (Int.Cl.6)
Y	US 3 933 035 A (ROCH ROGER HENRI) 20 January 1976 * abstract; figure 1 *	1-9	G01N3/08 G01N33/44 G01B11/30
Y	GB 1 116 400 A (THE DUNLOP CO. LTD.) 6 June 1968 * page 1; figure 1 *	1-9	
Y	POTLURI P ET AL: "A ROBOTIC FLEXIBLE TEST SYSTEM (FTS) FOR FABRICS" MECHATRONICS, vol. 5, no. 2/03, 1 March 1995, pages 245-278, XP000510167 kidlington, oxford, gb * page 246 - page 247; figure 1E *	1-9	
A	DE 43 29 051 A (PEG INGENIEURBUERO FUER PROJEK) 2 March 1995 * abstract; claim 7; figure 2 *	7	
A	GB 2 153 533 A (LD TESTERS OY) 21 August 1985 * the whole document *	10,11	TECHNICAL FIELDS SEARCHED (Int.Cl.6) G01N
A	RAMGULAM R B ET AL: "MEASUREMENT OF FABRIC ROUGHNESS BY A NONCONTACT METHOD" JOURNAL OF THE TEXTILE INSTITUTE, vol. 84, no. 1, 1 January 1993, pages 99-106, XP000345457 manchester, gb * abstract *	12,13	
A	FR 2 651 888 A (SUPERBA SA) 15 March 1991 * page 3, line 14-25; figure 1 *	1,7	
A	EP 0 403 988 A (ZELLWEGER USTER AG) 27 December 1990 * abstract; figure 1 *	1,7	

The present search report has been drawn up for all claims

Place of search	Date of completion of the search	Examiner
BERLIN	3 June 1999	Brison, O

CATEGORY OF CITED DOCUMENTS

X : particularly relevant if taken alone
Y : particularly relevant if combined with another document of the same category
A : technological background
O : non-written disclosure
P : intermediate document

T : theory or principle underlying the invention
E : earlier patent document, but published on, or after the filing date
D : document cited in the application
L : document cited for other reasons

& : member of the same patent family, corresponding document

EPO FORM 1503 03 82 (P04C01)

EP 0 866 327 A3

ANNEX TO THE EUROPEAN SEARCH REPORT ON EUROPEAN PATENT APPLICATION NO. EP 98 30 2145

This annex lists the patent family members relating to the patent documents cited in the above-mentioned European search report.
The members are as contained in the European Patent Office EDP file on
The European Patent Office is in no way liable for these particulars which are merely given for the purpose of information.

03-06-1999

Patent document cited in search report	Publication date	Patent family member(s)	Publication date
US 3933035 A	20-01-1976	CH 569968 A	28-11-1975
		CA 1009055 A	26-04-1977
		DE 2442901 A	07-08-1975
		FR 2244169 A	11-04-1975
		GB 1471997 A	27-04-1977
		JP 973038 C	28-09-1979
		JP 50057696 A	20-05-1975
		JP 54006391 B	28-03-1979
		SE 411076 B	26-11-1979
		SE 7411715 A	20-03-1975
GB 1116400 A		NONE	
DE 4329051 A	02-03-1995	NONE	
GB 2153533 A	21-08-1985	FI 840380 A	31-07-1985
FR 2651888 A	15-03-1991	CH 683799 A	13-05-1994
		DE 4029172 A	28-03-1991
		GB 2237884 A	15-05-1991
		IT 1244308 B	08-07-1994
		JP 3185174 A	13-08-1991
EP 0403988 A	27-12-1990	CH 678764 A	31-10-1991
		CN 1057716 A,B	08-01-1992
		DE 59008337 D	09-03-1995
		ES 2066042 T	01-03-1995
		JP 2844384 B	06-01-1999
		JP 3042538 A	22-02-1991
		US 5050437 A	24-09-1991

EPO FORM P0459

For more details about this annex : see Official Journal of the European Patent Office, No. 12/82